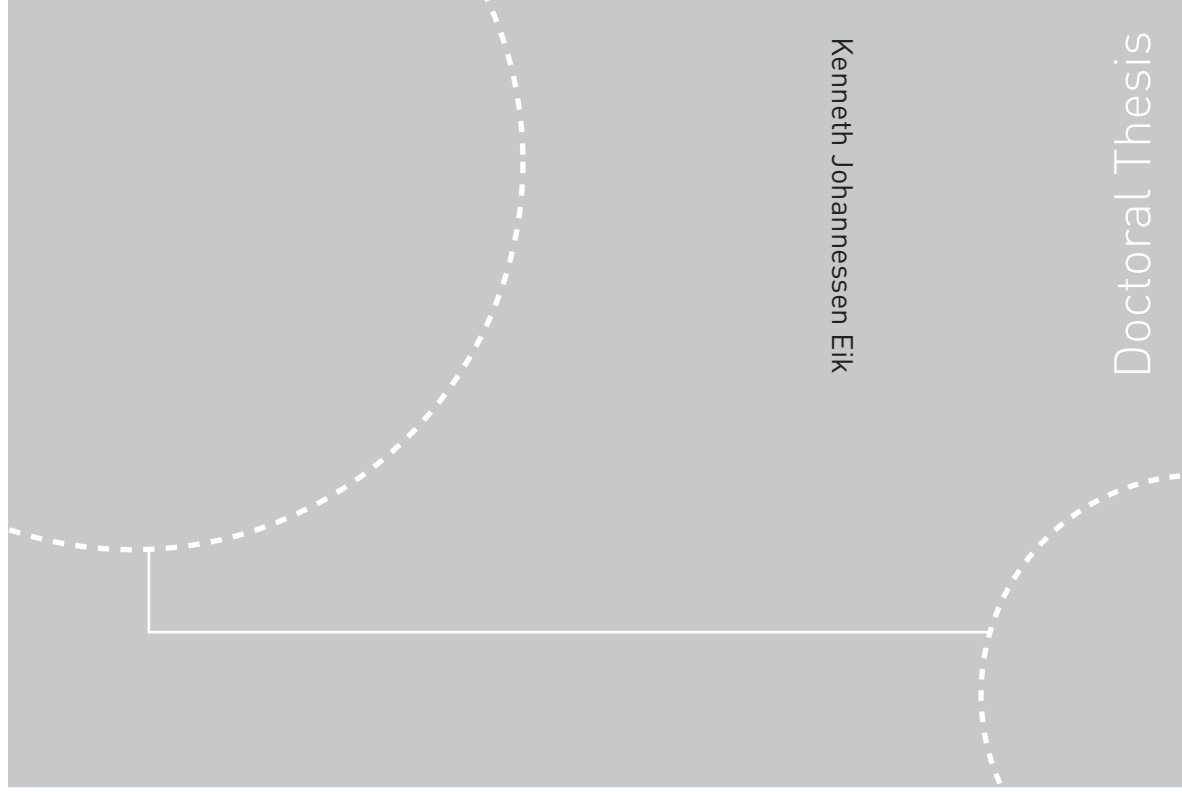


Doctoral theses at NTNU, 2010:276

Kenneth Johannessen Eik
**Ice Management in Arctic Offshore
Operations and Field Developments**



ISBN 978-82-471-2402-4 (printed ver.)
ISBN 978-82-471-2403-1 (electronic ver.)
ISSN 1503-8181

Doctoral theses at NTNU, 2010:210

NTNU
Norwegian University of
Science and Technology
Thesis for the degree of
philosophiae doctor
Faculty of Engineering Science and Technology
Department of Civil and Transport Engineering



Kenneth Johannessen Eik

Ice Management in Arctic Offshore Operations and Field Developments

Thesis for the degree of philosophiae doctor

Trondheim, November 2010

Norwegian University of
Science and Technology
Faculty of Engineering Science and Technology
Department of Civil and Transport Engineering



Norwegian University of
Science and Technology

NTNU

Norwegian University of Science and Technology

Thesis for the degree of philosophiae doctor

Faculty of Engineering Science and Technology
Department of Civil and Transport Engineering

©Kenneth Johannessen Eik

ISBN 978-82-471-2402-4 (printed ver.)

ISBN 978-82-471-2403-1 (electronic ver.)

ISSN 1503-8181

Doctoral Theses at NTNU, 2010:210

Printed by Tapir Uttrykk

ABSTRACT

The subject ice management has been studied with the main objective to deduce a methodology that incorporates the effect of ice management on the structural reliability of offshore installations. This was done by first studying Arctic projects in the past and summarizes the learning's. All available reports were unanimous and highlighted ice management as a key for the successes in the projects. Based on the reported experiences, an unambiguous definition of ice management was made:

“Ice management is the sum of all activities where the objective is to reduce or avoid actions from any kind of ice features”

Despite the number of similarities between sea ice management and iceberg management, it was decided to study each of the fields individually. The motivation for doing so was that iceberg management in general focus on reducing the frequency of impacts between icebergs and installations while sea ice management generally focus on reducing the sizes in the ice floe distributions and thereby reduces the severity of the ice actions. One methodology for including iceberg management and one for including sea ice management in the offshore installation design process has been proposed.

In order to develop the models for ice management efficiency a number of studies of the various elements were conducted. Individual papers regarding subsurface ice intelligence, iceberg drift modelling, iceberg deterioration, iceberg deflection in ice and ice load variability has been published and are included in this thesis. Each of these papers is of importance for the proposed models for ice management efficiency.

The possibility to disconnect an installation and escape the site has been considered both in the methodologies for iceberg management and sea ice management. When considering the number and magnitude of uncertainties both with respect to load calculations from icebergs and sea ice, it is concluded that disconnection capabilities should be considered in all Arctic projects. It was shown that icebreakers not necessarily are sufficient to reduce extreme or abnormal loads on a structure. However, there may

still be a number of reasons for why icebreakers also should be considered in Arctic projects.

The methodologies presented in this work provide adequate tools for evaluating the effect of various icebreaker fleets and iceberg management systems. However, the approaches rely on a number of tools and formulations with inherent weaknesses and advantages. The weaknesses are discussed and recommendations for further work in order to improve the models have been proposed.

ACKNOWLEDGEMENTS

The main motivation for writing a thesis on the subject “Ice Management” was based on the acknowledgement that future offshore developments will take place in Arctic environments and that this introduces a number of new challenges for the offshore industry. Personally, I had a strong motivation for being a part of these future projects and being able to contribute technically. When my colleague and later co-supervisor, Ove Tobias Gudmestad took the initiative to start a PhD on the subject, I was please to volunteer for the “mission”. Almost four years later, I can look back on a hectic but joyful time both with respect to work and private life. There are a number of persons I would like to express my gratitude to, for making it possible for me to undertake this work.

First, I would like to thank my employer, Statoil, for having faith in me and letting me do this study as a part of my work. The former chief researcher Arnt Olufsen supported the idea about doing a PhD in order to increase my competence. Ove Tobias Gudmestad, Einar Nygaard , Arne Gürtner and Hanne Greiff Johnsen ensured at different stages that funding were available to do the study. Our chief researcher Finn Gunnar Nielsen has been of great support by carefully reading my papers and contributing with constructive comments.

The unique milieu in the “PhD basement” at NTNU should be praised for being open, incorporating and a source for exchange of knowledge within a number of fields. We have an always enthusiastic supervisor in Professor Sveinung Løset which are full of new ideas and is able to make things happen. Amongst the PhD students I would like to emphasize my appreciation of Raed Lubbad, Nicolas Serre, Vegard Aksnes, Oddgeir Dalane, Christian Lønøy, Marit Reiso, Ada Repetto-Llamazares, Felix Breitschädel, Wolfgang Kappel, Sergiy Sukhorukov, Anton Kulyakthin, Haiyan Long, Kim Yangkyun and (now colleague in Statoil) Arne Gürtner. Further the post docs. Jenny Trumar, Alex Klein-Paste, Paul Thomassen, professors Knut Høyland and Alf Tørum and our administrator Marion Beentjes all contributes to the good and friendly environment in the basement.

The work with a PhD study may sometimes be considered as lonely as you are the one and only responsible for the progress. I have been able to enjoy the work from the start to the end and never experienced the phase where I get bored of the subject. This is thanks to my wife Nina Elise, and my sons Vegard, Sondre and Håvard which always brings me back to the reality and ensures that I have the right perspectives in life.

CONTENTS

1	INTRODUCTION.....	1
1.1	<i>General.....</i>	<i>1</i>
1.2	<i>Scope and organisation of the thesis.....</i>	<i>2</i>
1.3	<i>Readership.....</i>	<i>3</i>
2	REVIEW OF EXPERIENCES WITHIN ICE AND ICEBERG MANAGEMENT.....	6
3	ICE INTELLIGENCE.....	24
3.1	<i>General.....</i>	<i>24</i>
3.2	<i>Specifications for a subsurface ice intelligence system.....</i>	<i>26</i>
4	EFFICIENCY OF ICEBERG MANAGEMENT.....	36
4.1	<i>Iceberg drift.....</i>	<i>36</i>
4.2	<i>Iceberg deterioration.....</i>	<i>86</i>
4.3	<i>Physical iceberg management.....</i>	<i>104</i>
4.4	<i>Iceberg management and impact on design of offshore structures.....</i>	<i>132</i>
5	EFFICIENCY OF SEA ICE MANAGEMENT.....	148
5.1	<i>Ice load formulations.....</i>	<i>148</i>
5.2	<i>Ice load variability.....</i>	<i>150</i>
5.3	<i>Sea ice management and impact on design of offshore structures.....</i>	<i>166</i>
6	SUMMARY.....	208
6.1	<i>Summary and conclusions.....</i>	<i>208</i>
6.2	<i>Recommendations for further work.....</i>	<i>212</i>
7	REFERENCES.....	213

1 INTRODUCTION

1.1 General

In order to supply the world with sufficient hydrocarbons, the petroleum industry is expected to initiate an increasing number of offshore developments in Arctic waters. This introduces new challenges with respect to design philosophy as the standards established for open water developments may not be optimal for developments in ice covered waters or waters exposed to icebergs.

There is a number of reasons for why the open water philosophies for offshore installation design may be insufficient in ice covered waters. In this respect, uncertainties in ice and iceberg load calculations should be mentioned. Furthermore, significant uncertainties in available environmental data in most Arctic regions must be expected as such data are both expensive and complicated to collect. The challenges in ice load calculations and ice data collection calls for innovative thinking in the design process.

In spite of the increased uncertainties in Arctic projects, there are possibilities to include load reducing measures and thereby increase the overall safety. Examples of such measures may be use of icebreakers in ice covered waters or supply vessels for iceberg towing. Furthermore, if the offshore installations are designed with the possibility to disconnect and escape their site, an additional level of safety may be achieved. All means contributing to avoiding or reducing ice loads may be incorporated in the designation "Ice management". The present work focuses on the elements in sea ice and iceberg management with the objective of proposing approaches for how to include these elements in the offshore installation design process.

1.2 Scope and organisation of the thesis

The intent of this thesis is to gain increased knowledge about ice management in general and to transfer the knowledge from practical experiences into statistical design frameworks in particular.

The work is presented through nine papers each dealing with different elements of ice management. All papers except one have been published in international journals and conference proceedings. The last paper is presently pending on a journal review. The first paper, “Review of experiences within ice and iceberg management”, which is presented in Chapter 2, provides a proper introduction to the special field “ice management”. An unambiguous definition of ice management is proposed and lessons learned from all relevant Arctic projects are highlighted.

In order to include ice management in statistical frameworks for design calculations, a number of building blocks need to be in place. Examples of such building blocks may be; “ice detection models”, “ice and iceberg drift forecasting models”, “models for calculations of managed ice” and “models for iceberg deflection success”. In order to prepare all the building bricks for real Arctic offshore projects a substantial amount of work from a number of disciplines will be required. Obviously, it is not possible even within the scope of a PhD study to go into detail in all the sub-topics which fall under the special field “ice management”. Consequently, some selected fields are presented into detail through different papers while others are briefly described. In order to avoid duplicating information, references are made to Chapter 2 regarding general ice management subjects that are not treated in specific papers.

With respect to ice intelligence (Chapter 1), which is the first activity required in ice management operations, it was decided to look closer at the ability to detect ice features from the bottom side. Reasons for this was that novel technology such as AUVs and multi beam echo sounders is considered promising with respect to future ice management operations while more traditional intelligence means such as marine radars and satellites already have been considered for most ice management operations.

Therefore, a brief summary of ice detection means is presented in Section 3.1 while a more detailed subsurface ice intelligence system is presented and discussed in Section 3.2.

Despite the number of similarities between sea ice management and iceberg management, it was decided to treat each of these subjects individually. Thus, all information on iceberg management is found in Chapter 4 while all information on sea ice management is found in Chapter 5. Both of these chapters close with papers on how the management systems may be incorporated into the design process. Section 4.4 and Section 5.3 address iceberg management and sea ice management respectively. The bricks required for iceberg management evaluation such as iceberg drift, iceberg deterioration and iceberg deflection are presented through four papers in Sections 4.1 to 4.3. Corresponding bricks for sea ice management such as ice load models and ice load variability are presented in Section 5.1 and Section 5.2 respectively.

Each paper in this thesis includes both conclusions and references. However, some general discussion of the total work and main conclusions of the thesis have been included in Chapter 6. A few references that are cited outside the individual papers are listed in Chapter 7.

1.3 Readership

The present work deals with ice management in the context of Arctic offshore field developments. The primary readership targets for this thesis as a whole and for some particular parts are engineers and scientists working with:

- Hydrocarbon field development in ice-covered waters
- Design of any kind of structures subjected to loads from sea ice or icebergs
- Marine operations in ice-covered waters

As the thesis also highlight fields which require improved models, it can also serve as encouragement to scientists working within disciplines such as oceanography, meteorology, sea ice load modelling and iceberg load modelling.

Finally, the thesis should be read by personnel working actively with ice management operations as it shows how important their experiences are and how their learning's can contribute to increased efficiency and safety in future projects.

2 REVIEW OF EXPERIENCES WITHIN ICE AND ICEBERG MANAGEMENT



Royal Institute of Navigation
Land Air Sea Space

THE JOURNAL OF NAVIGATION

VOL. 61

OCTOBER 2008

NO. 4

Review of Experiences within Ice and Iceberg Management

Kenneth Eik

(Norwegian University of Science and Technology)
(Email: kenjo@statoilhydro.com)

A review of existing knowledge regarding how to manage ice during offshore work in cold waters has been carried out. The objective has been to contribute to increased safety and efficiency in future projects by learning from world-wide experiences. It was found that offshore drilling has been carried out in a wide range of ice conditions and at water depths spanning from five metres to more than a thousand metres. Icebergs in open waters have been handled safely over several years and the possibility of detecting icebergs is considered good. With respect to icebergs frozen in sea ice, both detection and deflection is considered difficult and the technology for doing so is not proven. Good ice management systems are considered to represent the main factors for operating successfully in the covered waters. Future work should focus on how to include the effect of ice management statistically in a design process.

KEY WORDS

1. Ice management. 2. Ice detection. 3. Risk evaluation. 4. Operability.

1. INTRODUCTION. Searching for oil and gas in regions infested by sea ice and icebergs has been ongoing for several decades. Considering the increasing price for hydrocarbons during recent years and a suggestion by the US Geological Survey that 25% of the remaining hydrocarbon resources in the world are located in the Arctic, a strong increase in Arctic offshore activities must be expected. One of the critical issues when drilling in waters subjected to sea ice or icebergs is how to

handle the ice. To ensure that new projects are planned and executed in a safe and efficient manner it is important to learn from the experience of the past. This paper gives a review of petroleum activities world-wide where the presence of sea ice or icebergs has influenced operations. The objectives have been to identify the type of ice regime, the tools and methodology used to keep track of the ice and how to avoid damage from ice actions.

Each Section in this paper provides a description of relevant projects from a region in the world characterized by the presence of sea ice or icebergs. The regional presentations are followed by a discussion on how existing knowledge, methodology and tools can be applied to future projects and finally some conclusions are drawn.

2. DEFINITION OF ICE MANAGEMENT. The terms ice management and iceberg management are only used in recent literature and no unambiguous definitions have been found. The associations with ice management may depend on the regions that are under consideration; in the Beaufort Sea ice management is typically about breaking and clearing sea ice while ice management at Grand Banks typically concerns iceberg deflection. In some areas the presence of both sea ice and icebergs will be expected. As there are many similarities in sea ice management and iceberg management there will be no differentiation between these terms. The following definition is proposed for ice management:

Ice management is the sum of all activities where the objective is to reduce or avoid actions from any kind of ice features. This will include, but is not limited to:

- *Detection, tracking and forecasting of sea ice, ice ridges and icebergs*
- *Threat evaluation*
- *Physical ice management such as ice breaking and iceberg towing*
- *Procedures for disconnection of offshore structures applied in search for or production of hydrocarbons*

3. BEAUFORT SEA ICE MANAGEMENT EXPERIENCES (*Wright, 2005*). With respect to offshore operations, the Beaufort Sea is known to be one of the most challenging regions in the world. A number of wells have been drilled in the Beaufort Sea at water depths in the range from a few metres and up to 80 m during periods with severe ice conditions. For water depths in the range 20 m–80 m floaters were applied for the exploratory drilling and relatively sophisticated ice management systems were developed.

3.1. *Canmar drillships*. From 1976 and until the late 1980s four conventional drillships were used by Canadian Marine Drilling Ltd. (Canmar) for exploratory drilling in the Beaufort Sea. Prior to mobilisation in the Beaufort Sea, the drillships had been reinforced to satisfy the requirements for the Baltic Class 1A Super level¹. Despite this, the drillships were only intended for use in the open water season and the early freeze-up period.

Each of the vessels was deployed with an eight point mooring system which overall had a capacity in the order of 100 tons. The vessels were aligned in a fixed direction

¹ Baltic Rules (Finnish Maritime Administration and Swedish Maritime Administration)
1A Super – vessel able to work in 1.0 m thick ice



Figure 1. Beaufort Sea drilling operations from a moored drillship, in the late 70s (from Keinonen et al., 2007).

and not able to vane in accordance with wind, waves, current or ice drift. Three of the four vessels had anchor lines piercing through the waterline while one had underwater fairleads. All anchor lines were equipped with remote anchor releases (RARs) that allowed the drillships to quickly disconnect and move off location.

With respect to physical ice management typical support for the drillship operations consisted of one or two supply vessels with ice class CAC 4 and at times with icebreakers in class CAC 3 and/or CAC 2². The icebreakers would typically work upstream from the drillship in circular patterns as seen in Figure 1. It is reported by Wright (1999) that ice monitoring, ice management and alert procedures were developed and had proven successful.

Considering the efficiency and safety of the operations no major incidents have been reported. However, in accordance with Keinonen (2006), on one occasion one of the supply vessels got stuck in the ice and drifted into the drillship it was supposed to protect. Wright (1999) reports that main problems with the operations were caused by large rough ice floes that could not be managed (independent of concentration). High ice concentrations, moderate to severe thick first-year ice and changes in ice drift directions caused ice forces in a transverse direction. Weak moorings, fixed orientation and mooring lines piercing through the waterline were all factors reducing the operability of the system.

Hnatiuk (1983) reports that average drilling period per year was 110 days while both drillships as well as their support systems were idle for eight or nine months due to ice conditions. A well drilled from one of the drillships could cost over \$100 million and take up to three years.

² Canadian Arctic Shipping Pollution Prevention Regulations:

CAC 4 – vessel designed to work in medium thick (0.7 m–1.2 m) first-year ice

CAC 3 – vessel designed to withstand thick (>1.2 m) first-year ice



Figure 2. The conical drilling unit, Kulluk, station keeping in late freeze-up pack ice conditions with two vessels managing the oncoming ice updrift (from Wright, 2000).

3.2. *Gulf conical drilling unit – Kulluk (Wright, 1999, 2000 and 2005).* In order to extend the drilling season and make exploration drilling more efficient, Gulf Canada Resources developed a conical drilling unit (named Kulluk) for operations in the Beaufort Sea (Figure 2). The structure was designed to resist significant ice forces and meet the requirements for CAC 2 standards. The hull was shaped conical at the waterline in order to break the ice in a flexural mode and thus reduce the global loads. An outwards flare was mounted near the bottom of the hull in order to clear broken ice pieces around the hull and not enter the moon-pool or get entangled in the mooring lines. Kulluk had a radially symmetric mooring system consisting of twelve 3½” wire lines running through the hull to underwater fairleads near the bottom of the hull. The system was designed to withstand global ice loads up to 750 tonnes during drilling. As with the drillships, all anchor lines were equipped with RARs in order to ensure the vessel could quickly move off locations when required. Despite all precautions with respect to actions from ice loads, the vessel was not however designed for year-round operations in the Beaufort Sea.

Kulluk drilled twelve wells in the Beaufort Sea at water depths in the range 20 m to 60 m in the period 1983 to 1993. Typically, operations would start in late May and end in late December (approximately 200 days). Suspension of drilling in the freeze-up season was usually caused by restrictions in relief well drilling rather than limitations in the station-keeping capabilities.

The elements of the Kulluk ice management system were:

- An ice monitoring and forecasting system
- A performance monitoring system

<u>KULLUK ENVIRONMENTAL ALERT STATUS</u>				
COLOUR CODE	MEANING	HAZARD TIME (HT) MINUS SECURE TIME (ST)	DRILLING RESPONSE	MARINE RESPONSE
Green	Normal operation	HT-ST is more than 12 hours	Normal operations	Normal watch
Blue	Early alert	HT-ST is less than 12 hours	Normal operations	Alert watch & ice management
Yellow	Early warning	HT-ST is less than 6 hours	Restrict operations to available lead time	Begin preparations for hazard and ice management
Red	Drilling must stop, vessel may move off	HT-ST is zero	Secure well as appropriate	Final preparations for hazard and ice management
Black	ICE: vessel must move off WEATHER/WAVE: vessel must stream off on moorings	HT for disconnect is less than 2 hours	Disconnect	ICE: Move Kulluk off site WEATHER/WAVE: Stream off moorings

Figure 3. Synopsis of Kulluks ice alert system (after Wright, 2000).

- An ice alert system (Figure 3)
- An icebreaker support system
- Well defined operating procedures

In monitoring and forecasting of ice conditions, one would distinguish between local and regional ice information. The typical local information would be about ice thickness, concentration, floe size, type of ice feature, drift velocity and velocity up-stream (primarily) the vessel for a distance up to 15 km. The time scale of the information would be from some few tens of minutes to a few hours. The information was typically based on visual observations from ice observers both on Kulluk as well as on the assisting icebreakers. Marine radars were frequently used and occasionally, helicopters. The regional ice information would in spatial scale be from tens of kilometres to 100 km or more and in timely scale for one to a few days. The regional information would focus on regional pack ice distribution and characteristics as well as general pack ice movements. Periodic airborne radar flights, in addition to some available satellite imagery, were important sources for the regional information. Sometimes, drift buoys were put on the ice in order to track the ice movements while drift forecasts usually were based on wind forecasts and some fairly simple models.

The purpose of the Kulluk alert system (Figure 3) was to define, in a timely manner, any hazards that could cause an interruption to the drilling operations or threaten the security of the well or the vessel and, in addition, ensure that appropriate responses could be taken. In order to evaluate the threat and respond correctly the two parameters *Hazard Time* (HT) and *Secure Time* (ST) were used. HT was the estimated time until occurrence of a potential hazardous ice conditions while ST would be the time needed to secure and disconnect from the well. For Kulluk the ST was in the range of four to six hours and included some safety margins in order to ensure an orderly mooring disconnect and move-off sequence.

Despite the fact that Kulluk was designed to withstand severe ice loads it typically depended on assistance from two to four CAC 2 icebreakers in order to meet the station-keeping requirements during drilling. The vessel was not self-propelled and

thus also needed assistance to move off location. Wright (2000) describes a wide range of icebreaker techniques used by the Kulluk assistance icebreakers depending on the various ice conditions. The effect of icebreaker support was, however, limited in situations with high ice pressure. Overly managed ice combined with high lateral ice pressure generated rafting and ridging and could cause even higher loads than in unmanaged ice.

During operations Kulluk experienced thick first-year ice, large pressure ridges, heavy rubble and/or large concentrations of drifting multi-year ice. During the first 6 drilling seasons Kulluk experienced 44.7 down days and 8 moves off location within a total of 585 operating days (92% operability). No severe accidental events have been reported from the drilling operations. However there were some events involving impacts from some large and heavily ridged ice floes. The most severe event occurred at an early stage in the Kulluk operations when a thick and heavily ridged ice floe with extension 5 km × 8 km impacted Kulluk with a speed of 0.6 m/s. Kulluk was pushed off location and some of the mooring lines broke. However, as a consequence of the ice management system and alert procedures all drilling activities had been safely suspended prior to the impact.

4. EAST COAST OF CANADA – GRAND BANKS. The occurrence of drifting icebergs is the dominating threat for the petroleum production at Grand Banks. On average 553 icebergs per year pass the 48°N parallel but the annual variability is significant (McClintoc et al., 2007). Typically, the icebergs are drifting from the north and going southwards. Along the Labrador coast a wide range of icebergs are sighted every year varying from small growlers to large ice islands.

Hibernia, which started oil production in 1997, is located at 80 m water depth and is designed to withstand an impact with an iceberg of six million tons in ALS condition³ (Hibernia, 2007). Hibernia was followed by the floating production vessels Terra Nova in 2002 and White Rose in 2005 at approximately 95 m and 120 m water depths, respectively. All these installations are in need of some sort of ice management support including Hibernia which has a loading system and associated shuttle tankers vulnerable for impact with icebergs (Crocker et al., 1998).

During the years with activities at Grand Banks, experiences from physical iceberg management operations have been collected, reported and presented in a publicly available database (PERD Comprehensive Iceberg Management Database, Rudkin et al., 2005). McClintock et al. (2007) provide a thorough overview of technology used for detection, tracking and deflecting icebergs. A general description regarding procedures for iceberg management is also given. It is stated that visual iceberg detections, whether from offshore facilities, supply vessels or aircraft are always best but severely limited by fog. Satellites are useful in a strategic sense but suffer from the trade off between area coverage and resolution in addition to a high risk for false alarms. While marine radars in general suffer under the influence of poor weather conditions such as rain and high waves, the introduction of coherent marine radars is reported to set a new standard for iceberg detection capabilities at Grand Banks. However, extensive field testing and detection model developments are needed in order to prove the technology. Most of the strategic and tactical iceberg detection for Grand Banks operations today is performed from fixed wing aircraft.

³ Abnormal Limit State – annual probability of exceedance shall be 10⁻⁴ or less.

Table 1. Calculated tow success (from Rudkin et al., 2005).

Category	Number of records	Percentage
Complete success	112	8%
Successful	391	27%
Acceptable	627	42%
Poor	346	23%

Table 2. Probability of success versus deflection method (after Rudkin et al., 2005).

Method	# Operations	# Successful	Percentage
Single Vessel Rope Tow	1303	1007	77%
Two Vessel Rope Tow	25	14	56%
Net Tow	45	30	67%
Propeller Wash	73	54	74%
Water Cannon Deflection	19	10	53%

Rudkin et al. (2005) developed a comprehensive methodology for evaluating the degree of success in an iceberg tow operation. By taking the various components in physical iceberg management into account and assigning numerical values to a set of key fields, each of the iceberg management operations in the PERD database were given a score between 0 and 100. If the score was above 90 the tow was considered a complete success while a score less than 55 would be considered as unsuccessful. Table 1 shows the results from an evaluation of 1500 tow operations included in the PERD database (Rudkin et al., 2005).

Rudkin et al. (2005) also investigated the correlations between the probability of success and a wide range of parameters such as:

- Iceberg size
- Iceberg shape
- Sea state
- Towing method

The results showed no significant correlations between iceberg size and probability of success. The correlation between iceberg shape and success was not distinct but indicated that it is more difficult to handle domed and wedge shaped icebergs than tabular shaped. With respect to correlation between success and sea state, the PERD database shows no general trend for towing in sea states with significant wave height, H_s , up to 5 m. For sea states with H_s between 5 m and 5.5 m there is a drop in the probability of success but this may be a consequence of a very limited amount of data in this interval. Usually, the single line towing method is used in the first attempt to move an iceberg. If this method is unsuccessful other approaches will be attempted. Due to this, the correlation between handling method and probability of success is somewhat biased. Table 2 shows the probability of success for the most recognised iceberg deflection methods. It should be noted that 87% of all operations in the database included single vessel floating tow rope, and that propeller wash and water cannon deflection usually is attempted only on minor icebergs. Details regarding the

various approaches for physical iceberg management are well documented by Crocker et al. (1998).

With respect to Probability Of Detection (POD) of icebergs, Rudkin et al. (2005) presented an overview of the detection tools applied at Grand Banks and evaluated their efficiency. It was concluded that no single instruments will provide a 100% POD but that the present practise of applying a suite of tools including satellites, aircraft, radars and visual observations ensures an acceptable POD. In the period 2000–2004, 450 icebergs entered the tactical zones at Grand Banks and only two icebergs were undiscovered until they appeared within the tactical zone. Both these icebergs were dome shaped. After ten years with oil production at Grand Banks no severe accidents caused by impact with icebergs have been reported.

5. WEST COAST OF GREENLAND-FYLLAS BANKE. Similarly to the Grand Banks, the coast offshore Greenland is recognized for the occurrence of drifting icebergs. The largest icebergs are found in the northern part of the West Greenland coast where icebergs up to 32 million tons have been observed. At the Fyllas Banke more moderate icebergs are expected with an average mass between 0.3 and 0.7 million tons and a maximum of 2.8 million tons, Mosbech et al. (2000).

Over a period of 10 weeks during the summer of 2000, Statoil carried out exploration drilling at a water depth of 1150 m offshore central west Greenland in the Fylla field. During the drilling, valuable information regarding icebergs as well as practical experience regarding iceberg management was gained. The experiences are well documented by McClintock et al. (2002). There are many similarities between iceberg management at Fylla and at Grand Banks, however, there are some additional notes from the Greenland drilling (McClintock et al., 2002):

- First, it was proved that it was possible to drill successfully at large water depth using dynamic positioning and comprehensive iceberg management services in an area subjected to an extreme number of drifting icebergs. During the ten weeks of drilling, 228 iceberg targets were tracked near the drillship. Out of these, 64 had to be physically deflected by the assisting supply vessels. Towing was successful 91% of the time and the reason for the unsuccessful cases was mainly towline slippage. Several icebergs with a mass over one million tons were successfully deflected; tow line slippage typically occurred during the towing of medium and small sized icebergs with smooth surfaces. The drill ship was forced off location on one occasion during the drilling. The cause was the approach of one unstable iceberg in poor weather and high sea conditions. Total downtime was 33 hours during the ten weeks of drilling.
- Three Norwegian supply vessels were hired for assistance during the drilling and none of these had any experience or training with respect to iceberg towing beforehand. Iceberg management experts from Canada were engaged in order to assist in iceberg handling. It is commented by McClintock et al. (2002) that all crew members picked up the deflection methods very quickly and performed extremely well. During the ten weeks, tow line fouling of the propellers occurred twice. In the first case the supply vessel had to go to shore for repair and was off site for three days.
- Despite a tow operation being considered successful, it was not always possible to tow the iceberg in the planned direction. In some events where wind, waves

and currents made it impossible to tow in the planned direction, the iceberg would typically be guided through the ice management zones.

- For detection capabilities the marine radar was identified as the main source for iceberg detection. Satellite images from Radarsat were considered useful in a strategic sense, i.e. whether to send one of the supply vessels to land for re-supply or not. However, the information from the satellite was not used for tactical decisions. Only one fixed-wing aerial reconnaissance was performed at the beginning of the programme but was generally not found to be viable due to prevailing fog and poor visibility.
- Finally, the need for reliable information regarding metocean data and in particular current data is highlighted by McClintock et al. (2002). There are examples of icebergs, initially deflected into safe areas, that returned into the safety zones and posed a threat to the drilling operations.

6. THE ARCTIC OCEAN. As a part of the International Ocean Drilling Program (IODP) a multiple vessel expedition was sent into the Arctic Ocean in August 2004 to drill and recover deeply buried sediments at the Lomonosov Ridge. A summary of the expedition is given by Moran et al. (2006) and briefly reviewed in this paper. The convoy consisted of three icebreaking vessels; Vidar Viking, Oden and Sovetskiy Soyuz. For the purpose of this expedition, Vidar Viking had been converted into a drillship, Vidar Viking (Ice-10). The other two icebreakers were used to break ice during transit and to protect the drillship during drilling. Sovetskiy Soyuz is a nuclear powered Polar icebreaker while Oden is a Polar-20 icebreaker with diesel-electric machinery. These icebreakers are considered to be amongst the most capable icebreakers in the world⁴.

The water depth at the drill sites was in the range 1100–1300 m and it was planned to use dynamic positioning during drilling. However, prior to drilling, station-keeping tests showed that it was not feasible to keep position within limits during drilling. By manual positioning it was however possible to maintain Vidar Viking within a watch circle of 50–75 m for drilling to proceed. The ice concentration was 9–10/10 with 7–8/10 consisting of hard multi-year ice. The ice floe thickness was in the range 1–3 m and drift speeds were up to 0.3 knots.

With respect to physical ice management the most powerful icebreaker would typically work in circles some distance upstream while the second icebreaker would work in circles with smaller radius somewhat closer to the drillship. This concept is shown in Figure 4. It is reported by Moran et al. (2006) that the situations where it was most difficult to keep the drillship on location were those with variations in drift directions. In such situations information regarding ice drift became crucial. In order to provide such information a number of sources were applied. Drift buoys were deployed by helicopter on to the ice floes providing real time ice drift information. Helicopter reconnaissance was also used to map the local ice conditions. To provide an overview of the ice conditions, satellite images from Radarsat were applied. Together with an onboard weather team and traditional wind forecasts, the ice management team was able to predict ice movements in a 24–48 hours window.

⁴ DNV Arctic Rules:

ICE-10: vessel intended for breaking way in 1 m thick ice on their own.

Icebreaker POLAR-20: vessel intended for icebreaking as main purpose in up to 2 m thick ice.

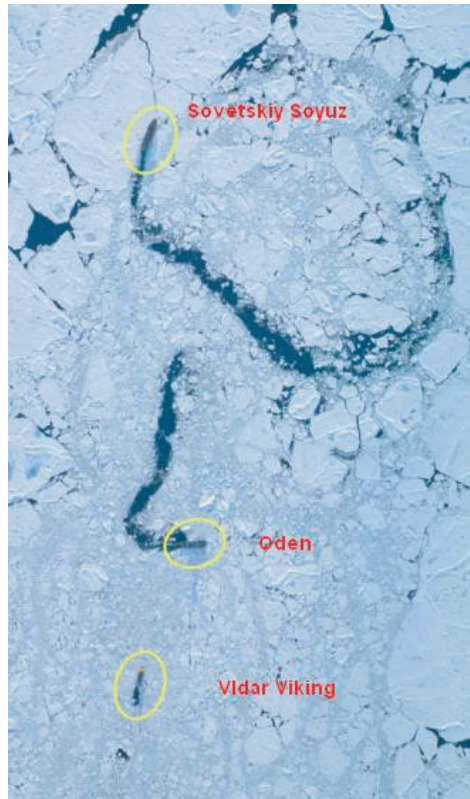


Figure 4. The expedition 302 fleet during drilling operations. Ice drift direction is from top to bottom (photo taken by Per Frejvall, ref. Moran et al., 2006).

Based on the results from the ice reconnaissance and information about the drilling activities, hands made ice alert reports which were submitted to the fleet manager. The reports included T-Time⁵ estimates. If ice management could not achieve a good ice condition window longer than the T-Time, drilling operations would be suspended. It was reported by Moran et al. (2006) that the ice alert reports served well as a tool for documenting the operations but were of limited value during critical times when rapid decision making was required. In such situations, the fleet manager relied most heavily on ice drift information and meteorological predictions. In total, during three weeks of stationary operations, drilling activities had to be suspended twice due to unmanageable ice conditions.

7. BARENTS SEA. Exploration for hydrocarbons in the Barents Sea started in the early 1980s in both the Norwegian and Russian sectors. So far there has not been any production from the part of the Barents Sea that is likely to be covered by ice or subjected to drifting icebergs. It is expected however, that the gas-condensate field Shtokmanovskoye, located in the central part of the Barents Sea, will be

⁵ T-Time was the time required to trip or recover the pipe from the hole so that the drillship would be free from the seabed and could move under heavy ice drift/ice forces.

developed in the near future. At this field, both occurrences of sea ice and icebergs (possibly at the same time) will have to be expected during operations.

During a data collection expedition in the North Eastern part of the Barents Sea, an attempt to tow an iceberg frozen into the sea ice was carried out (Stepanov et al., 2005). The iceberg with a mass slightly less than 200 000 tons was surrounded by a concentration of 10/10 slightly deformed first year sea ice approximately 0.5 m thick. First, a lead favourable for towing was identified in the vicinity of the iceberg. Secondly, the towrope was attached manually around the iceberg and the iceberg was broken free from the surrounding sea ice by an icebreaker. When the iceberg was floating freely, the tow vessel took up the slack in the towrope and the tow started. Maximum vessel speed during towing was 1.3 knots. During the tow, it appeared not to be possible to steer the tow vessel due to heavy tension in the tow line. In order to avoid entering an ice field, engines had to be stopped until new slack appeared in the tow rope. Thereafter the vessel course was changed towards the nearby lead and the slack was taken up once more. When the tow was continued, one of the branches in the tow line ruptured and the experiment stopped. The tow line rupture was partly explained by damage caused by interaction with the ice and partly by uneven loads in the two tow line branches. Two of the important lessons highlighted from the experiment were the difficulty in keeping the planned course and the risk of being trapped in the sea ice during towing.

8. PECHORA SEA. Oil production on land in the Timan-Pechora basin started in 1985 and at about the same time shipments of crude oil started in the Pechora Sea. In 2000 an offshore oil-loading facility was built at Varandey in the Pechora Sea. The terminal is operated by Lukoil and has been operational from 2002 on a year-round basis. Oil is brought to the terminal by pipelines running from several onshore fields and is loaded into shuttle tankers by a Submerged Loading Terminal (ASLT).

The shuttle tankers connect to a single loading hose which also functions as a mooring line when approaching the terminal site. In order to connect to the hose, a pick up line and pick up buoy are used. The submerged buoy is released by acoustic link and is designed to break through the ice to bring the pick up line to the surface. The water depth is 12 m. The loading hose, which penetrates through the waterline, is designed to withstand forces from the sea ice. However, at least one diesel electric icebreaker is used to break and clear the ice around the hose. The loading operation spans over three tidal cycles (34 hours) so that the ice drift direction varies through the loading operation.

In accordance to APL (2007), loading operations have been carried out successfully since 2002. The system has been used in ice up to 1.5 m thick and in air temperatures down to -32°C . The hose has been replaced twice due to damage but the damage was not caused by ice. Ongoing loading has never been terminated but sometimes it has been necessary to wait for a suitable “ice window”.

9. SAKHALIN. The first oil production offshore Sakhalin Island started in 1999 from Sakhalin 2. Later, in 2005, oil from Sakhalin 1 also came on stream. So far, the production from Sakhalin 2 has been limited to approximately six months per year due to unmanageable ice conditions during wintertime.

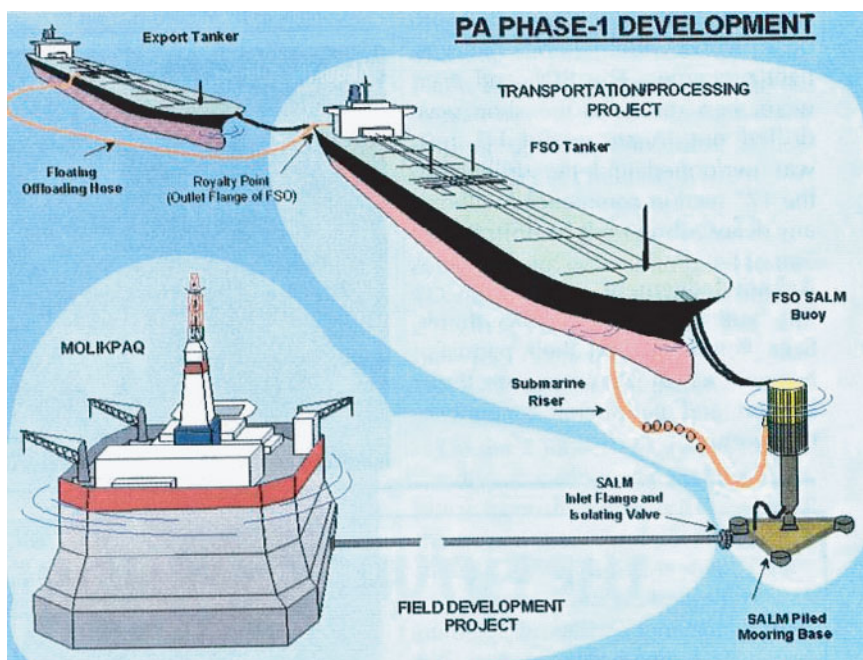


Figure 5. Vityaz Production Complex (from Offshore E-news, 2001).

In order to produce oil from the Piltun-Astokhskoye field (Sakhalin 2), the Vityaz Production complex was developed (Figure 5). The concept consists of the Molikpaq platform previously applied in the Beaufort Sea, a Single Anchor Leg Mooring (SALM) buoy and a Floating Storage and Offloading (FSO) tanker. In operation, the loading from the SALM buoy to the FSO is vulnerable to impact from ice (Keinonen, 2006), thus operations are limited within the timeframe June to December. Both in the early and in the late season, ice management operations are required. There are many similarities with respect to methodology and tools applied at Sakhalin and in the Beaufort Sea. However, with respect to T-Time it takes a relatively long time (36–48 hours) to lower the SALM buoy safely to the seafloor. With respect to efficiency and operability it is reported by Keinonen (2006) that no failure in the risk control system has occurred since the start in 1999. However, potential production time has been lost due to presence of ice.

With respect to new technology, it has been reported by Keinonen (2007) that the introduction of icebreaking support vessels, equipped with azimuth propeller systems, has significantly improved the ice management capabilities during the recent seasons.

10. NORTH CASPIAN SEA. An exploration program was first started in the North Caspian Sea by the Kazakhstan government in 1992. The most recognised field in this region, Kashagan, was discovered in 2000 and production is now estimated to begin around 2010. The water depths in the North Caspian Sea are in the range 0–10 m and large long-term fluctuation in mean sea level have been

seen over the last three decades. Short-term variations of ± 2 m in water level may occur during periods with persisting winds from south/north. Due to the somewhat special conditions, attention is given to the use of physical ice barriers and development of low draft azimuth icebreaking supply vessels.

A barge drill rig was initially designed (Evers and Kuehnlein, 2001) for all season exploration drilling in the North Caspian. In order to improve the ice clearing capability and reduce the ice loads, steel piles were driven into the soil in front of the barge. Physical barriers made of ice, gravel or steel caissons have also been used as passive ice management protection during exploration drilling in the North Caspian Sea. With respect to icebreaker support, two shallow draft Ice Breaking Supply Vessels (IBSV) were tailor-made for operations in the North Caspian (Arpiainen, 1999). In accordance with specifications, the two vessels are able to perform ice management in waters as shallow as 3 metres and in level ice up to 90 cm thick (Wagenborg, 2007). One of the challenges when working in the shallow waters is to avoid getting ice under the hull and thus get stuck. The vessels are also supposed to influence the local ridging thus contributing to development of grounded ridges shielding the drill barge from ice actions. As for most modern icebreakers, the IBSVs are equipped with azimuth thrusters.

11. DISCUSSION. It is evident that offshore operations have been, and still are, successfully conducted in almost any kind of ice regime. Spanning from ultra shallow waters of 3 m in the Caspian to depths more than 1000 m in the Arctic Basin, various types of drilling operations have been carried out. Oil production is safely carried out in the iceberg stream at Grand Banks and even the heavily ridged multi-year ice in the Beaufort Sea has been handled in a safe way.

It is important to recognise that the ice management system has been a key factor when operating in ice covered waters. Without proper ice intelligence, risk evaluation, ice breaker assistance and the possibility to escape the drilling site it would probably not have been possible to work in the strong multi-year ice in the Beaufort. It is however, also important to note some shortcomings with respect to technology when working in ice covered waters:

- The possibility of handling icebergs when frozen into the sea ice is not documented.
- No single detector is able to detect all kind of ice features. It is likely that future projects will include a wide range of tools for ice detection as illustrated in Figure 6. Satellites, airborne ice reconnaissance, marine radars, ice drift buoys and visual observations from supply vessels have already been applied. The possibility of using Unmanned Aerial Vehicles (UAVs), multi beam sonar and Autonomous Underwater Vehicles (AUVs) should be considered in the future. An important challenge connected to this is the need to develop tools for gathering, analysing and presenting all data in a quick and efficient manner.
- Use of Dynamic Positioning systems is not well documented for vessels working in the sea ice. This means that use of mooring lines will be required. Use of manual positioning should be avoided due to the high risk of human errors.

With respect to new technology, it is noted that the ability to work in ice has been significantly increased by the use of Azimuth thrusters. Such thrusters have been reported to work well in connection with icebreaker escort services for more than a



Figure 6. Illustration of a possible future physical ice intelligence system.

decade and new experience from Sakhalin and the North Caspian Sea indicates that the Azimuth equipped vessels also work efficiently when protecting drilling and loading operations.

One of the most important lessons from the various projects is that ice management systems need to be included at an early stage in the operation planning and concept evaluation. In particular, ice management systems need to be taken into account when considering whether to use a fixed structure or a structure with the ability to move off location when threatened by ice. A question arising in connection with new projects is how to quantify the effect of ice management in the design of a concept. Further work should focus on how to use historical ice management data together with environmental and structural information in a probabilistic analysis in order to ensure that the concept's integrity is kept.

12. CONCLUSIONS. The major conclusions regarding ice management are:

- Exploration and/or production drilling have been performed successfully in a wide range of Arctic conditions and at water depths ranging from a few metres to more than thousand metres.
- Comprehensive use of ice management is explained as a key factor for the success.
- Technology for iceberg handling in open water is considered as proven.
- Technology for handling icebergs frozen in the sea ice is not considered proven.

- Technology for breaking sea ice is proven for a wide range of severe conditions including multi-year ice and ice ridges. However, it is expected that there may be ice conditions more severe than the most powerful icebreakers can handle.
- Use of azimuth propeller systems on icebreakers have been seen to contribute to significant improvements in the ice breaking capability and more important for offshore operations; the ability to clear ice around a structure.
- Technology for detection and tracking of ice features will have to include a wide range of tools. Use of unmanned aeroplanes, unmanned underwater vehicles and multi beam sonar may be considered as possible future supplements to existing ice detection tools.
- It is recommended that evaluation of ice management capabilities is performed at an early stage when planning new operations and in the evaluation of new drilling and production concepts.
- Future work regarding methodology for implementation of ice management capabilities in concepts/operations is recommended.

REFERENCES

- Advanced Production and Loading (2007). Christian Mosgren, personal communication
- Arpiainen, M., Backström, M., Juurmaa, K., Wilkman, G. and Veldman, K. (1999). Development of the new icebreaking supply vessel for Northern Caspian Sea, *Proceedings of the 15th International conference on Port and Ocean Engineering under Arctic Conditions (POAC)*, Helsinki, Finland, pp. 545–551.
- Crocker, G., Wright, B., Thistle, S. and Bruneau, S. (1998). *An assessment of Current Iceberg Management Capabilities*. Report submitted to National Research Council Canada, Prepared by C-CORE and B. Wright and Associates Ltd., C-CORE Publication 98-C26.
- Evers, K.U. and Kuehnlein, W.L. (2001). Drilling Exploration in the North Caspian Sea. HSVA Newswave, The Hamburg Ship Model Basin, Newsletter. Hamburg, Germany, 2001, 6–7.
- Hibernia (2007). About Hibernia – Hibernia Ice management. Website: www.hibernia.ca/html/about_hibernia/ [cited 1 September 2007]
- Hnatiuk, J. (1983). Exploration Methods in the Canadian Arctic. *Journal of Cold Regions Science and Technology* 7, 181–193.
- Keinonen, A. (2006): Personal communication.
- Keinonen, A., Evan, M., Neville, M. and Gudmestad, O. T. (2007): Operability of an Arctic Drill Ship in Ice With and Without Ice Management, *Proceedings of the 19th annual Deep Offshore Technology International Conference & Exhibition (DOT)*, Stavanger 2007.
- McClintock, J., Bullock, T., McKenna, R., Ralph, F. and Brown, R. (2002). *Greenland Iceberg Management: Implications for Grand Banks Management Systems*. PERD/CHC Report 20–65, Report prepared by AMEC Earth & Environmental, St. John's, NL, and C-Core, St. Johns, NL., 84
- McClintock, J., McKenna, R. and Woodworth-Lynas, C. (2007). *Grand Banks Iceberg Management*. PERD/CHC Report 20–84, Report prepared by AMEC Earth & Environmental, St. John's, NL, R.F. McKenna & Associates, Wakefield, QC, and PETRA International Ltd., Cupids, NL.
- Moran, K., Backman, J. and Farrell, J.W. (2006). *Deepwater Drilling in the Arctic Ocean's permanent Sea ice*. In Backman, J. Moran, K., McInroy, D.B. Mayer, L.A. and the Expedition 302 Scientists, Proc. IODP, 302; Edinburgh (Integrated Ocean Drilling Program Management International, Inc.). doi:10.2204/iodp.proc.302.106.2006.
- Mosbech, A., Anthonen, K.L., Blyth, A., Boertmann, D., Buch, E., Cake, D., Grøndahl, L., Hansen, K.Q., Kapel, H., Nielsen, N., Von Platen, F., Potter, S. and Rasch, M. (2000). *Environmental Oil Spill Sensitivity Atlas for the West Greenland Coastal Zone*. Ministry of Environment and Energy, The Danish Energy Agency, ISBN 87-7844-183-8, URL <http://www.ens.dk>.
- Offshore E-news (2001). *ABS brings experience, flexibility to Sakhalin II project offshore Russia*. Publication of the ABS Project Development Team, Houston, USA, May 2001, Website: www.eagle.org/prodserv/offshore-eneews-3/sakhalin.html [cited 1 September 2007]

- Rudkin, P., Boldrick, C. and Barron Jr., P. (2005). *PERD Iceberg Management Database*. PERD/CHC Report 20-72, Report prepared by Provincial Aerospace Environmental Services (PAL), St. John's, NL
- Wagenborg (2007). Website: www.Wagenborg.com [cited 1 September 2007]
- Wright, B. (1999). *Evaluation of Full Scale Data for Moored Vessel Stationkeeping in Pack Ice*. PERD/CHC Report 26-200, report prepared by B. Wright & Associates Ltd.
- Wright, B. (2000). *Full Scale Experience with Kulluk Stationkeeping Operations in Pack Ice*. PERD/CHC Report 25-44 prepared by B. Wright & Associates Ltd.
- Wright, B. (2005). *Ice-related R&D Requirements for Beaufort Sea Production Systems*. PERD/CHC Report 35-60 prepared by B. Wright & Associates Ltd.

3 ICE INTELLIGENCE

3.1 General

The first component of an ice management system is detection and monitoring of ice. Before one can make decisions to mitigate the threat of ice contact with an installation, one must first be aware of the condition of ice in the region including classification details such as ice type, floe size, drift speed etc. The acquisition of detection information in a timely manner is critical as operations protocols to mitigate the risk to ensure the safety of the installation and crew are time dependent.

By studying previous Arctic operations (Chapter 2), it can be seen that the primary detection methods include satellite imagery both from optical as well as radar sensors, marine radars both on vessels and installation, visual detection from ship, helicopters, and fixed wing reconnaissance. It should be noted that 100% Probability Of Detection (POD) can never be guaranteed by any of the detection means. In future projects, it is likely that various detection means will be combined in different ways both depending on character of the project and the costs connected to the surveillance activities. There is a number of papers and reports in the public domain dealing with ice and iceberg detection. Information on the detection means can be found in e.g., McClintock et al. (2007) while Timco and Gorman (2007) presented statistics on the use of various means in icebreaker operations.

In addition to the existing ice surveillance means, there is a number of novel devices with a large potential for surveillance improvements in future projects. Examples are autonomous aeroplanes or helicopters (drones), autonomous underwater vehicles (AUVs) and multibeam sonars. With respect to the subsurface devices, a study on their feasibility in ice management operations is presented in Section 3.2.

3.2 Specifications for a subsurface ice intelligence system

OMA2009-79606

Specifications for a subsurface ice intelligence system

Kenneth Eik
 Statoilhydro

Norwegian University of Science and Technology (NTNU)
 Trondheim, Norway

Sveinung Løset

Norwegian University of Science and Technology (NTNU)
 Trondheim, Norway

ABSTRACT

In connection with offshore activities in waters exposed to sea ice and/or icebergs, ice management (IM) systems need to be applied. An ice intelligence system is one of several required elements in an IM system. This paper presents possible solutions for Subsurface Ice Intelligence Systems (SIIS). Capabilities of technology for sonars, unmanned underwater vehicles, and communication nodes are highlighted and need for further development is commented.

KEY WORDS

Ice management, ice intelligence, sonar, UUV

1. INTRODUCTION

In connection with offshore activities in waters exposed to sea ice and/or icebergs, ice management (IM) systems need to be applied. In general, IM includes all activities where the objective is to reduce or avoid actions from any kind of ice [1]. Such activity may include ice detection, tracking, forecasting, threat evaluation, ice breaking, iceberg towing etc.. An ice intelligence system is one of several required elements in an IM system. The ice intelligence system has to ensure that all information regarding ice conditions, that might influence marine operations, is collected and presented for relevant personnel in due time. For ice intelligence, typically surface scouting tools such as satellites, airborne recognizance, marine radars, drift buoys and visual observations from icebreakers have been used. All these methods may be limited by the weather conditions. SAR

images from satellites, that are unaffected by the weather, are also limited by the trade off between spatial coverage and resolution. With respect to airborne recognizance and deployment of drift buoys, there is generally some degree of risk for the personnel involved in these operations.

Considering that the ice characteristic is more distinct under water, the development of a Subsurface Ice Intelligence System (SIIS) seems to be a promising subject for future technology focus. This paper presents two possible systems for subsurface ice intelligence and describes the type of instruments that are needed and the requirements these instruments must fulfill. The proposed specifications will be relevant for water depths in the range 100 to 300 m. Existing technology has been reviewed and evaluated towards the different requirements of the SIIS. Further, a discussion regarding the feasibilities of the systems has been included. Finally, some conclusions are drawn regarding the applicability of the SIIS.

2. PROPOSALS FOR SUBSURFACE ICE

INTELLIGENCE SYSTEMS

2.1 Acoustic Fence

Both exploration and production drilling will usually involve some sort of structure or vessel, either moored or dynamic positioned at a fixed location. The structure must either be able to withstand the actions from all ice features in the area or be able to escape location if ice loads are assumed

to exceed the design criteria. Icebreakers or iceberg towing vessels may be used in order to reduce or avoid actions from the ice.

Generally, ice may approach the structure from all directions. Sudden changes in ice drift direction are generally known to be difficult to predict unless there is a strong dominance by the tidal currents. Hence, it is proposed that ice conditions are monitored in a continuous circle around the structure (Figure 1).

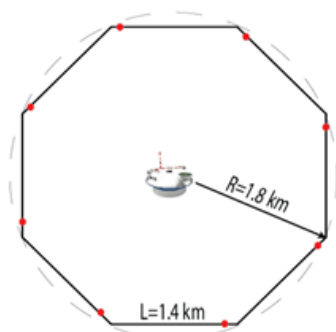


Figure 1. Configuration of eight sonars around an installation. R is the preferred distance from installation to the fence while L is the required footprint length for one sonar. Red dots indicate where the sonars should be located.

2.1.1 Multi Beam Sonars. An acoustic fence can be achieved by deploying a number of multi beam upward looking sonars arranged in a circle around the structure (Figure 1). The sonars are used to determine the distance from the sonar to the bottom of the ice surface. If Acoustic Doppler Profilers (ADPs) are installed in the same rigs as the sonars, parameters such as ice thickness, ice drift speed and ice drift direction can be monitored.

The preferred solution is to cover a continuous circle around the operating structure (Figure 1). In the Barents Sea and at the Grand Banks, the average ice drift speed is reported to be around 20 cm/s while it can be slightly higher than 1 m/s in more extreme situations (valid for both sea ice and icebergs) [2,3]. Assuming that a drilling operation will need at least 30 minutes¹ to safely disconnect and leave drilling site, ice features must be identified and managed when they are at least 1.8 km away from the structure in the extreme case.

¹ The time it will take to close down operations and prepare for disconnect will depend on a number of factors. The proposed value of 30 min should be considered as a minimum for most types of operations. Further, an ice intelligence system that not provides at least 30 minutes warning would be considered disqualified for Ice Management operations.

The required footprint length in the water line for each sonar will depend on the water depth as well as the radius in the alarm circle. For practical reasons, the required number of sonars must be kept at a minimum level. Since the sonars are indented to cover a circle, it is important that the footprint length is maximized. In order to capture the most important details in the underwater ice sheet, a resolution around 1 x 1 m within the entire footprint seems reasonable.

This requires instruments that have a significant coverage and excludes devices such as single beam sonars. By applying multi beam sonars and in addition mount them in a tilted orientation, as shown in Figure 2, a fairly long footprint may be achieved for a given water depth. However, the resolution will not be uniform within the footprint and due to this; there will be a trade off between resolution and coverage.

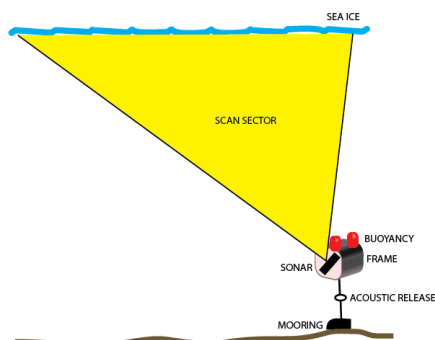


Figure 2. Illustration showing a multi beam sonar installed tilted in a frame.

To cover a circle with radius 1.8 km with eight sonars, the footprint under the ice must be at least 1.4 km long for the extreme ice drift events (Figure 1).

Table 1 shows the required length of the footprint for some other possible combinations of ice drift speeds and number of instruments. The requirements with respect to width of the footprints are however, less strict. If sonar scans are available every minute, ice drifting with speed 1 m/s will move maximum 60 m between each scan. This means that a footprint width of 60 m is sufficient to capture all ice features passing the sonar.

Table 1. Required lengths of sonar footprint [km] for various combinations of ice drift speed and number of sensors.

Number of sensors	Ice drift speed		
	20 [cm/s]	50 [cm/s]	100 [cm/s]
4	0.6	1.4	2.8
8	0.3	0.7	1.4
12	0.2	0.5	0.9

With respect to power capacity, the sonars should ideally be able to function throughout the ice season without the need of battery exchange. Battery consumption will vary significantly based on location and ice regime. However, power capacity for at least two months in operation should be a minimum requirement.

The sonars need to be connected to software in order to generate the required information. Based on the information from incoming signals, the distance from sonar to underwater ice surface may be calculated. If there is a sudden drop in the distance, an alarm must be sent from the sonar to the ice management crew at the surface. The alarm must include information about position and time for the change in depth.

2.1.2 Unmanned Underwater Vehicles (UUVs). If an alarm is sent from one of the sonars and transmitted to the surface, an Autonomous or Unmanned underwater vehicle will be convenient for further investigations. In general, it is strongly recommended to avoid having lines and cables through the ice or water surface in areas subjected to sea ice. This excludes the use of a Remotely Operated Vehicle (ROV).

It will be required that the UUV can be launched either from the moonpool in a vessel/rig or alternatively in the wake of an icebreaker. The UUV should be equipped with a sidescan sonar and multi beam sonar. In addition, the vehicle should be equipped with a video camera. The UUV should be maneuvered to the area where the ice feature was reported. In order to capture the drift speed and direction of the ice feature, the UUV should also be able to install a log or transmitter on the feature keeping track of its relative changes in position. Alternatively, routines for interpretation of data should be made in a way making it possible to identify speed and drift direction of the ice feature.

All information from sonar and camera can either be stored in the UUV or ideally be transferred in real time acoustically to its base. If data is stored in the UUV, it must be possible to download and analyze data within some few minutes.

The UUV should have power capacity for operations up to 3 hours. With an operating speed around 2 m/s, the UUV will have 2.5 hours available for inspection and then 30 minutes for transit. It should be noted that such use of the UUV will not be relevant in situations with extreme drift speeds where there only are 30 minutes available for shut down and disconnect. However, in situations with thicker ice or possibilities for multi year ice with moderate drift speeds, the UUV may be considered as a good supplement to the acoustic fence.

2.1.3 Communication and data handling. A crucial part of the SIIS will be the ability to transfer a sufficient amount of data from the sensors to the ice management team which typically will be onboard the drilling structure or an assisting icebreaker. This will most likely call for an underwater communication system ensuring that all data are transferred quickly over large distances underwater.

An ice management system will require that all necessary information is transmitted in a timely manner. A system able to transmit signals 1.8 km horizontally and up to 300 m vertically will be required. The following information must be transmitted from the sonars:

- All positions where ice thickness exceeds certain thresholds.
- Time of measurement.
- Option: Image of underwater ice surface

From the UUV, the following information must be sent to/from the surface:

- UUV position
- UUV velocity
- Steering signals to the UUV
- Options: Images from camera and images from sonars

All information needs to be transferred to a dedicated ice management software for further analyzes. In such a system, the subsurface data should be merged with other relevant data such as surface observations, satellite observations, ice drift forecasts etc.

2.2 Patrolling Unmanned Underwater Vehicles (UUVs)

A second solution, where one or two UUVs are continuously patrolling the area around or upstream the structure, should also be considered as a less comprehensive alternative to the acoustic fence.

In a situation with strong ice drift speed (1 m/s) it will be sufficient to patrol in a limited area upstream the structure (Figure 3). If two UUVs are available and dedicated to monitor ice thickness along a section with the same length as the coverage from one of the proposed sonars (1400 m), the following requirements should be sufficient to ensure efficient operations:

- Operation depth – 200 m (to avoid keels from icebergs)
- Footprint length of 400 m (corresponding to beam inclination up to $\pm 45^\circ$ at 200 m depth)
- Footprint width of 200 m (from UUV at 200 m depth)
- Resolution 1 x 1 m
- UUV speed 3 m/s or higher
- Power capacity 24 hours
- Footprint of surface must be updated with 1 minute intervals or more frequent.

Situations with very low ice drift speed are a concern for weather and ice vaning vessels because sudden changes in drift direction may occur. In a situation with ice drift speed 10 cm/s or less, the UUVs need to cover a circle with distance 180 m to the structure (Figure 4). In this case one UUV satisfying the abovementioned requirements will be sufficient.

Data from the sonar attached to the UUVs can either be processed in software built into the UUVs and transmitted as images showing the ice underwater surface, or alternatively, raw data from the UUVs have to be transmitted to the structure and analyzed from external software.

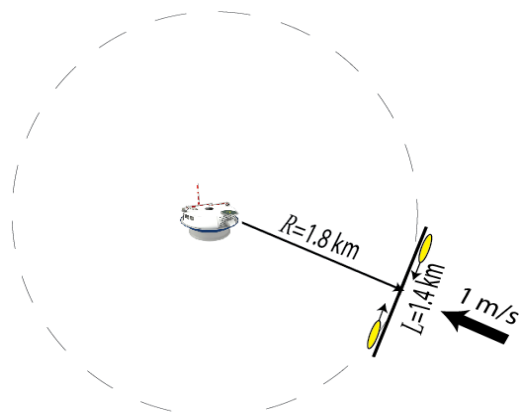


Figure 3. Illustration of a structure assisted by two UUVs collecting ice information 1.8 km upstream. The distance patrolled by the UUVs depends on the ice drift forecasts but 1.4 km is suggested in this example. The ice drift speed is 1 m/s.

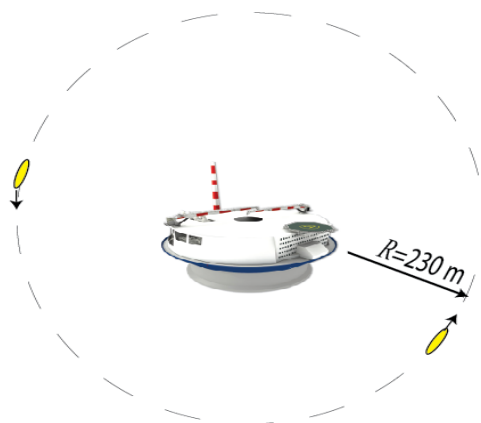


Figure 4. Illustration of a structure assisted by two UUVs collecting ice information continuously around a circle with radius 230 m. The ice drift speed is 10 cm/s or less. The structure radius is 50 m in this example.

3. TECHNOLOGY STUDY

3.1 Sonar Technology

Upward looking sonars (ULS) have been, and are, the primary tool for long term observations of ice thickness. Single beam sonars have been used successfully both in the Barents Sea [4], Sea of Othotsk [5], The Fram Strait offshore Greenland [6] and the Weddel Sea [7]. The devices have typically been deployed between 50 and 200 m below the surface with a limited horizontal footprint at the surface (less than 10 m diameter). These devices are useful in the sense that they collect important statistical data for climatic studies. However, the applicability in ice management operations is limited since only a small area is monitored. So far, there is not found documentation on real time acoustic data transfer from these sensors.

More recent multibeam sonars such as the Geoswath [8] or Kongsberg EM 2000 [9] and 3D sonar such as the Echoscope [10] have been tested under the ice and shown promising results. These types of instruments may be mounted on the seabed, in a rig or on a UUV/ROV in order to map large areas of the bottom topography of the ice surface. According to Wadhams and Doble [11], it may be possible to distinguish between first-year ice and multi-year ice by use of a multibeam sonar. It is also proven to be possible to identify cracks in the ice and refrozen leads [11].

With respect to power consumption, long term operations powered by batteries are expected to be possible in the near future. For instance, the Echoscope will be tested without

cable power supply for a longer period during the winter 2008/2009 [12].

The range and resolution of maps made by sonars, depends on several parameters. The distance from the sensor to the mapped surface as well as tilt angle for the instrument and local sound profiles, will determine the resolution in the generated maps. Today, multibeam sonars may operate at depths exceeding 1000 m. However, when the instrument is tilted, the resolution will vary depending on the distance from the surface to the instrument. There is not found any documentation on sonars capable of making ice surface maps with resolution 1 x 1 m from a water depth in the range 200 – 300 m which covers a horizontal distance of 1.4 km.

3.2 UUV Technology

A number of Autonomous Underwater Vehicles (AUVs) such as Maridan Martin 150, Autosub and Gavia have been operated successfully under the ice [9,11,13]. With respect to possibilities for implementation in an ice management system, the Gavia AUV can be considered as relevant due to its compact size. The final size of the AUV will depend on the instruments on it. During tests under the ice in the Beaufort Sea, 2007, the dimensions of the AUV Gavia were 3.1 m long and with a weight of 80 kg [11]. The Gavia AUV may operate down to 2000 m water depth and has both inertial and acoustic navigation options [14]. The cruising speed is 3 m/s while the operation range will depend on the type and number of batteries installed on the AUV.

Deployment and recovery of UUV's from vessels/installations in ice has not been documented. So far, deployment and recovery have been done in open water outside the ice edge or by personnel on the ice making a hole.

It should also be noted that during the tests in the Beaufort Sea, 2007, a line had to be attached to the Gavia AUV as the navigation systems were not sufficiently accurate to bring the AUV back to the 3 x 1 m large hole were it was deployed [11].

3.3 Underwater Acoustics

Both the performance of sonars as well as ability for underwater communication depends on the local conditions in the area. For instance, the surface range covered by a near bottom mounted sonar will depend on local sound speed profiles and bottom topography. As the sound speed profiles vary through the seasons, the performance of underwater acoustic systems will also vary correspondingly.

Hovem et al. [15] developed an acoustic propagation model which based on sound speed profiles, bathymetry and a geoacoustic model of the bottom, calculates the acoustic fields. The model was used to produce acoustic rays for

different seasons in the Barents Sea and the Norwegian Sea [15] and the results indicate that a direct transmission of 1.8 km horizontally and 300 m vertically may be possible. However, it should be emphasized that seasonal changes and local variations in the sound speed profile may significantly affect the coverage in range and depth both with respect to the sonars as well as data transfer.

With respect to absorption, the damping should be less than one dB/km conditional the frequency is in the range 10 – 100 kHz [15].

With respect to data transmission under water, there may be alternative ways to solve this than with direct transmission. It is worth mentioning the ongoing research projects, NNN-UTS, in Norway [16]. This project investigates the possibility for developing a comprehensive underwater network for simple and robust subsurface data transfer. The network is intended to be based on a number of seabed mounted nodes that transfer information over distances up to 5 km.

4. DISCUSSION

There seems to be a fairly good match between some of the requirements in the proposed systems for subsurface ice intelligence and specifications for sonars and UUVs in the open market. Multi beam sonars and UUVs with the ability to work under the ice exist but have so far not been used in ice management operations. Successful testing of deployment and recovery from a vessel or installation in ice has so far not been documented.

There is a gap between the required and documented skills in present sonar technology regarding resolution and horizontal coverage. If the grid resolution is too coarse, there is a risk for ice features drifting unnoticed through the "fence". If the horizontal coverage is insufficient, it will not be possible to provide a continuous "fence" around a structure. This problem could be solved by applying a large number of sensors but this again is considered to be impractical and with no value for real life operations. From a practical point of view, approximately 10 sensors is considered as the maximum in a SIIS for a permanent installation while 4 sensors is considered to be maximum for operations like exploration drilling.

An absolute requirement for successful use of sonars and UUVs in ice management operations is that the systems are robust and easy to handle. If deployment/recovery/data transfer is complicated or time consuming the instruments will be more of a disadvantage than a help.

There are presently no documented available solutions for real time, un-cabled transfer of sonar and UUV information under the ice. The use of one or several communication nodes at the seabed may be promising but thorough testing will be required

prior to development of ice management SIIS. It must also be taken into account that drilling operations may generate significant noise that may complicate subsurface communication.

The use of a Subsurface Ice Intelligence System should only be considered as a supplement to existing systems for ice intelligence. Patrolling icebreakers, helicopters, airplanes and satellite will still be required in order to monitor a sufficiently large area. A possible full ice intelligence system is illustrated in Figure 5.

Finally, it must be clarified whether or not there actually is a need for a subsurface ice intelligence system. Present solutions using a number of surface sensors combined with visual observations seem to ensure a sufficient level of safety on existing installations. From the last two decades there have not been reported any damages from undiscovered ice features.² However, in new areas such as the Northern Beaufort Sea, the North East coast of Greenland, the Chukchi Sea and so on, there is potential for discovering both icebergs and multi-year ice embedded in first-year ice. It seems evident that technology for creating maps of the underside of the ice identifying both multi-year ice and icebergs will contribute to increased operational safety.



Figure 5. Illustration of a possible future ice intelligence system.

² There have been reported several incidents between multi-year ice and vessels in transit but in this study only oil and gas exploration/exploitation have been considered.

5. CONCLUSIONS AND RECOMMENDATIONS

Two Subsurface Ice Intelligence Systems have been presented including requirements for components such as multi beam sonars, UUVs and communication nodes.

Existing technology matches some of the requirements in the proposed systems, but not all. In particular, requirements with respect to both range and resolution are yet not met. Thorough testing and further development with respect to deployment/recovery solutions and data transfer is required.

Use of a system for subsurface ice intelligence that is robust and easy to operate is considered to contribute to increased safety for oil and gas production in waters subjected to severe ice conditions.

It is recommended that further work focuses on establishing technology useful for ice data collection. When solutions have proven to be robust and efficient for such tasks, the next step would be to consider this technology for ice management operations.

6. REFERENCES

- [1] Eik, Kenneth, 2008, "Review of Experiences within Ice and Iceberg Management", *The Journal of Navigation*, Vol. 61, No. 4, October 2008, pp. 557 – 572.
- [2] Spring, W., 1994, "Ice Data Acquisition Summary Report", Mobil Research and Development Corporation, Texas, US.
- [3] Bruneau, S. E., 2007, "Icebergs of Newfoundland and Labrador – Frequently asked questions with short answers and pointers", URL: www.worldplay.com/tourism/icebergs, cited Dec. 2008.
- [4] Abrahamsen, E. P., Østerhus, S. and Gammelsrød, T., 2006, "Ice draft and current measurements from the north-western Barents Sea, 1993-96", *Polar Research* Vol. 1, 2006, Blackwell Publishing Ltd., Oxford, UK, 2006.
- [5] ASL Environmental Science, 2008, "Ice studies - 1996 to 2003 – Sakhalin Island, Russia", <http://www.aslenv.com/sakhalin001.htm>, cited Dec. 2008.
- [6] Østerhus, S. and Widell, K., "Fram Strait – Sea Ice and Freshwater Fluxes, 2008," Nansen Environmental Research Centre, www.nersc.no/~torel/WSOct2003/Talks/Svein_BCCR2003Freshwater.pdf, cited Dec. 2008.
- [7] Harms, S., Fahrbach, E. and Strass, V. H., 2001, "Sea Ice transport in the Weddel Sea, *Journal of Geophysical Research*, Vol. 106, No. C5, pp. 9057-9073.

[8] GeoAcoustics, 2008, "GeoSwath ROV/AUV Swath Bathymetry with co-reisterred Side Scan for Survey ROV's & AUV's, GeoAcoustics specification sheet, <http://www.geoacoustics.com/specifications.htm#GeoSwath> , cited Dec. 2008.

[9] Wadhams, P., Wilkinson, J. P. and McPhail, S. D., 2006, "A New View of the Underside of Arctic Sea Ice", Geophys. Res. Lett., 33, L04501, doi:10.1029/2005GL025131.

[10] CodaOctopus, "Real-time 3D Acoustic Imaging", CodaOctopus technical specification, http://www.codaoctopus.com/3d_ac_im/index.asp# , cited Dec. 2008.

[11] Wadhams, P. and Doble, M. J., 2008, "Digital terrain mapping of the underside of sea ice from a small AUV", Geophysical Research letters, Vol. 35, L01501, doi: 10.1029/2007GL031921.

[12] Kvingedal, B., 2008, personal communication.

[13] Wadhams, P., Wilkinson, P. J. and Kaletzky, A., 2004, "Sidescan sonar imagery of the winter marginal ice zone obtained from an AUV", J. Atmos. Oceanic Technol., 21, pp. 1462-1470.

[14] Hafmynd, "Gavia – The Great Northern Diver", <http://www.gavia.is/index.html> , cited Dec. 2008.

[15] Hovem, J. M., Shefeng, Y., Xueshan, B. and Hefeng, D., 2008, "Modelling Underwater Communication Links", Sensor technologies and Applications, 2008, SENSORCOMM'08. Second International Conference on, Cap Esterel, France, pp. 679-686.

[16] Forskningsrådet, 2007, "Lydsignaler på dypet", Forskningsrådet newsletter 2, http://www.forskningsradet.no/servlet/Satellite?c=GenerellArtikkel&cid=1182237399736&p=1092128011667&pagename=verdict%2FGenerellArtikkel%2FVis_i_dette_menypunkt&site=verdict , cited Dec. 2008.

4 EFFICIENCY OF ICEBERG MANAGEMENT

4.1 Iceberg drift

4.1.1 Numerical ice drift modelling



Contents lists available at ScienceDirect

Cold Regions Science and Technology

journal homepage: www.elsevier.com/locate/coldregions

Iceberg drift modelling and validation of applied metocean hindcast data

Kenneth Eik*

Norwegian University of Science and Technology, Norway
 StatoilHydro, Trondheim, Norway

ARTICLE INFO

Article history:

Received 5 November 2008

Accepted 21 February 2009

Keywords:

Iceberg drift

Hindcast validation

Barents Sea

ABSTRACT

An iceberg drift model covering the Barents and Kara Seas has been developed. The skills of the model relies both on the ability to describe physical actions from the environment on the icebergs and the accuracy of the applied metocean variables (wind, waves and currents). Experiences from the East Coast of Canada show that iceberg modelling may work reasonably well and indicate that iceberg drift models are able to fulfil both of the above mentioned requirements. By applying similar models in other regions, it may be assumed that wind, waves and currents affect the iceberg in a similar way as at the East Coast of Canada. However, the reliability of available metocean data sources will vary significantly from region to region. Due to this, a study with the objective to evaluate the quality of the underlying metocean models has been performed.

A significant amount of recorded wind, wave and current data from various regions in the Barents Sea have been applied in comparisons with hindcast data from selected atmospheric and oceanographic models. Results show that the quality of wind and wave data applied by the iceberg drift model is very good. Regarding current velocity, there is a poor match between data from the applied oceanographic model and measurements. A method for improving the current magnitude has been introduced.

The relative importance of winds, waves and currents on iceberg drift has also been investigated. In general, currents are most important for iceberg drift. However, in open waters, the wave drift may become the most important forcing. The presented iceberg drift model is considered to provide good results in situations with strong winds (and waves) and low currents while situations with low winds will give less reliable results. It is concluded that the quality of incorporated metocean data in any iceberg drift model need to be documented in order to fully understand possible limitations in iceberg drift simulations. Further work should focus on improvements in oceanographic modelling in order to establish a more reliable oceanographic hindcast for the Barents Sea.

© 2009 Elsevier B.V. All rights reserved.

1. Introduction

Searching for oil and gas in regions infested by sea ice and icebergs has been ongoing for several decades. Considering the increasing price for hydrocarbons during the recent years and a suggestion by the US Geological Survey that 25% of the remaining hydrocarbon resources in the world are located in the arctic, a strong increase in arctic offshore activities must be expected.

As offshore activities are moving northwards the presence of icebergs in some areas will affect both designs of new installations as well as plans for marine operations. Knowledge regarding frequency and characteristics of icebergs will be crucial in order to ensure safe and efficient operations. During the recent decades, a number of

iceberg drift models have been presented for various regions and one of these models is presently used operationally with great success offshore the East Coast of Canada (Kubat et al., 2005). However, common for most of the published models, is an insufficient validation of the underlying atmospheric and oceanographic model skills. The validations are typically limited to some few comparisons between iceberg drift trajectories from the model and from physical recordings. In order to get the proper understanding regarding why (or why not) the iceberg drift model gives a good description of the physical iceberg drift, it is proposed to perform validation studies of the oceanographic and atmospheric models that provide input to the iceberg drift model. The validations include comparisons between modelled and measured metocean data both over large geographical areas as well as over a relatively long time period.

This paper presents an iceberg drift model valid for the Barents Sea (Fig. 1) and the basic metocean models that it is based on. The objective has been to establish tools to evaluate model quality both with respect to directionality as well as strength in wind, current

* Fax: +47 73 59 70 21.

E-mail address: kenjo@statoilhydro.com.

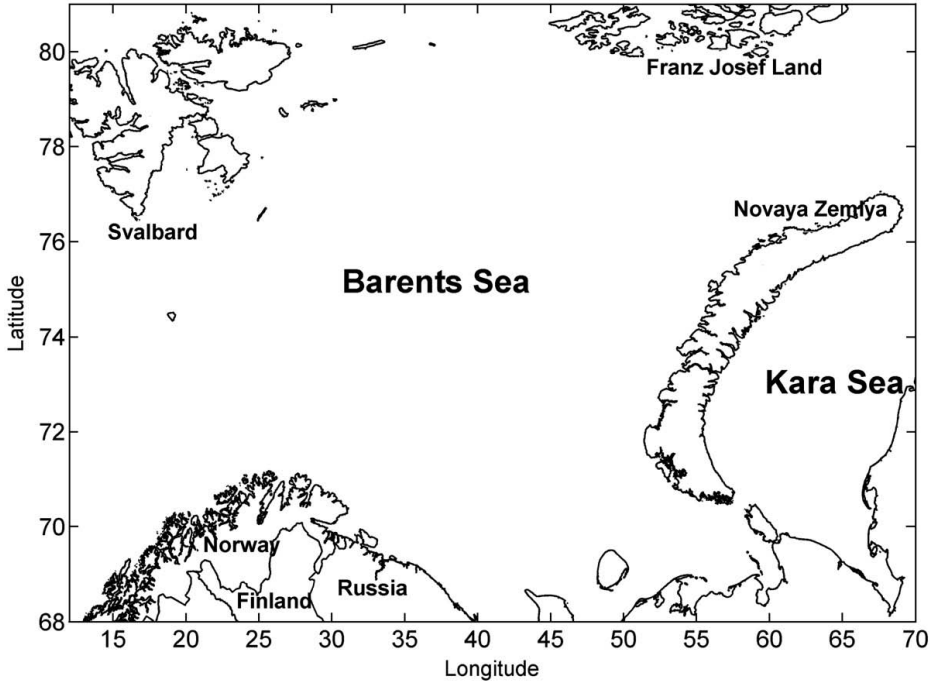


Fig. 1. Map showing the region covered by the iceberg drift model.

and waves. A methodology for improving current data has also been introduced. Finally, a comparison between iceberg drift trajectories from model and from physical recordings has been included.

The model evaluations are followed by a discussion regarding results and the methodology that has been applied. Conclusions are drawn based on the results and recommendations for future work are highlighted.

2. Iceberg drift model

The iceberg drift model presented in this paper is basically an update version of the iceberg drift model presented by Johannessen et al. (1999).

2.1. Momentum balance

To find the movement of an iceberg in an initially known position, we integrate the speed that the iceberg is moving with. To find the speed we integrate the acceleration given by Newton's 2. law:

$$m \frac{d\mathbf{V}_i}{dt} = -m\mathbf{f}\mathbf{k} \times \mathbf{V}_i + \mathbf{F}_a + \mathbf{F}_w + \mathbf{F}_{wd} + \mathbf{F}_{si} + \mathbf{F}_p \quad (1)$$

where $m = m_0(1 + C_m)$ and m_0 is the physical mass and C_m is the coefficient of added mass. \mathbf{V}_i is the local velocity of the iceberg, $-\mathbf{f}\mathbf{k} \times \mathbf{V}_i$ is the Coriolis parameter and k is the unit vector in vertical direction. Further, $\mathbf{F}_{a,w}$ is the air and water form drag, respectively. \mathbf{F}_{wd} is the

mean wave drift force, \mathbf{F}_{si} is the sea-ice drag and \mathbf{F}_p is the horizontal gradient force exerted by the water on the volume that the iceberg displaces.

2.2. Numerical integration

The momentum balance of the iceberg is given by Eq. (1). On the basis of Eq. (1) the iceberg drift track $x_i(t)$ is determined by solving the two following coupled differential equations:

$$\frac{dx_i}{dt} = (\mathbf{V}_i - \mathbf{V}_w) + \mathbf{V}_w \quad (2)$$

$$m \left(\frac{d(\mathbf{V}_i - \mathbf{V}_w)}{dt} \right) = -m\mathbf{f}\mathbf{k} \times (\mathbf{V}_i - \mathbf{V}_w) + \mathbf{F}_a + \mathbf{F}_{res} + \mathbf{F}_{tc} + \mathbf{F}_{wd} + \mathbf{F}_{si} \quad (3)$$

with given initial conditions, i.e. start position and start velocity. Note that all drag forces on the right-hand side of Eq. (3) are expressed as functions of relative velocities and that the difference between iceberg and water velocity is considered as the unknown variable. F_{res} is the drag force from residual (weekly averaged) current while F_{tc} is the drag force from tidal current. Further, the water velocity V_w is found by adding the residual current, V_{res} and tidal current, V_{tc} .

Eqs. (2) and (3) are decomposed into two directions, north-south and east-west, and that gives a system of four equations with four unknown variables. The system is solved with the Matlab ODE15S solver (The Mathworks, 2008). This function is called with intervals equal to a time step until specified simulation time is reached.

Table 1
Metocean models included in the iceberg drift model.

Model	Parameters	Sampling	Name	Period	Reference
Coupled ice/oceanographic model	Current velocity Water temperature Salinity Ice velocity Ice thickness Ice concentration Sea surface height	1 week	NERSC Barents Sea model	1987–1992	Keghouche et al. (2007)
Tidal model	Tidal surface elevation Tidal current velocities	Flexible	Tidal model	NA	Gjevik et al. (1994)
Coupled wave/atmospheric model	Wind velocity Wave heights Wave periods Wave direction	6 h	Winch model	1955–2006	Reistad and Iden (1998)

Selection of time step is flexible but usually 2 h are considered adequate. The initial iceberg velocity is set equal to the residual current at the initial iceberg position.

Wind and current forces are described as drag forces and expressions are found in Bigg et al. (1997). Mean wave drift force depends on the icebergs capability to generate waves. Potential theory has been applied in the iceberg drift model. The total fluid velocity potential is written as the sum of encountered and diffracted

potential. This approach is justified by making the following assumptions:

- Iceberg velocity and oscillations are small so radiation effects can be neglected.
- Wavelengths are small compared to the iceberg.
- Iceberg walls are vertical so all the encountered waves are reflected.
- Viscous effects are neglected.

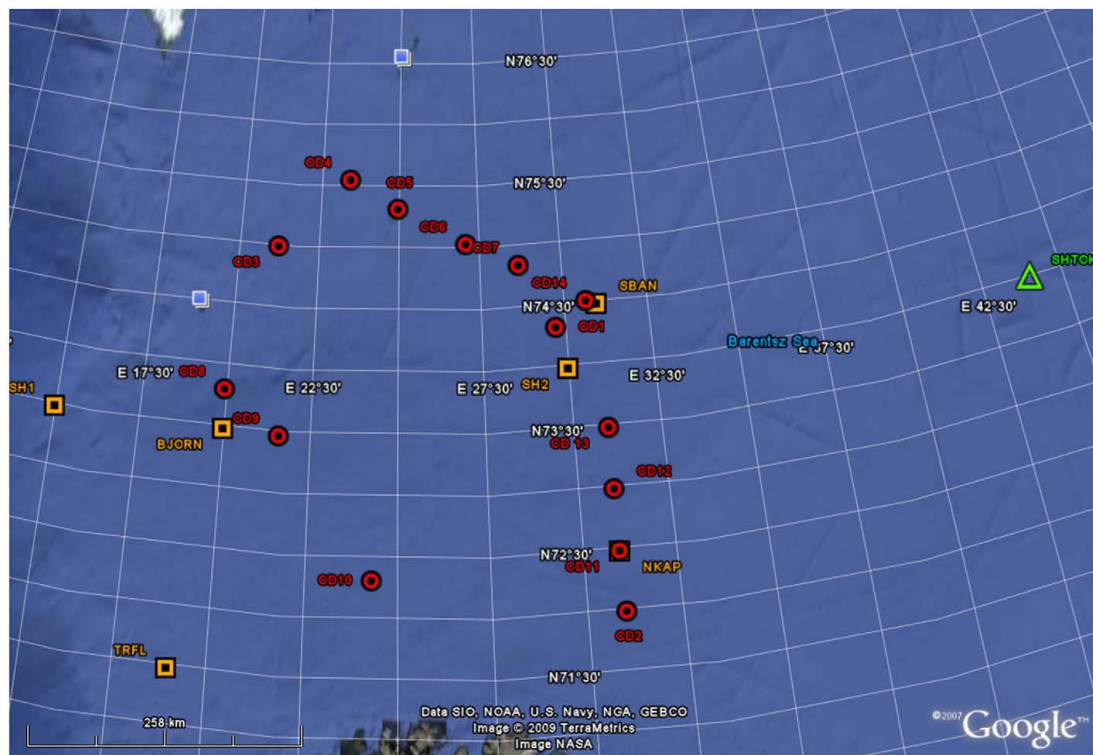
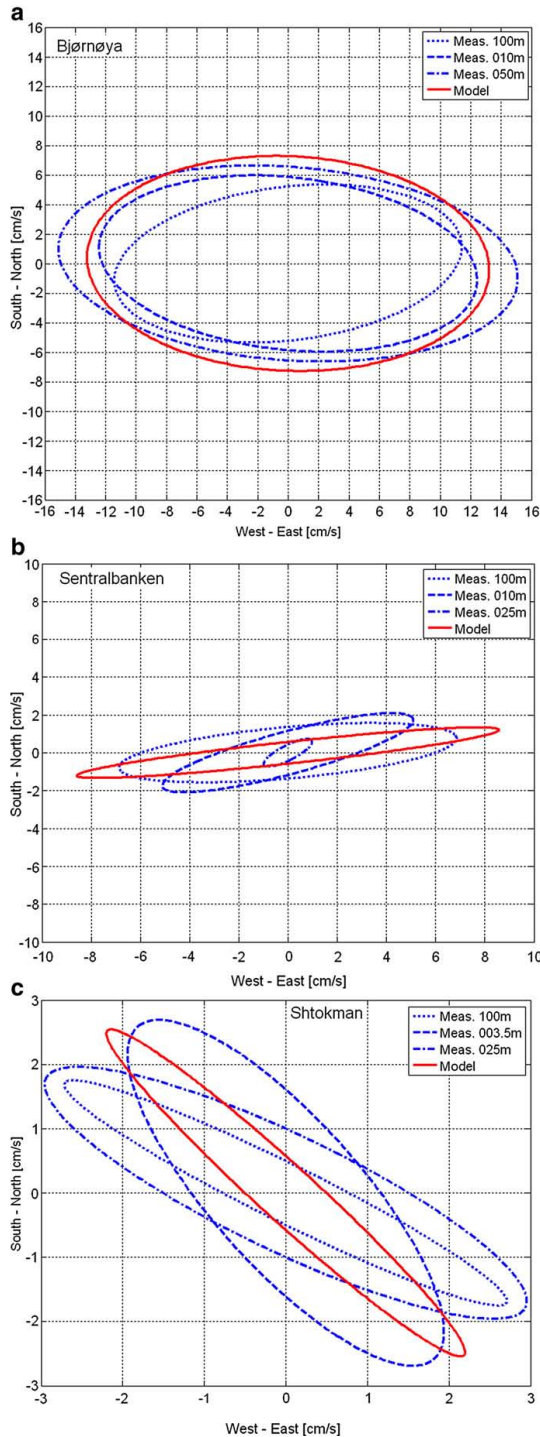


Fig. 2. Map showing locations for current, wave and wind recordings in the Barents Sea. Current recordings are marked with red circles while wind and wave recordings are marked with orange squares. Wind, wave and current recordings are available from the Shtokman location (green triangle). (For interpretation of the references to color in this figure legend, the reader is referred to the web version of this article.)



In order to take into account, that not all these assumptions are perfectly fulfilled, the wave drift force is multiplied with a wave drift coefficient, C_w . This factor will in general depend on ratios between parameters such as iceberg characteristic length, iceberg draft, wave length and water depth (Isaacson, 1988). In the present iceberg drift model, a constant value has been applied for C_w . Expressions for all forces in the model are presented in Appendix A.

Expression for sea-ice loads on iceberg is based on recommendations from Lichey and Hellmer (2001). In general, in moderate ice concentrations, the sea-ice force is considered as a drag-type force where the relative velocity between iceberg drift speed and sea-ice drift speed is applied. For high ice concentrations (more than 90%) combined with sufficiently thick ice, the iceberg is locked into the sea ice and follows the sea-ice drift. Forces from waves and sea ice are not allowed to act simultaneously. For ice concentrations less than 15%, force from sea ice is set to zero. For ice concentrations up to 40%, sea ice force is included only if there are no waves. For ice concentrations above 40%, wave drift forces are omitted. All expressions including recommended values for all required parameters are presented in Appendix A.

3. Data sources

3.1. Model data

A summary of the metocean data models that have been used to generate input to the iceberg drift model are given in Table 1. More detailed information on the models are presented in Sections 3.1.1–3.1.3.

3.1.1. Coupled ice and oceanographic model

Presently, several ice and oceanographic models covering the Barents and Kara Seas have been established by international recognised institutes such as the Nansen Environmental and Remote Sensing Center (NERSC), the Arctic and Antarctic Research Institute (AARI) and the Norwegian Meteorological Institute (met.no). However, none of these models have been used to generate a complete long term hindcast archive which is required by the iceberg drift model. Due to this, NERSC was contracted by StatoilHydro in 2006 in order to establish an ice/ocean hindcast archive covering the period 1987 to 1992 continuously. The NERSC Barents Sea model was used to generate weekly averaged values for current at 3, 10, 50 and 100 m depths and sea ice with a grid resolution of 10 km.

The ocean velocities provided by NERSC are based on a model system consisting of an improved version of the Hybrid Coordinate Ocean Circulation Model (HYCOM) coupled to a sea-ice model based on Elastic Visco Plastic rheology. The model system use ERA-40 atmospheric forcing from the European Center for Medium range Weather Forecasting (ECMWF) and boundary conditions given by the TOPAZ forecasting system for the Atlantic and Arctic Oceans. Details and references on the models are found in Keshouche et al. (2007).

In the iceberg drift simulation model, the currents from the four levels are averaged over the depth of the iceberg.

3.1.2. Tidal model

The tidal potential is usually described by a sum of several periodic elements and may be used for predictions of tidal currents. The tidal

Fig. 3. Tidal ellipses representing M2 from Bjørnøya (a), Sentralbanken (b) and Shtokman (c). The model currents (red circles) are averaged over the entire water column at the location. (For interpretation of the references to color in this figure legend, the reader is referred to the web version of this article.)

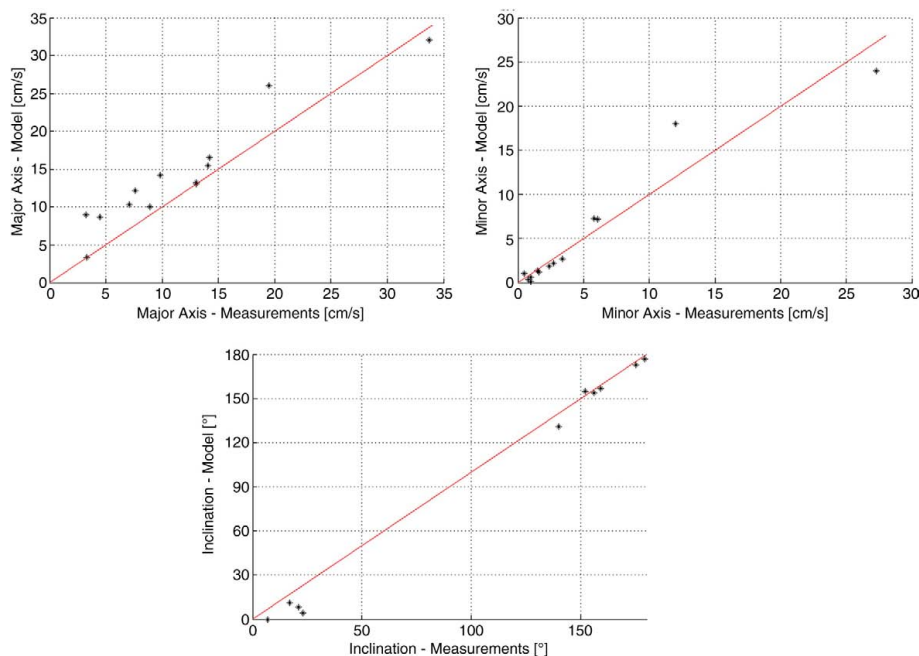


Fig. 4. Comparisons of tidal constituent M2 from tidal current model (Gjevik and Straume, 1998) and measurements (Oceanor, 1998). M2 is specified by magnitude of major axis (upper left), minor axis (upper right) and inclination (lower left). Each dot corresponds to data from an oceanographic station (ref. Appendix B).

model used in the iceberg drift model is described in Gjevik et al. (1994) and provides information on four of the most common periodic constituents; M2, N2, S2 and K1. Both M2 and N2 are due to gravity forces from the moon while S2 is caused by the sun. Forcing from these three constituents is repeated twice per day. K1 is caused by both the sun and the moon and has a diurnal period. In the iceberg drift model, tidal currents, which have been generated from these constituents, have been superposed on the weekly averaged currents from the oceanographic model (Keghouche et al., 2007). The tidal currents in the iceberg drift model are averaged over the entire water depth.

3.1.3. Coupled wave and atmospheric model

In similarity to the oceanographic models, several meteorological and wave models have been developed for all or parts of the Barents and Kara Seas. As input to the iceberg drift model, it was decided to use the Winch hindcast archive developed by the Norwegian Meteorological Institute (Reistad and Iden, 1998). The wind/wave hindcast archive were selected as it provides a uniquely long data set (1955–2006) that covers both the Barents and the Kara Seas with a grid resolution of $1.5^{\circ} \times 0.5^{\circ}$ East/West and North/South respectively. Sampling interval is 6 h. A second reason for selecting this hindcast to the iceberg drift model was that historical comparisons with data from this model and wind/wave recordings from the North Sea and the Norwegian Sea have documented fairly good quality on the model data.

With respect to winds, the model calculates geostrophic winds based on gridded mean sea level pressure data. A two layered boundary layer model is applied to derive 10 m wind based on the geostrophic wind. Surface roughness over sea has been applied for the entire model domain thus reliability of winds over sea ice and land is reduced compared to winds over open water.

With respect to waves, the Winch model is a deep water discrete wave prediction model developed by Oceanweather Inc. and run by the meteorological institute. The propagation scheme is a downstream advection scheme. The wave spectrum is divided into 24 direction bands with 15° bandwidth and 15 frequency bands ranging from 0.04 Hz to 0.24 Hz. The parametric wave growth is derived from empirical fetch limited growth data and forces the wind sea to conform to a reference spectrum of the JONSWAP type. The fetch will depend on the ice conditions thus monthly average ice borders have been applied in the model. If ice concentration in a grid point is less than 40% the grid point is treated as open water in the wave model. If the ice concentration is higher than 40% the wave energy has been set to zero.

Details on the model and references on the Winch model are found in Reistad and Iden (1998).

Table 2
Validation studies and intention with study.

Comparison	Purpose
1 Time series	Indicates differences in magnitude and whether physical variations have been captured by the model
2 Scatter plot of current magnitudes	Shows potential bias in model data and visualise uncertainties in the model
3 Quantile–Quantile (QQ) plots	Shows potential bias in model data. Compares values at different statistical levels (quantiles) from model and measurements.
4 Directional distributions	Shows potential bias in directionality in model data
5 Trajectories	Illustrates the skills of the model with respect to use in an iceberg drift model.

3.2. Measured data

3.2.1. Current recordings

Measured currents from water depths 3, 10, 25, 50 and 100 m from 12 different sites in the Norwegian part of the Barents Sea and from the Shtokman site in the Russian sector of the Barents Sea have been used in the validation of model data. The locations are presented in the map shown in Fig. 2. The recordings from the Norwegian sector come from an initiative by the Norwegian Petroleum Directorate (NPD) in the eighties and are reported by Oceanor (1998). Recordings from the Shtokman field were carried out by Oceanor in the period 1992–1997 and were reported by Kleiven and Meisingset (2003). Presently, recordings from the Shtokman field are not publicly available. Time spans of Barents Sea current measurements applied in this study are presented in Appendix B.

3.3. Wind and wave recordings

As for the currents, the majority of available wind and wave recordings are available thanks to the NPD initiative in the eighties. Both various buoys as well as meteorological vessels (AMI and Endre Dyrøy) were used in the data acquisition programme. In this study, recordings from Tromsøflaket, Bjørnøya, Nordkappbanken and Sentralbanken have been applied (Oceanor, 1998). In addition, wind and wave recordings from buoys at Shtokman have been applied (Kleiven and Meisingset, 2003). Finally, wind and wave data have been collected at two locations from 2007 after an initiative by StatoilHydro. These data are also applied in this study, despite that data yet not have been reported. All locations are shown in Fig. 2 while time spans for the recordings are presented in Appendix B.

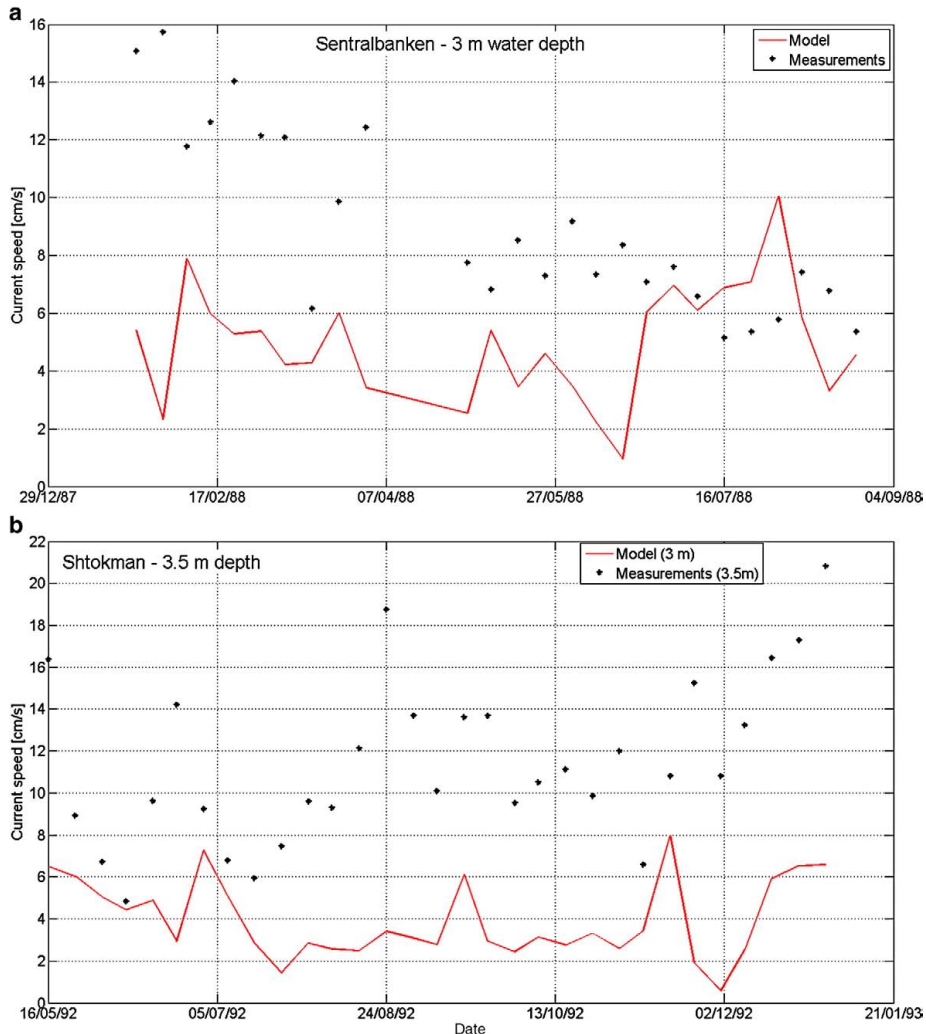


Fig. 5. Time series of measured and model current speed from Sentralbanken (a and c) and from Shtokman (b and d) at 3 and 100 m depth respectively.

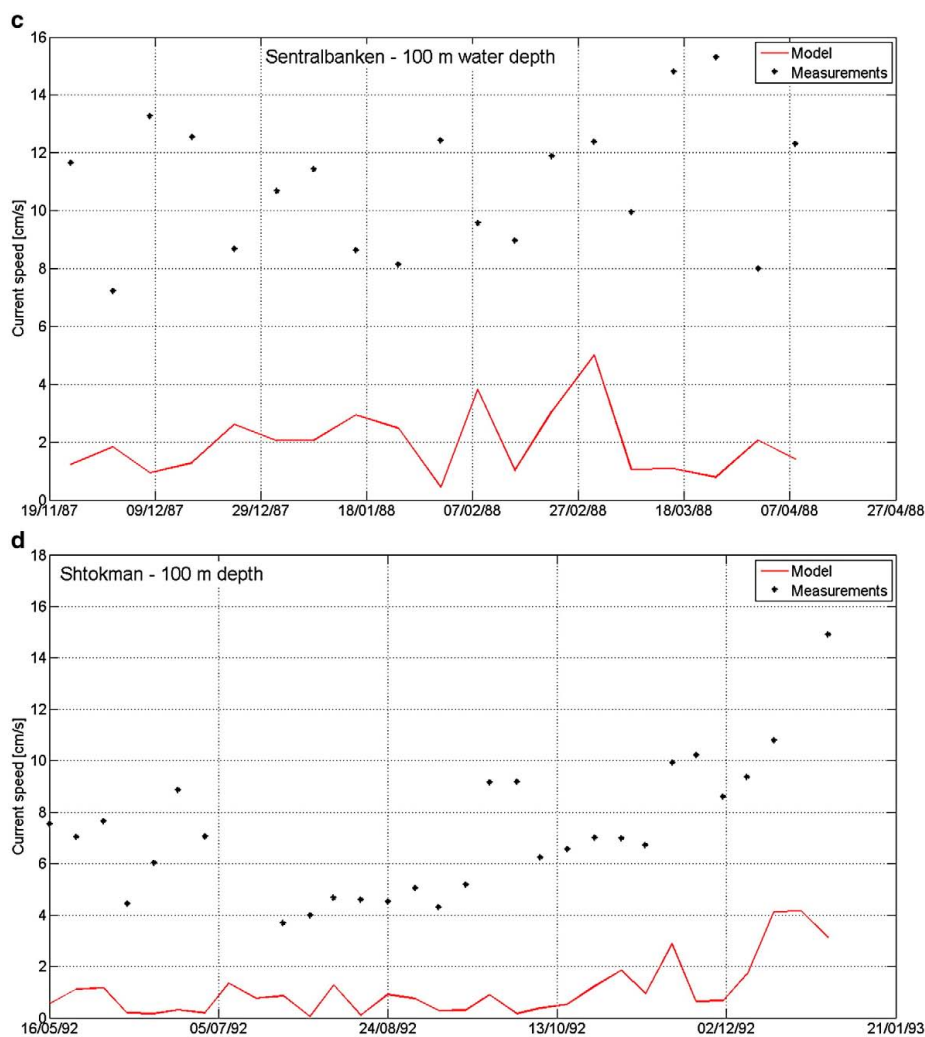


Fig. 5 (continued).

3.3.1. Iceberg trajectories

During the Ice Data Acquisition Program (IDAP) 1988–1994, totally 53 drift buoys were deployed on icebergs (Spring, 1994). Data from these buoys were filtered and smoothed to hourly sampled time series. Of these trajectories, 26 have been stored in the StatoilHydro database and are applied in these studies. It should be noted however, that a number of these trajectories show that a large number of the icebergs were grounded for long periods thus not particularly suited for validation of the iceberg drift model. Other iceberg trajectories have been excluded from the study due to lack of knowledge regarding the iceberg size and geometry. Remaining icebergs (7) have been used in comparisons with model trajectories.

Two iceberg trajectories were also recorded close to Franz Josef Land and Novaya Zemlya respectively by the Arctic and Antarctic Research Institute (AARI) in 2005 (Dmitriev and Nesterov, 2007). Both these trajectories have been included in the validation studies.

4. Validation studies

4.1. Oceanographic validations

As the currents applied in the iceberg drift model come from two different models, the validation is split into two different types of analyses. With respect to tidal currents, comparisons of four constituents (M2, N2, S2 and K1) from tidal model and measurements are carried out. With respect to weekly averaged currents, simultaneous currents from measurements and oceanographic model are compared both with respect to magnitude and directionality.

4.1.1. Tidal currents

Harmonic analyses have been performed with data from all oceanographic stations listed in Appendix B. The Harmonic analyses have been done in accordance with software and recommendations published by Foreman (1978). In total, 60 constituents are estimated

by the harmonic analyses. However, only four constituents are included in the tidal model, thus only M2, N2, S2 and K1 have been included in the validations. It has previously been reported that M2 and K1 are the major diurnal and semidiurnal constituents in the Barents Sea (Gjevik and Straume, 1998). With respect to magnitude of

the major axis in the tidal ellipses, the harmonic analyses showed that M2 in general is approximately twice as high as any of S2, N2 and K1. Due to this, results only for M2 are presented in this paper. However, it should be noted that results for the other constituents show similar trends as for M2.

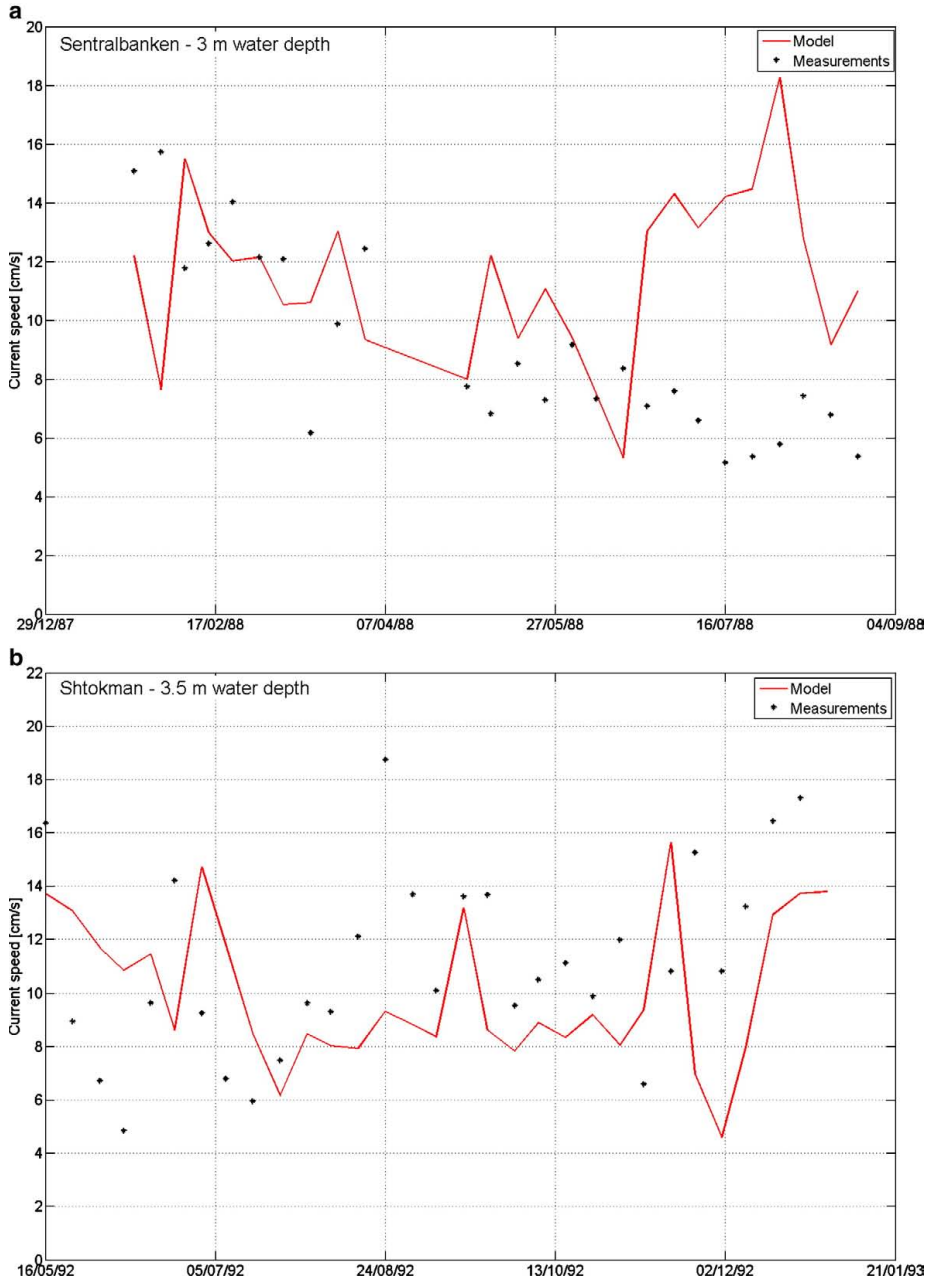


Fig. 6. Time series of measured and modified model current speed from Sentralbanken (a and c) and from Shtokman (b and d) at 3 and 100 m depth respectively.

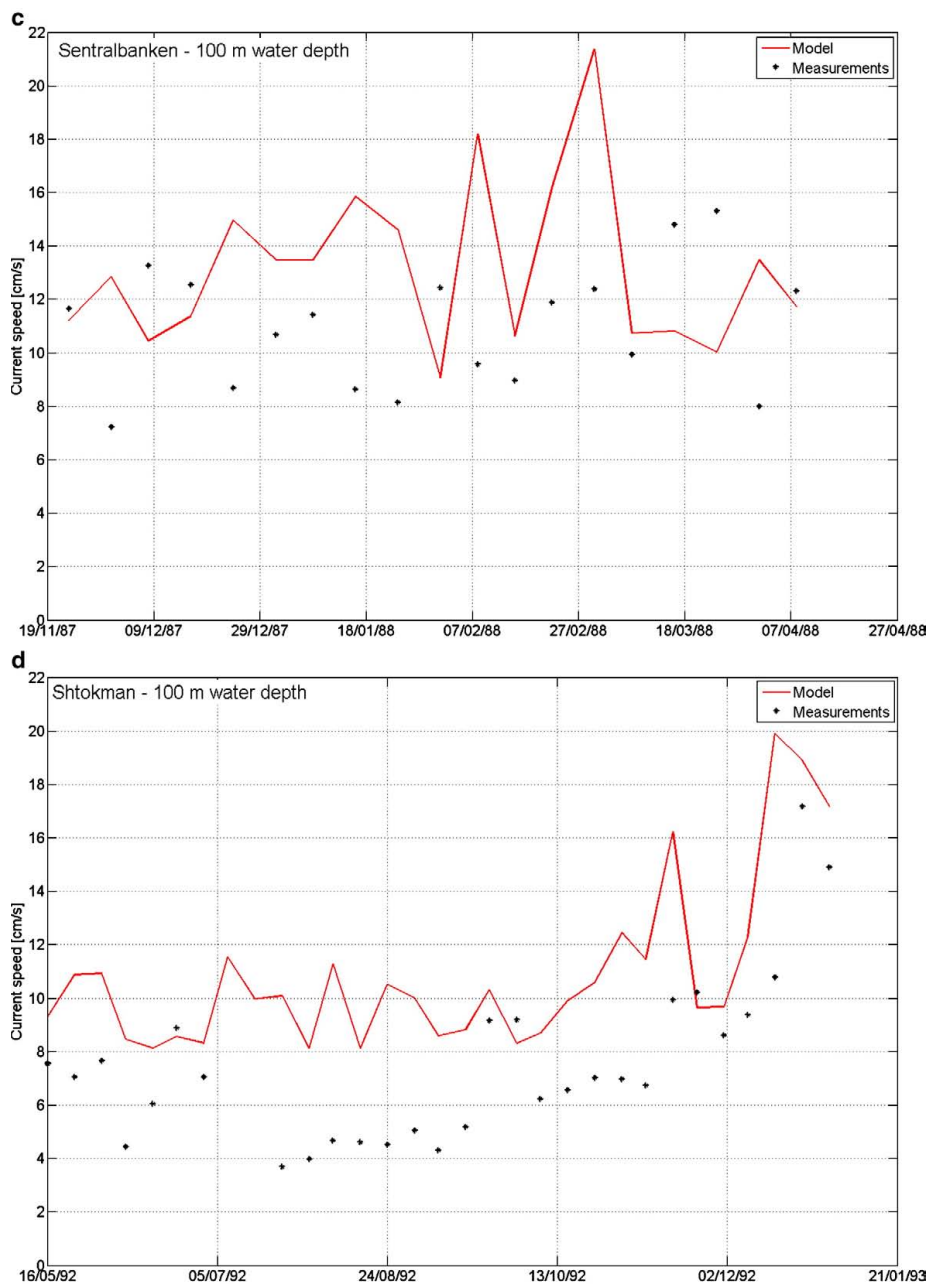


Fig. 6 (continued).

Tidal ellipses have been drawn for all locations and plots including ellipses from both measurements and model have been generated. These ellipses comprise information regarding magnitude and direction of currents caused by the constituents. As the model generates a depth averaged current, only one ellipse represents the

model at each site. With respect to measurements, ellipses based on data from 10 m, 25 m and 100 m depths have been drawn. Fig. 3 shows the comparisons of ellipses from Bjørnøya, Sentralbanken and Shtokman for the constituent M2. The locations are denoted OD8, OD7 and SHTOK in Fig. 2. Fig. 4 shows scatter diagrams comparing M2 major

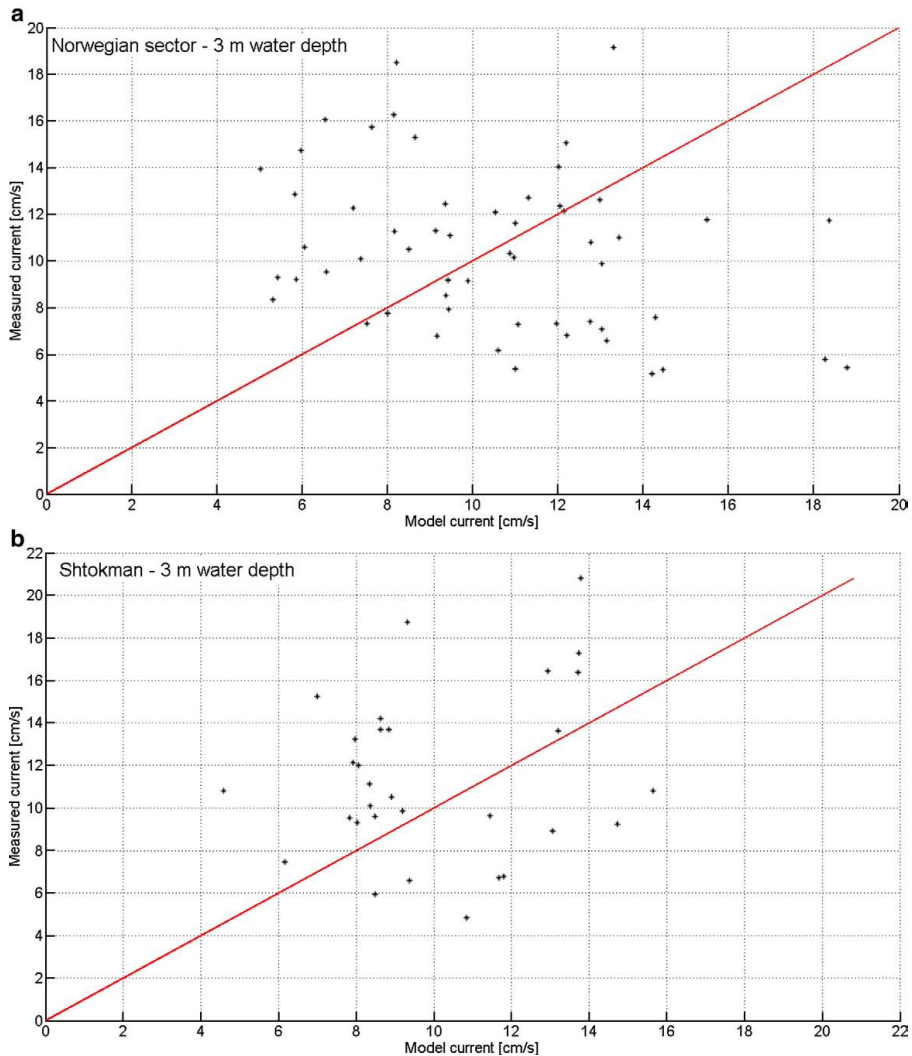


Fig. 7. Scatter diagram showing modified model current speed versus current speed from measurements at 3 m (a and b) and 100 m (c and d) water depth. Scatter a) and c) are based on all recordings in Norwegian sector while b) and d) are from the Shtokman field. Red line shows the equation $y=x$. (For interpretation of the references to color in this figure legend, the reader is referred to the web version of this article.)

axis, minor axis and inclination from model and measurements. The measured amplitudes have been averaged over the measurement depths before the comparison.

4.1.2. Residual currents

For each of the measured records, five types of comparisons with model have been carried out (Table 2). While the first four types of analyses are traditional type of analyses and considered as more or less self-explaining, the trajectory-study needs some further explanation.

The analysis in itself is fairly simple as it is restricted to follow a water particle moving with the speed recorded at the fixed station. With respect to current measurements, typical sampling is 1 h which

means that trajectories with 1 h time step may be generated by the recorded datasets. The recorded current value is assumed to be constant both with respect to magnitude and direction throughout the sampling interval. With respect to model currents, the sampling is 1 week¹ which means that model trajectories will be smoother than the measured trajectories. Both sailed distances as well as difference in end position have been stored for each measurement location. The trajectories visualise the quality of the oceanographic

¹ In the iceberg drift model, linear interpolation is used to provide currents with more frequent sampling. In most of the validations of the oceanographic model it has however been preferred to smooth the recordings to get the same sampling interval as the model currents, i.e. 1 week sampling.

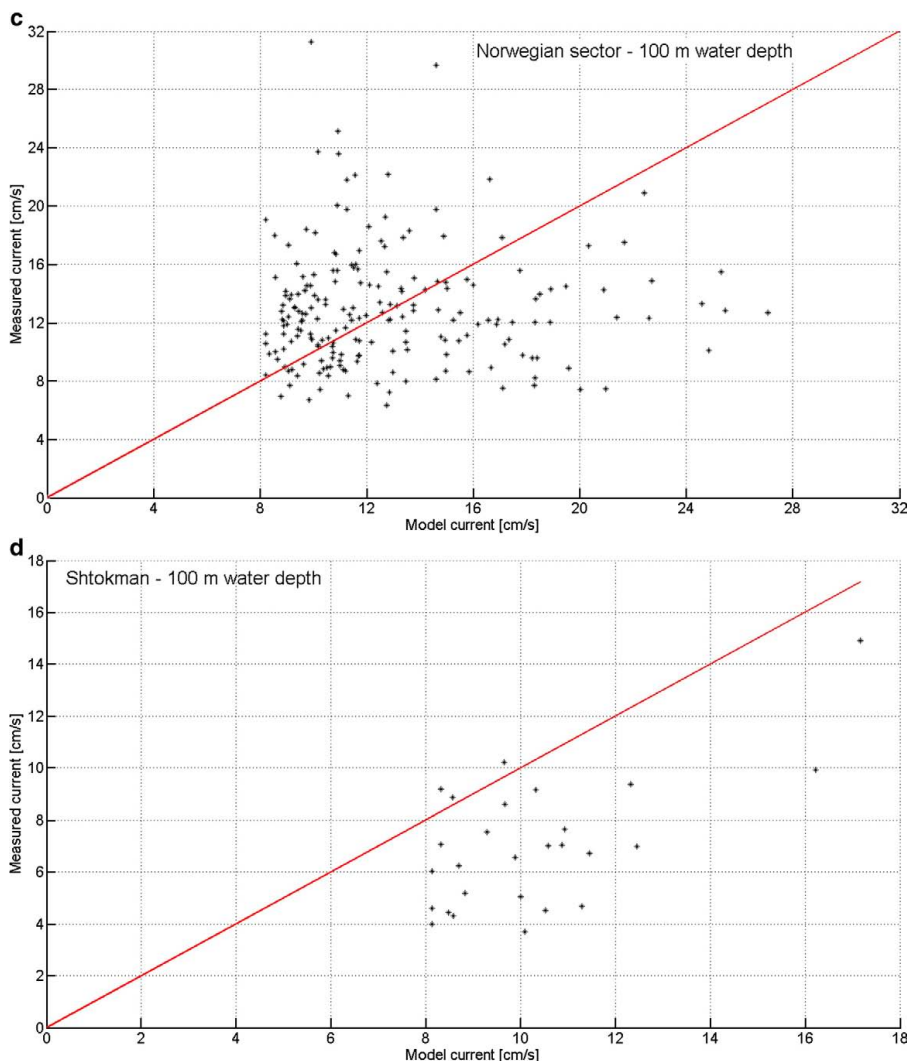


Fig. 7 (continued).

model. Only simultaneous model and measurement data have been applied.

With respect to comparisons type 1 to 4 (Table 2), recorded currents were averaged over the exact same weeks as given by the model. All studies revealed that the oceanographic model provides too low currents at all depths and all locations. The differences are illustrated in Fig. 5 for 3 and 100 m water depth at Sentralbanken and Shtokman, respectively. Since bias was more or less constant at all locations a method for correcting the current model was introduced. The methodology for corrections is as follows:

- Statistical distributions (3-parameter Weibull) were fitted to all measured recordings in the Norwegian sector at a certain water depth (3, 50 and 100 m).
- Corresponding distributions were fitted to simultaneous data from the model.

- The hindcast Weibull distribution is adjusted to the measurement distribution by requiring that both distributions shall give equal values for an equal probability level.
- Corrected hindcast current is then expressed by:

$$C_{hc_cor} = \left[\frac{C_{hc} - \varepsilon_{hc}}{\theta_{hc}} \right]^{\left(\frac{\gamma_{hc}}{\gamma_m} \right)} \cdot \theta_m + \varepsilon_m \quad (4)$$

where C_{hc} is current speed from hindcast, ε_{hc} and ε_m are location parameters in the Weibull distribution for hindcast and measurements, respectively. Correspondingly θ_{hc} and θ_m are Weibull scale parameters while γ_{hc} and γ_m are Weibull shape parameters. All further results presented in this paper are referring to the modified hindcast currents.

Time series of measured versus modified current speed at Sentralbanken and Shtokman are presented in Fig. 6. An extract of the comparisons are presented in Figs. 7–10. Comparisons that are not included in this paper show similar results as those included herein.

4.2. Meteorological validations

As for currents, simultaneous model and measured winds and waves have been subjected to comparisons both with respect to scatter, magnitude and direction. A representative extract of the results for winds are presented in Figs. 11–14 while corresponding results for waves are presented in Figs. 15–18.

4.2.1. Wind

See Figs. 11 to 14 in pages 17 to 18.

4.2.2. Waves

See Figs. 15 to 18 in pages 18 to 19.

4.2.3. Wind and wave trajectories

In order to investigate the effect of winds and waves on the drift of an iceberg, the iceberg drift model has first been used with only wind speeds as input. Currents have been set constant to zero during the simulations while waves and sea ice have not been included. A tabular shaped iceberg with length 100 m, width 80 m and sail 5 m has been used. Trajectories based on measured and model winds in the same

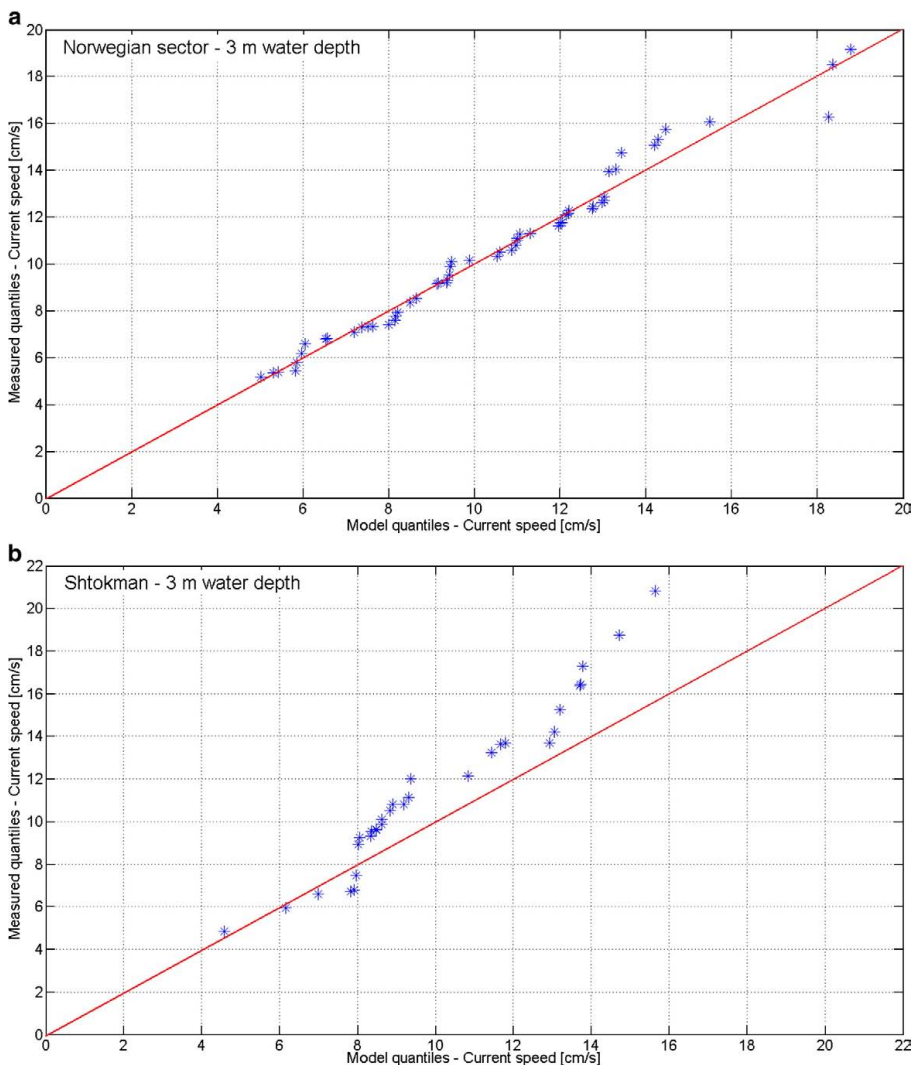


Fig. 8. QQ-plots showing modified model current speed versus current speed from measurements at 3 m (a and b) and 100 m (c and d) water depth. QQ-plot a) and c) are based on all recordings in Norwegian sector while b) and d) are from the Shtokman field. Red line shows the equation $y = x$. (For interpretation of the references to color in this figure legend, the reader is referred to the web version of this article.)

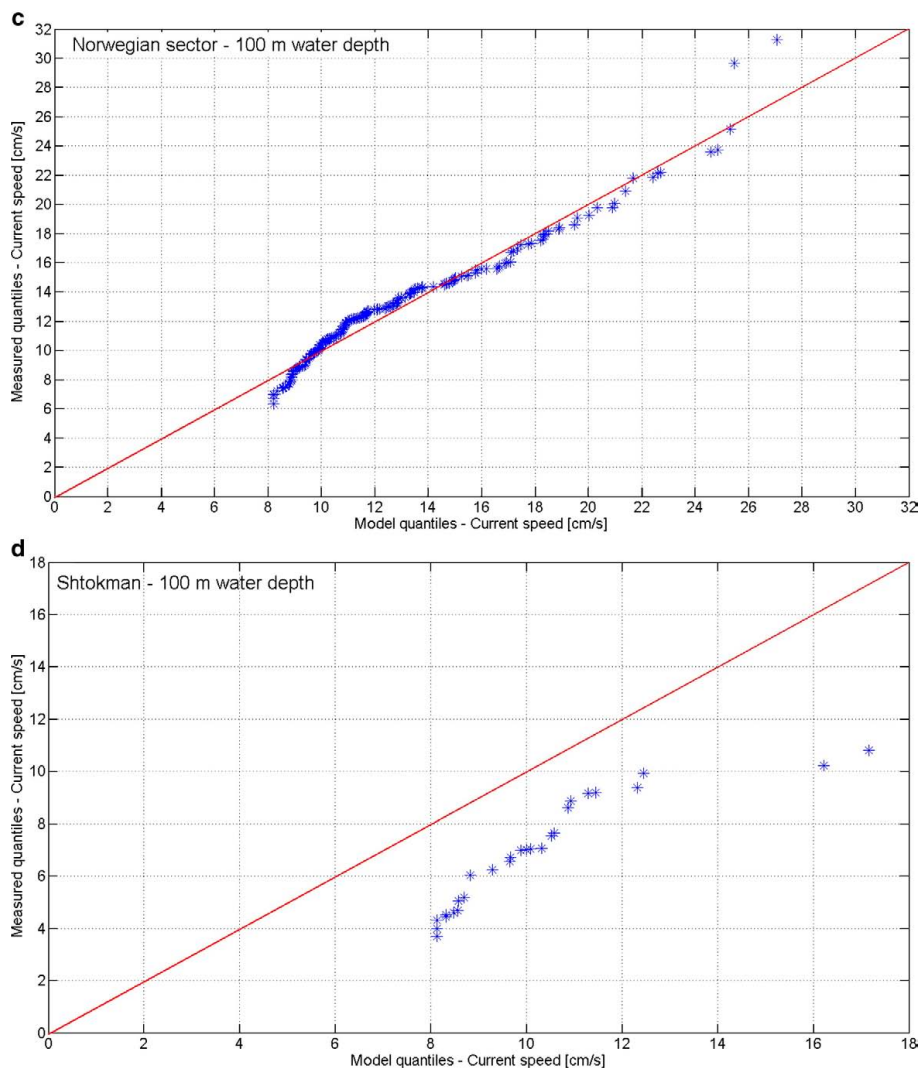


Fig. 8 (continued).

plot have been established for all locations where measured winds are available. As some of the datasets span over several years, only some limited periods have been simulated. These periods are the same as the periods with generated current trajectories thus making it possible to compare the effect of winds versus currents on the iceberg drift. Corresponding trajectories for icebergs subjected only to wave forces have also been generated. Representative trajectories are presented in Fig. 19. Formulations for wind and wave forcing are found in Appendix A.

Based on the length of trajectories from simulated icebergs when subjected only to winds, waves or currents, it is possible to provide information regarding the relative importance of each of the parameters. By summing up the length of the trajectories caused by the various forces (wind, waves and currents), the importance of,

for example current, is found as the length of the current trajectory divided by the total length. Importance based on the various datasets and corresponding recorded metocean data are presented in Table 3.

4.3. Iceberg drift validations

Trajectories from the model have been compared with totally nine measured trajectories. In light of the quality of underlying metocean data, it was considered meaningful to compare only the three first days of the measured trajectories. Initially, all forcing as described in Section 2 were included. However, two of the trajectories showed that the icebergs were locked into the sea ice during most of the simulation period. As can be seen from Fig. 20 the simulated trajectories show a

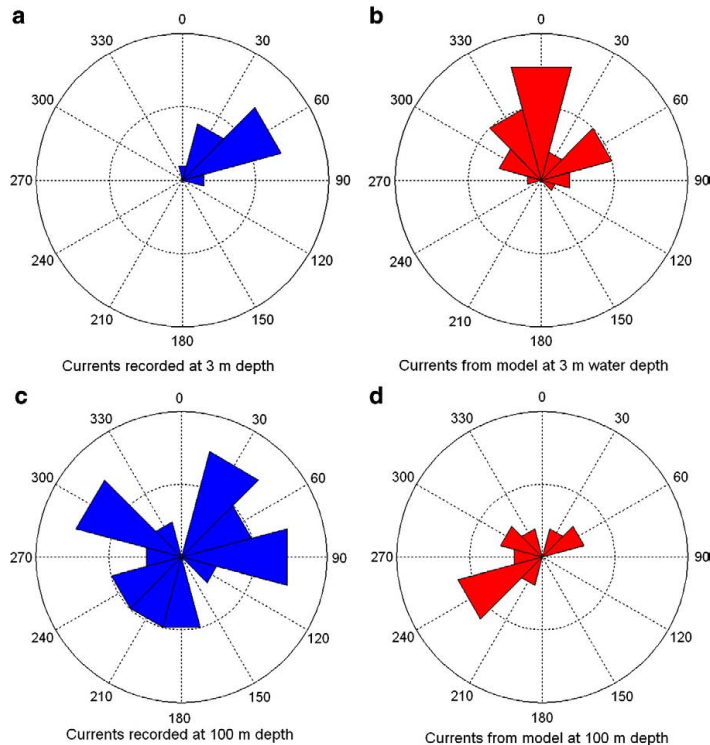


Fig. 9. Directional distributions from measurements (a and c) versus directional distributions from model (b and d) at 3 m and 100 m depth respectively.

poor match to the measured ones. These two icebergs were simulated over again but without including the forces from surrounding sea ice. As can be seen from Fig. 20 the match between simulated and measured trajectories improved significantly when excluding the sea ice drift.

Three of the comparisons between simulated and recorded iceberg drift trajectories are included in Fig. 21. Metocean statistics extracted from the simulations are presented in Table 4. The first trajectory is presented because it shows a fairly good match between recordings and simulations. The second is included because it shows a very good match the first 12 h and that the inertial oscillations are well described. However, this trajectory also illustrates a situation where the model simulates too high drift speed. It should further be noted that forces from surrounding sea ice has been excluded from this particular simulation. The third shows a situation where the simulated iceberg missed the initial drift direction with 90° but which still match the last 24 h of the recordings very well. It should be noted that weekly averaged residual currents were not included in this last simulation.

Despite that only the three first days of each trajectory were used in the comparisons, simulations were also carried out for the full periods with recordings. Average drift speeds and standard deviations based on both simulations and recordings are shown in Table 5.

In order to investigate the importance of wind, waves and currents on iceberg drift, the simulations were repeated with only one of these components included at a time. Based on these simulations, average drift speed due to currents, winds and waves respectively were found. By averaging all speeds from the seven

selected IDAP icebergs, it was found that the currents contribute to almost 50% of the total forcing. Corresponding values for wind and waves are presented in Table 6. It should be noted that the IDAP icebergs in significant periods were surrounded by sea ice in various concentrations thus some of the icebergs were not affected by waves at all. With respect to the AARI icebergs, simulations did not include the residual currents thus relative contribution from currents (tide) were much less than for IDAP icebergs. The southernmost AARI trajectory showed, however, that wave forces were equally important as wind.

5. Discussion

With respect to oceanographic data, it is clear that the skills of the applied oceanographic model are far from good. The statistical corrections resulted in a reasonable level for weekly averaged currents both in the eastern as well as the western Barents Sea. However, the usefulness of these data is still limited as the directional information in the oceanographic model also is of poor quality.

The skills of the tidal model may however be considered as good both with respect to magnitude as well as directionality. The tides are considered important in iceberg drift forecasting and in local collision risk analyses. With respect to investigation of long term drift patterns, however, the importance of tidal currents is less important.

The magnitude of wind and waves from the atmospheric and wave models showed good agreement with the recorded data. It could be seen that the model had a tendency to give higher values for high winds compared to the recordings. However, when considering that the majority of recorded winds are from buoys which suffer from

sheltering in high sea states, it seems reasonable that model winds are slightly higher. It can also be seen that changes in the wind and waves are well captured at the correct time. With respect to directionality,

there is still a need for improvement. In particular, the wave energy in the model is focused in a narrow sector while the recordings show a more spread directionality in the waves.

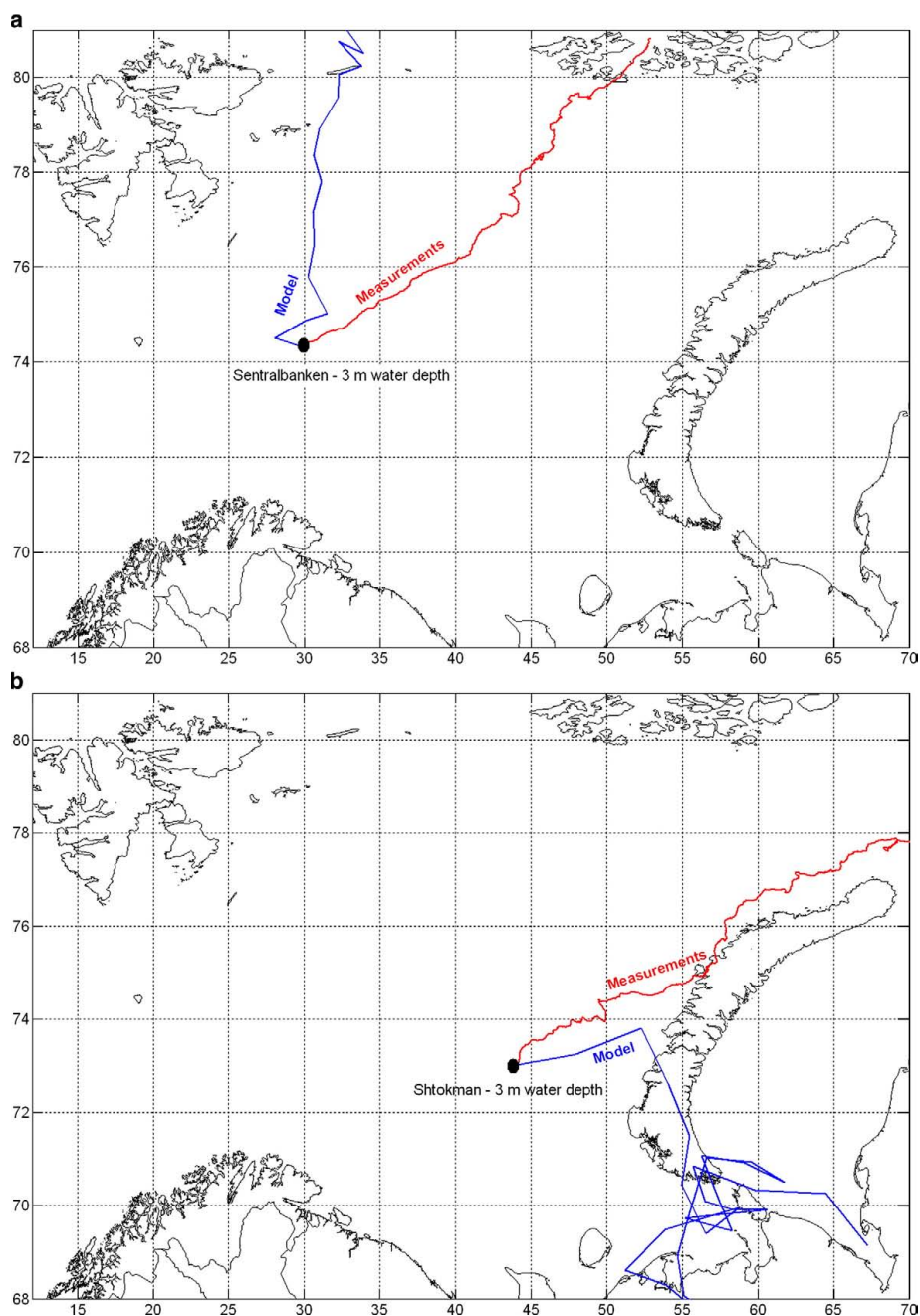


Fig. 10. Trajectories showing displacement of a water particle when subjected to currents from a fixed location spanning over approximately 7 months. Model currents (blue) from 3 m and 100 m versus measured currents (red) from the same depths at Sentralbanken are shown in (a) and (c) respectively. Corresponding values from Shtokman are presented in (b) and (d). (For interpretation of the references to color in this figure legend, the reader is referred to the web version of this article.)

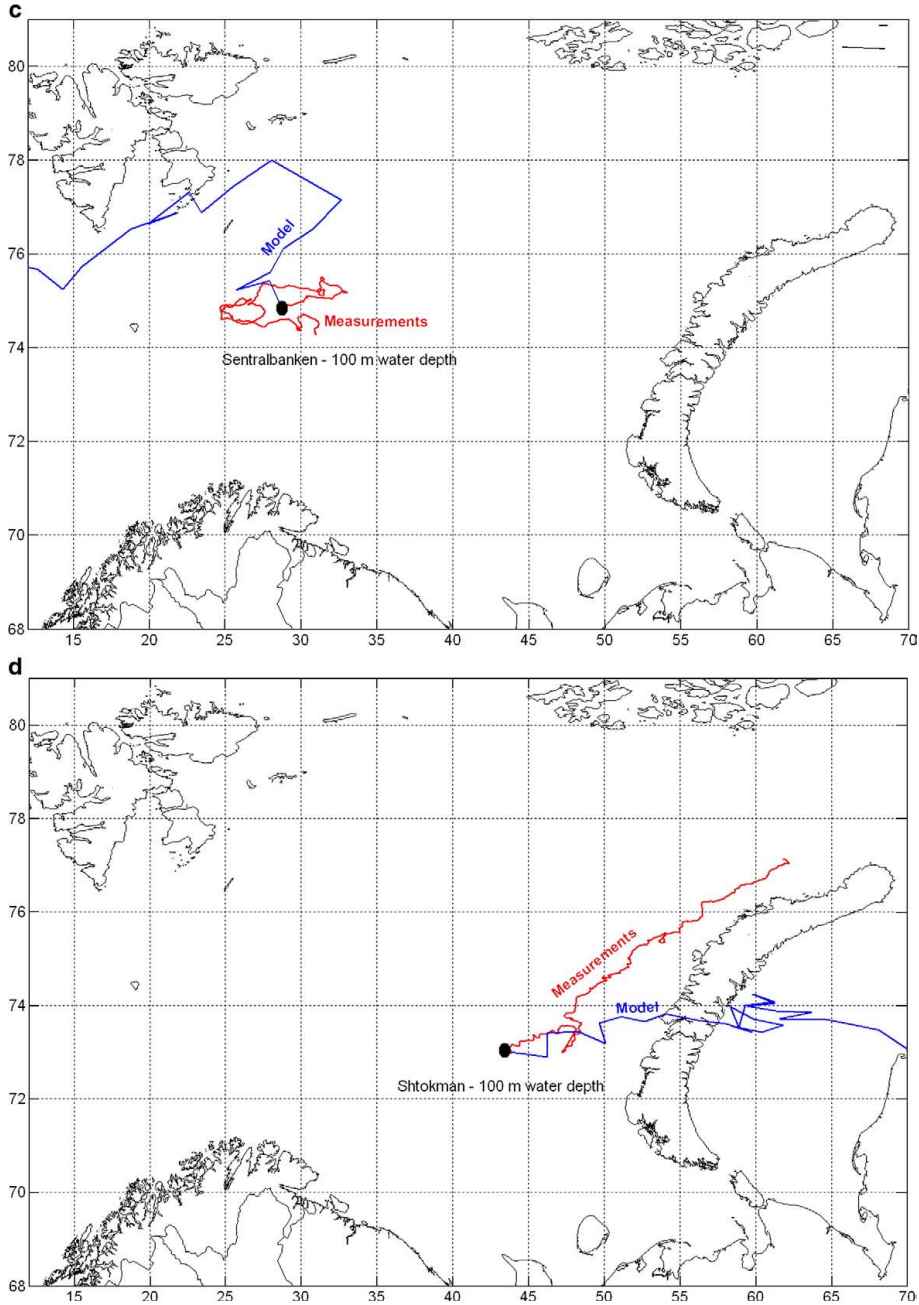


Fig. 10 (continued).

As expected, there was no perfect match between simulated and measured trajectories. A few of the simulation could be considered as “disqualifying” if the model were to be applied in a forecasting mode.

However, in all of the trajectories, there were clear correspondences between recorded and modelled trajectories. It is evident that changes in the wind conditions were captured well. Further, circular patterns,

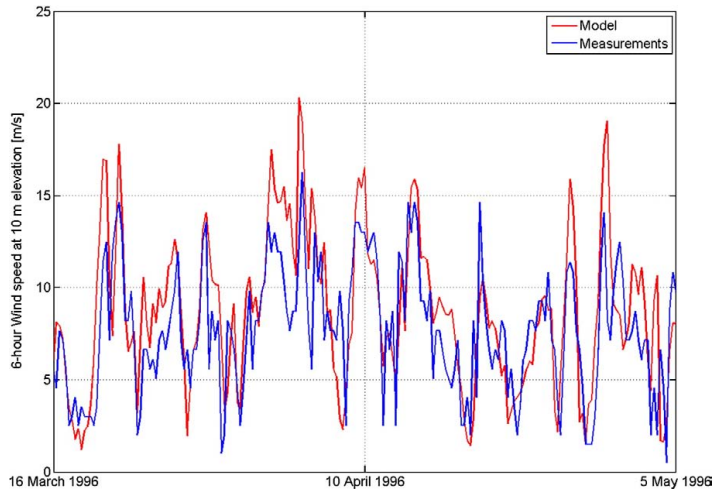


Fig. 11. Extract of time series with measured versus model wind speed at Shtokman.

either due to tidal currents or inertial oscillations seemed to be captured well.

The model does also provide useful information regarding the relative importance of the forces. It is evident that the currents are important, and often the most important parameter in iceberg drifts. In open water, at some distance from the ice edge however, the wave drift forces seem to be more important.

The model shows examples where icebergs get locked in the sea in accordance to the AWI criteria (Lichey and Hellmer, 2001). This happens when the sea ice concentration is higher than 90% and the sea ice strength is sufficiently high. The sea ice strength is formulated as a function of the ice thickness and ice concentration. When an iceberg is locked in the sea ice, it follows the sea ice drift patterns. Trajectories from icebergs, which in accordance to simulations were locked in the sea ice, generally show a very poor match with recorded trajectories. There may be several

reasons for this; first of all there is no information whether the physical icebergs were locked into the sea ice or not. Secondly, there is reason to believe that the numerical sea ice drift model, which is coupled to the oceanographic model (Keghouche et al., 2007), does not provide realistic sea ice drift patterns. The third explanation may be that the theoretical formulation from Lichey and Hellmer (2001) is not adequate for iceberg drift in the Barents Sea. The present study has not included validations of the sea ice/iceberg forces thus it is not possible to conclude on this subject. However, validation of sea ice forces on icebergs should be considered for further work on iceberg drift.

The validation studies performed on the underlying meteocean models provide important knowledge regarding the skills of the iceberg drift model. In situations with strong winds and high waves, there is reason to expect reliable results from the iceberg drift model. However, when ocean currents are dominating, the model

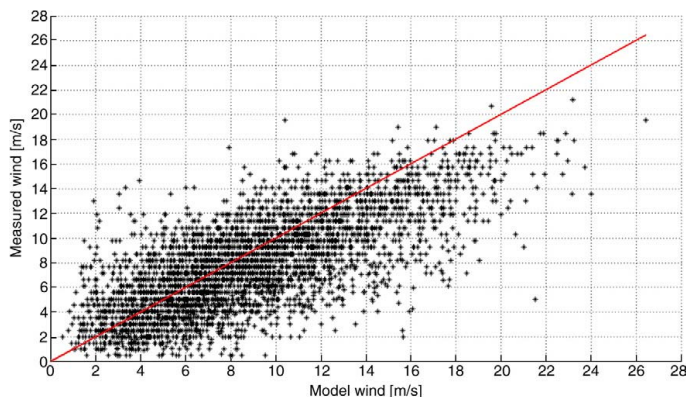


Fig. 12. Scatter diagram showing simultaneous values from measured and model wind speeds. Based on 6 hour averaged winds at Shtokman. Red line shows the equation $y = x$. (For interpretation of the references to color in this figure legend, the reader is referred to the web version of this article.)

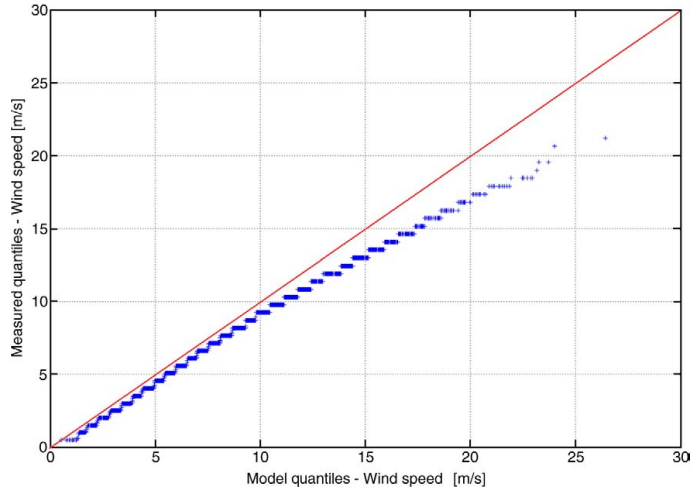


Fig. 13. QQ-diagram showing quantiles from measured and model wind speeds. Based on 6 hour averaged winds at Shtokman. Red line shows the equation $y = x$. (For interpretation of the references to color in this figure legend, the reader is referred to the web version of this article.)

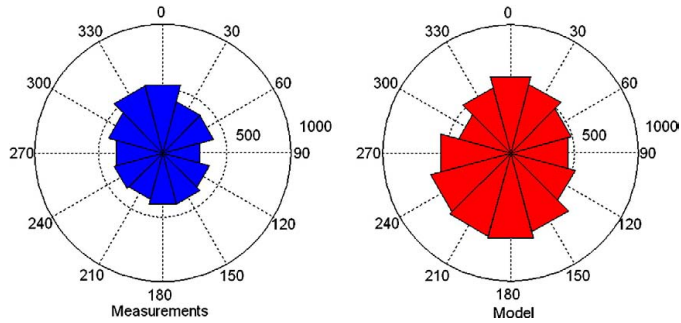


Fig. 14. Comparison of directional distributions from measurements and model at Shtokman. NB! Due to gaps in the measured data set, the model rose is based on more data than the rose representing the measurements.

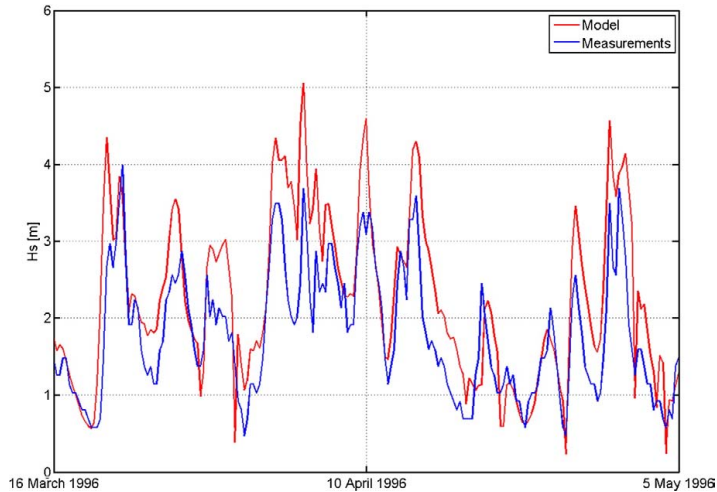


Fig. 15. Extract of time series with measured versus model significant wave height at Shtokman.

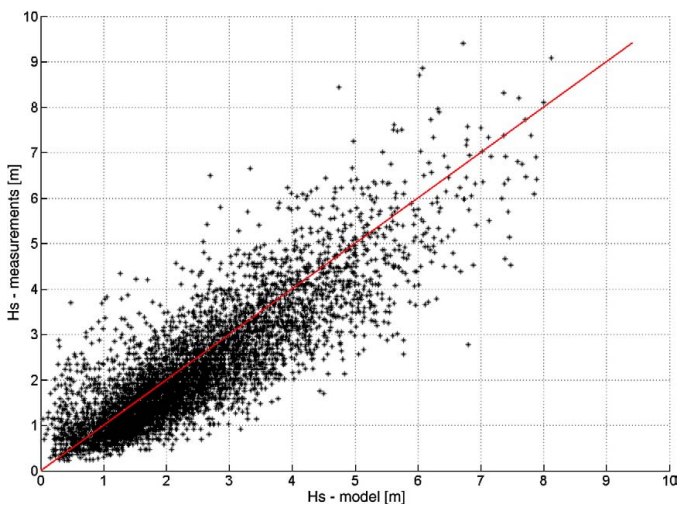


Fig. 16. Scatter diagram showing simultaneous values from measured and model significant wave height at Shtokman. Red line shows the equation $y = x$. (For interpretation of the references to color in this figure legend, the reader is referred to the web version of this article.)

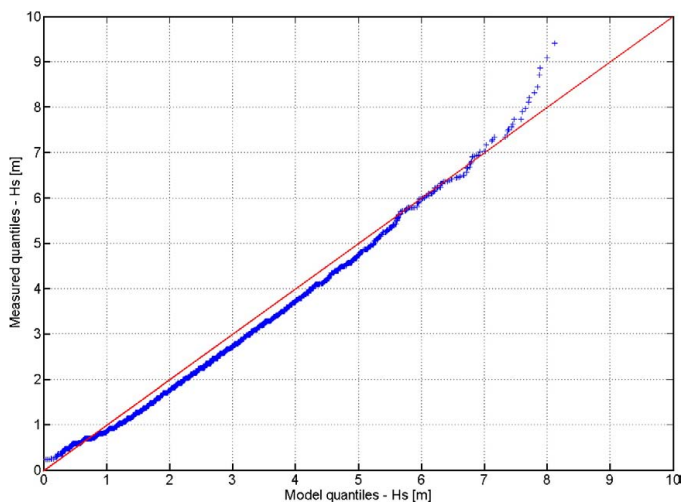


Fig. 17. QQ-diagram showing quantiles from measured and model significant wave height at Shtokman. Red line shows the equation $y = x$.

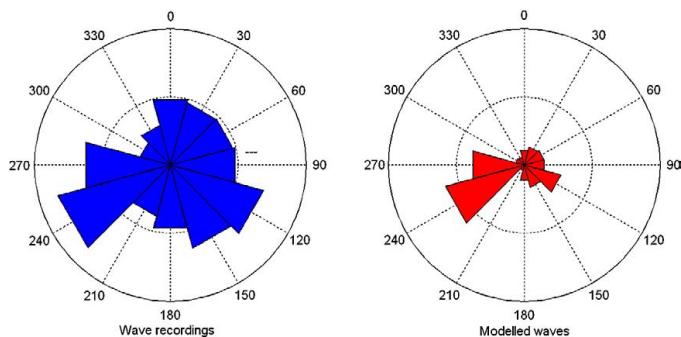


Fig. 18. Comparison of directional distributions from measurements and model at Sentralbanken. NB! Due to gaps in the measured data set, the model rose is based on more data than the rose representing the measurements.

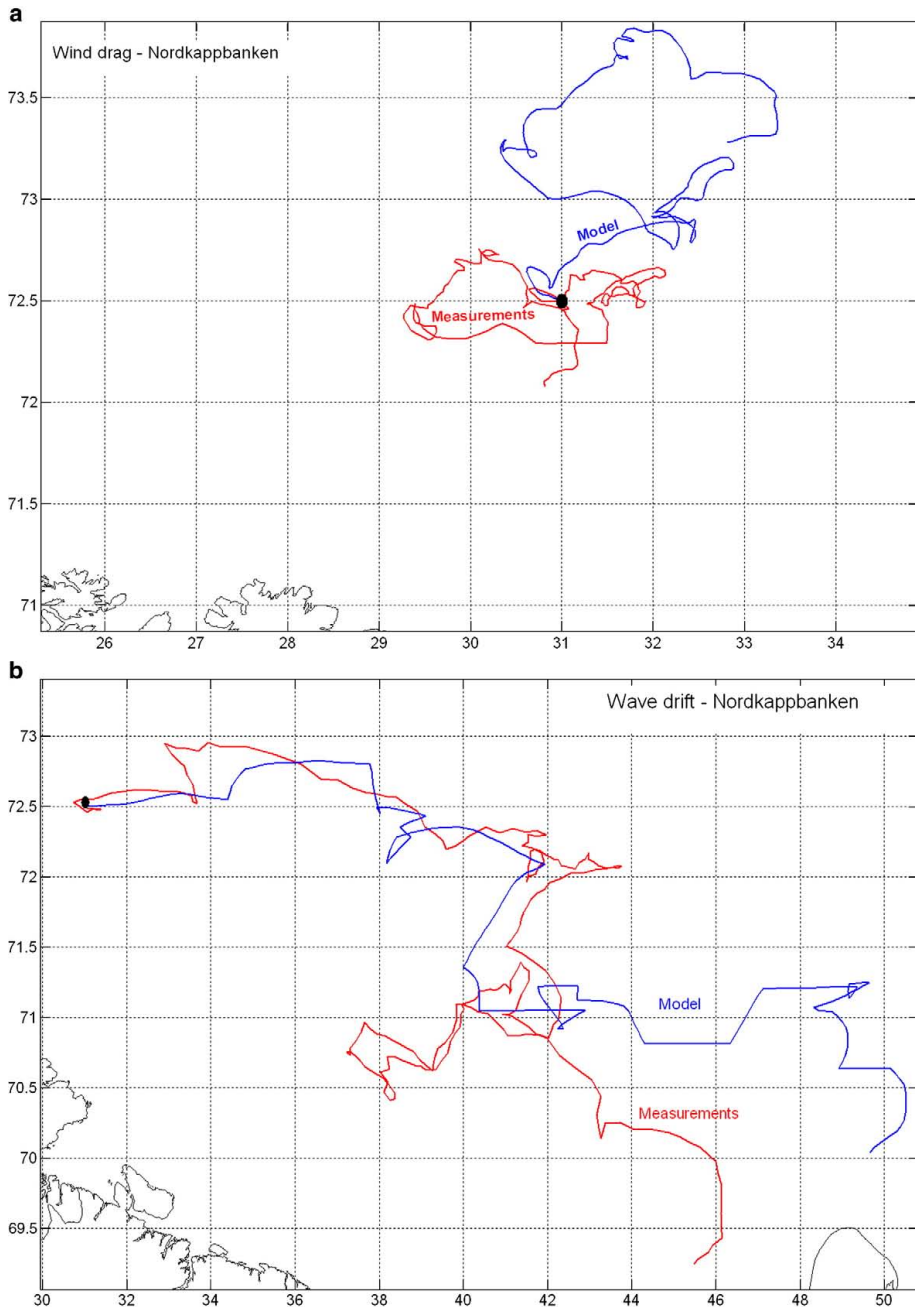


Fig. 19. Iceberg drift trajectories due to forcing from a) wind drag and b) wave drift. Iceberg dimensions (length×width×sail): 100×80×5 m. Based on recorded data from Nordkappbanken in the period 19.09.1989 to 22.11.1989 and wind/wave data from the Winch hindcast model (Reistad and Iden, 1998) for the same period.

skills may not be satisfactory. In order to ensure a more reliable iceberg drift model further efforts should be given to oceanographic modelling.

Iceberg deterioration has not been treated in this paper. However, it should be noted that iceberg deterioration may affect the iceberg drift significantly. The operational iceberg drift model applied at the East Coast

Table 3
Summary of relative importance and associated metocean parameters.

Data location ^a	Relative importance [%]			Average recorded parameters		
	Currents	Winds	H _s	Currents [cm/s]	Winds [m/s]	H _s [m]
Sentralbanken/OD 1 (3 m depth)	15	19	66	9	8.2	1.9
Bjørnøya/OD 8 (50 m and 100 m depth)	40	12	43	17	5.5	1.5
Nordkappbanken/OD 11 (100 m depth)	25	20	55	12	7.0	2.3
Shtokman (3.5 m depth)	23	17	60	12	6.2	2.0

Based on drift lengths.
^a Data locations are shown in Fig. 2.

of Canada (Kubat et al., 2007) has been implemented in the presented iceberg drift model. Preliminary simulations indicate that deterioration due to waves in storm situation is significant and that the iceberg drift speed seems to increase as the mass is reduced during the storm.

6. Conclusions

A numerical iceberg drift model for the Barents Sea has been established spanning the period 1987–1992 continuously with wind, wave and current data. The underlying oceanographic and atmospheric models have been subjected to comprehensive validations.

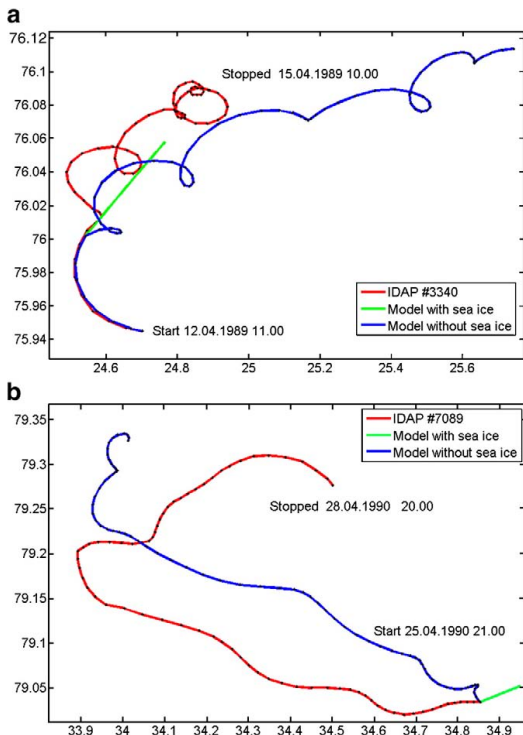


Fig. 20. Plot of two iceberg drift trajectories from recordings (red), simulations including sea ice forces (green) and simulations excluding sea ice forces (blue). (For interpretation of the references to color in this figure legend, the reader is referred to the web version of this article.)

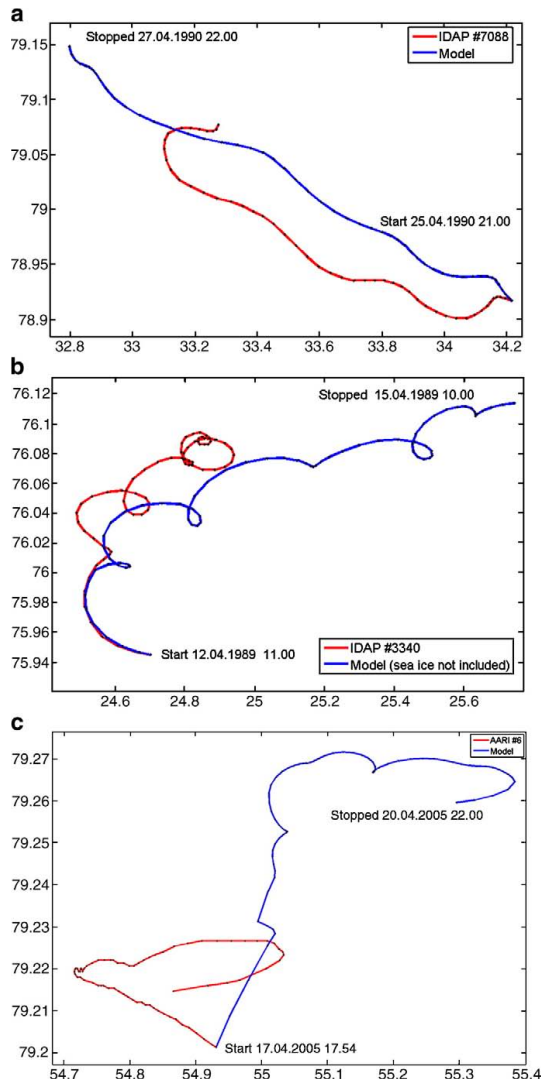


Fig. 21. Selection of comparisons between model and measured iceberg drift trajectories. Start and end of simulation time, which is identical with the first and the last data point in the measured trajectory, are included.

Validations show that both magnitude and directionality in model currents are of poor quality at all locations and at all times in the model domain. A methodology for adjusting the magnitude has successfully been introduced. However, better directional current information must be required from the oceanographic model.

The skills of the atmospheric and wave models are considered good and adequate for iceberg drift modelling. The directionality in both winds and waves may be improved.

Currents are considered as the most important parameter for icebergs drifting in waters close to the ice edge or within the sea ice. In more open water conditions, waves become the most important iceberg drift parameter.

Table 4
Metocean statistics extracted during three iceberg drift simulations.

Parameter	Source	Iceberg buoy number		
		IDAP 3340	IDAP 7088	AARI 6
Current speed [cm/s]	NERSC Barents Sea model Recordings	20	12	
Current direction (towards)	NERSC Barents Sea model Recordings	ESE	NW	
Wind speed [m/s]	Winch model	6.5	10.8	7.1
Wind direction (from)	Winch model	SSW	SE	S
Sea ice concentration [%]	NERSC Barents Sea model Recordings	94	87	
Sea ice thickness [m]	NERSC Barents Sea model Recordings	1	0.7	
Sea ice drift speed [cm/s]	NERSC Barents Sea model Recordings	4	1	
Sea ice drift direction (towards)	NERSC Barents Sea model Recordings	NE	NNE	

Iceberg dimensions and start of simulations correspond to size and time for physically recorded trajectories. Recorded ice and metocean conditions are from Løvås et al. (1990) and Jensen et al. (1990). Only mean values based on simulation period (3 days) are included. Empty fields mean that no information on the parameter is found.

Table 5
Statistical characteristics of iceberg drift according to simulations and recordings.

Iceberg buoy no.	Length × width × height	Simulations		Measurements	
		Average speed (cm/s)	Standard deviation (cm/s)	Average speed (cm/s)	Standard deviation (cm/s)
IDAP 3108 ^a	80 × 54 × 18	6	2.9	18	
IDAP 3337 ^a	65 × 47 × 11	32	11.8	29	
IDAP 3340	80 × 55 × 5	24	12.1	27	
IDAP 7086	90 × 60 × 10	18	8.1	12	
IDAP 7087	63 × 56 × 10	14	8.1	14	
IDAP 7088 ^a	95 × 80 × 20	22	9.2	10	
IDAP 7089 ^a	95 × 90 × 15	17	8.5	12	
Average IDAP		19	8.7	19	10.0
AARI 6	95 × 63 × 3.7	12	7.4	11	8.2
AARI 8	106 × 70 × 4.5	15	5.2	13	8.3

IDAP recordings are reported by Spring (1994) while AARI recordings are presented in Dmitriev and Nesterov (2007). Note: Some of the simulated trajectories are shorter than recorded trajectories due to grounding in the simulation model.

^a Simulated iceberg grounded before end of simulation time.

Table 6
Summary of relative importance and associated metocean parameters.

Data location	Relative importance [%]			Average associated values from metocean models		
	Currents	Winds	Waves	Currents [cm/s]	Winds [m/s]	Waves [m]
IDAP (7 icebergs)	49	44	7	17	8.8	0.2
AARI – Franz Josef Land ^a	33	67	0	5	6.6	0.2
AARI – Novaya Zemlya ^a	18	41	41	4	6.6	0.8

Based on forcing in the iceberg drift simulation model.

^a Only tidal currents were included in addition to wind and waves in the simulations.

Further work, should focus on improvement in oceanographic models for the Barents Sea.

Appendix A. Specifications for iceberg drift model

Expression for drag forces due to wind (F_a) and current (F_w) (Bigg et al., 1997):

$$F_{a,w} = \rho_{a,w} \cdot C_{a,w} \cdot A_{a,w} \cdot |\mathbf{V}_{a,w} - \mathbf{V}_i| (\mathbf{V}_{a,w} - \mathbf{V}_i) \quad (A1)$$

Expression for wave drift forces based on potential theory (Faltinsen, 1990):

$$F_r = \frac{1}{4} \rho_w \cdot g \cdot d^2 \cdot L \cdot \frac{V_{wa}}{|V_{wa}|} \quad (A2)$$

Expression for sea ice forces (F_i) (Lichey and Hellmer, 2001):

$$F_{si} = \begin{cases} 0 & : A \leq 15\% \\ \frac{1}{2} \rho_{si} C_{si} A_{si} |\mathbf{V}_{si} - \mathbf{V}_i| (\mathbf{V}_{si} - \mathbf{V}_i) & : 15\% < A < 90\% \\ -(\mathbf{F}_a + \mathbf{F}_w + \mathbf{F}_p + \mathbf{F}_{cor}) & : A \geq 90\% \text{ and } h \geq h_{min} \end{cases} \quad (A3)$$

Expression for pressure gradient force (F_p) (Kubat et al., 2005)

$$F_p = m \left(\frac{dV_{mw}}{dt} + \mathbf{f} \times \mathbf{V}_{mw} \right) \quad (A4)$$

Expression for Coriolis force (F_{cor}) (Bigg et al., 1997):

$$F_{cor} = -m \cdot \mathbf{f} \times \mathbf{V}_i \quad (A5)$$

Table A1
Parameter descriptions.

Parameter	Description	Recommended value	Reference
ρ_a	Air density	1.225 [kg/m ³]	
ρ_w	Water density	1027 [kg/m ³]	
ρ_{si}	Sea ice density	900 [kg/m ³]	
C_a	Air drag coefficient	1.3 [–]	Bigg et al. (1997)
C_w	Water drag coefficient	0.9 [–]	Bigg et al. (1997)
C_{si}	Sea Ice drag coefficient	1.0 [–]	Lichey and Hellmer (2001)
A_a	Cross sectional area above the water surface and normal to the wind speed	iceberg – sail · $\frac{\text{width} + \text{length}}{2}$	
A_w	Cross sectional area below the surface and normal to the wind speed	7.1 · sail · $\frac{\text{width} + \text{length}}{2}$	
A	Sea ice concentration	From ice-ocean model	Keghouche et al. (2007)
V_a	Wind velocity	From Winch model	Reistad and Iden (1998)
V_w	Current velocity	From ice-ocean model	Keghouche et al. (2007)
V_i	Iceberg velocity	Calculated	
V_{si}	Sea ice velocity	From ice-ocean model	Keghouche et al. (2007)
V_{mw}	Mean water current velocity	Current velocity averaged over the iceberg draft is applied	
g	Gravity	9.81 [m/s ²]	
a	Wave amplitude	$\frac{1}{2} \cdot H_s$	Faltinsen (1990)
H_s	Significant wave height (average height of the 1/3 highest waves in a sea state)	From Winch model	Reistad and Iden (1998)
C_w	Wave drift force coefficient	0.6 [–]	Isaacson (1988)
$\frac{V_{wa}}{ V_{wa} }$	Wave direction	From Winch model	Reistad and Iden (1998)
L	Iceberg length		
m	Iceberg mass	Physical mass + added mass = 1.5 times the physical mass	Kubat et al. (2005)
h	Sea ice thickness		
h_{min}	Minimum ice thickness needed to lock an iceberg in the sea ice	$h_{min} = \frac{p}{\rho \cdot \exp(-20 \cdot (1 - A))}$	Lichey and Hellmer (2001)
p	Sea ice strength	Average 660.9 [N/m]	Lichey and Hellmer (2001)
p^*	Sea ice coefficient	20,000 [N/m ²]	Lichey and Hellmer (2001)

References

- Bigg, G.R., Wadley, M.R., Stevens, D.P., Johnson, J.A., 1997. Modelling the dynamics and thermodynamics of icebergs. *Cold Regions Science and Technology* 26, 113–135.
- Dmitriev, N. Ye, Nesterov, A.V., 2007. Iceberg drift in the Barents sea according to observation data and simulation results. *Proceedings 17th International Offshore and Polar Engineering Conference, ISOPE'07*, Lisbon, Portugal, pp. 633–638.
- Faltinsen, O.M., 1990. *Sea Loads on Ships and Offshore Structures*. Cambridge University Press, Great Britain.
- Foreman, M.G.G., 1978. *Manual for tidal currents, analysis and prediction*. Institute of Ocean Sciences, Patricia Bay, Sidney, BC Canada. Pacific Marine Science Report 78-6, revised October 2004.
- Gjevik, B., Straume, T., 1998. Simulations of the M2 and K1 tide in the Nordic Seas and the Arctic Ocean. *Tellus, Ser. A*, vol. 41, pp. 73–96.
- Gjevik, B., Nøst, E., Straume, T., 1994. Model simulations of the tides in the Barents Sea. *Journal of Geophysical Research* 99, 3337–3350.
- Isaacson, M., 1988. Influence of Wave Drift Force on Ice Mass Motions. *Proceedings 7th International Conference on Offshore Mechanics and Arctic Engineering (OMAE)*, vol. 2, pp. 125–130.
- Jensen, H., Løvås, S.M., Vinje, T., Løyning, T., 1990. B IDAP 90 R/V Lance Deployment. Field observations and analysis, vol. 2. Report from the Ice Data Acquisition Programme (IDAP), Sintef project 604872, 82 pp.
- Johannessen, K., Løset, S., Strass, P., 1999. Simulation of iceberg drift. *Proceedings 15th International conference on Port and Ocean Engineering under Arctic Conditions, POAC'99*, Helsinki, Finland, pp. 97–105.
- Keghouche, I., Bertino, L., Sandven, S., 2007. Iceberg modelling in the Barents Sea: Part I, initial Tests. *NERSC Tech. Rep.* 280.
- Kleiven, G., Meisingset, H.C., 2003. Analysis of metocean data from the Shtokman Area. *Norsk Hydro report NH-00199965*.
- Kubat, I., Sayed, M., Savage, S.B., Carrieres, T., 2005. An operational model of iceberg drift. *International Journal of Offshore and Polar Engineering* 15 (2), 125–131 ISSN 1053-5381.
- Kubat, I., Sayed, M., Savage, S.B., Carrieres, T., Crocker, G., 2007. An operational iceberg deterioration model. *Proceedings of 17th International Offshore and Polar Engineering Conference, ISOPE'07*, Lisbon, Portugal, pp. 652–657.
- Lichey, C., Hellmer, H.H., 2001. Modeling giant-iceberg drift under the influence of sea ice in the Weddell Sea, Antarctica. *Journal of Glaciology* 47 (158), 452–460.
- Løvås, S.M., Løyning, T.B., Jensen, H., Johnsen, Å., 1990. IDAP 90 R/V Lance Deployment. Re-analysis of Iceberg drift data from 1988 and 1989, vol. 3. Report from the Ice Data Acquisition Programme (IDAP), Sintef project 604872, 100 p.
- The Mathworks, 2008. *Matlab Function Reference*. Website: http://www.mathworks.com/access/helpdesk/help/techdoc/index.html?access/helpdesk/help/techdoc/ref/ode113.html&http://www.mathworks.com/cgi-bin/texis/webinator/search/?db=MSS&prox=page&rorder=750&rprox=750&rdfreq=500&rwfreq=500&rlead=250&sufs=0&order=r&sis_summary_on=1&ResultCount=10&query=ODE15s&submitButtonName=Search [cited 1 September 2007].
- Oceanor, 1998. *Innsamling av naturdata i Norskehavet og Barentshavet, Sammendrag 1976–1997*. Summary report OCN R-98038 delivered to Norwegian Petroleum Directorate (NPD) 1998.
- Reistad, M., Iden, K., 1998. Updating, correction and evaluation of a hindcast data base of air pressure, wind and waves for the North Sea, the Norwegian Sea and the Barents Sea. *Norwegian Meteorological Institute, Research report No. 9*, 1998.
- Spring, W., 1994. *Ice Data Acquisition Summary Report*. Mobil Research and Development Corporation, Texas, US.

4.1.2 Iceberg wave drift – model tests



POAC09-86

WAVE DRIFT FORCE ON ICEBERGS – TANK MODEL TESTS

Kenneth Eik^{1,3}, Aleksey Marchenko^{2,3}, Sveinung Løset^{3,2}

¹StatoilHydro, Trondheim, NORWAY

²The University Centre in Svalbard (UNIS), Svalbard, NORWAY

³Norwegian University of Science and Technology (NTNU), Trondheim, NORWAY

ABSTRACT

As offshore activities move northwards, the presence of icebergs will in some regions affect both marine operations and design of new installations. Access to reliable iceberg drift forecasts will be crucial in order to ensure safe and efficient operations. Calculation of wave drift forces is an important element in iceberg drift modelling thus the effect of waves on iceberg drift has been investigated.

Six models of icebergs have been made of wax in scale 1:150 and exposed to regular waves in a wave tank. The models represent three cylindrical and three tabular icebergs with length/diameter 30 m, 60 m and 90 m. All models have been exposed to calm, moderate and severe waves (corresponding to sea states with significant wave height 1.5 m, 2.5 m and 3.5 m). The iceberg drift speed has been measured and compared with expected speeds from recognised wave drift formulas. It was found that the assumptions done in standard iceberg wave drift calculations were not fulfilled and that the discrepancy between calculated and measured drift speeds was larger for smaller icebergs. Based on the observations, an expression for wave drift coefficient as a function of wave height and iceberg length was derived. By introducing the wave drift coefficient in iceberg drift models, the quality of iceberg drift predictions may be improved. A few tests with iceberg models in irregular seas were also conducted. Results from these tests do not indicate any significant difference between wave drift coefficient in irregular and regular waves.

There are a number of uncertainties and potential sources for errors in the conducted tests. It is recommended that further tests are carried out in a larger scale and that iceberg accelerations are measured simultaneously with the velocity. Further, use of sophisticated numerical software and/or analytical solutions for wave drift on floating bodies may be applied in order to establish efficient tools for iceberg wave drift predictions.

INTRODUCTION

Searching for oil and gas in regions infested by sea ice and icebergs has been ongoing for several decades. Considering the suggestion by US Geological Survey that 25% of the remaining hydrocarbon resources in the world are located in the Arctic, a strong increase in Arctic offshore activities must be expected.

As offshore activities are moving northwards the presence of icebergs in some areas will affect both designs of new installations as well as plans for marine operations. Knowledge regarding frequency of occurrence of icebergs as well as abilities to perform reliable predictions of iceberg drift will be crucial in order to ensure safe and efficient operations. During the recent decades, a number of iceberg drift models have been presented for various regions and been applied both in iceberg drift hindcasting and forecasting. Most of the models include some sort of forcing component due to wave actions on the icebergs. The objective with the present study has been to perform some simple tank model tests in order to measure wave drift and thereby evaluate the usefulness of wave drift formulations for icebergs.

In total, six iceberg models were made and each was exposed to six sets of regular wave conditions in a physical wave tank. The wave positions were recorded making it possible to calculate the drift speed caused by the waves. Based on the results, a function for wave drift coefficient was established that is considered useful for implementation in wave drift models.

This paper highlights recognised theory on mean wave drift. Thereafter, the set up of the model tests is presented before results and development of functions for wave drift coefficient are described. Model tests were also performed in irregular sea and a comparison of results in regular versus irregular waves is included. The paper is closed with a brief discussion on the results and conclusions that follows from this.

THEORY ON WAVE DRIFT FORCES

Contributions to wave drift

Wave propagation on the surface of ideal fluid is realized by the excitation of oscillating currents and deformation of the fluid surface. Wave propagation in the vicinity of a surface piercing body influences the excitation of oscillating currents circumfluent the body surface and the production reflected waves and vortices. It is convenient to distinguish three forces influencing the displacement of the body in the direction of wave propagation: the force due to the influence of the oscillating current (F_c), the force due to wave reflection (F_{wd}), and the drag force (F_d). The force F_c is related to the added mass effect in case of body motion in oscillating current, and can be estimated using the solution of the problem about potential flow near an oscillating body. The oscillating current can either produce or not produce vortices depending on wave frequency,

wave amplitude and body sizes (Lienhard, 1966). The drag force \mathbf{F}_d is related to the production of vortices due to the separation of boundary layer from the body surface. In addition, a buoyancy force (\mathbf{F}_b) will influence the displacement of the body in vertical direction.

Finally the momentum balance of a floating body under the influence of surface waves can be written as follows

$$M \frac{d\mathbf{v}}{dt} = \mathbf{F}_c + \mathbf{F}_r + \mathbf{F}_d + \mathbf{F}_b, \quad (1)$$

where M is the mass of the body, \mathbf{v} is the vector of the velocity of the body gravity centre, and t is the time. A sum of above considered four forces is equal to the integral from water pressure by the submerged surface of the body. The water pressure also creates angular momentums causing rolling and pitching of the body.

The direction of the forces \mathbf{F}_c and \mathbf{F}_d is almost horizontal and the direction of buoyancy force \mathbf{F}_b is almost vertical when the wave amplitude is much smaller than the wave length. In this case, a sum of their horizontal projections can be estimated with Morison's formula (Sarpkaya and Issacson, 1981)

$$F_c + F_d = \rho_w C_m V \frac{d(v - v_w)}{dt} + \frac{1}{2} \rho_w C_d S |v - v_w| (v - v_w), \quad (2)$$

where v is the velocity of the body, v_w is the velocity of water particle at the water surface induced by incoming wave, V is the volume of submerged part of the body, S is the representative area of vertical cross-section of submerged part of the body, ρ_w is the water density. The dimensionless coefficients C_m and C_d depend on the shape of submerged part of the body, the Keulegan-Carpenter number ($K = \Delta v_m T / L$), the Reynolds number ($Re = \Delta v_m D / \nu$) and kD . T and k are wave period and wave number, L is body diameter in transversal direction to the incoming wave propagation, and ν is kinematic viscosity of fluid. Further, Δv_m is the amplitude of the velocity $v - v_w$ of the oscillating current. Typically, the drag coefficient, C_d , is determined by experiments (see, e.g., Sarpkaya and Issacson, 1981), while the coefficient C_m can be calculated analytically (Moe, 1999).

When the body sizes are comparable with wave length: $|dv/dt| \ll |dv_w/dt|$, the body accelerations should be much smaller than the accelerations of water particles in orbital motion. Therefore, it is natural to assume that $\overline{F}_c = 0$ when the body moves under the influence of periodic wave. Symbol $\overline{\quad}$ means that the force is averaged over the wave period. Let us average the projection of Equation (1) on the direction of wave propagation over one wave period

$$M \frac{d\overline{v}}{dt} = \overline{F}_{wd} + \overline{F}_c, \quad (3)$$

Equation (3) can be used for the description of mean wave drift of a floating body by periodical surface wave. The forces \bar{F}_{wd} and \bar{F}_d can be called as mean wave drift force and mean drag force respectively.

A major contribution to the horizontal mean wave drift force is due to the relative vertical motion between the structure and the waves. This causes some of the body surface to be part of the time in the water and part of the time out of the water. When examining the pressure on a point in the surface zone, it can be seen that the result is a non-zero mean pressure around the structure (Figure 1). If the relative vertical motion differs around the waterline, the result will then be a non-zero mean force. This is typical for large volume structures where the waves are modified by the structure. The mean wave drift force on a structure may be calculated by a far field momentum conservation methodology or alternatively by direct pressure integration. Both approaches are well described by Faltinsen (1990).

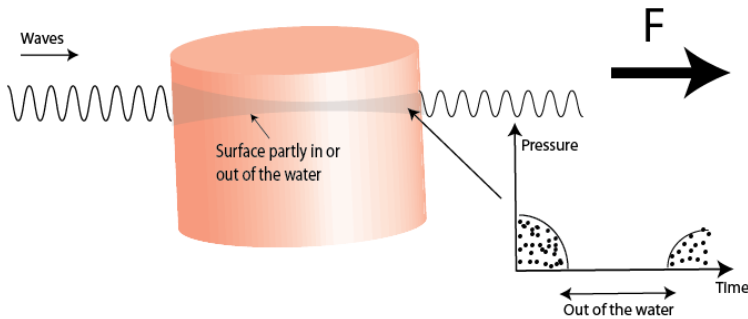


Figure 1. Horizontal mean wave force contribution due to pressure forces on the free-surface zone of an iceberg.

Expression for mean wave drift forces and moments

Mauro (1960) derived a recognised formula for mean wave drift force on a two dimensional body in incident regular deep-water waves:

$$\bar{F}_{wd} = \frac{1}{2} \cdot \rho_w \cdot g \cdot A_R^2 \quad [\text{N/m}] \quad (4)$$

where g is the gravitational acceleration and A_R is the wave amplitude of reflected waves. This formula is valid both for a fixed and a floating body oscillating around a mean position.

Equation (3) shows that wave-drift forces are connected to the body's ability to generate waves. The waves caused by an iceberg will be the sum of (a) the radiating waves when the body is forced to oscillate in each mode of motion and (b) the diffracted waves when the iceberg is restrained from oscillating and subject to incident waves. For long wavelengths relative to the cross-sectional dimensions, the iceberg will not disturb the wave field. This means that the reflected amplitude, A_R and the wave drift become negligible. When the wavelengths are very short and the side walls are vertical however, the incident waves are totally reflected from the

iceberg. In this case, the reflected wave amplitude is equal the incident wave amplitude, $A_R = \zeta_a$. By integration over the effective iceberg length¹, L_{eff} , the traditional expression for wave drift forces in regular waves is achieved:

$$\bar{F}_{wd} = \frac{1}{2} \cdot \rho_w \cdot g \cdot \zeta_a^2 \cdot L_{eff} \quad [\text{N}] \quad (5)$$

This formula has been applied in various forms in different drift models such as for instance the operational iceberg drift model at Grand Banks offshore the East Coast of Canada (Kubat et al., 2005).

Faltinsen (1990) derived an expression for mean wave drift force in irregular seas by linearly adding the force contributions from each of the wave components:

$$\bar{F}_{wd_irr} = \frac{1}{16} \cdot \rho_w \cdot g \cdot H_s^2 \cdot L_{eff} \quad [\text{N}] \quad (6)$$

where H_s is the significant wave height in a sea state. This formula has been applied in iceberg drift models by Bigg et al. (1997) and Eik (2009).

In order to estimate mean wave drift forces at finite water depths, Longuet-Higgins (1977) generalised Eq. (6) by multiplying with $\left(1 + \frac{2kh}{\sinh(2kh)}\right)$, where h is the water depth. However, this term has not been introduced in any of the herein referred publications for iceberg drift models. In this respect, it should be noted that there may be a lack of detailed information regarding water depths in the domains for iceberg drift models.

When iceberg motions are large, for instance due to heave resonance, the reflected wave amplitude, A_R , is likely to be large. This means that the wave drift-force may show a peak in a wave frequency range around the resonance frequency.

From the derivation of Eq. (3) it can be seen that the expression is only correct if the incident waves are reflected from a wall that is parallel to the wave crests. This will not be the case for an iceberg shaped like a circular cylinder where some of the waves will be reflected sideways. In accordance to Faltinsen (1990) the wave drift force on an infinitely deep structure with circular water plane area of radius, r will be:

$$\bar{F}_{wd} = \frac{2}{3} \cdot \rho_w \cdot g \cdot \zeta_a^2 \cdot r \quad [\text{N}] \quad (7)$$

With respect to floating bodies, sophisticated tools for wave drift calculations exist such as i.e. Wamit (Wamit, Inc., 2006). Comparisons between analytical solutions and numerical

¹ The effective iceberg length depends on the iceberg orientation and is usually less than the iceberg length but longer than the iceberg width.

calculations have been carried out, i.e. by Mansour et al. (2002). In the present paper however, attention has been given to the physical tank model tests with the emphasis to establish an efficient tool for iceberg drift calculations. Consequently, limited emphasis has been given to the numerical software and analytical solutions.

Wave drift coefficients

As many of the recognised iceberg drift models have applied some variant of Eq. (3) to take into account wave drift forces, these models implicitly assumes that the following conditions are met:

- Iceberg velocity and oscillations are small so radiation effects can be neglected
- Wavelengths are small compared to the iceberg
- Iceberg walls are vertical so that all the encountered waves are reflected.

For most icebergs, these assumptions are not perfectly fulfilled and therefore it has been convenient to introduce a wave drift coefficient, C_{wd} :

$$C_{wd} = \frac{\overline{F_{wd}}}{\frac{1}{2} \rho_w g L \zeta_a^2} \quad (8)$$

Isaacson (1988) studied the influence of wave drift force on ice mass motions and calculated wave drift force coefficients as function of seven independent parameters; L is ice mass horizontal size, d is ice mass draft, h is wave height, λ is wave length, D is water depth, ρ_w is water density and g is gravitational acceleration.

Based on a dimensional analyses and use of linear diffraction theory, Isaacson (1988) was able to express the wave drift coefficient as a function of three dimensionless parameters;

- size parameter, $\frac{L}{\lambda}$
- shape parameter $\frac{d}{L}$
- bottom proximity parameter $\frac{d}{D}$

Further, Isaacson (1988) developed curves for C_{wd} representing various combinations of the non-dimensional parameters both for circular cylinders and square cylinders. For the iceberg dimensions and sea states applied in the presented experiments, the wave drift coefficient would, in accordance to calculations by Isaacson (1988), be around 0.65 and 0.90 for circular and squared cylinders, respectively.

For icebergs forced only by waves, the wave drift force will have to be balanced by a drag force. When the mean acceleration is zero, the following balance from Equation (3) will provide information on the iceberg drift speed:

$$F_{wd} - \frac{1}{2} \rho_w C_d S v^2 = 0 \quad (9)$$

For icebergs, the value 0.9 is used for drag coefficient (C_d) in some models (Smith, 1993). It is important to note that all calculated drift velocities in this paper correspond to this value for C_d . It should however also be noted that F_{wd} varies as a function of the relative difference in speed between the body and the surrounding water.

MODEL TESTS – SET UP

The tests were executed in the Marine Civil Engineering Group's tank at NTNU in Trondheim, Norway. The applied tank is 60 m long, 5 m wide and with water depth varying within the range 0.8 m to 1.1 m. The actual tests were performed in a part of the tank with constant water depth at 1.06 m. The tank is equipped with a wave generator capable of making both regular and irregular waves. During the present work, regular waves were used in most of the tests. In the other end of the tank there was a beach in order to avoid reflection of waves.

In total, six iceberg models were made (Figure 2 and Table 1); three of rectangular shapes and three of cylindrical shapes. A model scale of 1:150 was applied on both icebergs and waves. The largest icebergs correspond to "normal iceberg" sizes in the Barents Sea in accordance to reports from the IDAP project (Spring, 1994). Correspondingly, the smallest icebergs would represent typical bergy-bits. In accordance to the Arctic and Antarctic Research Institute (AARI, 2005) bergy-bits will represent about 70 % of the icebergs observed in the Shtokman region, Barents Sea. A rectangular shape was intended to serve as a model for tabular icebergs while a cylindrical shape was intended to represent pinnacle icebergs. The iceberg models were made of wax with density 870 kg/m^3 . Observations from icebergs in the Barents Sea were used to establish realistic relations between iceberg length versus width and iceberg length versus draft.

Each iceberg model was planned to be tested in six sets of regular waves (Table 2). The waves would typically be representative for mild, average and severe sea states in the central part of the Barents Sea. The "severe" waves would correspond to a 90 % non-exceedance probability level. For each wave height, the tests were planned to be executed with two different wave periods; a "normal" wave period which would be the expected wave period for the given wave height and a "long" wave period which would represent a period that only is exceeded in one of ten sea states for the given wave height. Unfortunately, the wave generator was not able to make sufficiently short waves thus all tests were done with somewhat longer periods than planned.

In order to keep track of the iceberg drift, and thereof speed, the iceberg positions were monitored continuously by use of two laser distance sensors. The positions from the primary laser were logged with one second sampling while positions from the second laser were used only for corrections of positions for those icebergs that did not drifted straight along the centre line in the tank. The set up is shown in Figure 3. The elevation of the water surface was measured simultaneously with the iceberg positions and with a sampling frequency of 10 Hz. The wave sensor was located closed to the initial iceberg positions in the tests. The surface current was also

measured prior to the tests in order to consider the effect of possible return currents in the tank. Currents were measured with a Nortek Acoustic Doppler Velocimeter (ADV).

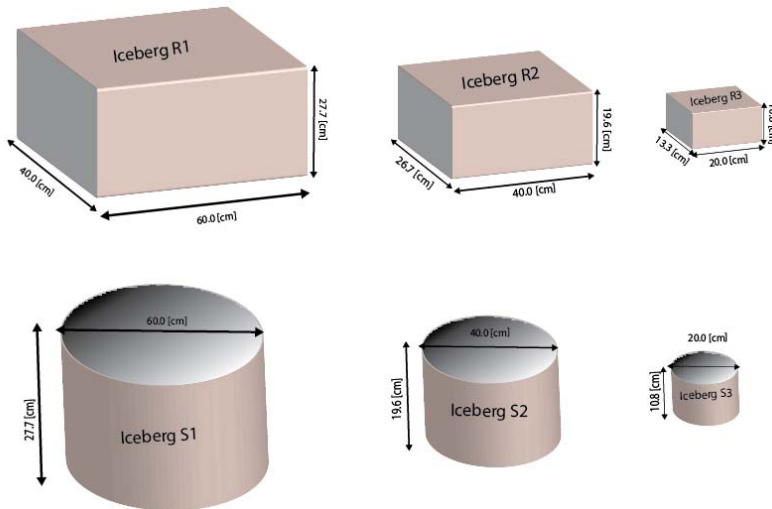


Figure 2. Iceberg shapes and dimensions in model scale

Table 1. Iceberg dimensions in full scale and model scale

	Full scale			Model scale		
	Length [m]	Width [m]	Height [m]	Length [cm]	Width [cm]	Height [cm]
Rectangular shape	30	20	16.2	20	13.3	10.8
	60	40	29.4	40	26.7	19.6
	90	60	41.6	60	40.0	27.7
Cylindrical shape	Diameter [m]		Height [m]	Diameter [cm]		Height [cm]
	30		16.2	20		10.8
	60		29.4	40		19.6
	90		41.6	60		27.7

Table 2. Wave test conditions in full scale and model scale.

	Full scale ²	Model scale	Run no.
Wave height, h [cm]	94	0.63	a,b
	157	1.04	c,d
	219	1.46	e,f
Wave period, t [s]	7.6	0.6205	a
	8.7	0.7104	c
	9.7	0.7920	e
	10.7	0.8737	b
	11.5	0.9390	d
	12.1	0.9880	f

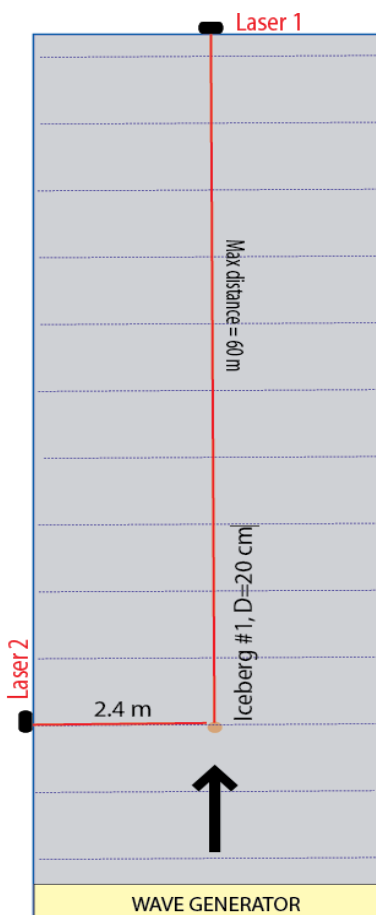


Figure 3. Test set up and illustration of position measurements. Photos of iceberg models.

² Wave heights correspond to average heights in sea states characterised by significant wave height of 1.5 m, 2.5 m and 3.5 m.

RESULTS OF TANK TESTS

Resulting drift speeds for the tabular icebergs are presented in Table 3 while results for cylindrical icebergs are given in Table 4. Measured velocities have been compared with expected velocities based on Eqs. (6 and 8) for tabular icebergs and Eqs. (7 and 8) for cylindrical icebergs. From the ratios between estimated and measured velocity wave, drift coefficients, C_{wd} , have been calculated³. With respect to the data provided in Tables 3 and 4, the following information should be noticed:

- The wave generator was not able to make perfectly regular waves.
- The wave generator was not able to provide waves with sufficiently low wave periods, thus all wave periods were somewhat longer than targeted and were also slightly longer than real wave periods for these wave heights.
- As all icebergs used some time to accelerate in the initial phase of the tests, the velocities have been estimated by averaging the drift speed over the last 50 % of the recordings.
- The wave drift did not converge towards a constant value in any of the tests. Figure 4 shows 30 s averaged drift speeds and simultaneous wave recordings from one of the tests as an example.
- The ratio between the longest wave lengths and water depth was approximately 0.5 thus application of deep water wave theory may be justified.
- The rectangular icebergs tended to orient themselves with the short side perpendicular to the wave crests independent on the initial orientation.

Table 3. Results from wave drift velocity measurements on *tabular* iceberg models. Data correspond to full scale values.

Iceberg Length	Wave amplitude [m]	Zero upcrossing period [s]	Measured drift speed [cm/s]	Theoretical drift speed [cm/s]	Wave drift coefficient [-]
30 m	0.20	14.3	0.5	17.8	0.03
	0.41	14.5	2.4	36.2	0.07
	0.72	14.5	1.7	63.1	0.03
	0.80	14.5	3.9	69.7	0.06
	0.88	14.5	7.7	76.9	0.10
60 m	1.01	14.5	8.3	88.1	0.09
	0.44	14.5	6.7	28.8	0.23
	0.44	14.4	3.3	28.8	0.11
	0.65	14.3	15.7	42.5	0.37
	0.80	14.5	13.6	52.2	0.26
90 m	0.82	14.4	21.7	53.2	0.41
	0.88	14.5	16.4	57.1	0.29
	0.13	14.2	8.1	7.0	1.16
	0.16	13.4	8.2	8.6	0.95
	0.70	14.4	28.9	38.2	0.76
90 m	0.77	14.4	29.3	41.9	0.70
	0.95	14.4	38.8	52.1	0.74
	1.15	14.4	37.7	62.8	0.60

³ NB! All values for C_{wd} in this paper, both tabular and cylindrical, are related to a drag coefficient with value 0.9 [-]

Table 4. Results from wave drift velocity measurements on *cylindrical* iceberg models. Data correspond to full scale values.

Iceberg Length	Wave amplitude [m]	Zero upcrossing period [s]	Measured drift speed [cm/s]	Theoretical drift speed [cm/s]	Wave drift coefficient [-]
30 m	0.13	11.0	0.2	9.1	0.03
	0.18	11.7	0.6	12.9	0.05
	0.51	14.3	1.3	36.5	0.04
	0.75	14.5	3.6	53.7	0.07
	0.89	14.5	7.8	63.4	0.12
	0.92	14.5	8.1	65.5	0.12
60 m	0.14	13.8	2.0	7.6	0.26
	0.14	13.1	0.2	7.6	0.03
	0.55	14.5	17.9	29.1	0.61
	0.68	14.4	23.1	36.3	0.64
	0.83	14.4	23.6	43.8	0.54
	0.98	14.5	30.5	52.2	0.58
90 m	0.13	11.9	1.0	5.7	0.17
	0.18	12.8	1.3	8.0	0.17
	0.59	14.4	24.1	26.5	0.91
	0.74	14.5	28.7	32.9	0.87
	1.01	14.5	47.3	44.9	1.05
	1.16	14.4	42.0	52.0	0.81

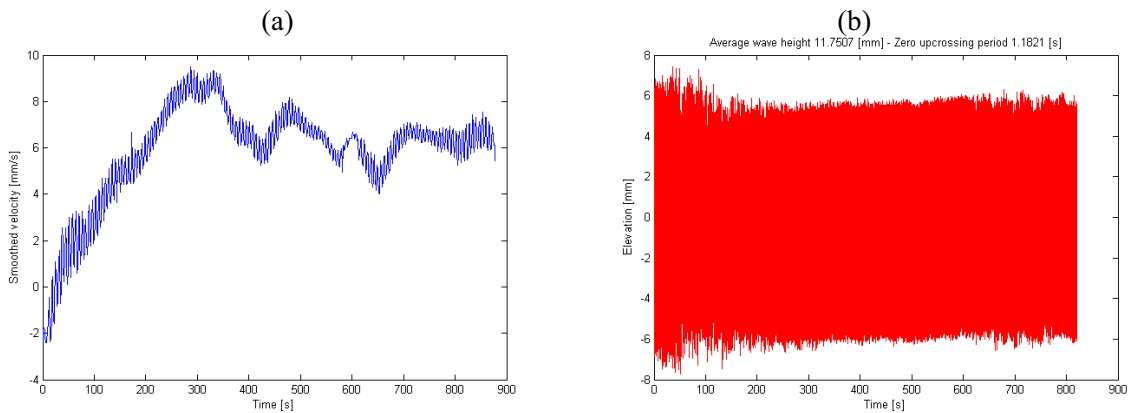


Figure 4. Example of velocity and wave recordings. The velocity plot (a) shows 30 s running average values.

WAVE DRIFT FORCE COEFFICIENT

The data presented in the Tables 3 and 4 were sorted in four classes in accordance to the respective wave heights. For each wave class, C_{wd} was plotted versus the iceberg length and diameter for rectangular and cylindrical icebergs respectively (Figure 5). The following function was fitted visually to the observations:

$$C_{wd} = A + 0.3 \cdot \tan^{-1}[B(L - 60)] \quad (10)$$

where L is the total iceberg length for the rectangular icebergs, alternatively the diameter of the cylindrical icebergs. A and B are coefficients which are functions of the wave height (h):

$$\begin{aligned}
 A &= 0.39 + 0.15 \cdot \exp(-h) \\
 B &= 0.05 + 5.5 \cdot \exp(-h \cdot 3.5)
 \end{aligned}
 \tag{10}$$

Figure 6 shows $C_{wd}(L, h)$ based on Equation (10) together with measured values from the model tests.

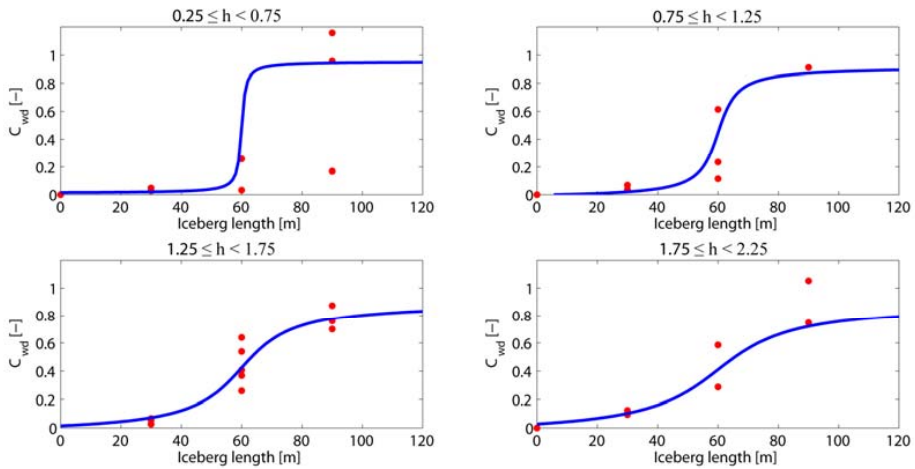


Figure 5. Wave drift coefficient given wave height based on data from model tests and from a smoothed function.

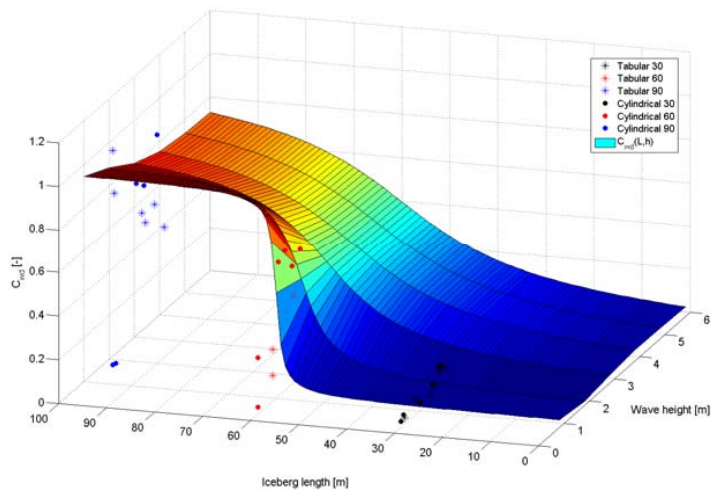


Figure 6. Wave drift coefficients as a function of iceberg length (diameter) and wave height. Measurements from tank model tests are included.

REGULAR VS IRREGULAR WAVES

Instrumentation for generation of irregular waves were made available for the project one day during the tests making it possible to re-run some of the experiments. It was decided to test only the largest two icebergs (90 m length) in irregular waves. Sea states corresponding to significant wave height of 2.5 m and 3.5 m and in accordance to a JONSWAP spectrum with peak-enhancement factor of 2.2 were generated. It was intended to make sea states with spectral peak periods 9.7 s and 12.1 s corresponding to average and long periods for the given wave heights. Results from the tests in irregular seas are presented in Table 5 while Figure 7 shows how the results fit to the empirical function in Equation (10).

Table 5. Results from wave drift velocity measurements on *tabular and cylindrical* iceberg models in irregular seas. Data correspond to full scale values.

Iceberg Length	Significant wave height [m]	Average wave amplitude [m]	Zero upcrossing period [s]	Measured drift speed [cm/s]	Theoretical drift speed [cm/s]	Wave drift coefficient [-]
90 m Tabular	2.6	0.80	10.0	35.4	43.5	0.81
	2.7	0.85	11.9	28.5	46.8	0.61
	3.7	1.14	11.8	43.2	62.0	0.70
	4.0	1.20	10.4	53.2	65.7	0.81
90 m Cylindrical	2.7	0.82	9.9	32.8	44.8	0.73
	3.1	0.95	11.6	39.2	51.7	0.76
	4.0	1.21	10.3	55.1	66.1	0.83
	4.1	1.27	11.5	48.9	69.4	0.70

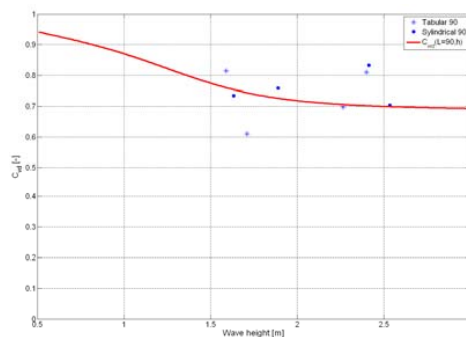


Figure 7. Estimated and measured wave drift coefficient for 90 m long icebergs in irregular seas.

DISCUSSION

First of all, it is important to note the wave drift coefficient should, for a given water depth, be a function of the wave length in addition to the iceberg size and shape and not the wave height as presented in this work. However, as it was not possible to create waves with sufficiently low periods in the tank tests, the wave heights, which are strongly correlated to the wave lengths, seemed to be an acceptable alternative. Some of the observations are not explained by the proposed empirical function for C_{wd} . Cancellation and/or resonance effects may explain this but

further work focusing on the wave period dependency is required before any conclusions can be drawn.

From the results, it can be seen that the wave drift theory (Eqs. 4 and 5) can be applied on icebergs with length or diameter around 90 m and higher with only a small reduction in the total drift force. With respect to smaller icebergs such as i.e. bergy bits, the wave drift is more or less negligible and the theoretical framework highlighted in this paper not really applicable. The empirical function for C_{wd} derived in this work may still, when used together with the traditional wave drift formulations, introduce an improvement in iceberg drift modelling.

For small icebergs, it can be seen that higher waves indicate a higher wave drift coefficient. A possible explanation for this is the effect of viscous forces which generally are excluded from iceberg drift predictions. When the reflected waves from the iceberg are negligible, the viscous forces may be more important. Since the viscous wave drift force is proportional with the cube of the wave amplitude, the wave drift will increase with increasing wave heights.

It has not been taken into account that the wave drift force will depend on the iceberg drift speed caused by other forcing components such as winds and currents. Further, it should be noted that the expression for C_{wd} is related to a constant value for the water drag coefficient. However, for a body oscillating under the influence of waves, the drag coefficient will vary and it will depend on the wave amplitude.

The model tests suffer by a too small scale. Due to the limited size of the model icebergs and the limited wave drift forces exerted on the models, it was not possible to measure movements in heave, pitch and surge which may be relevant for iceberg drift. Further, due to the scale, it was not possible to create waves of the planned height with reasonable wave periods. Due to this, it is not possible to conclude what effect the wave periods may have on the drift.

CONCLUSIONS

Wave drift of icebergs have been investigated in tank tests in scale 1:150. Wave drift was measured for icebergs with different shapes and sizes when exposed to both regular and irregular waves.

Results where compared with wave drift theory and an expression for wave drift coefficient as a function of iceberg length and wave height was developed. The expression may improve existing iceberg drift models as it quantifies differences between a simplified theoretical framework and actual wave drift.

The results show that small icebergs (bergy-bits) will experience only limited wave drift while the traditional wave drift theory may be applied on larger icebergs with a small reduction factor.

The actual tests suffer by a number of uncertainties and it is recommended to follow up the tests in a larger test facility. It will also be possible to apply sophisticated numerical simulations or alternatively analytical solutions for wave drift of cylinders and rectangular blocks in order to improve the mean wave drift contribution in existing numerical iceberg drift models.

REFERENCES

- AARI, 2005, Glaciers at Novaya Zemlya/Sources for icebergs in the Barents Sea. Research report ordered by Statoil, 87 p.
- Bigg, G. R., Wadley, M. R., Stevens, D. P. and Johnson, J. A., 1997. Modelling the Dynamics and Thermodynamics of Icebergs. *Cold Regions Science and Technology* 26, pp 113-135.
- Eik, K., 2009. Iceberg Drift Modelling and Validation of Applied Metocean Hindcast Data, *Cold Regions Science and Technology*, in press.
- Faltinsen, O. M., 1990. Sea Loads on Ships and Offshore Structures. Cambridge University Press, 328 p.
- Isaacson, M., 1988. Influence of Wave Drift Force on Ice Mass Motions, Proceedings 7th International Conference on Offshore Mechanics and Arctic Engineering (OMAE), Vol. 2, pp. 125-130.
- Kubat, I., Sayed, M., Savage, S. B., Carrieres, T. and Crocker, G., 2007. An Operational Iceberg Deterioration Model. Proceedings of 17th International Offshore and Polar Engineering Conference, ISOPE'07, Lisbon, Portugal, pp. 652-657.
- Lienhard, J.H., 1966. Synopsis of Lift, Drag and Vortex Trail Dynamics, *Physics of Fluid*, Vol. 31, pp. 991-998.
- Longuet-Higgins, M. S., 1977. The Mean Forces Exerted by Waves on Floating or submerged Bodies with Applications to Sand Bars and Wave Power Machines, Proceedings of the Royal Society of London, Series A, Mathematical and Physical Sciences, Vol. 352, Issue 1671, pp. 463-480.
- Mansour, A. M., Williams, A. N. and Wang, K. H., 2002. The diffraction of linear waves by a uniform vertical cylinder with cosine-type radial perturbations. *Ocean Engineering* 29, pp. 239-259.
- Mauro, H., 1960. The Drift of Floating Bodies in Waves. *Journal of Ship Research* 4, pp. 1-10.
- Moe, G., 1999. Linear wave theory. In book "Basics of offshore petroleum engineering and development of marine facilities", M: Neft' I Gaz, pp.144-157.
- Sarpkaya, T. and Isaacson, M., 1981. Mechanics of Wave Forces on Offshore Structures. Van Nostrand Reinhold, New York, 651 p.
- Smith, S. D., 1993. Hindcasting iceberg drift using current profiles and winds, *Cold Regions Science and Technology*, 22 (1), pp.33-45.
- Spring, W., 1994. Ice Data Acquisition Summary Report. Mobil Research and Development Corporation, Texas, US.
- Wamit, Inc. 2006. Wamit[®] User Manual version 6.3PC, USA.

4.1.3 Iceberg wave drift – numerical calculations

As described in Section 4.1.2, there are some limitations with respect to the use of the expression which was derived for the wave drift coefficient, C_{wd} (Eq. 10 in Section 4.1.2). The main concern is that the wave drift becomes a function of iceberg length (L) and wave height (H). It would however be more correct to express it as a function of iceberg length (L) and wave length (λ). In this respect, references are made to Mauro (1960), Kudou (1977), Isaacson (1988) and Faltinsen (1990). With the objective to improve the expression for the wave drift coefficient it was decided to perform a comparison between results from the physical tank model tests with calculations from a sophisticated numerical simulation tool.

In order to avoid duplications, the theoretical framework for iceberg wave drift is not repeated in this section. However, in order to avoid confusion the expressions for wave drift forces in regular and irregular seas are presented in Eq. (4-1) and (4-2) respectively. In iceberg drift models, it is likely that waves are represented by parameters such as significant wave height, spectral peak period or zero up-crossing and a dominating wave direction. Due to this, it will be convenient to use Eq. (4-2) for calculation of wave drift.

$$\overline{F}_{wd} = \frac{1}{2} \cdot \rho_w \cdot g \cdot \zeta_a^2 \cdot L_{eff} \quad (4-1)$$

$$\overline{F}_{wd_irr} = \frac{1}{16} \cdot \rho_w \cdot g \cdot H_s^2 \cdot L_{eff} \quad (4-2)$$

where ρ_w is the sea water density, g is the gravity, ζ_a is the wave amplitude of a regular wave, H_s is the significant wave height representing a sea state while L_{eff} is the width of the iceberg perpendicular to the incoming waves. For circular icebergs, L_{eff} will be the diameter while for tabular icebergs, L_{eff} will be the iceberg width in surge motion or iceberg length in sway motion.

When the wave lengths are short relatively to the iceberg lengths ($\lambda < L$) it is likely that more or less all of the incoming wave is reflected in some direction by the iceberg. In such situations, Eqs. (4-1) and (4-2) will be more or less correct for the tabular iceberg shapes as long as they are oriented with either parallel or perpendicular to the incoming waves. For circular icebergs, only a portion of the incoming waves will be reflected in opposite direction thus the wave drift force will be somewhat reduced compared to Eq. (4-1) and Eq. (4-2). For longer wave lengths however, both cancelation and resonance effects may occur in heave, pitch and roll motions contributing to changes in the wetted iceberg surface and thus also changes in the wave drift speeds. Such effects should be captured in the wave drift coefficient, C_{wd} and used as a correction to the forces from Eqs.(4-1) and (4-2):

$$C_{wd} = \frac{\overline{F}_{wd}}{\frac{1}{2} \cdot \rho_w \cdot g \cdot \zeta_a^2 \cdot L_{eff}} \quad (4-3)$$

During the tank model tests, which are presented in Section 4.1.2, little attention was given to resonance or cancellation effects and the value of the results would therefore be limited. In order to provide more reliable formulations for the C_{wd} , the advanced wave-structure interaction software, WAMIT was applied (WAMIT Inc., 2006). WAMIT use potential theory and calculates the wave drift in accordance to the formulations presented in Section 4.1.2. However, as WAMIT also calculates the iceberg motions exerted by the incoming waves, all dynamic effects are included in the calculation of wave drift forces.

Figure 4-1 shows C_{wd} as a function of a size parameter $\left(\frac{L}{\lambda}\right)$ based on the 3 cylindrical models that were used in the tank tests. Correspondingly Figure 4-1b shows C_{wd} for the tabular icebergs in surge motions. With respect to the tabular iceberg models, it should be noted that during more or less all of the tests, the icebergs would tend to orient themselves with their short axis perpendicular to the incoming waves.

With respect to the wave drift coefficient it is also important to note that the following assumptions have been made:

- Deep water ($\frac{Depth}{\lambda} > 0.5$)
- The wave steepness is not important with respect to wave drift
- The ratio between iceberg draft and length is not important with respect to wave drift

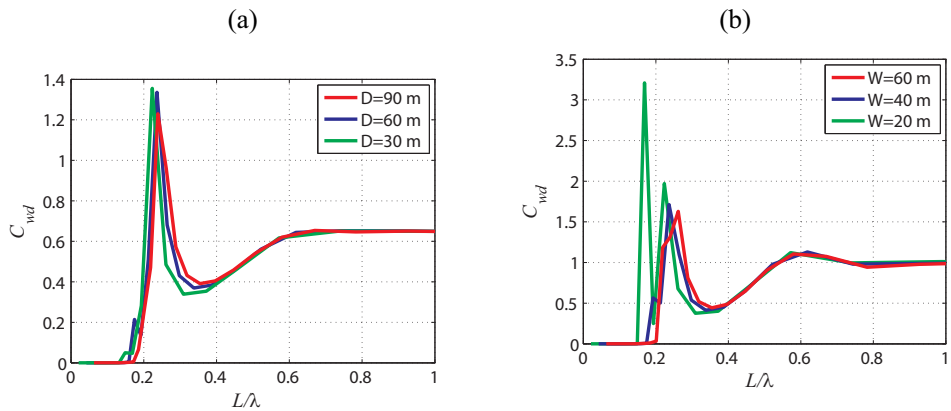


Figure 4-1. Wave drift coefficient as a function of size parameter for a) cylindrical icebergs with diameters of 30, 60 and 90 m and b) tabular icebergs with widths of 20, 40 and 60 m. Based on numerical calculations in WAMIT.

As can be seen from Figure 4-1, there are only minor variations in C_{wd} for the various iceberg sizes. In order to establish expressions which can be used in numerical iceberg drift models, two functions were fitted visually to the WAMIT results for cylindrical and tabular icebergs. These functions are presented in Eqs. (4-4) and (4-5) respectively. A comparison between WAMIT results, the proposed empirical functions and results from tank model tests are shown in Figure 4-2 and Figure 4-3. It can be seen that there is a fairly good agreement between WAMIT calculations and the coefficients from the model tests and further that the formulations in Eqs. (4-4) and (4-5) provide a good representation of C_{wd} . Eqs. (4-6) to (4-9) present functions which are included in

Eqs. (4-4) and (4-5) and which take into account resonance and cancelation effects in the wave drift.

$$C_{wd_cyl} = 0.40 \tan^{-1} \left(\frac{\pi}{2} \exp \left[-20 + 100 \frac{L}{\lambda} \right] \right) + C_{add_cyl} \quad (4-4)$$

$$C_{wd_tab} = 0.62 \tan^{-1} \left(\frac{\pi}{2} \exp \left[-20 + 100 \frac{L}{\lambda} \right] \right) + C_{add_tab} \quad (4-5)$$

where

$$C_{add_cyl} = -870 \cdot \left(\frac{L}{\lambda} \right)^2 + 470 \cdot \frac{L}{\lambda} - 50 \quad \text{if} \quad 0.21 < \frac{L}{\lambda} < 0.27 \quad (4-6)$$

$$C_{add_cyl} = 13.018 \cdot \left(\frac{L}{\lambda} \right)^2 - 10.414 \cdot \frac{L}{\lambda} + 1.863 \quad \text{if} \quad 0.27 < \frac{L}{\lambda} < 0.53 \quad (4-7)$$

and

$$C_{add_tab} = -497.96 \cdot \left(\frac{L}{\lambda} \right)^2 + 248.98 \cdot \frac{L}{\lambda} - 30.512 \quad \text{if} \quad 0.215 < \frac{L}{\lambda} < 0.285 \quad (4-8)$$

$$C_{add_tab} = 55.882 \cdot \left(\frac{L}{\lambda} \right)^2 - 43.309 \cdot \frac{L}{\lambda} + 7.804 \quad \text{if} \quad 0.285 < \frac{L}{\lambda} < 0.49 \quad (4-9)$$

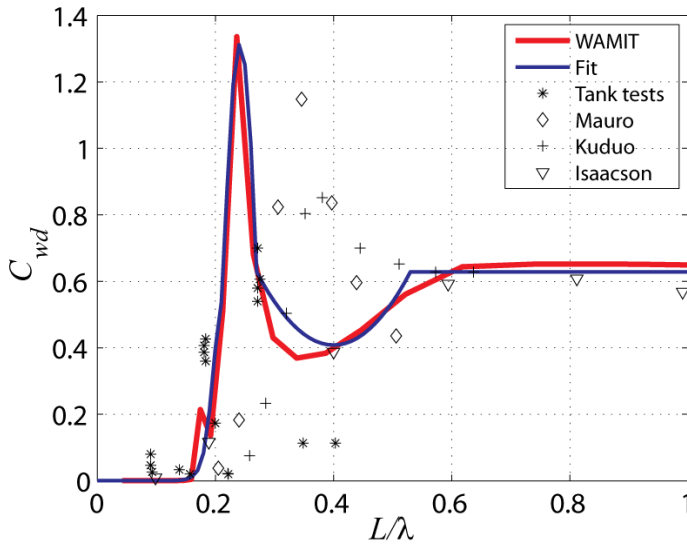


Figure 4-2. Wave drift coefficient versus size parameter based on numerical results from WAMIT for a cylindrical iceberg with diameter 60 m, a function fitted to WAMIT data and data from physical tank model tests. In addition results from analysis of Mauro (1960), experiments and analysis of Kudou (1977) and numerical calculations of Isaacson (1988) are included.

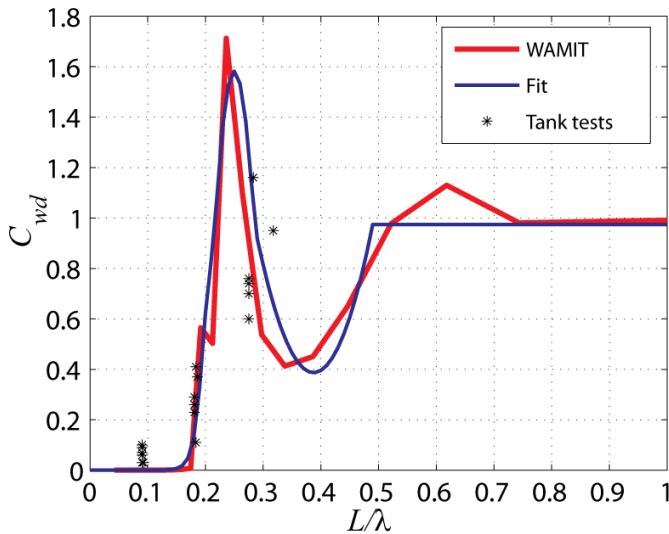


Figure 4-3. Wave drift coefficient versus size parameter based on numerical results from WAMIT for a tabular iceberg with length 60 m and width 40 m, a function fitted to WAMIT data and data from physical tank model tests.

4.2 Iceberg deterioration



Iceberg Deterioration in the Barents Sea

Kenneth Eik^{1,2}

¹StatoilHydro, Trondheim, NORWAY

²Norwegian University of Science and Technology

ABSTRACT

An iceberg drift model for the Barents Sea has been developed and the iceberg deterioration model developed by the Canadian Hydraulics Centre (CHC) has been implemented within the iceberg drift model. The deterioration model includes contributions from wave erosion, calving, solar radiation, buoyant convection and forced convection. The model relies on wave and wind data from the Norwegian hindcast archive and regional temperature and salinity recordings. Iceberg drift simulations in the Shtokman region show that wave erosion process is the main contribution to iceberg deterioration causing almost 71% of the mass reduction. Forced convection on the submerged part of the iceberg is the second most important contribution to the deterioration causing 18% of the reduction. Further, calving, which is a consequence of the wave erosion, explains about 8% of the reduction. While reduction in length of icebergs drifting in open waters may be several meters pr day, the deterioration of icebergs embedded in sea ice is limited and generally less than 25 cm/day.

A sensitivity study reveals that the sea surface temperature that affects both wave erosion and forced convection, is the most important parameter with respect to iceberg deterioration. Also significant wave height with associated wave period and iceberg lengths are important for the deterioration. As a part of an ice management system, logging of these parameters will be important in order to estimate the size of the iceberg when it later approaches the iceberg prevention zone.

Calculations of mass loss from the wave erosion model has been compared with physical measured mass loss in a model test. Results indicate that the physical mass loss may be even more severe than estimated from the model. Further work should aim to verify the deterioration model skills in the Barents Sea. For instance, in situ observations and monitoring of real icebergs over one or two weeks would provide important information.

INTRODUCTION

Icebergs are a concern for offshore installations in several Arctic regions such as the East Coast of Canada, East and West Greenland, the Barents Sea and the Kara Sea. So far, permanent installations have only been installed at Grand Banks offshore Canada while the remaining regions are considered as potential candidates for future oil and gas developments. The Central part of the Barents Sea is considered to be the next gas province by the development of the Shtokman field.

The partners developing the Shtokman field have the advantage by benefitting from experiences and technology developed for the Grand Banks fields. With respect to the iceberg threat, operational models both for iceberg drift and for iceberg deterioration have been developed by Canadian Institutes. This study focuses on the CHC model for iceberg deterioration (Kubat et al., 2007) and how applicable this will be in the Barents Sea. Empirical relations of the deterioration mechanisms have been implemented in an iceberg drift model for the Barents Sea (Eik, 2009) and local metocean data such as winds, waves, currents, ice and water temperatures have been used in the deterioration calculations.

The paper starts with a brief presentation of the iceberg drift model and how this has been applied in the simulations for this study. Further, a more comprehensive description of the deterioration model is included with emphasis on the applied metocean inputs. Drift simulations of 8000 icebergs in the Shtokman region during the period 1987-1992 have been performed and deterioration has been calculated every 2nd hour for all icebergs. The relative importance of the various deterioration contributions has been identified.

In order to identify which metocean parameters are most important for the deterioration, a sensitivity study has been conducted. The results are included but not details regarding the methodology. A proper reference is included for those interested in the details.

In lack of physical deterioration measurements from the Barents Sea, wave erosion calculated by the model has been compared with wave erosion loss measured in a physical wave tank in 1990.

All results are discussed and the conclusions presented. All relevant references are provided in the last section.

ICEBERG DRIFT MODEL AND SIMULATIONS

The iceberg drift model is well described in Johannessen (1999) and validated in Eik (2009) so only a brief description is provided herein. The drift of icebergs is calculated by modelling icebergs as rectangular bodies forced by winds, waves, currents, sea ice and Coriolis acceleration. The movement is found by balancing the forces with the product of mass and accelerations in accordance to Newton's 2nd law:

$$m \frac{d\mathbf{V}_i}{dt} = -mf\mathbf{k} \times \mathbf{V}_i + \mathbf{F}_a + \mathbf{F}_w + \mathbf{F}_{wd} + \mathbf{F}_{si} + \mathbf{F}_p \quad (1)$$

where $m=m_0(1+C_m)$ and m_0 is the physical mass and C_m is the coefficient of added mass. \mathbf{V}_i is the local velocity of the iceberg, $-f\mathbf{k} \times \mathbf{V}_i$ is the Coriolis parameter and \mathbf{k} is the unit vector in vertical direction. Further, $\mathbf{F}_{a,w}$ are the air and water form drag, respectively. \mathbf{F}_{wd} is the mean wave drift force, \mathbf{F}_{si} is the sea-ice drag and \mathbf{F}_p is the horizontal gradient force exerted by the water on the volume that the iceberg displaces.

In this work, icebergs were distributed along the border of a 73105 km² large area, denoted as the Shtokman region (Figure 1a). All icebergs were randomly given a start time within the period

1987-1992 before simulations were started. Simulations were carried out with an update of metocean parameters every 2nd hour. At every 2nd hour, the deterioration was calculated and the iceberg size was updated. The simulations would be stopped if the simulation time exceeded 50 days, if the iceberg grounded or if the iceberg left the Shtokman region.

It is well documented that the majority of icebergs in the Central Barents Sea originates from Franz Josef Land, alternatively Svalbard, the Northern Part of Novaya Zemlya, Kara Sea (not Kara gate) or the Arctic Ocean. Due to this 75% of all simulated icebergs were distributed uniformly along the northern boundary of the Shtokman region. Further, 12% of all icebergs were distributed along the western and eastern border of the region. The last 1% of the icebergs were started at the southern border of the region, uniformly distributed along the border (Figure 1b).

In total, 20 000 iceberg simulations were started but only 8000 of these entered the Shtokman region. Results in this presentation are based on these 8000 simulations.

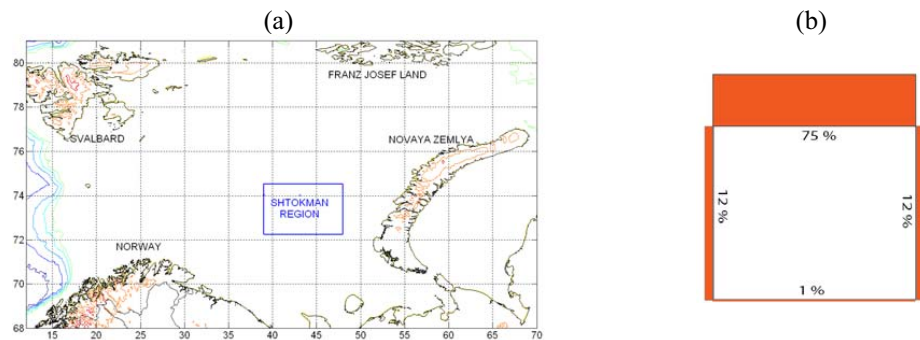


Figure 1. a) Map of the Barents Sea and the Shtokman region (72.25°N – 74.50°N, 39.0°E-48.0°E) and b) Illustration showing percentage of iceberg simulations that were started along each border of the Shtokman region.

DETERIORATION MODEL AND METOCEAN DATA IN THE BARENTS SEA

The iceberg deterioration model that has been applied is the same model as presented by Kubat et al. (2007). However, with respect to the required input parameters, local metocean data from the Barents Sea has been applied. The following sections present the deterioration terms included in the model and specify which input data that has been applied in the Barents Sea simulations.

All contributions to deterioration (except of calving of overhanging slabs) are generally expressed as reduction in iceberg water line length (L). The reduction in iceberg width and iceberg draft is implicitly expressed through the reduction in L since the mass of the icebergs are given by the following formula:

$$M = C_b \cdot \rho_i \cdot L^3 \quad (1)$$

where M is the iceberg mass, C_b is a block coefficient and ρ_i is the ice density. A value of 0.45 is recommended for the block coefficient by Kubat et al. (2007). However, in the present study

statistics for iceberg lengths, and iceberg sail height based on observations in the Barents Sea have been applied. The iceberg widths (W), which are measured perpendicular to the lengths, have been assumed to be 2/3 of the lengths. For each simulated iceberg, the block coefficient has been calculated and further used in order to estimate iceberg mass loss per time unit. Table 1 shows average value and a 90% confidence interval for the block coefficient for icebergs in the Central Barents Sea.

Table 1. Mean value and a 90% confidence interval for iceberg block coefficient in the Central Barents Sea

	Block coefficient, C_b [-]
Mean value	0.38
P5	0.25
P95	0.54

The total iceberg deterioration per time step is found by summing up the reductions caused by solar radiation (V_s), buoyant vertical convection (V_b), forced convection to air and water (V_f), wave erosion (V_{we}) and wave calving (V_{cal}):

$$V_{total} = V_s + V_b + V_{f\ air} + V_{f\ water} + V_{we} + V_{cal} \quad (2)$$

Surface melting due to solar radiation

The following expression recommended by Savage (2001) was used for estimating melting caused by incoming solar radiation (insolation):

$$V_s = \frac{I}{\Gamma \cdot \rho_i} (1 - \alpha) \quad (3)$$

where Γ is the latent heat of melting of ice ($3.34 \cdot 10^5$ J/kg) and α is the iceberg surface albedo. An average value of 0.55 seems reasonable for iceberg albedo in the Barents Sea (Løset, 1992). The insolation, I , varies both seasonally and geographically. In lack of site specific data, measurements from the Labrador Sea have been applied and vary from $1.26 \cdot 10^6$ J/m²/day in January to $17.57 \cdot 10^6$ J/m²/day in July (De Jong, 1973). Values for the remaining months are found by linear interpolation. It should be noted that insolation used by Løset (1992) indicate that these values may be too high for the Central Barents Sea. The density of the glacial ice, ρ_i was set to 910 kg/m³ in all calculations.

Melting due to buoyant vertical convection

The difference between the freezing point temperature, T_{fp} and far field water temperature, T_∞ as given by Neshyba and Josberger (1979) was used to estimate the melt rate due to buoyant vertical convection (Eq. 4).

$$V_b = 2.78 \cdot (\Delta T) + 0.47 \cdot (\Delta T)^2 \quad (4)$$

where $\Delta T = T_\infty - T_{fp}$. It is important to note that Eq. (4) gives loss in length (L) per year. For the far field water temperature, monthly average values for surface temperatures (water depths in the range 0-5 m) from the Shtokman region have been used (Figure 2). The sea surface temperature data are based on statistics from the World Ocean Database 2001 and approximately 2400 temperature records have been applied (National Oceanographic Data Center, 2001). Values for T_{fp} are found by applying the equations recommended by Josberger (1977) (Eq. 5) and Løset (1993) (Eq.6).

$$T_{fp} = T_f(S) \cdot e^{-0.19 \cdot (T_\infty - T_f(S))} \quad (5)$$

$$T_f(S) = -0.036 - 0.0499 \cdot S - 0.000112 \cdot S^2 \quad (6)$$

S is the sea water salinity and $T_f(S)$ is the sea water freezing temperature based on the salinity. By using (Eq. 5) it is taken into account that the sea water surrounding the iceberg will mix with the fresh water that has melted from the iceberg. In accordance to the records from the World Ocean Database (National Oceanic Data Center, 2001) salinity in the surface layer in the Shokman region should be around 34.8 PSU.

Forced convection

Forced convection both due to influence of water currents and winds are taken into account. The forced convection can, in accordance to Kubat et al. (2007) be expressed as:

$$V_f = \frac{q_f}{\rho_i \cdot \Gamma} \quad (7)$$

where q_f is the heat flux

$$q_f = Nu \cdot k \cdot \frac{\Delta T}{L} \quad (8)$$

and k is the thermal conductivity of the fluid while ΔT in the case of convection to air is the difference between air temperature and iceberg surface temperature. Average monthly air temperatures and iceberg surface temperatures are shown in Figure 2. Nu is the Nusselt number:

$$Nu = C \cdot Re^{0.8} \cdot Pr^{0.4} \quad (9)$$

where C is 0.058 in accordance to Kubat et al. (2007). Re is the Reynolds number (Eq. 10a) and Pr is the Prandtl number (Eq. 10b).

$$Re = V_r \cdot \frac{L}{\nu} \quad (10a)$$

$$Pr = \frac{\nu}{k_f} \quad (10b)$$

V_r is the relative velocity between fluid and iceberg, ν is the kinematic viscosity and k_f is the thermal diffusivity. The values applied for k , ν and k_f are presented in Table 1. In calculations of forced convection in the sea water, sea surface currents at the iceberg location are based on model data from a coupled ice ocean numerical model (Keghouche et al., 2007). Further, current speeds have been adjusted based on the methodology presented by Eik (2009). With respect to forced convection caused by winds, the iceberg drift velocity has been neglected as it is very small compared to the wind speed. The wind speed is found from the Norwegian hindcast archive, grid point 640 (Reistad and Iden, 1998).

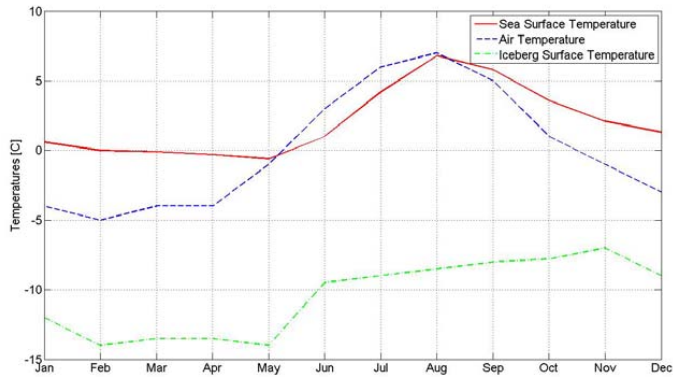


Figure 2. Average monthly values for i) Sea Surface Temperature (National Oceanic Data Center, 2001), ii) Air Temperature (European Centre for Medium-Range Weather Forecasts, 2009) and iii) Iceberg Surface Temperature (Løset, 1993).

Table 1. Viscosity, conductivity and diffusivity used in the iceberg deterioration model.

Parameter	Notation	Value
Kinematic viscosity – sea water	ν_{water}	$1.6438 \cdot 10^{-6}$ [m ² /s]
Kinematic viscosity – air	ν_{air}	$1.32 \cdot 10^{-5}$ [m ² /s]
Thermal conductivity – sea water	k_{water}	0.6 [W/mK]
Thermal conductivity – air	k_{air}	0.025 [W/mK]
Thermal diffusivity – sea water	$k_{f\ water}$	$1.37 \cdot 10^{-7}$ [m ² /s] NB! Only valid for salinity 35 PPU and temperature 0°C
Thermal diffusivity– air	$k_{f\ air}$	$D1 \cdot (273 + T_{air})^2 + D2 \cdot (273 + T_{air}) - D3$ [m ² /s] $D1 = 9.1018 \cdot 10^{-11}$ $D2 = 8.8197 \cdot 10^{-8}$ $D3 = 1.0654 \cdot 10^{-5}$

Wave erosion

In accordance to White et al. (1980), the waterline melt rate for the case of a rough wall can be expressed as:

$$V_{we_waterline} = 0.000146 \left(\frac{R}{H} \right)^{0.2} \cdot \left(\frac{H}{\tau} \right) \cdot \Delta T \quad (11)$$

where R is the roughness height of the ice surface (0.01 m) while H and τ are mean wave height and wave period respectively¹. Wave data are taken from the Norwegian hindcast archive, Winch grid point 640 (Reistad and Iden, 1998). This formulation of waterline melt rate (Eq. 11) is only used as input in calculations of calving interval as is done in the model described by Kubat et al. (2007).

In order to estimate wave erosion for the entire iceberg, it must be taken into account that wave actions cause forced convection over the entire depth of the iceberg. Based on linear wave theory, White et al. (1980) established the following expression for total wave erosion:

$$\overline{V_{we}}' = 5.22 \cdot 10^{-6} \cdot \Delta T \cdot g \cdot H \cdot \tau \cdot P \cdot \left(\frac{R}{H} \right)^{0.2} \quad (12)$$

where $\overline{V_{we}}'$ is the total rate of volume loss due to wave erosion. $P \approx 3L$ is the waterline perimeter and L is the waterline length. Further, by use of Eq. (1) the rate of volume loss may be expressed as:

$$\overline{V_{we}}' = 3 \cdot C_b \cdot L^2 \frac{dL}{dt} \quad (13)$$

Consequently the waterline melt rate due to wave erosion which is used in the model is expressed as:

$$V_{we} = 5.22 \cdot 10^{-6} \cdot \frac{\Delta T \cdot g \cdot H \cdot \tau \cdot P}{3 \cdot C_b \cdot L^2} \left(\frac{R}{H} \right)^{0.2} \quad (14)$$

Calving

Due to wave erosion in the waterline, overhanging slabs of ice are developed on the icebergs. As the erosion progresses, a notch at the waterline deepens and the size of the overhanging slab increases and eventually collapse when the bending stresses cause fracture. White et al. (1980) developed the following expression for critical length of an overhanging slab at which fracture (calving) occurs:

¹ Mean wave height: $H = 0.63 \cdot H_s$ (Significant wave height)

Mean wave period: $\tau = 0.7143 \cdot T_p$ (Spectral peak period). NB! The formulation is based on the assumption that the wave energy may be described by a PM spectrum.

$$F_l = 0.33 \cdot (37.5 \cdot H + h^2)^{\frac{1}{2}} \quad (15)$$

where h is the thickness of the overhanging slab (in metres). Savage (1999) studied the overhanging ice geometry and established an expression for the slab thickness, h , as a function of the iceberg length, L .

$$h = 0.196 \cdot L \quad (16)$$

Savage (1999) analysed the shape of the overhanging ice and established an expression for the calved ice volume, \overline{V}_c :

$$\overline{V}_c = 0.64 \cdot L \cdot F_l \cdot h \quad (17)$$

The calving interval, t_c , is estimated by considering the ratio between critical length and reduction in waterline length caused by wave erosion (Eq. 11):

$$t_c = \frac{F_l}{V_{we_waterline}} \quad (18)$$

The mass loss per time step in the simulation model is found by:

$$\frac{dM}{dt} = \frac{\overline{V}_c}{t_c} \cdot \rho_i \quad (19)$$

The reduction in L per time unit is found by using Eq. (1) with updated mass after each time step. By doing so, the deterioration due to calving, V_{cal} , is smoothed in time in the model.

RESULTS FROM SIMULATIONS IN THE SHTOKMAN REGION

Based on all the simulations, reduction in iceberg waterline length was stored at each time step. Further, these data were converted to represent reduction in iceberg waterline length per hour. Figure 3a shows the distribution of the reduction rate from these data. The difference between median (P50) and mean deterioration should be noted. This difference is explained by the relatively “fat” tail in the deterioration distribution which indicates that some icebergs in a few occasions are subjected to extremely rapid deterioration. The maximum deterioration in the calculations was 3.7 m/h. Figure 3b shows mean deterioration and 95 percentile per month based on the same data. Statistics from icebergs drifting surrounded by sea ice were also generated based on the model simulations. It was found that the average deterioration rate in ice was 18 cm/day while the 95 percentile was 24 cm/day.

Table 2 shows the individual deterioration contributions from the all deterioration processes included in the model. Since the wave erosion together with the calving impose the most significant deterioration contribution, a scatter diagram showing deterioration rate versus significant wave height is included in Figure 4a. The correlation coefficient between iceberg

deterioration rate and significant wave height was calculated to 0.39. Similar scatter plots were made in order to investigate the importance of iceberg length, water temperature and relative drift speed on the deterioration rate, respectively (Figure 4, b-d). It was found that only the minor icebergs (length less than 50 m) experienced high deterioration rates. For larger icebergs a small negative correlation between length and deterioration rate is indicated.

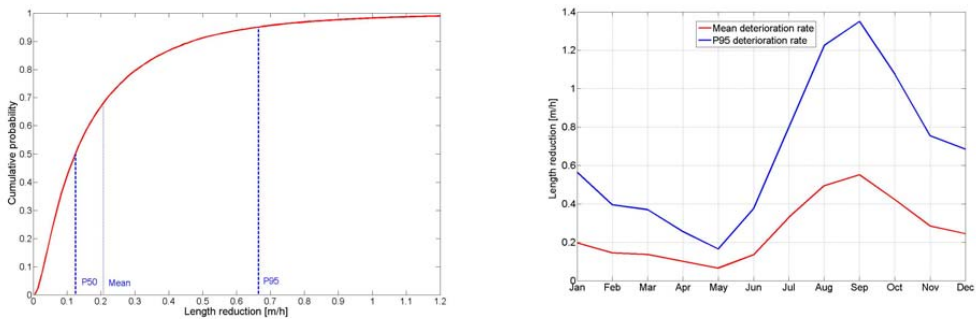


Figure 3. Deterioration based on data from iceberg drift simulations a) Cumulative distributions for deterioration rate. Median, average and 95 percentile are shown. b) Average and 95 percentile deterioration rate per month.

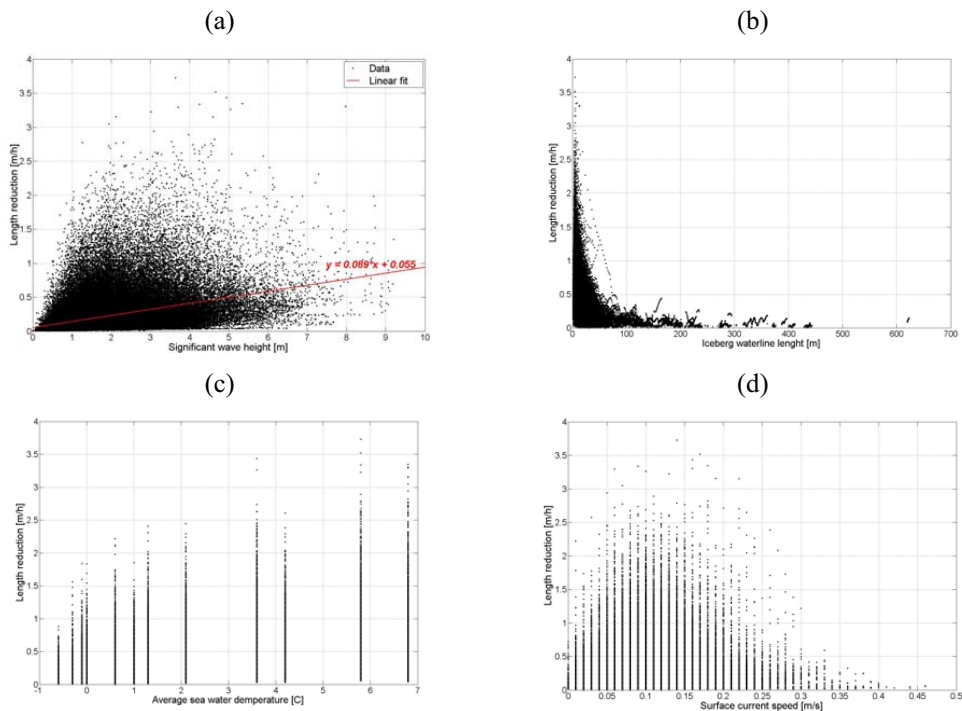


Figure 4. Scatter plots of iceberg deterioration rates and simultaneous values for a) significant wave height, b) iceberg length, c) sea surface temperature and d) surrounding current speed.

Table 2. Contributions to total deterioration (in %) from processes included in the iceberg deterioration model.

Process	Relative contribution (%) Barents Sea Model	Relative contribution (%) Labrador and Grand Banks (El-Tahan et al., 1987)
Solar radiation	0.9	2.8
Buoyant vertical convection	1.0	1.4
Forced convection - air	0.4	1.4
Forced convection - water	18.0	16.2
Wave erosion	71.3	61.3
Calving	8.4	16.8

SENSITIVITY STUDY

Even though the wave erosion was identified as the main contributor to the iceberg deterioration, the importance of each metocean parameter is not evident. In order to investigate the importance of the parameters contributing to iceberg deterioration, a two-level factorial design was carried out. The methodology, which is well described by Box et al. (1978), is based on a number of simulations where all variables are set to either a low or high level. Only variables which are expected to be of importance are included in the analysis. Based on the results presented in Table 2 and the formulations in Eqs. (1-19), the following four variables were selected:

- Iceberg waterline length (L)
- Sea surface temperature (T_{∞})
- Significant wave height (H_s)
- Relative drift speed between iceberg and water current (V_r)

Each variable was given either a high or a low value and the reduction in iceberg length per hour was calculated for totally 2^4 possible combinations of these variables. All other variables were kept constant. For all parameters, except L , the low levels were corresponding to a 90% exceedance probability level in the Central Barents Sea. All the high levels were correspondingly referring to a 10% probability level of exceedance. It is commented by Kubat et al. (2007) that formulations for wave erosion are not valid for bergy bits and growlers. As approximately 70% of the glacial ice observations in the Central Barents Sea refer to icebergs with lengths 30 m or less, the selection for high and low level iceberg length was done without considering probability of occurrence. Table 3 shows the combinations of the variables and calculated deterioration rates.

Table 3. Selection of test parameters and test results

Combination no.	L [m]	T_{∞} [°C]	H_s [m]	V_r [m/s]	Deterioration rate [cm/h]
1	80	-1.5	1	0.1	0.47
2	80	-1.5	1	0.3	0.59
3	80	-1.5	4	0.1	1.31
4	80	9	1	0.1	14.01
5	300	-1.5	1	0.1	0.29
6	80	-1.5	4	0.3	1.43
7	80	9	1	0.3	18.06
8	300	-1.5	1	0.3	0.38
9	80	9	4	0.1	43.18
10	300	-1.5	4	0.1	0.58
11	300	9	1	0.1	8.12
12	80	9	4	0.3	47.23
13	300	-1.5	4	0.3	0.29
14	300	9	1	0.3	11.23
15	300	9	4	0.1	18.16
16	300	9	4	0.3	21.27
<i>Average</i>					11.66

Further, the main effect of each parameter and interaction effects were calculated. All effects that are of comparable size as mean deterioration rate may be suspected to have a significant impact on the resulting deterioration rate. Table 4 shows all main and interaction effects from these tests. Details on how the calculations are done, can be found in Box et al. (1978). From Table 4, it can be seen that the effect from T_{∞} is most significant. Also H_s and L are considered to have a significant effect while V_r has little effect. With respect to interactions, it can be seen that both interactions $L \times T_{\infty}$ and $T_{\infty} \times H_s$ may be suspected to have significant effects. In order to confirm or refute these results all effects were plotted in a normal probability distribution plot (Figure 5). Outliers from a straight line in such a plot reveal the significant effects. The one evident outlier in Figure 5 corresponds to the effect of T_{∞} while the other effects are less obvious.

Table 4. Calculated effects

Mean effects		2-factor interactions		3-factor interactions		4-factor interaction	
L	-8.25	$L \times T_{\infty}$	-7.68	$L \times T_{\infty} \times H_s$	-4.6	$L \times T_{\infty} \times H_s \times V_r$	0.05
T_{∞}	21.99	$L \times H_s$	-4.97	$L \times T_{\infty} \times V_r$	-0.18		
H_s	10.04	$L \times V_r$	-0.29	$L \times H_s \times V_r$	-0.05		
V_r	1.80	$T_{\infty} \times H_s$	9.57	$T_{\infty} \times H_s \times V_r$	0.05		
		$T_{\infty} \times V_r$	1.79				
		$H_s \times V_r$	-0.05				

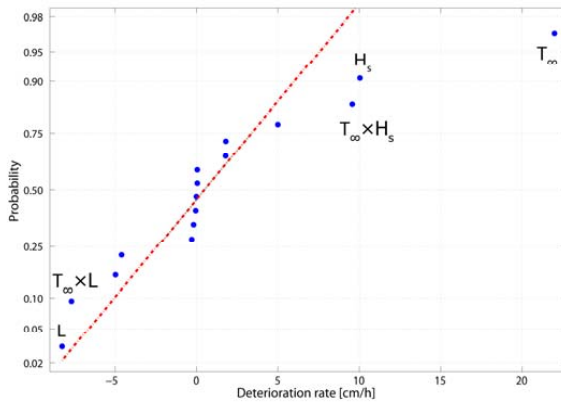


Figure 5. Normal probability plot of effects.

VALIDATION OF WAVE EROSION MODEL – TANK MODEL TESTS

As wave erosion seems to be the most important contribution to deterioration on icebergs drifting in open water, results from the model have been compared to physically measured wave erosion on an ice block in a wave tank. A tank model test was conducted in 1990 at the Marine Civil Engineering Group's tank at NTNU in Trondheim, Norway. Figure 6 shows the ice block and dimension before and after the tests. Table 5 shows details with respect to temperatures, wave heights and mass loss. The same set of input was converted to "full scale" data and a deterioration simulation was done with the model recommended by White et al., 1980 Eq. (12). Froude scaling and geometrical similarity was applied with scale factor 200. In accordance to the tank tests, the total mass loss in relation to the initial mass was 34%. Unfortunately, the wave period during the experiments is not known. By assuming average wave periods of 7 s, 10 s and 13 s, the percentage mass loss due to wave erosion was calculated to 18%, 26% and 33%, respectively. For the wave height specified in Table 5, a corresponding zero up-crossing wave periods would normally be around 7-8 seconds.

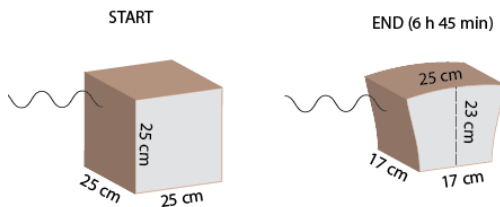


Figure 6. Shape and dimensions of ice block in tank tests before and after being exposed to waves. The final shape is very approximate!

Table 5. Specifications of initial dimensions and parameters in wave tank tests. Scale is 1:200.

Parameter	Model scale	Full scale
Temperature - sea water	-0.5 [°C]	
Salinity - sea water	30.5 [‰]	
Density – sea water	1024.5 [kg]	
Density – ice	925 [kg/m ³]	
Freezing point temperature	-1.3 [°C]	
Iceberg length	25 [cm]	50 [m]
Iceberg sail height	2.4 [cm]	4.9 [m]
Wave Height	2.9 [cm]	5.7 [m]
Wave Period	3.2 [s] (guess)	10 [s] (guess)
Duration of experiment	6h 45 min	95.5 [h]
Mass of ice block prior to tests	14.45 [kg]	115 625 [tons]
Mass of ice block after tests	9.53 [kg]	76 265 [tons]

DISCUSSION

The relative importance of the various deterioration processes (Table 2) are in good agreement with findings from the Labrador Sea and Grand Banks as reported by El-Tahan et al. (1987). It is noted, however, that the contribution from wave erosion is even more significant in the presented model while the mass loss due to calving is less significant. One possible explanation to this is that the sea surface temperatures in the model have been slightly higher than average for the three icebergs reported by El-Tahan et al. (1987) while the wave heights may have been lower. It is also likely that there are differences in both temperatures and wave climate which may explain differences in deterioration contributions in the various regions.

The correlation between sea surface temperature and iceberg deterioration is evident both by considering the monthly deterioration statistics as well as the results from the sensitivity study. Also the wave heights (and associated wave periods) are of importance. However, as the waves in the Barents Sea in general are more severe during the winter, one would expect higher deterioration during the winter time. As shown in Figure 3b, this is not the case and indicates once more that the sea surface temperature is more important. These observations are also supported by the results in the sensitivity study.

With respect to iceberg size, it is reported by Savage (2001) that the expressions for wave erosion are not applicable for icebergs with length less than 20 m. The reason for this is that the small icebergs are expected to be carried along with the wave motion to a larger extend than larger icebergs. This has not been taken into account in the presented model and the results showing high deterioration rates for the smallest icebergs are probably not correct. The strong increase in deterioration for icebergs with length even up to 80 m may indicate that the wave erosion is over estimated even for icebergs larger than bergy bits. Further work should focus on implementing more relevant formulations for deterioration of small icebergs.

With respect to ice management operations in connection with oil and gas developments in Arctic waters, the ability to estimate iceberg deterioration will be of strategic importance. By monitoring the important parameters such as sea surface temperatures, wave heights and periods, current speed etc. good estimates for iceberg sizes may be achieved at an early stage. This type of

information will be useful when considering methodology for iceberg deflection, which vessels to use and sometimes the number of vessels required for towing operations.

The comparison between wave erosion in tank and from the simulation model indicates that the wave erosion at least not is overestimating the real erosion. Unfortunately, there are too many uncertainties connected to the physical experiment in order to rely fully on these results. Even if the iceberg deterioration model applied in the Barents Sea indicate similar results as at the East Coast of Canada, a thorough validation of all terms should be conducted. This can be done by monitoring real icebergs in the Barents Sea, or other relevant seas, and simultaneous metocean parameters.

CONCLUSIONS

An iceberg deterioration model has been implemented in a numerical iceberg drift model for the Barents Sea. Simulations carried out in the Central Barents Sea show that the wave erosion is the primary cause for deterioration (71%) followed by forced convection to water (18%) and calving (8%). Forced convection to air, deterioration due to solar radiation and buoyant convection provide only minor contributions to the total iceberg deterioration.

A sensitivity study shows that the most important parameter with respect to iceberg deterioration is the sea surface temperature. Also wave height (and associated wave period) as well as iceberg lengths are of significant importance. The deterioration rate increases for decreasing iceberg size. For small icebergs (length less than 80 m) the expressions for wave erosion are over probably overestimated.

Further work should focus on comparing model results with data from real iceberg deterioration monitoring.

REFERENCES

- Box, G. E. P., Hunter, W. G., Hunter, J. S. (1978). Statistics for Experimenters: An Introduction to Design, Data Analysis and Model Building, Chapter 10, John Wiley & Sons, ISBN 0-471-09315-7.
- De Jong, B. (1973). Net Radiation Received by a Horizontal Surface at the Earth, Delft University Press, Rotterdam, Netherland, 55 p.
- Eik, K. (2009). Iceberg Drift Modelling and Validation of Applied Metocean Hindcast Data, *Cold Regions Science and Technology* (in press).
- El_Tahan, M., Venkatesh, S. and El-Tahan, H. (1987). Validation and Quantitative Assessment of the Deterioration Mechanisms of Icebergs, *J. Offshore Mech. Arctic Eng.*, 109, pp. 102-108.
- European Centre for Medium-Range Weather Forecasts (2009). ECMWF 40 Re-analysis – Data Archive 1957-2002, <http://www.ecmwf.int/>, cited March 2009.
- Johannessen, K., Løset, S. and Strass, P. (1999). Simulation of Iceberg Drift. *Proceedings 15th International conference on Port and Ocean Engineering under Arctic Conditions*, POAC'99, Helsinki, Finland, pp. 97–105.
- Josberger, E.G. (1977). A Laboratory and Field Study of Iceberg Deterioration, *Proceeding of the first International Conference on Iceberg Utilization*, New York, USA, pp 245-264.
- Keghouche, I., Bertino, L. and Sandven, S. 2007. Iceberg Modelling in the Barents Sea: Part I, initial Tests. NERSC Tech. Rep. 280.
- Kubat, I., Sayed, M., Savage, S. B., Carrieres, T. and Crocker, C. (2007). An Operational Iceberg Deterioration Model, *Proceedings of the Seventeenth International Offshore and Polar Engineering Conference*, Lisbon, Portugal, July 1-6, 2007, pp. 652 – 657.
- Løset, S. (1993). Numerical Modelling of the Temperature Distribution in Tabular Icebergs, *Cold Regions Science and Technology* 21, pp 103-115.
- Løset, S. (1992). Heat Exchange at the Air Exposed Surface of Icebergs, *Proceedings of the IAHR 11th International Symposium on Ice*, Alberta, Canada, pp.
- National Oceanographic Data Center (2001). World Ocean Database 2001, http://www.nodc.noaa.gov/OC5/WOD05/pr_wod05.html
- Neshyba, S. and Josberger, E.G. (1979). On the Estimation of Antarctic iceberg melt rate, *Iceberg Dynamics Symposium*, St. John's Newfoundland, June 4-5, 1979.
- Reistad, M. and Iden, K. (1998). Updating, Correction and Evaluation of a Hindcast Data Base of Air Pressure, Wind and Waves for the North Sea, the Norwegian Sea and the Barents Sea. Norwegian Meteorological Institute, Research report No. 9, 1998.
- Savage, S. B. (2001). Aspects of iceberg deterioration and drift. *Lecture Notes in Physics Series: Geomorphological Fluid Mechanics*. N. J. Balmforth and P. A. Berlin, Springer-Verlag 582, pp. 279-318.
- Savage, S.B. (1999). Analyses for iceberg drift and deterioration code development, Technical report 99-03 prepared for Canadian Ice Service, Contract KM149-9-85-035, 50 p.
- White, F.M., Spaulding, M.L. and Gominho, L. (1980). Theoretical Estimates of the Various Mechanisms Involved in Iceberg Deterioration in the Open Ocean Environment, Rep. CG-D_62_80, U.S. Coast Guard, Washington, D.C. 126 p.

4.3 Physical iceberg management

The main task of physical iceberg management is to deflect all threatening icebergs. In order to achieve it, an offshore installation will have to be assisted by sufficiently strong vessels dedicated to iceberg management (70 – 140 tonnes bollard pull based on experience from Grand Banks). The approach for managing the iceberg(s) is to send one (or two) vessels dedicated to iceberg management to the location where the iceberg(s) were detected and prepare for physical iceberg deflection. There are five approaches which are proven to be efficient for deflections of icebergs drifting in open water (Crocker et al., 1988):

- Single vessel iceberg tow
- Dual vessel iceberg tow
- Iceberg net tow
- Propeller washing
- Water cannon washing.

The methodologies are described in the following including recommendations for when to use each approach and requirements for vessel and equipment. Under some circumstances, iceberg deflection has not yet been documented and should consequently not be considered as feasible. Examples of such conditions are:

- Significant wave height (H_s) above 5.5 m
- Iceberg waterline length (L) above 450 m
- Occurrence of medium or thick sea ice in concentrations higher than 20%. (ref. Section 4.3.2).

A contour plot indicating the expected success probabilities in different sea states and for different iceberg sizes is presented in Figure 4-4. The definition of a successful iceberg deflection operation is found in Section 4.4. The duration of the deflection

operations will depend on both meteorological and oceanographic conditions in addition to the planned tow duration. The cumulative distribution for the elapsed time in real iceberg deflection operations offshore the east coast of Canada is presented in Figure 4-5. This figure is included in order to indicate approximate durations of iceberg tows.

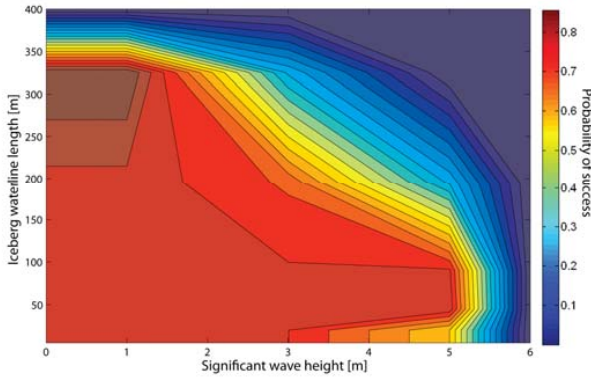


Figure 4-4. Probability of successful physical iceberg management operation as a function of sea state and iceberg waterline length. Based on data from the PERD Comprehensive Iceberg Management Database (2005).

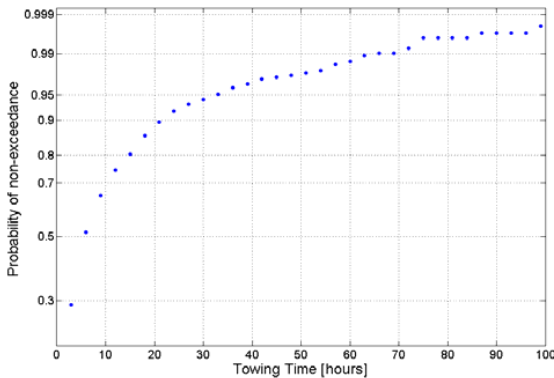


Figure 4-5. Cumulative probability distribution for elapsed deflection time (PERD Iceberg management database, 2005). The average duration of a tow is 6 hours ($P=0.5$), while 90% of the tows are completed successfully within 21 hours ($P=0.9$).

4.3.1 Iceberg towing in open waters (Crocker et al., 1998)

4.3.1.1 Single vessel iceberg towing

The primary method for iceberg towing will be single vessel towing as this generally is the simplest and most efficient method to deflect an iceberg. For larger ice masses, the objective of the towing procedure is to deflect the ice mass by a few degrees from its preferred route. The methodology involves a single vessel pulling a floating synthetic tow line looped around an iceberg (Figure 4-6). The line is paid out over the stern as the towing vessel approaches the iceberg. The vessel circles the iceberg and pulls the towline around, then recovers the end of the line which is marked by a buoy on a tag line. In situations with high winds and waves, it is recommended that the iceberg is approached from its lee-side, i.e. the tow line end and marker buoy is thrown in the water on the iceberg lee side. When the connection is made, a minimum of 100 m of steel towing hawser is paid out to sink the towing line. The hawser will serve several purposes:

- It depresses the line of the tow force to bring it closer to the iceberg's centre of hydrodynamic drag, thereby reducing the overturning moment.
- It prevents sudden recoil in the event of towline failure or slippage.
- It serves as a shock absorber to compensate for surges in the line tension caused by sea state or iceberg movement.

With the tow line installed, the towing vessel shall slowly increase the force in the lines until the desired towing force is attained in the predetermined direction. Typical towing speed will be in the range 1 to 2 knots.

Deployment of the tow line will usually require ½ to 2 hours. Iceberg rolling and tow line slippage are key problems. In all tow operations, it will be crucial that no personnel remain unprotected on deck during towing.

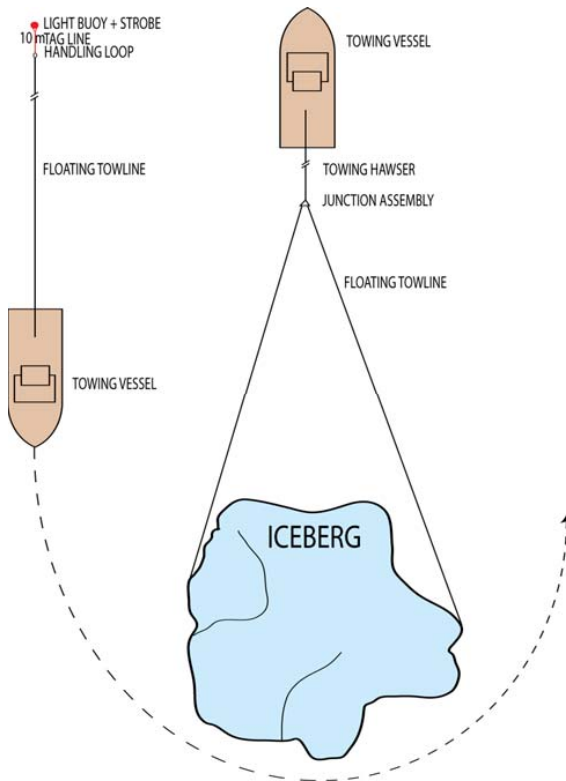


Figure 4-6. Illustration of a single vessel, iceberg tow operation (after McClintock et al., 2007).

In general, any supply vessel in the vicinity of the site can be used for iceberg towing as long as the bollard pull is within the range of 70 -140 tons. More powerful vessels may be an advantage, in particular in light ice conditions, but one should be aware of that higher power also will increase the risk for towline rupture, slippage or iceberg overturning.

The floating tow line shall be sufficiently strong for the vessel doing iceberg management, that it is easy to handle and torque free. Typically, a 15-20 cm diameter floating polypropylene line is used. Approximately 1200 m of floating tow line is normally used. With respect to strength, the tow line must be capable of at least 60 tons towing force.

4.3.1.2 *Dual vessel towing*

A two vessel towing technique may be attempted as an alternative to the single vessel tow on very large icebergs or unstable icebergs (Figure 4-7). One vessel is positioned near the iceberg aligned on the desired tow heading. The second vessel trails a section of tow rope by the first vessel which recovers it and connects to its tow hawser. The second boat then proceeds around the iceberg. Both vessels proceed away from the iceberg in the direction of the desired tow heading. Although the applied tow force can be significantly greater than with single vessel towing, there are some problems associated with this method and which the operational personnel need to be aware of. Basically, the challenge is to balance the vessel thrusts during tow. Uneven thrusts give two effects:

1. The tow rope saws back and forth around the iceberg during towing
2. It is difficult to maintain the depth control over the tow wire. If the tow line rises above the water, there will be a risk for tow-line snapping.

The equipment that is required for dual vessel towing is essentially the same as for single vessel towing, except that two sufficiently powered vessels are used. Generally, the probability of success for dual vessel tows is lower than for single vessel tows. However, it should be noted that this method is usually applied on more “complicated” icebergs than single vessel tows.

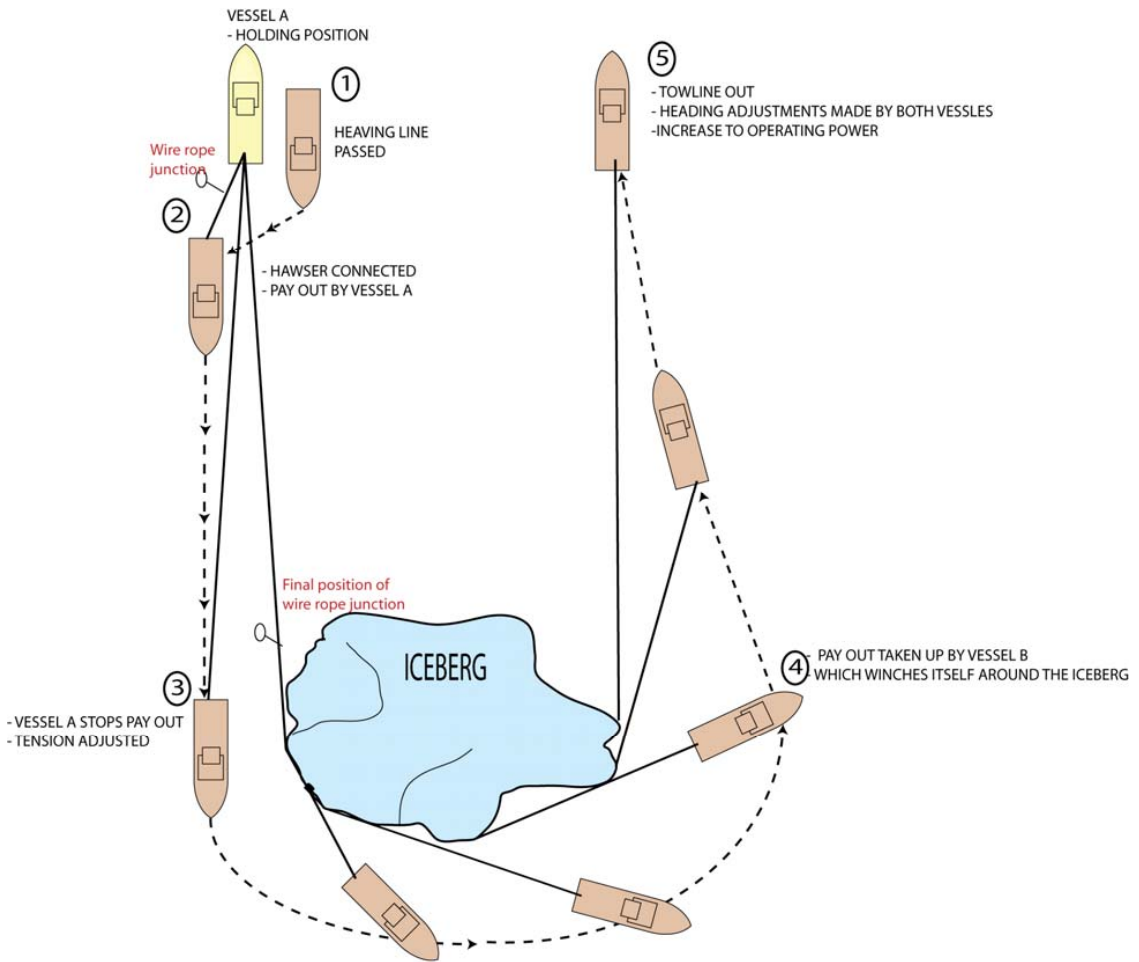


Figure 4-7. Illustration of a dual vessel tow operation (after Crocker, 1998).

4.3.1.3 Net towing

The inherent difficulty with towing small and rounded ice masses is their propensity to roll, and for the line to slip. An alternative approach is to use a net rather than a single line. An efficiently designed net will cradle the ice mass and distribute the towing force

both above and below the centre of drag, thus minimising the potential for rolling and slippage (Figure 4-8).

Net towing can normally be conducted from a standard supply vessel. Since the net tow generally is suitable for smaller ice pieces, vessels with relatively small bollard pulls may also be suitable. As for the other towing methods, a synthetic tow line, steel hawser and winch are required in addition to ice net and net drum.

Based on experiences from the Canadian East coast it is found that about 65% of the net towing operations have been successful. It should be noted that more or less all of the net towed icebergs could not have been towed successfully with the traditional tow line. Reason for using the tow line rather than the net is in general that it is somewhat simpler and quicker to use the line compared to the net.

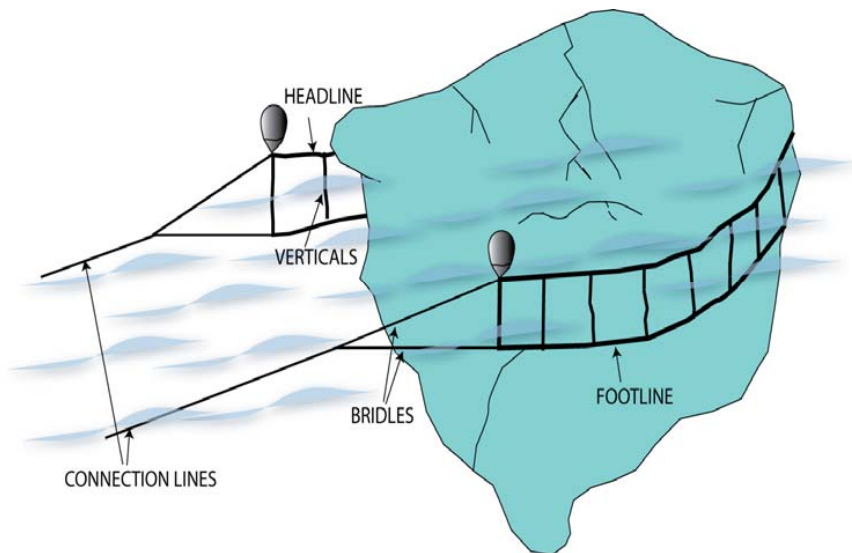


Figure 4-8. Illustration of net towing

4.3.1.4 Deflection by water cannon

In order to deal with small ice masses such as bergy bits or small icebergs that are often characterised by smooth faces due to erosion, thrust from water cannons may be applied. The vessel manoeuvres close to the iceberg and direct the high pressure stream of seawater on the iceberg or just in front in order to generate a flow in the desired direction.

Typically support vessels have water cannons mounted on the top of the bridge for fire fighting purposes. For iceberg management, it is however recommended to have the water cannon(s) installed in the bow. A capacity around 3600 m³/hr or higher is considered adequate for this purpose (may generate a pushing force around five tons).

High winds can make vessel positioning difficult and disperse the water jet which again reduces the applied force on the iceberg. Further, high seas may make it difficult to aim and maintain the water jet in front of or on the iceberg. Another limitation may be due to icing from the water blowing back on the vessel. Water cannon deflection is successful only in about 50% of the operations.

4.3.1.5 Deflection by propeller wash

Small ice masses can be successfully deflected by propeller washing. In this procedure, the vessel slowly backs or swings towards the ice mass and accelerates forward. This results in a water current pushing the ice away from the stern. Sufficient deflection can often be achieved by repeated propeller washing. This technique requires precision boat handling, which is difficult in rough seas. High sea states also tend to dissipate the vessel's wake quickly, reducing the effectiveness of the method.

It should be noted that use of azimuth thrusters are expected to increase the efficiency of this method. For example, vessels with twin azimuth thrusters can be angled in such a way as to deliver constant power from one engine while the other

engine is used to maintain the close position. In addition to making the deflection more efficient, this will make propeller washing more economic and easier on main engine components. So far, use of azimuth thrusters for iceberg deflection has not been tested.

4.3.2 *Iceberg towing in sea ice*



Contents lists available at ScienceDirect

Cold Regions Science and Technology

journal homepage: www.elsevier.com/locate/coldregions

Model tests of iceberg towing

Kenneth Eik^{a,*}, Aleksey Marchenko^b^a Norwegian University of Science and Technology / Statoil, Trondheim, Norway^b The University Centre in Svalbard, Svalbard, Norway

ARTICLE INFO

Article history:

Received 18 September 2009

Accepted 4 December 2009

Keywords:

Iceberg towing

Tank model tests

Tow line tension

ABSTRACT

Icebergs may cause a threat to offshore installations, vessels and operations in a number of Arctic regions. In order to increase the understanding of what happens when an iceberg tow is started in ice covered waters; physical tank model tests have been carried out in various concentrations of sea ice. The objectives with these tests have been to evaluate the practical arrangements for iceberg towing and to collect data regarding tow loads and iceberg behaviour during the tow.

The tank model tests were carried out in scale 1:40 in the ice tank at Hamburg Ship Model Basin (HSVA), Germany. Two different iceberg models were used and each towed in four different ice concentrations. From all tests, tow line forces, iceberg displacements and rotations were recorded.

It was concluded that towing in 50% ice concentrations and higher were not realistic due to high resistance. During the tows in high concentrations, ice was breaking in flexural mode, crushing, rafting and ridging continuously in front of the iceberg models. With respect to the tow line, the line was fully extended and lifted up from the water/ice. In real operations this may increase the risk for tow line rupture and subsequent “snapping”. In 50% ice concentration, total loads in the tow line will most of the time be lower than maximum bollard pull for powerful diesel electric icebreakers indicating that towing up to this concentration may be feasible. However, tow lines will have to resist even the highest peak loads during a tow and it is unclear whether sufficiently strong tow lines can be produced. With respect to tows in 20% concentration and open water, loads are significantly lower indicating that towing in low ice concentrations should be feasible.

Measured loads seem to be reasonable well described by a log-normal distribution. The concentrations of surrounding sea ice are found to be most important for the load magnitude while variations in speed, acceleration, course and iceberg shape seem to be less important.

A log-normal distribution, in which the parameters are functions of the sea ice concentration, has been fitted to recorded data. Combined with information regarding expected tow length, this distribution may be applied in order to provide crude estimate on extreme loads during an iceberg tow. By performing additional model tows in different ice conditions and with larger variations in iceberg size, this model may be further developed to be applicable in a wide range of scenarios.

© 2009 Elsevier B.V. All rights reserved.

1. Introduction

Icebergs may cause a threat to installations, vessels and operations in a number of Arctic and Antarctic regions. If icebergs are detected and considered to be a threat, it has been documented that they can be deflected around installations in approximately 75% of the events (Rudkin et al., 2005). The preferred method for iceberg deflection is single vessel tow rope (Fig. 1). A two vessel towing technique has also occasionally been used to tow large icebergs or large unstable icebergs.

While all successful iceberg towing operations so far has taken place in open water, future oil and gas developments are expected to

take place in regions with occurrence of icebergs embedded in sea ice. The possibility of being able to manage icebergs in such conditions will contribute to increased safety in future operations. The potential for handling icebergs in sea ice may also directly influence the design of offshore structures in Arctic waters.

In order to investigate the feasibility for iceberg towing both in open waters and in waters prone to sea ice, a number of iceberg tow tests were carried out in the large tank of the Hamburg Ship Model Basin (HSVA). The tests were run in different ice concentrations and for two different model shapes. For each iceberg shape and ice concentration, two different tow types were tested; one linear test including an acceleration phase and one test where a change in tow course was simulated. This paper describes the experiments conducted (Section 2) and the test results (Section 3). The results also include a study of the tow load distributions and the introduction of an approach for estimating extreme loads during an iceberg tow. The

* Corresponding author. Fax: +47 73 59 70 21.
E-mail address: kenjo@statoil.com (K. Eik).

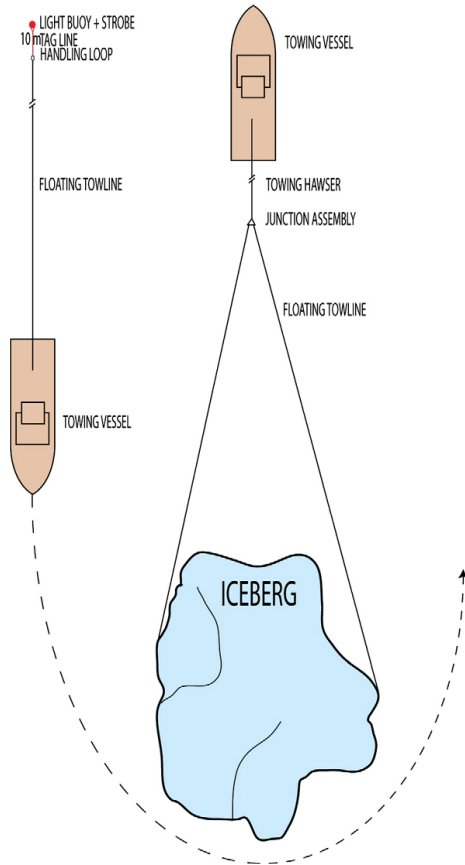


Fig. 1. Illustration of a single vessel, iceberg tow operation (after McClintock et al., 2007).

results and test set up have been discussed and final conclusions have been highlighted. It should further be noted that all numbers presented in this paper are scaled to full scale, unless otherwise mentioned.

2. Model test set-up

2.1. Scaling

The model tests were conducted with a geometrical scaling of 1:40 (scale factor, $\lambda = 40$). In order to ensure correct ratio between inertia forces and gravity forces, Froude scaling was applied. This means that the Froude number (F_n) shall be the same for the model scale and the full scale iceberg:

$$\frac{v_m}{\sqrt{gL_m}} = \frac{v_f}{\sqrt{gL_f}} = F_n \quad (1)$$

where v_m and v_f is the velocity in model scale and full scale respectively, g is the gravity and L_m and L_f is the iceberg length (diameter) in model and full scale. It should be noted that it was not possible at the same time to achieve the same Reynolds number in

model and full scale. Table 1 shows the Froude scaling multiplication factors which were relevant for these tests.

2.2. Iceberg models

Two iceberg models were made by building wooden shapes and filling these with small blocks of fresh water ice. These shapes were thereafter filled with fresh water and stored in the ice tank for a few days. When the ice was frozen into solid blocks, the wooden forms were removed and the models were ready for use. Illustrations, photos and dimensions of the models are presented in Fig. 2. Initial volume, mass and densities are given in Table 2.

2.3. Sea ice characteristic

Three sheets of level ice were grown naturally from a 0.7% sodium chloride solution. The ice was of a fine-grained columnar type and the preparation technique is described by Evers and Jochmann (1993). After the desired thickness was reached, the ice was heated to achieve a certain flexural strength as required by a different project being run in parallel. Measurements of flexural strength (σ_f) were performed before the tests by means of cantilever beam tests as recommended by Schwarz et al. (1981). As can be seen from Table 3, the flexural strength in full scale will in these tests be somewhat higher than what is normal in real sea ice (around 300 kPa). However, as ice breaking in flexural mode was not expected to be dominating during the towing operations, this was not expected to have any significant impact on the test results. With respect to compressive strength, Evers and Jochmann (1993) indicate that this is in the interval 2–3 times the flexural strength. This means that this parameter was within the range 2–4 MPa when converted to full scale.

The modulus of elasticity (E) was estimated by measuring the deflection of a cantilever beam under a certain applied vertical force on the free end. These measurements were only performed on ice sheets number 2 and 3.

The ice thickness (h_i) was measured at a number of locations along the entire tank prior to the tests. The values for ice thickness reported in this document are average values from each ice sheet. It should be noted that the spatial variation in ice thickness was low.

The salinity (S_i) of the sea ice was measured on two samples from four different locations in the basin. Salinity values in this report are average values from each ice sheet. Reliable density values were only performed for the third ice sheet and only the average value is presented herein.

The tests were conducted in ice 80%, 50%, 20% concentrations and open water ($C = 80, 50, 20$ and 0). Prior to the tests, the sea ice in each sheet was cut into triangular peaces with size about 0.5 m². The ice floes were typically reduced in size during the tests, either because they broke or because the sharp edges were worn of. Due to this, tests in 20% ice concentration were performed in ice floes which were smaller and more rounded than in tests with 50% or 80% ice concentrations.

Table 1
Multiplication factors from model scale (M) to full scale (F) with Froude scaling.

Physical parameter	Unit	Multiplication factor
Length	[m]	λ
Structural mass	[kg]	$\lambda^3 \cdot \frac{\rho_F}{\rho_M}$
Force	[N]	$\lambda^3 \cdot \frac{\rho_F}{\rho_M}$
Acceleration	[m/s ²]	$a_F = a_M$
Time	[s]	$\sqrt{\lambda}$

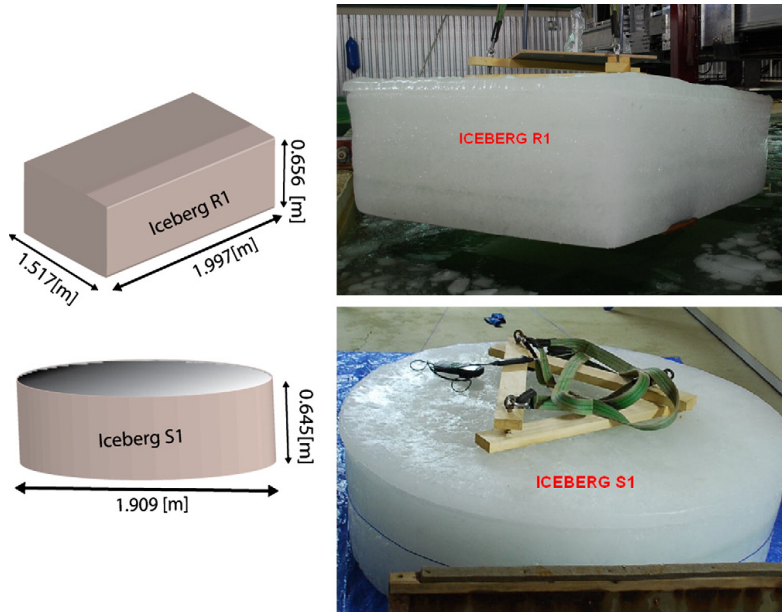


Fig. 2. Illustration and photos of iceberg models. Dimensions are given in model scale.

2.4. Tow rope

The tow rope consisted of two parts; one floating tow line made of Dyneema® and one part consisting of a steel wire. The set up is illustrated in Fig. 3 while tow line specifications are presented in Table 4. In full scale, the tow line length would be 920 m and the diameter 16 cm. For a steel hawser, full scale values would be 82 m length and 12 cm in diameter.

Table 2

Initial volume, mass and density of iceberg models (model scale).

Shape	Volume [m ³]	Mass [kg]	Density [kg/m ³]
Tabular	1.99	1784.7	898.6
Cylindrical	1.85	1637.2	887.0

Table 3

Sea ice parameters.

Ice sheet #	Parameter	Full scale	Model scale
1	Ice thickness, h_{si}	1.28 m	32 mm
	Flexural strength, σ_f	1.40 MPa	35 kPa
	Modulus of elasticity, E	NA	NA
	Sea ice salinity, S_{si}	3.2 ppt	3.2 ppt
	Sea ice density, ρ_{si}	$\approx 930 \text{ kg/m}^3$	$\approx 930 \text{ kg/m}^3$
2	Ice thickness, h_{si}	1.16 m	29 mm
	Flexural strength, σ_f	1.08 MPa	27 kPa
	Modulus of elasticity, E	$\approx 2.8 \text{ GPa}$	$\approx 70 \text{ MPa}$
	Sea ice salinity, S_{si}	3.2 ppt	3.2 ppt
	Sea ice density, ρ_{si}	$\approx 930 \text{ kg/m}^3$	$\approx 930 \text{ kg/m}^3$
3	Ice thickness, h_{si}	1.12 m	28 mm
	Flexural strength, σ_f	1.00 MPa	25 kPa
	Modulus of elasticity, E	$\approx 2.0 \text{ GPa}$	$\approx 50 \text{ MPa}$
	Sea ice salinity, S_{si}	3.2 ppt	3.2 ppt
	Sea ice density, ρ_{si}	929 kg/m ³	929 kg/m ³

2.5. Description of test runs

With respect to speed during the tow, it was of interest to investigate what happens after an acceleration or if the tow heading is changed. Due to this, two types of tow tests were performed (Fig. 4):

1. Tests where the icebergs were subjected to a change in tow speed
2. Tests where the icebergs were subjected to a change in tow direction.

A test matrix including parameter specifications during the tests is included in Table 5.

2.5.1. Type 1 tests – 1D (all values refer to model scale)

Initially, the iceberg was floating in the centre line in one end of the tank (Fig. 4a). The iceberg was then accelerated from $v_x = 0 \text{ m/s}$ to $v_x = 0.11 \text{ m/s}$ within a period of 70 s. Thereafter, the iceberg was towed with a constant speed of $v_x = 0.11 \text{ m/s}$ for the next 130 s. After this, the iceberg was accelerated from $v_x = 0.11 \text{ m/s}$ to $v_x = 0.13 \text{ m/s}$ over a period of 19 s. This speed was then kept constant until the carriage reached the end of tank.¹

2.5.2. Type 2 tests – 2D (all values refer to model scale)

In this test, the iceberg was located on the side of the tank while the tow line initially was attached straight ahead of the iceberg in the tow direction. During the tow, the end of the towline was moved to the opposite side of the carriage (Fig. 4b). Total displacement of the transversal carriage was 3.85 m and lasted for 32 s.

¹ The approximate distance was 45 m corresponding to approximately 1.8 km in full scale. Velocities and time correspond to model scale values.

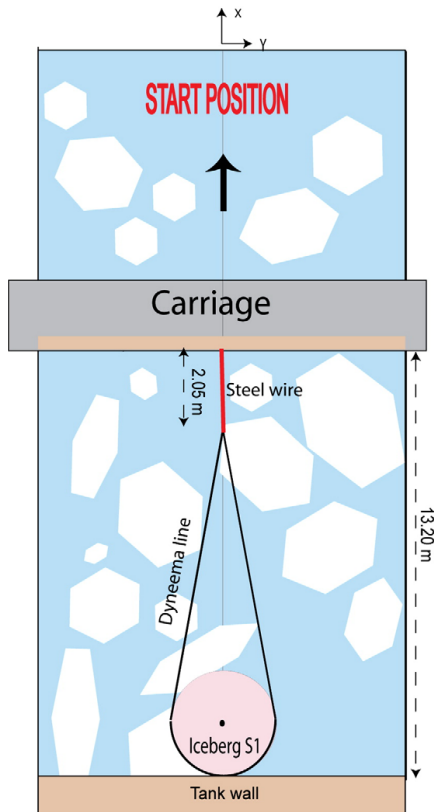


Fig. 3. Illustration of the tow line configuration before tow start. Dimensions are given in model scale.

2.6. Instrumentation

The tension in the tow line was recorded at three locations (Fig. 5). From evaluations of the test results, it is evident that some of the load cells in some of the tests were “drifting”. This can be seen from either the start or the end of the recorded data (i.e. negative loads in one of the sensors from the start). However, since records from three sensors were available, it has been possible to manually correct these offsets. The time series seem reasonable after these corrections, but nevertheless, this will cause some unfortunate uncertainties in the load results. The effect of this is considered to be most important in the open water tests.

Table 4
Tow rope properties (model scale).

Property	Unit	Tow rope – Dyneema®	Steel wire
Length	[m]	23.00	2.05
Weight	[kg]	0.187 ^a	0.102
Diameter	[m]	0.004	0.003
Density	[kg/m ³]	550.1	7039.0
Ultimate load	[N]	12500	–
E-Module	[GPa]	95	–

^a Including metal shackles in the ends (28 g).

With respect to movement and rotation of the icebergs, this was recorded in all six degrees of freedom with a Qualisys–Motion Capture System. In addition, all tests were recorded with two video cameras.

3. Results of towing tests

As indicated in Fig. 4, the tests can be divided into different stages. In order to be able to analyse the results in a systematic matter the resulting data have been sorted into four different phases:

1. Constant tow speed $v_x = 0.7$ m/s and straight tow direction.
2. Constant tow speed $v_x = 0.8$ m/s and straight tow direction.
3. Acceleration from $v_x = 0.7$ m/s to $v_x = 0.8$ m/s within 2 min, straight tow direction
4. Constant tow speed $v_x = 0.7$ m/s and change in course from 0° to 344° .

From all of the phases, average and maximum total tow load have been calculated and are presented in Figs. 6 and 7.

Time series of the recorded total tow line loads are presented in Section 3.1. Some examples on corresponding plots based on recordings in each of the tow branches are presented in Section 3.2 together with general descriptions on how the loads are distributed in the tow line branches. Section 3.3 describes the recorded movements of the iceberg models in the various tests while an analysis of the tow load distributions are presented in Section 3.4.

3.1. Time series

In all test phases, the magnitude of tension in the tow lines varied significantly with variations in sea ice concentrations. This can be shown, i.e. from the time series of total load on the cylindrical iceberg shape plotted in Figs. 8 and 9. Time series of total load on the rectangular iceberg shape show similar behaviour as for the cylindrical shape.

3.2. Branch loads

The loads measured in each of the branches show similar characteristic as the total loads at a generally lower level as the loads are distributed in two branches. However, in order to identify potential critical scenarios with respect to iceberg towing the following approach was used:

1. For each test, the 10 largest peaks in time series for total loads were identified.
2. The simultaneous recordings in the load sensors in the branches were thereafter identified. In this respect, it should be noted that all branch recordings within the interval ± 30 s relative to the time of occurrence for total peak load were considered. The highest recording within this interval was considered as branch load peak.
3. The ratios between the branch load and the simultaneous total load were calculated and investigated.

Unfortunately, as described in Section 2.6, some of the load cells were drifting in some of the tests. Even if the load cell that measured total loads seemed to be reliable with two exceptions (open water type 1 and 2 tests with the rectangular shape), it is likely that at least one of the branch load cells were biased in a number of the tests. Due to this, only a limited number of the time series with branch loads have been used in the analyses.

Fig. 10 shows the results from type 2 tests with the cylindrical shape in 50% ice concentration. It can be seen that the peaks in the branches are not evenly distributed (in this plot, there are generally higher loads in the starboard branch but this varied from test to test). Further, there is also one event where the load in the port branch is exceeding the total peak load with a factor of more than 2. At the same time, the peak load in the starboard branch is at the same level as the

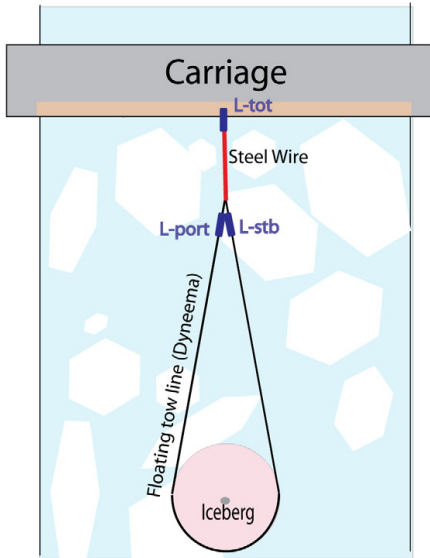


Fig. 5. Location of load cells during iceberg tow (L-tot, L-port and L-stb).

order to better understand which effects that cause the high loads. In this section, iceberg movements in surge, sway and yaw are presented in Figs. 13–15. All plots refer to full scale values. With respect to heave, roll and pitch, these motions were relatively small through all tests and are therefore not shown in this paper. Iceberg instability was not a concern in these studies. With respect to surge and sway, attention should be given to test type 2 with the cylindrical shape in open water. During this test, an extreme high load peak occurred after the change in course. The reason for this is not known, but it is interesting to note the reduction in tow length and also that there were an increase in heave occurring simultaneously.

3.3.1. Surge

Time series of the horizontal distance between the tow carriage and the iceberg show that the surge motions are significantly reduced in high sea ice concentrations compared to open water tests (Fig. 13). Reason for this is that in high concentrations, the tow line tension is high and the tow line stiffness is nearly constant (i.e. only elastic stiffness). In lower concentrations, the geometrical and thus total stiffness is reduced allowing for larger displacements (surge) of the towed body.

3.3.2. Sway

Time series of the sideways motion show that the sway motions after a course change in open water are more significant than in high sea ice concentrations (Fig. 14).

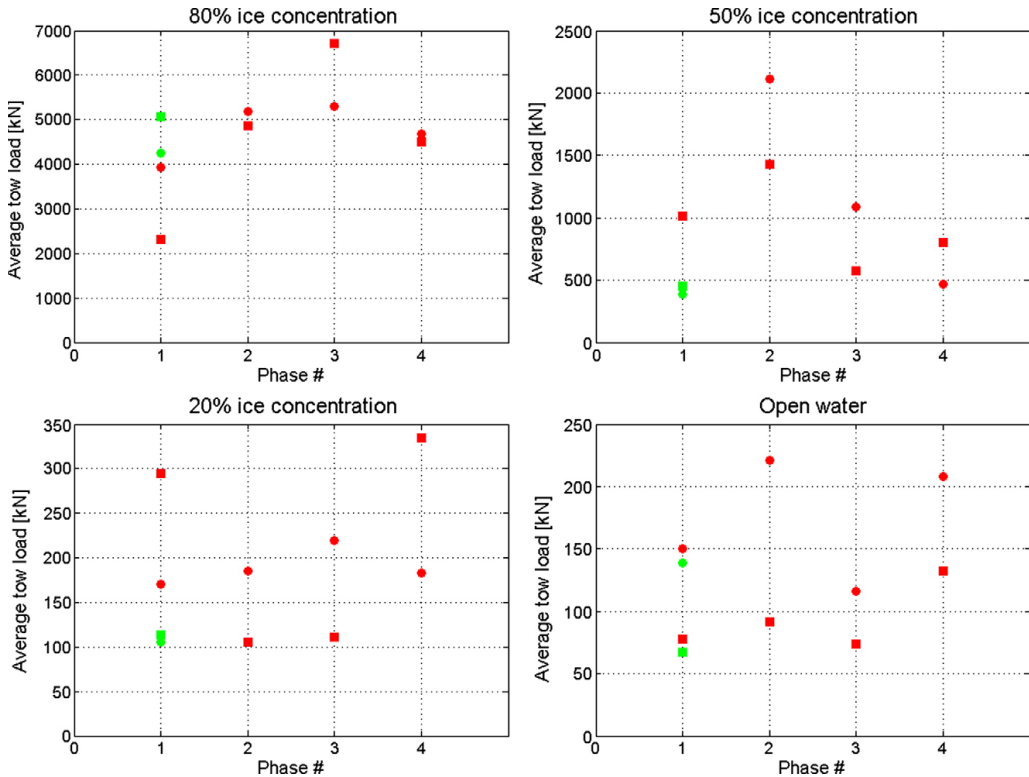


Fig. 6. Average tow loads in different phases; 1) Const. velocity $v_x = 0.7$ m/s, 2) Const. velocity $v_x = 0.8$ m/s, 3) Acceleration from $v_x = 0.7$ m/s to $v_x = 0.8$ m/s and 4) Change in course 16° to the port. Tows with cylindrical model are marked with circular dots while tows with rectangular model are marked with squares. In phase 1, records are available both from type one and type two tests – green points in phase one are based on records from type two tests.

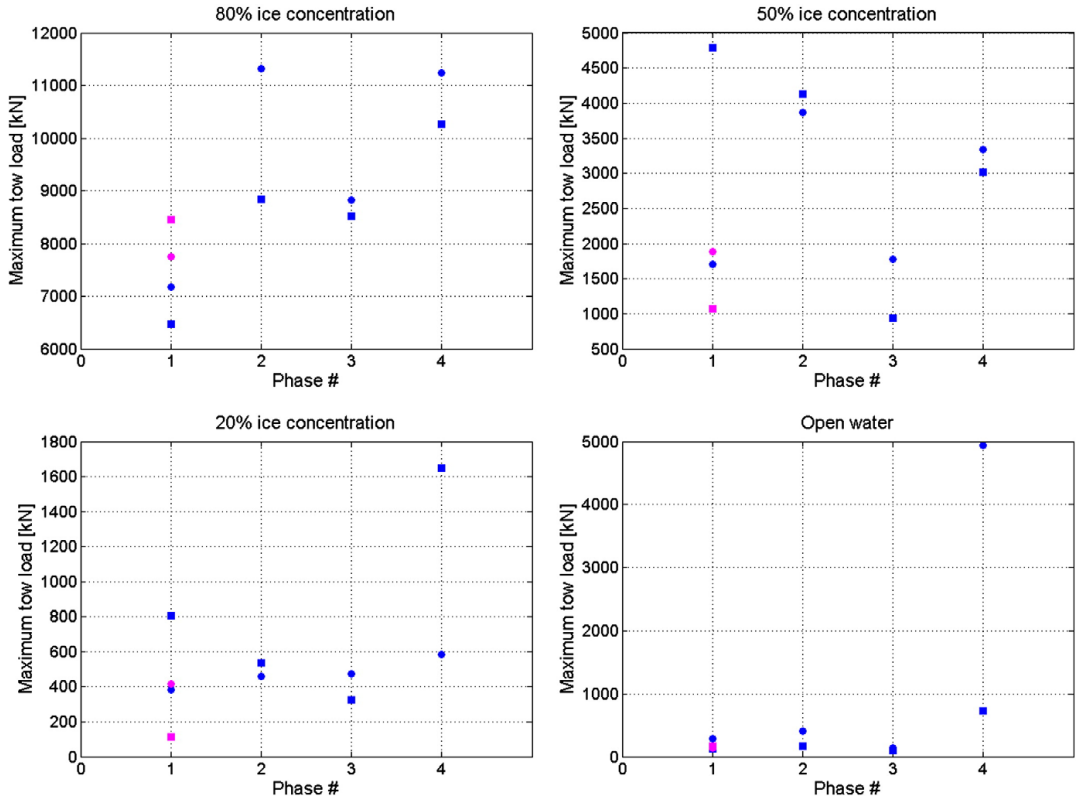


Fig. 7. Maximum recorded tow loads in different phases; 1) Const. velocity $v_x=0.7$ m/s, 2) Const. velocity $v_x=0.8$ m/s, 3) Acceleration from $v_x=0.7$ m/s to $v_x=0.8$ m/s and 4) Change in course 16° to the port. Tows with the cylindrical shape are marked with circular dots while tows with the rectangular shape are marked with squares. In phase 1, records are available both from type one and type two tests – magenta points in phase one are based on records from type two tests.

3.3.3. Yaw

With respect to yaw motions, most attention was investigations to friction between the tow line and the iceberg. There was not

observed sliding between the tow rope and the iceberg models and as can be seen from the time series in Fig. 15 b and d, the rotations caused by the course change were also reasonably fast damped.

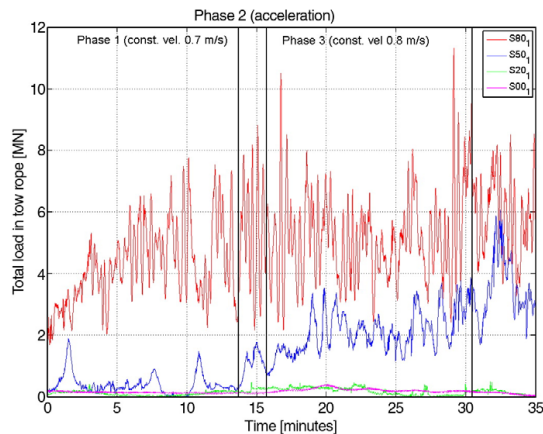


Fig. 8. Time series plot of total loads recorded during tow of cylindrical model in 80, 50, 20 and 0% ice concentration. Test profile type 1.

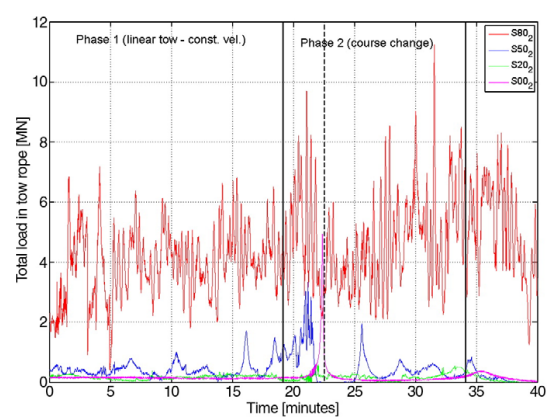


Fig. 9. Time series plot of total loads recorded during tow of cylindrical model in 80, 50, 20 and 0% ice concentration. Test profile type 2. Dashed line shows the time when transversal carriage movement stopped.

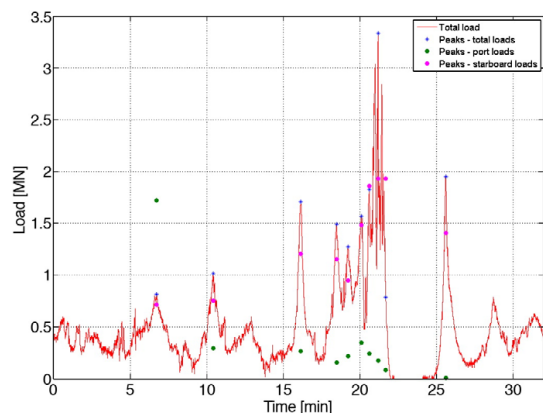


Fig. 10. Time series of total load measured during type 2 tests with cylindrical model in 50% ice concentration. The 10 highest peaks in total load in the dataset are highlighted with blue stars while corresponding peak loads in port and starboard tow line branches are marked with green and magenta dots respectively.

3.4. Probability distributions

From the recorded time series of tow loads, probability distributions of load peaks have been generated (*pdfs*). Load peaks are simply defined as all local maxima in the time series. In this paper, only density distributions from type 1 tests with the cylindrical shape is shown (Fig. 16). However, remaining density functions from the other tests show similar behaviour. In particular, the significant differences in tow load from 80% ice concentration to open water should be highlighted.

3.4.1. Total loads

The probability density functions based on recorded total tow line loads are shown in Fig. 16. It can be seen that the loads are strongly affected by the sea ice concentration.

3.4.2. Branch loads

As shown in Section 3.2, it is likely during some particular events that loads in the individual tow line branches exceeds the total loads in the entire tow. In order to investigate the importance of this, *pdfs* based on branch loads have been compared with *pdfs* from the

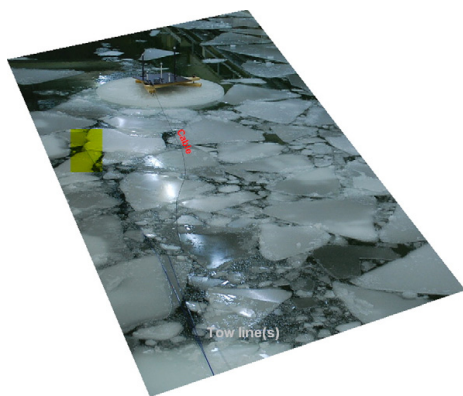


Fig. 11. Photo from test in 50% ice concentration. The ice floes are pushed together in front of the iceberg model. At some stage, the floes close to the iceberg are pushed sideways. If the tow line is close to the surface, it is moved sideways with the ice floes (highlighted region).

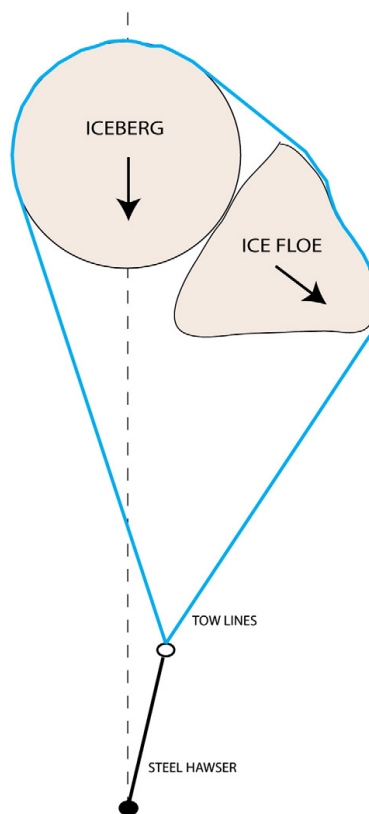


Fig. 12. Illustration of an event where ice floes push the tow line sideways and thereby creating high tension in the tow line branches.

recordings of total loads in all model tests. As can be seen from Fig. 17, tension loads in the tow rope branches are statistically less severe than the total tension load in the steel hawser. In this report, only two of the comparisons have been included but more or less all of the remaining comparisons show a similar relationship between branch loads and total loads.

3.4.3. Statistical distributions for tow load calculations

As can be seen from the figures in Section 3.4.1, a number of the load distributions seem to have a relatively “fat tail”, i.e. a few infrequent events causing very high loads making the distributions asymmetric. This type of behaviour is often well described by use of a log-normal distribution. By use of probability plots, this suspicion was strengthened. Fig. 18 shows the probability plots for log-normal distribution from two of the tests. Most of the other comparisons showed similar behaviour. In a number of the comparisons, at high probability levels (P99 and higher), the log-normal distributions showed a tendency to curve upwards and the same tendency could also be seen for the lowest probability levels (P20 and lower). Data that are perfectly log-normal distributed should follow a straight line in the probability plots, thus use of log-normal distributions for tow loads will therefore give a reasonable good description of the main bulk of data but will provide too high load values for the highest and lowest probability levels.

By calculating the mean value and variance from the records of tow loads, log-normal distributions were fitted to the observed

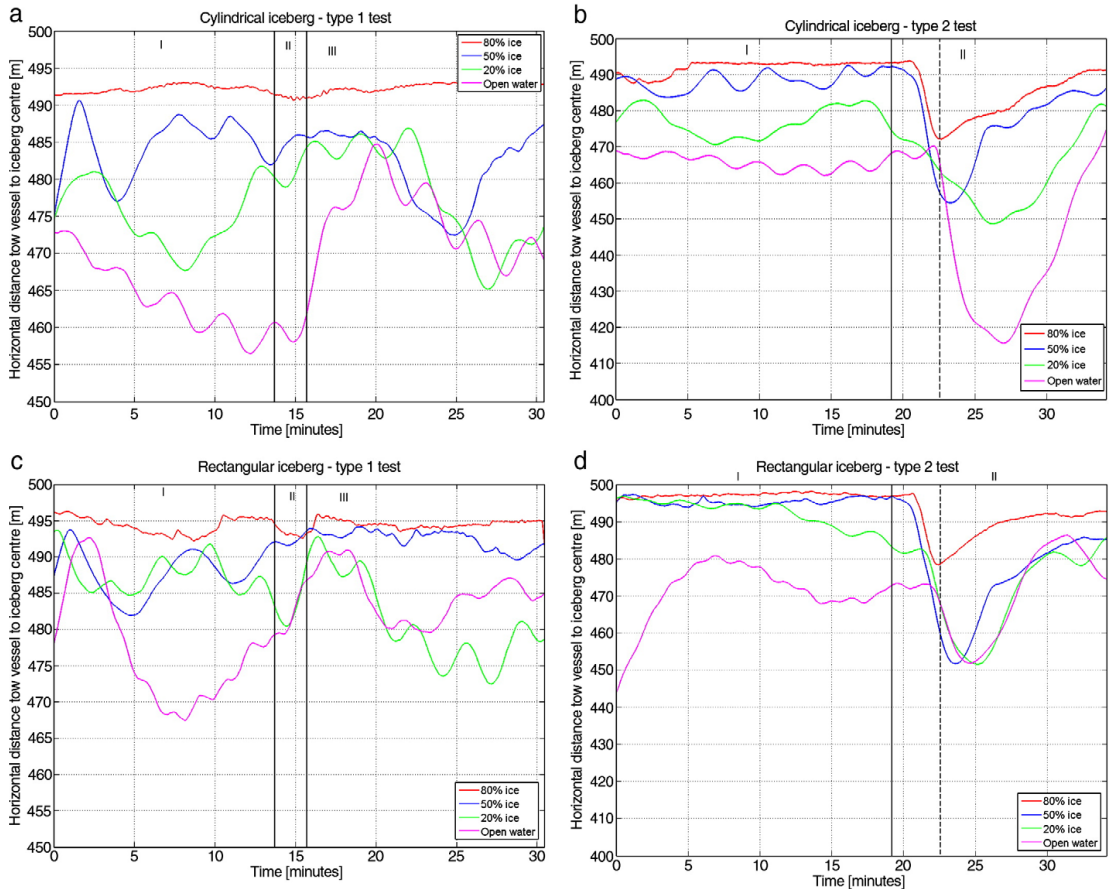


Fig. 13. Horizontal distance between tow vessel (carriage) and centre of iceberg at different ice concentrations and from four different test sets; a) Cylindrical iceberg – type 1 test, b) Cylindrical iceberg – type 2 test, c) Rectangular iceberg – type 1 test and d) Rectangular iceberg – type 2 test. Phases with constant speed $v_x = 0.7$ m/s, acceleration/course change and constant speed $v_x = 0.8$ m/s is marked with I, II and III respectively.

data for all tests and in the different test phases. Generally, there is good agreement with the fitted distributions and the observed data as can be seen in Fig. 19 which includes data from two of the tests.

In order to establish a generalised distribution for tow loads, the parameters in the log normal distributions fitted to data in each test were plotted against the sea ice concentration (Fig. 20). With respect to the mean value of the natural logarithm to the load, a clear correspondence between concentration and magnitude can be seen despite some scatter. It was suggested to use a cubic expression to estimate the mean value. The cubic expression in Eq. (2) was found by using a least squares fit to the average values from each concentration level (Fig. 20a). For the variance of the natural logarithm of the load, no clear correlation with ice concentration could be found. Due to this, it has been suggested to use a constant value for the variance, Eq. (2). By use of Eq. (2), smoothed probability distributions for tow loads at 80, 50 and 20% ice concentrations as well as open water have been established and plotted in Fig. 21.

$$E[\ln(T)] = \mu = \div 8.1 \cdot 10^{-6} \cdot C^3 + 0.0012 \cdot C^2 \div 0.00012 \cdot C + 4.7 \quad (2)$$

$$\text{Var}[\ln(T)] = \sigma^2 = 0.3483$$

where T is the tension load in the steel hawser [kN] and C is the sea ice concentration in %, μ and σ are the mean and standard deviation of the variable's (T) natural logarithm.

3.4.4. Extreme tow loads

The maximum loads during a tow will mainly depend on the sea ice concentration and the duration of the tow. Based on full scale experiences from Grand Banks (Rudkin et al., 2005) it is known that average duration of an open water tow is 6 h while a few tows need more than 48 h (5% of all tows need more than 48 h). The tests done in the tank will, when converted to full scale, correspond to an approximately 30 minute's long tow. The extreme loads measured during the tests will therefore not be representative for the extreme loads in a real tow. However, by use of the smoothed distribution presented in Section 3.4.3 and considering the highest load of totally N load peaks, a crude estimate on the maximum load can be provided. Evidently, N , which is the total number of load peaks during the entire tow, will be a function of the duration of the tow. In this work, a load peak is simply defined as local maxima in the recorded time series. The average number of load peaks for the various ice concentrations are presented in Table 6.

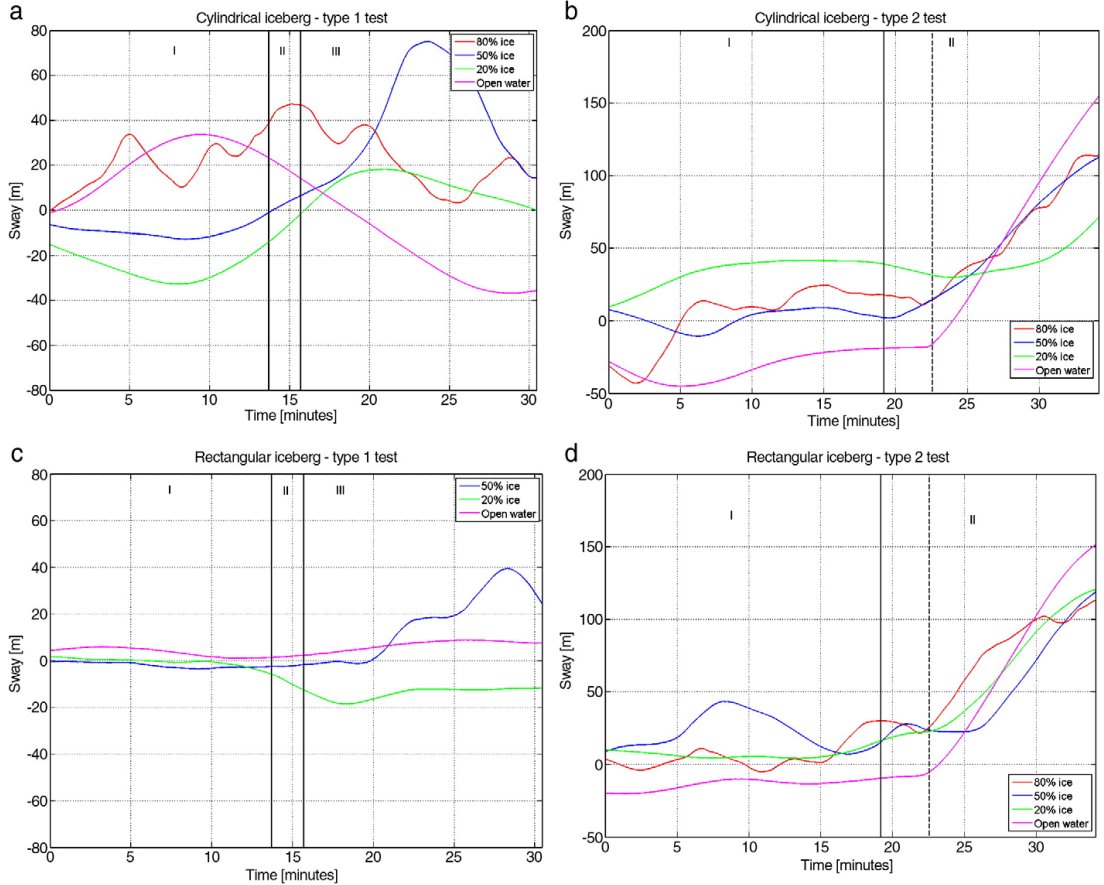


Fig. 14. Sideways movement relative between fixed point at tow vessel (carriage) and centre of iceberg at different ice concentrations and from four different test sets; a) Cylindrical iceberg – type 1 test, b) Cylindrical iceberg – type 2 test, c) Rectangular iceberg – type 1 test and d) Rectangular iceberg – type 2 test. Phases with constant speed $v_x = 0.7$ m/s, acceleration/course change and constant speed $v_x = 0.8$ m/s is marked with I, II and III respectively. Sway is positive to the port side.

The following scenario illustrates how the maximum tow load can be estimated prior to a tow:

3.4.5. 20% ice concentration, 6 hour tow

$$1 \div P(T_{\max}) = \frac{1}{N}$$

$$N = 2856 \cdot 6 = 17136 \text{ peaks during 6h}$$

T_{\max} is the maximum load during the tow and since the loads are log-normal distributed with the parameters given in Eq. (2), we get:

$$P(T_{\max}) = \Phi\left(\frac{\ln(T_{\max}) \div \mu}{\sigma}\right) = 1 - \frac{1}{N} \quad (3)$$

where Φ is the standard normal distribution. By using the inverse normal distribution we get:

$$\frac{\ln(T_{\max}) \div \mu}{\sigma} = 3.85 \quad (4)$$

From Eq. (2) with 20% concentration we get $\mu = 5.11$ and $\sigma = 0.59$. Solving Eq. (4) with respect to T_{\max} gives the maximum tow load during the entire tow:

$$T_{\max} = 1\,614 \text{ [kN]}$$

Average tow load for this tow case will be around 200 kN (20% ice concentration, 80 m iceberg length, speeds around 0.7 m/s).

4. Discussion

Before making any conclusions regarding full scale iceberg towing based on these model tests, it is important to note that there are some concerns that limit the use of these data. For instance, it should be noted that the sea ice as been made in model scale both with respect to geometrical parameters as well as strength while the iceberg models have been made geometrically in model scale but with the same physical parameters as full scale ice. With respect to tow rope, the rope applied in the tests was extremely robust and static while in full scale some dynamic effects caused by strain in the tow ropes might be expected. Since Froude scaling was applied, it must also be

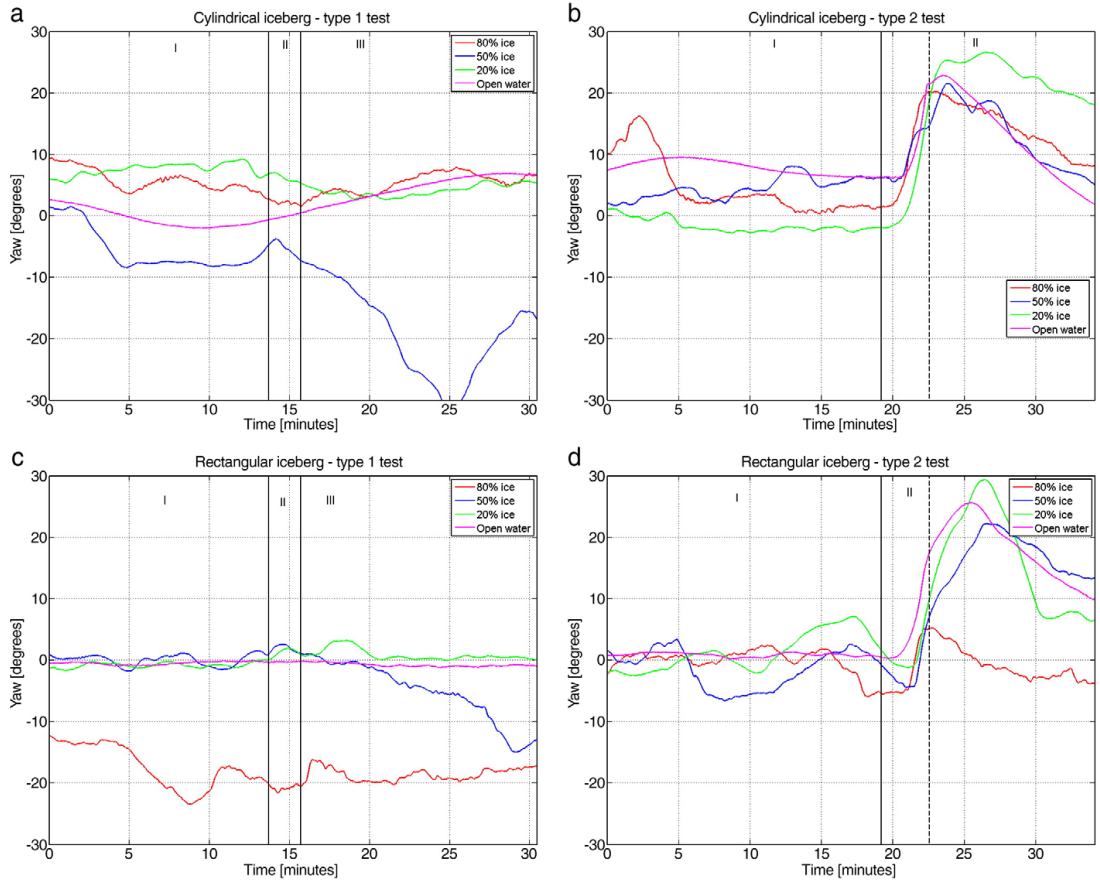


Fig. 15. Iceberg yaw in different ice concentrations and from four different test sets; a) Cylindrical iceberg – type 1 test, b) Cylindrical iceberg – type 2 test, c) Rectangular iceberg – type 1 test and d) Rectangular iceberg – type 2 test. Phases with constant speed $v_x = 0.7$ m/s, acceleration/course change and constant speed $v_x = 0.8$ m/s is marked with I, II and III respectively. The yaw is positive when the iceberg front is rotated towards port side.

accepted that the Reynolds numbers in model scale and full scale will be different and thus water drag coefficients from the tests will not necessarily be representative for full scale icebergs.

Another issue is the accuracy of the instruments used for load measurements. As mentioned in Section 2.6, some of the load cells “drifted” during the test period. Even if corrections were made based on comparisons between the different load cells, the trustworthiness of the results has been reduced. This is particularly important for the open water tests which recorded very low loads (around 2–3 N).

When towing with a vessel one will generally apply a constant load to the tow line and the resulting tow speed will vary depending on the resistance from the towed object. In real operations, the tow speed would have been reduced (or stopped) thus the model tests will not be fully realistic. The effect of this is uncertain.

With respect to the practical performance, the most important difference between the model test and a real life operation is probably that the carriage applied in the tank did not create any ice free wake such as will be the case when using an icebreaker as a tow vessel. On the other hand, there was no opposite wake from the vessel thrusters either. This make it complicated when transferring the model results to “real life” scenarios. The first effect is however, considered to be more important than the last one as long as the sea ice is present. Due

to this it is assumed that the model results when transferred to “real life” are somewhat conservative.

From Figs. 6 and 7, together with plot of time series in Section 3.1, it seems evident that the tow loads are highly stochastic of nature. It is difficult to make any unambiguous conclusions regarding importance of factors such as tow speed, tow acceleration, changes in tow direction or iceberg shapes. However, it is evident that the tow loads increase significantly with the ice concentrations.

By a closer look at Figs. 6 and 7 and having in mind that the load cells in some of the test not worked optimally, the following observations can be made:

1. In open water, tow loads are higher for the cylindrical shaped iceberg than the rectangular. This is expected as the water drag dominates and the projected surface under water is larger for the cylindrical iceberg than the rectangular model used in these tests.
2. In ice covered water, it seems random which model that experience the largest tow loads. This may indicate that both shape and size (within a certain range) are not very important for the tow loads.
3. Tow loads are higher for higher speeds (phase 2 compared to phase 1). There are however some exceptions that may be

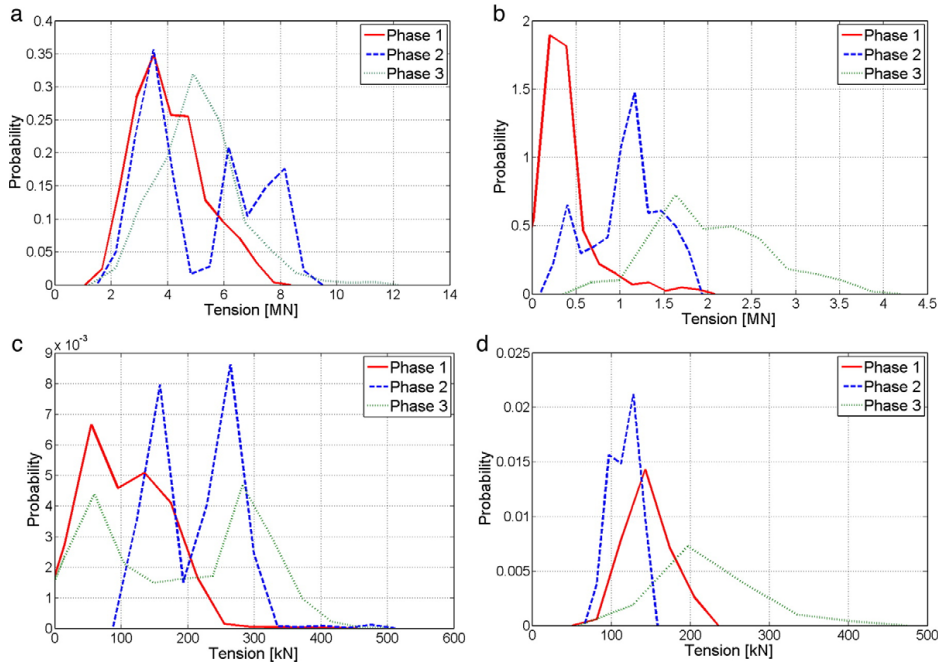


Fig. 16. Probability density functions for peak loads recorded in different phases in a) 80, b) 50, c) 20 and d) 0% ice concentrations. Phase 1 – constant speed $v_x = 0.7$ m/s. Phase 2 – acceleration. Phase 3 – constant speed $v_x = 0.8$ m/s. Cylindrical iceberg model – test profile type 1.

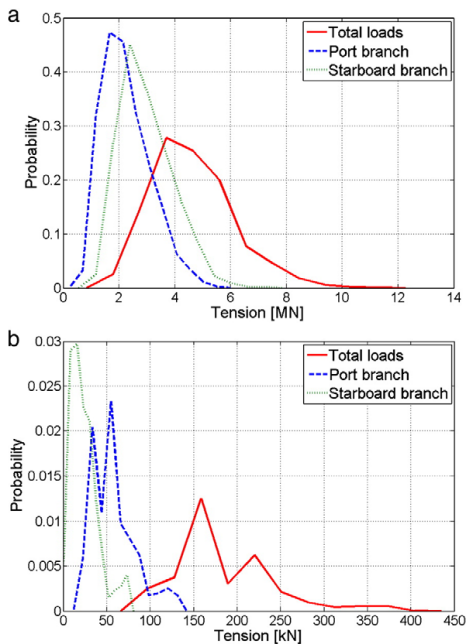


Fig. 17. Probability density functions for peak loads in steel hawser (total load) and tow line branches during tow tests in a) 80% and b) 0% ice concentrations. Cylindrical iceberg model – test profile type 1.

explained either by differences in ice floe configurations in front of the tow or by errors in the load measurements. The differences in tow loads due to speed are however negligible compared to differences in loads at different ice concentrations.

4. There is no significant increase in tow loads during the acceleration period. In this respect, it should be noted that the icebergs were accelerated quite slowly as also will be the case in real life iceberg towing operations.
5. With respect to tow loads during and after a change in course, there is not a significant increase in loads when towing in high ice concentrations. However, in low concentration and open water there is a significant peak in the load record for the cylindrical model. The reason for this is probably that that iceberg in open water continues to drift in longitudinal direction even after the course change while this drift is stopped immediately by the sea ice in high concentrations.

With respect to extreme loads during iceberg towing, it is evident that the loads will depend on parameters such as iceberg size, iceberg shape, sea ice thickness, floe size etc. However, for medium sized icebergs (60 m–100 m long) at tow velocities around 1.5 knots, results from these tests have indicated that the sea ice concentration is extremely important. In regions free of ice ridges with level ice thickness around 1 m to 1.5 m, the load distribution presented in this report should be applicable for making crude estimates on average and maximum required tow force. In order to evaluate the sensitivity for iceberg tow loads to the other parameters, further tank model tests will be required.

When considering the results from these tests it is also relevant to consider the results from some other model tests with a flexible boom in sea ice (Løset and Timco, 1993). In order to investigate the possibility to remove all ice prior to conventional cleaning of oil spills,

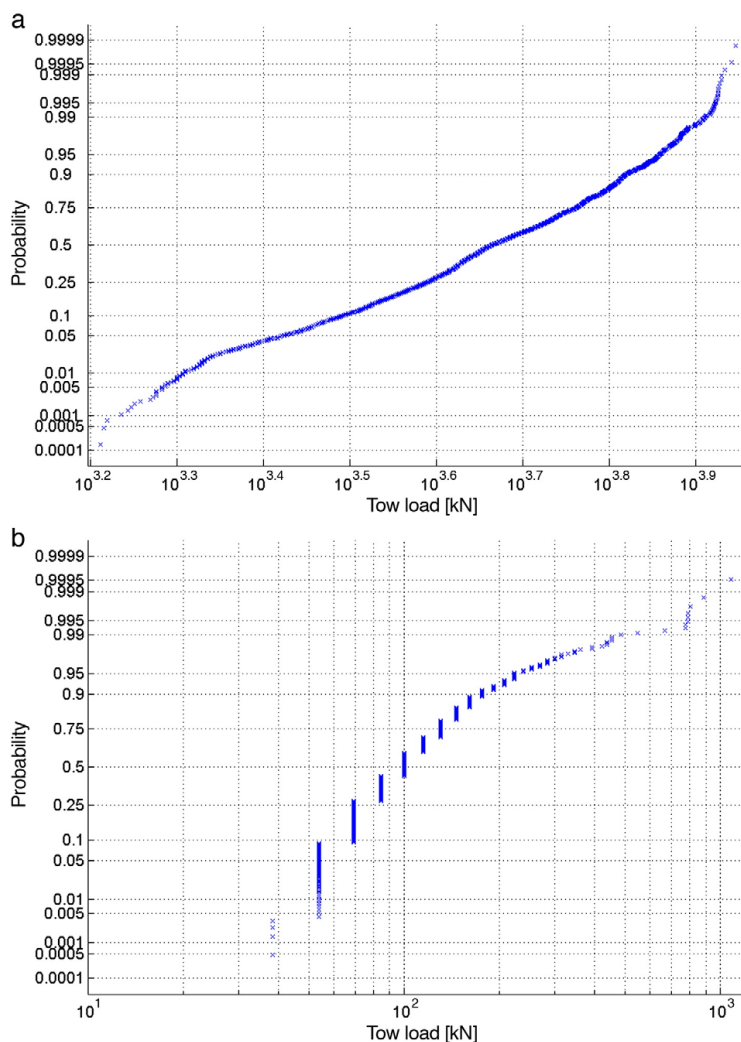


Fig. 18. Log-normal probability plots for total tow loads based on recordings from type 1 tests with the rectangular iceberg model in a) 80% ice concentration and b) open water.

Løset and Timco (1993) towed a flexible boom through sea of various concentrations and at two different speeds. In full scale, the length of the boom would be comparable with the width of the towed icebergs and the sea ice would also be of similar thickness as in the iceberg towing experiments. The boom was towed with somewhat slower speeds than the icebergs but no clear correlation between tow speed and tow loads were found. With respect to sea ice concentration and tow loads, a strong correlation was found, indicating that the major tow resistance in high sea ice concentrations is due to the amount of ice piling up in front of the iceberg/boom.

According to Crocker et al. (1998), typical iceberg towing operations in open water would require tow lines with capacity up to 0.6 MN and supply vessels with bollard pull in the range 0.7–1.4 MN. When comparing these numbers with the average tow loads from the tank tests, it seems obvious that iceberg towing in high ice concentrations will not be feasible. The strongest diesel electric

icebreakers have bollard pull up to about 2.3 MN while the strongest nuclear icebreakers have bollard pull up to 4.8 MN (BIM, 2008). This means that average tow loads in 80% ice concentration is of the same magnitude as maximum vessel force when nuclear icebreakers are applied. With respect to the most powerful diesel electric icebreakers, their bollard pull is of the same magnitude as the expected tow load in 65% ice concentration. However, in order to perform an efficient tow, the icebreaker thrust should be significantly higher than the average resistance caused by the iceberg. In 50% ice concentration, the average tow load plus two times the standard deviation is around 2.3 MN indicating that tows in sea ice up to this concentration may be feasible with the strongest diesel electric icebreakers.

With respect to tow lines, these will have to resist the highest peak loads. In 50% ice concentration, the highest load during a 48 hour tow will be about 11 MN. It has not been investigated whether it is possible to produce such strong tow lines or not. Due to thus, it is still

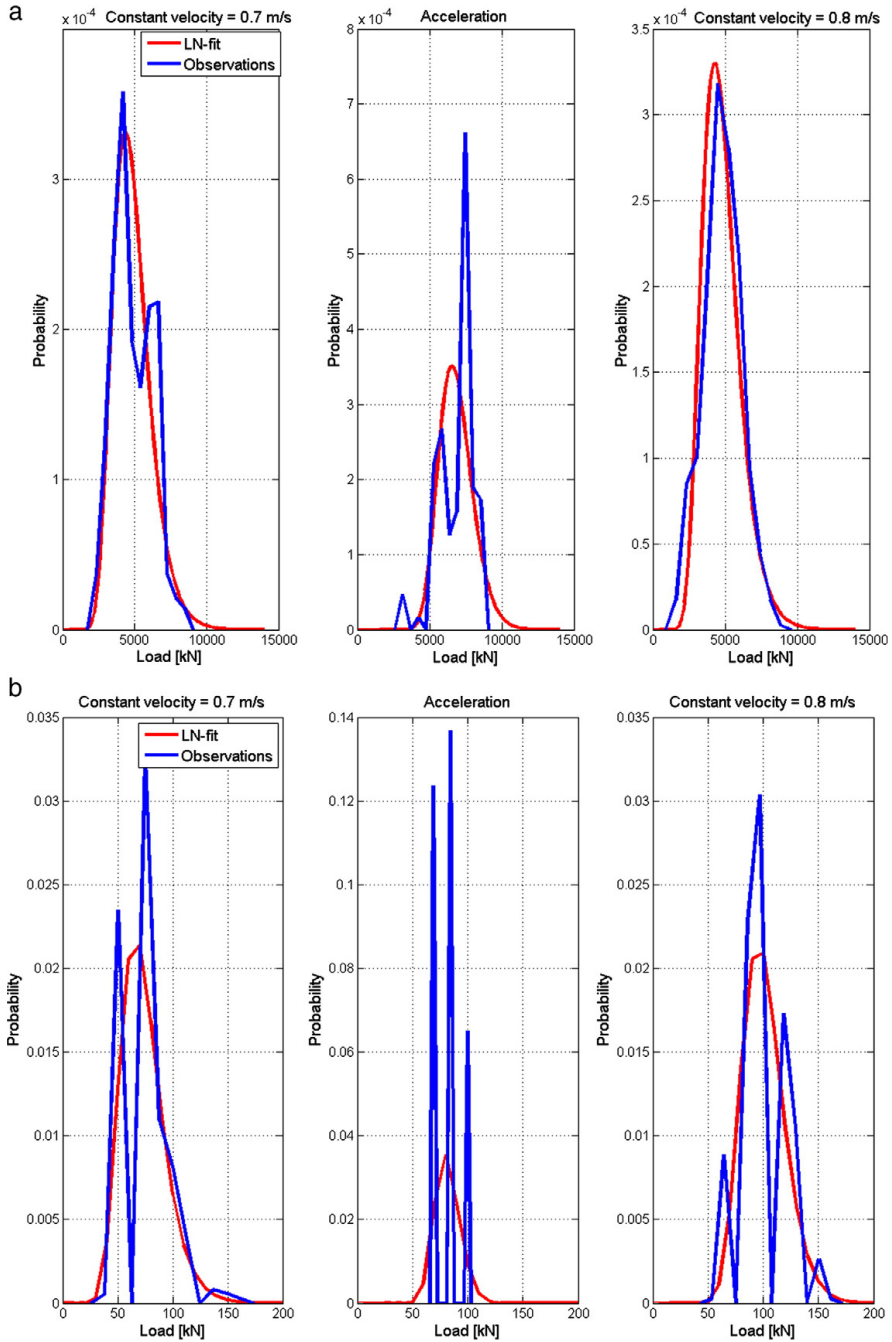


Fig. 19. Probability density functions based on observations of tow loads in different tow phases and fitted log-normal distributions. Based on model type 1 tests with rectangular iceberg model in a) 80% ice concentration and b) open water.

not possible to conclude that iceberg towing in ice conditions up to 50% is possible. One should also have in mind that a traditional 16 cm thick tow rope made of polypropylene has a maximum capacity

around 800 kPa (The Engineering Toolbox, 2009). This means that much stronger tow lines need to be developed for towing in sea ice compared to open waters.

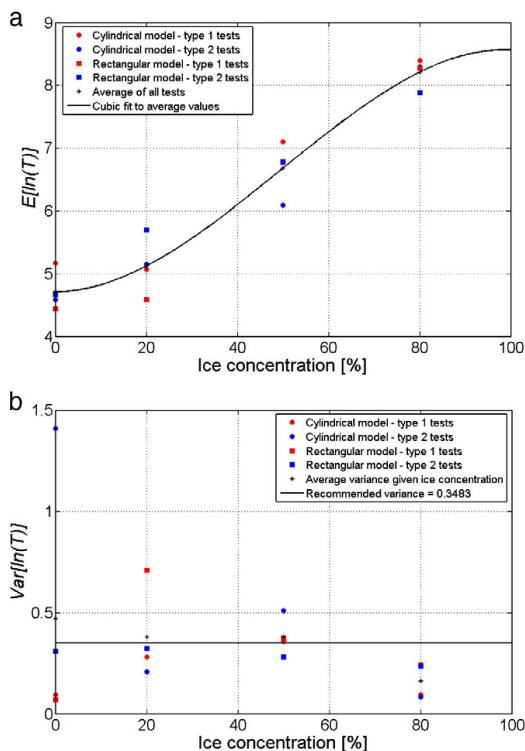


Fig. 20. Parameters in log-normal distribution based on observations from model tests. T refers to the tension loads in the tow line in full scale [kN]. a) Mean value (μ), b) Variance (σ^2).

Table 6

Average number of local load maxima per hour in recorded time series.

Ice concentration	80%	50%	20%	Open water
Number of peaks per hour	5585	4647	2856	2439

With respect to tow line capacity, it should also be noted that tow lines in ice covered waters will be exposed to significant wear compared to tow lines in open waters and this will probably reduce the capacity of the tow lines. Observations from the tank tests show that the tow lines frequently saw themselves into the ice floes or are squeezed between ice floes. It should also be noted that the tow rope applied in the tank model tests were extremely static. If more elastic tow ropes would be used in iceberg towing, it is likely that the load distributions will be different from what is presented in this report.

Stability was not a concern in the present tests. Roll and pitch motions were always less than 0.7° . With respect to yaw, both models experienced rotations up to approximately 30° during some of the tests. However, no sliding was observed between the iceberg and tow line and the rotations initiated by a change in tow course were rapidly damped. As a consequence of the change in course some tilting (roll) could be observed. Basically, the same oscillations and level of magnitude in roll and pitch occur whether the iceberg is floating in open water or in high concentrations of sea ice. However, in some events, the sea ice is piling up or moving sideways causing a more or less permanent trim angle.

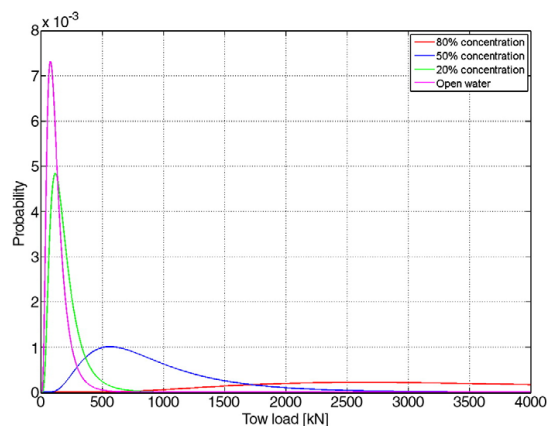


Fig. 21. Smoothed log-normal distributions representing tow loads in various ice concentrations.

With respect to surge, such movements are clearly dependent on the sea ice concentrations. Icebergs towed in 80% ice will experience very little surge movements simply because all drift is rapidly stopped by the surrounding sea ice. In open water, icebergs will keep a momentum straight ahead even after a course change and the sideways displacements (sway) will be more significant than in the sea ice. Some special attention should be given to test type 2 with the cylindrical model in open water. During this test, an extreme high load peak occurred after the change in course. Reason for this is not known, but it is interesting to note the reduction in tow length and increase in heave occurring simultaneously. This incident shows that under some manoeuvres, tow loads may become very high even in open water (Fig. 9, minute 23).

5. Conclusion

Tank model tests of iceberg towing in open water and in sea ice have been carried out and the most important findings are as follows:

- Towing of medium size icebergs in moderate thick sea ice is considered not to be feasible in concentrations higher than 50% due to high resistance caused by the sea ice actions on the iceberg.
- Towing in ice concentrations in the range 20–50% may be feasible conditional that sufficiently strong tow lines are available. Traditional polypropylene tow lines are not considered to have sufficient strength for iceberg towing in sea ice.
- Iceberg tow loads are highly stochastic and log-normal distributions seem to represent the load distributions fairly well. The log-normal distribution parameters will depend on the sea ice concentration.
- A model for estimating extreme tow loads prior to a tow has been demonstrated.
- The general arrangements for single vessel iceberg towing in open waters seems applicable also when towing in light ice conditions. However, in high ice concentrations the tow line will be lifted above the surface and cause risk for rupture and consequent “snapping”.
- The importance of tow speed, acceleration and change of tow course is found to be small compared to the importance of the sea ice concentration. The importance of ice thickness, ice floe size distribution, iceberg size, and metocean conditions has not been evaluated.
- There are not found any significant differences with respect to iceberg stability when towed in sea ice compared to open water. Both tow load and load from sea ice will act in the same vertical level and all recordings show small roll and pitch rotations in all tests.

With respect to the surge and sway of the icebergs, such movements will be more significant in open water as the sea ice stops all free drift very rapidly.

It is extremely important to note that all the test results and the abovementioned conclusions are based on the assumption that model results can be scaled up and representative for real life operations. Due to uncertainties both in scaling and instrument accuracy as well as discrepancies between model arrangements and real life arrangements, these assumptions are not necessarily fulfilled. This should be taken into account if the results are to be used for practical purposes.

Acknowledgements

The work described in this report was supported by the European Community's Sixth Framework Programme through the grant to the budget of the Integrated Infrastructure Initiative HYDRALAB III, Contract no. 022441(RII3). The authors would like to thank the Hamburg Ship Model Basin (HSVA), especially the ice tank crew, for the hospitality, technical and scientific support and the professional execution of the test programme in the Research Infrastructure ARCTECLAB. In addition, PhD students Christian Ulrich from Hamburg University of Technology and Aleksey Shestov from the University Centre in Svalbard should be acknowledged for their professional assistance during the test period.

References

- Baltic Icebreaking Management (BIM, 2008. The World Icebreaker and Icebreaking Supply Vessel Fleet, Finland 2008, 15 pp.
- Crocker, G., Wright, B., Thistle, S. and Bruneau, S., 1998. An assessment of Current Iceberg Management Capabilities. Contract report for National Research Council Canada, Prepared by C-CORE and B. Wright and Associates Ltd., C-CORE Publication 98-C26, 108 p.
- Evers, K.U., Jochmann, P., 1993. An advanced technique to improve the mechanical properties of model ice developed at the HSVA ice tank. Proceedings of the 12th International Conference on Port and Ocean Engineering under Arctic Conditions, Hamburg, Germany, pp. 877–888.
- Løset, S., Timco, G.W., 1993. Laboratory testing of a flexible boom for ice management. Journal of Offshore Mechanics and Arctic Engineering, JOMAE 115 (3), 149–153.
- McClintock, J., McKenna, R. and Woodworth-Lynas, C., 2007. Grand Banks Iceberg Management. PERD/CHC Report 20–84, Report prepared by AMEC Earth & Environmental, St. John's, NL, R.F. McKenna & Associates, Wakefield, QC, and PETRA International Ltd., Cupids, NL, 84 p.
- Rudkin, P., Boldrick, C. and Barron Jr., P., 2005. PERD Iceberg Management Database. PERD/CHC Report 20–72, Report prepared by Provincial Aerospace Environmental Services (PAL), St. John's, NL, 71 p.
- Schwarz, J., Frederking, R.M.W., Gavrillo, V., Petrov, I.G., Hirayama, K.I., Mellor, M., Tryde, P., Vaudrey, 1981. Standardized testing methods for measuring mechanical properties of ice. Cold Regions Science and Technology 4, 245–253.
- The Engineering Toolbox, 2009. Elastic properties and young modulus for some materials – pressure vs Flow control. http://www.engineeringtoolbox.com/young-modulus-d_417.html, cited 25.08.2009.

4.4 Iceberg management and impact on design of offshore structures



Contents lists available at ScienceDirect

Cold Regions Science and Technology

journal homepage: www.elsevier.com/locate/coldregions

Iceberg management and impact on design of offshore structures

Kenneth Eik^{a,b,*}, Ove Tobias Gudmestad^{a,c}^a Norwegian University of Science and Technology, Trondheim, Norway^b Statoil, Trondheim, Norway^c University of Stavanger, Stavanger, Norway

ARTICLE INFO

Article history:

Received 9 December 2009

Accepted 15 April 2010

Keywords:

Iceberg drift modelling

Iceberg management

Offshore installation design

ABSTRACT

A methodology is presented for the systematic evaluation of the need for an iceberg management system and the efficiency of various components such as detection, deflection and disconnection. The approach involves the numerical modelling of iceberg drift and probabilistic analysis. Experiences from the Canadian iceberg detection studies and iceberg deflection operations have been incorporated into the approach.

The methodology describes the concept: an offshore installation and an iceberg management system, as a traditional industrial system, i.e. a system which is designed so that it works well under normal conditions. Under some circumstances, an event occurs which stops the operation of the system. In order to prevent such a stop, different types of safety functions may be considered in order to increase the redundancy in the system and thereby increase the operability. In the present work, the iceberg management means are treated as such safety functions.

For a selected site in the Barents Sea, it was found that the maximum impact load corresponding to a 10000 year event was 85 MJ for a concept without any iceberg management capabilities. An alternative system with iceberg detection, iceberg deflection and disconnection capabilities including emergency disconnect indicated a corresponding abnormal load of about 1.8 MJ.

© 2010 Elsevier B.V. All rights reserved.

1. Introduction

Icebergs may cause a threat to production and exploration installations, vessels and operations in a number of Arctic and Antarctic regions. With respect to permanent offshore installations, the presence of icebergs is of concern already in the concept selection phase. Different design philosophies may be applied depending both on the iceberg regime and the field conditions. On the Grand Banks, offshore the East Coast of Canada, this is best illustrated by the lay-out of the three fields: Hibernia, Terra Nova and White Rose. While a fixed and robust gravity based structure (GBS) was selected for the first of these fields (Hibernia, 2009), the subsequent fields were developed with Floating Production, Storage and Offloading vessels (FPSOs). The GBS is designed to withstand impact with a 1 million ton iceberg without damage and contact with icebergs up to 6 million tons with repairable damage (accidental limit state) (Hibernia, 2009). The FPSOs on the other hand, are designed to withstand collisions only with smaller icebergs and otherwise, when threatened by larger icebergs, shut down the production, disconnect and move off location when threatened by larger icebergs.

In order to reduce the probability of an iceberg collision, all installations and operations on the Grand Banks are protected with an

ice management system. The philosophy adopted for such a system is that a large region is surveyed with respect to iceberg threats. All icebergs that may impose a threat are deflected along drift directions that are considered safe for the installations and their ongoing operations. It has been documented that icebergs in that area can successfully be deflected around installations in approximately 75% of all events (Rudkin et al., 2005). The preferred method for iceberg deflection is single vessel tow rope (Fig. 1) while a two vessel towing technique or towing with nets occasionally is used to tow large icebergs or unstable icebergs respectively. Smaller icebergs such as bergy bits and growlers may be deflected by use of water cannons or propeller wash.

Most of the internationally recognized codes for offshore structures require that some sort of limit state check is carried out, e.g. ISO (2007), CSA (1992) and NORSOK (2007). In such a check, it must be documented that extreme loads are lower than the structural resistance. With respect to loads from a collision between an iceberg and a structure there are methodologies for estimating this based on distributions of parameters such as iceberg frequency, iceberg size distribution, iceberg velocity distribution, installation size and shape etc (Fuglem et al., 1999). With respect to iceberg management capabilities, this has also been taken into account in a probabilistic framework by Fuglem et al. (1999). However, in order to achieve reliable results from the probabilistic framework, reliable statistics must be available that describe not only the relevant parameters but also the correlations between the parameters. In more remote regions

* Corresponding author. Norwegian University of Science and Technology, Trondheim, Norway. Fax: +47 73 59 70 21.

E-mail address: kenjo@statoil.com (K. Eik).

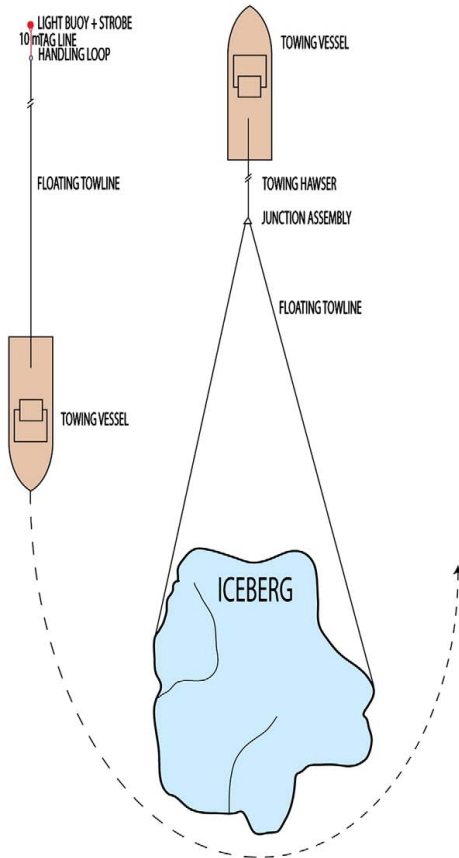


Fig. 1. Illustration of a single vessel iceberg tow operation. After McClintock et al., 2007.

such as the e.g. the Barents Sea and the Kara Sea only limited information regarding the iceberg regimes is known. The objective of this work has been to combine the advantages from the probabilistic framework with the physical description of the iceberg drift and thereby be able to estimate extreme impact load concepts for offshore installations with various degrees of iceberg management capabilities.

In this study, a physical iceberg drift model has been applied together with collected data on iceberg detection and physical iceberg management capabilities in order to study the effect of iceberg management on design loads. The general methodology, which is adopted from system reliability theory, is presented in Section 2. The physical iceberg drift model and use of this is presented in Section 3. In Section 4, data regarding iceberg detection and data from the PERD iceberg management database, have been analysed and distributions prepared for a “semi-probabilistic” load analysis. In Section 5 the methodology has been demonstrated at a location in the Shtokman region in the Barents Sea. The results are discussed in Section 6 and conclusions presented in Section 7.

2. Event tree philosophy

Information on event tree analysis can for example be found in Rausand and Høyland (2004). In many accident scenarios, the initiating event may have a wide spectrum of possible outcomes ranging from

consequences to catastrophic. The accident progression is best analysed by an inductive method and the most commonly used method is the event tree analysis. In most well designed industrial systems, a number of safety functions, or barriers, are provided to stop or mitigate the consequences of potential accidental events. The safety functions may generally comprise technical equipment, human interventions, emergency procedures etc. The consequences of the accidental event are determined by how the accident progression is affected by subsequent failure or operation of the safety functions, by human errors made in responding to the accidental event, and by various factors such as weather conditions and time of the day.

An event tree is a logic tree diagram that starts from a basic initiating event and provides a systematic coverage of the time sequence of event propagation to its potential outcomes or consequences. In the development of the event tree, we follow each of the possible sequences of events that result from assuming failure or success of the safety functions affected as the accident propagates. Each event in the tree will be conditional on the occurrence of the previous events in the chain. The outcomes of each event are most often assumed to be binary (true or false) but may also include multiple outcomes.

Event tree analyses have been used in risk and reliability analyses of a wide range of technological systems. In this study, we propose to model the operation of an offshore installation as such a system and the occurrence of icebergs as accidental events. The event tree analysis has been carried out in six steps in accordance with (AIChE, 1992):

1. Identification of initiating event
2. Identification of the safety functions that are designed to deal with the initiating event
3. Construction of the event tree
4. Description of the resulting accident sequences
5. Calculation of probabilities/frequencies for the identified consequences
6. Compilation and presentation of the results from the analysis

2.1. Initiating event

Usually, a number of different zones have been defined around an installation which works in an environment prone by sea ice and or icebergs. In each zone, there are certain pre-defined activities that will commence if ice is observed (e.g. Wright, 2000). An example of such an action may be to send out a vessel for inspection if an iceberg that has been detected by the radar. Other types of actions may be to stop ongoing operations and prepare installation for disconnection (e.g. Gudmestad et al., 2009).

One of the zones used in Arctic operations is typically named the ice monitoring zone and is defined as a region in which continuous iceberg surveillance is carried out. In this study, we have selected to define the initiating event as an event where an iceberg is entering the ice monitoring zone. The size of such a zone will depend on the quality and range of devices used for iceberg detection. One of the most commonly used instruments is however the marine radar. In a study by Miller and Satterfield (1984), the performance of marine radars for iceberg detection was investigated. They found that the average distance between radar and iceberg in the first detection was about 28 km while maximum distance was 87 km. It is important to note that the range of such radars depends strongly on the radar elevation and in the present study it has been assumed that there is an FPU at site that offers the possibility to install a radar a relatively high level (60–80 m above the sea level). Use of satellite sensors may both improve the detection range significantly and increase the overall probability of detection (POD) but may also increase the risk of false alarms. Due to this and to simplify the demonstration of the event tree approach, use of satellite sensors have not been included in this paper.

The reliability of the marine radars used in iceberg detection is further treated in Section 4. Based on the numbers in Miller and Satterfield (1984) however, it was suggested to use 35 km radius for the iceberg monitoring zone. The initiating event may therefore be stated as:

"An iceberg appears 35 km or closer to the installation."

It should be noted however, that an iceberg monitoring zone may very well be defined based on a criteria which states in time how far away the iceberg is.

2.2. Safety functions

In the event tree approach, the intention is that the ice management systems serve as safety functions.

The first step in the ice management system will be to identify the icebergs. The probability of detection (POD) will be a function of the quality of the detection system and the time the icebergs spend within the ice monitoring zone. Recognized instruments for iceberg detection such as marine radars, satellite images, aerial reconnaissance, ice intelligence vessels etc. will all to some degree be weather dependent and this needs to be taken into account.

Independent on whether the iceberg in the monitoring zone is detected or not, it may only cause damage to the installation if parts of the iceberg interact with the installation. Despite that iceberg detection actually is not a safety function since it does not involve any type of activities that physically prevents an iceberg collision in itself, this is brought into the event tree model as one of the safety functions. The motivation for doing so is to get the correct probabilities for the various outcomes in the event tree. Further, it should also be emphasized that it is not possible to manage icebergs that not are detected.

The next step in the ice management system will be to deflect the threatening icebergs from colliding with the installation. Typical methods for iceberg deflection are single or dual vessel towing, net towing, propeller wash or deflection by use of water cannon. The first of these methods is illustrated in Fig. 1. Selection of method will depend on a number of factors such as iceberg size, shape, available time and available vessels. However, the single vessel tow is usually the preferred method in most of the tows while the other methods are used if the first attempt fails (Rudkin et al., 2005).

If the physical iceberg management fails, some installations and rigs may have the possibility to disconnect and escape the site. For a disconnectable floating concept, guarantee for successful disconnection can never be given. The question regarding making a fixed versus a disconnectable installation is also generally challenging for the designers as the last solution is expected to be more complicated technically and more expensive. On the other hand, a disconnectable concept may reduce the expected number of interactions with icebergs and thereby reduce the expected extreme loads. The ability to disconnect is therefore considered as a last safety function.

2.3. Construction of event tree

The event tree is constructed with binary outcomes. The statements regarding performance of the safety functions are either true or false. The statements will all express that the safety functions fail. At each branch there will be a certain probability for the outcomes true and false. The sum of the probabilities at one branch shall always be 1. An illustration of an event tree for an iceberg-structure collision is presented in Fig. 2. Since this illustration is intended only to demonstrate the event tree philosophy, failure probabilities are not included. For offshore installations, one typical requirement will be that the installation shall remain its structural integrity after accidental events with annual probability of 10^{-4} or less. One way to document that such a requirement is fulfilled with respect to

iceberg collisions will be to show that the sum of the frequencies F_1 and F_3 in Fig. 2 is lower than 10^{-4} . If one considers a system without any sort of ice management systems, all frequencies F_3 to F_6 will be zero and the annual probability of collision will be F_1 . If F_1 ends up being higher than acceptable, one may introduce physical iceberg management as a next step and the frequency of collisions will be reduced. If the probability for collision still is unacceptable, another mean to prevent collision will be to include disconnection and escape capabilities and one ends up with the system illustrated in Fig. 2.

2.4. Resulting accidental sequences

With respect to outcome of the various sequences in the event tree, this is somewhat simplified in Fig. 2. If any impact between iceberg and structure would result in loss of structural integrity, the event tree could have been used as it is. However, since some installations may withstand loads from smaller icebergs, it is not sufficient only to distinguish between impact versus no impact. The way of dealing with this is, however, simple when combining the event tree model with results from a physical iceberg drift model. From the physical drift model information regarding iceberg mass and drift velocity will be available making it possible to calculate the kinetic energy of the iceberg at the moment it collides with the structure. This is described in more detail in Section 3.

2.5. Probabilities/frequencies for identified consequences

The main challenge when using the event tree model is to establish reliable probabilities for the various events. The methodologies used for doing this are explained in Sections 3 and 4.

2.6. Compilation and presentation of the results from the analysis

The intention with introducing the event tree model is to document statistically the effect of various iceberg management systems. By using the event tree combined with a physical iceberg drift model one ends up with various frequencies for interactions between the structure and icebergs depending on the iceberg management systems that are considered. In addition, the analyses will also result in various distributions for iceberg kinetic energy in the moment of collision. By combining the frequency of collisions with the kinetic energy distributions, extreme and abnormal collision loads corresponding to return periods such as 100 years and 10000 years respectively may be estimated.

3. Iceberg drift modelling

In order to establish statistics regarding frequencies of the various events and sequences in the event tree, realistic iceberg drift trajectories are required. These trajectories must include all information which is relevant for iceberg detection and physical iceberg management. This means that, in addition to iceberg positions, the trajectories should include parameters such as wave height, wind speed, current speed, iceberg shape and size at each time step. In this work, an iceberg drift model described by Eik (2009a) has been applied to generate iceberg drift trajectories. The model is capable of performing historical iceberg drift simulations (hindcast) within the period January 1987 to December 1992.

Iceberg drift may be modelled by balancing the forces with the product of mass and accelerations in accordance with Newton's 2nd law:

$$m \frac{d\mathbf{V}_i}{dt} = -m f \mathbf{k} \times \mathbf{V}_i + \mathbf{F}_a + \mathbf{F}_w + \mathbf{F}_{wd} + \mathbf{F}_{si} + \mathbf{F}_p \quad (1)$$

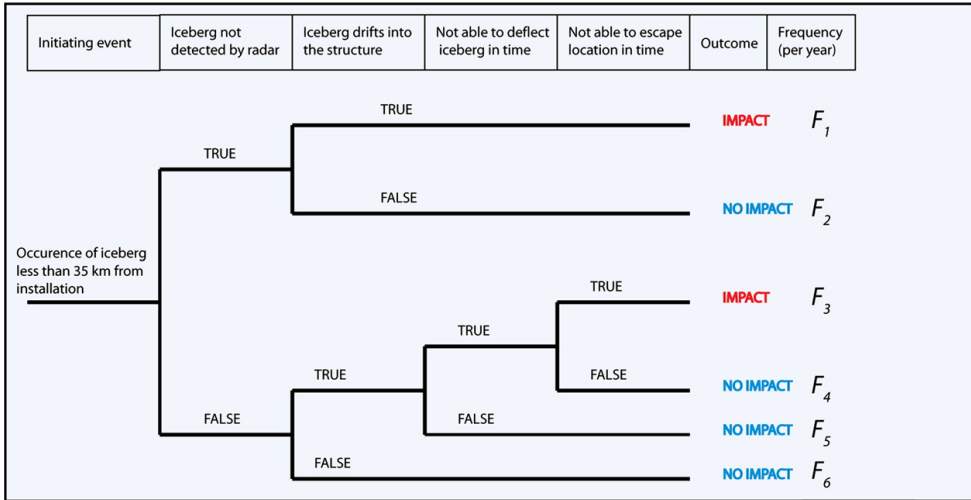


Fig. 2. Illustration of an event tree for iceberg-structure collision.

where $m = m_0(1 + C_m)$ and m_0 is the physical mass and C_m is the coefficient of the added mass. V_i is the local velocity of the iceberg, f is the Coriolis parameter and k is the unit vector in vertical direction. Further, F_a and F_w are the air and water drag, respectively. F_{wd} is the mean wave drift force, F_{si} is the sea ice drag and F_p is the horizontal gradient force exerted by the water on the volume that the iceberg displaces. Information regarding all the required metocean input and parameters is found in Eik (2009a). It should further be noted that an iceberg deterioration model is included in the drift model (Eik, 2009b) making the iceberg decaying as it drifts through the open water.

In this work, icebergs were distributed along the border of a 73 105 km² large area, denoted as the Shtokman region (Fig. 3). All icebergs were randomly given a start time within the period 1987–1992 before simulations were started. With respect to size iceberg lengths and drafts these parameters were generated in a similar way

but with use of appropriate statistical distributions for these parameters based on observations during the IDAP programme (Vefsnmo et al., 1992). It should be noted that the iceberg observations during the IDAP campaign were done either to the east of Shtokman (Spitsbergenbanken) or to the north of Shtokman (Frans Josef Land). Observations done in the Shtokman region (Zubakin et al., 2005) indicate however, that a significant number of the icebergs observed in the region are bergy bits. The bergy bits were probably neglected during the IDAP programme and are consequently not included in statistical distributions for i.e. iceberg length. The IDAP iceberg length distribution has still been used in this study under the assumption that it represents the parameter at the border to the region (Fig. 3).

Simulations were carried out with an update of metocean parameters every 2 h. At every 2 h, the deterioration was calculated and the iceberg size was updated. The simulation of the individual

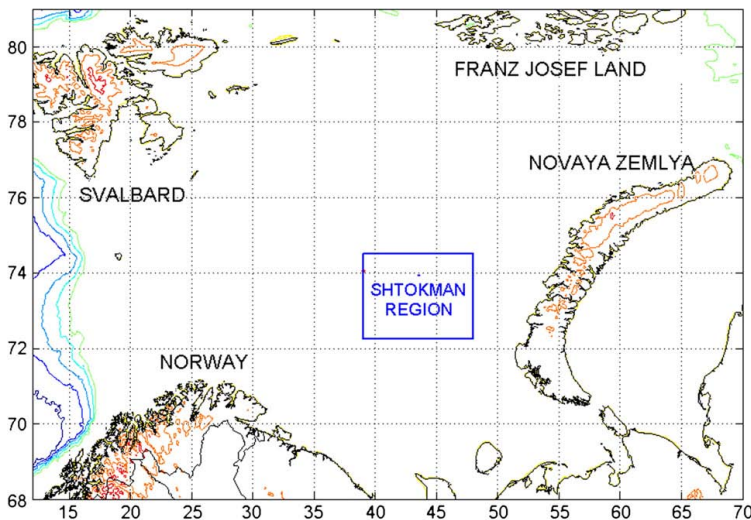


Fig. 3. Map of the Barents Sea and the Shtokman region (72.25°N–74.50°N, 39.0°E–48.0°E).

icebergs would be stopped if the simulation time exceeded 50 days, if the iceberg grounded, if the iceberg were fully deteriorated (length less than 1 m) or if the iceberg left the Shtokman region. At each time step simultaneous data for winds, waves and currents were stored together with information on iceberg position and iceberg size.

It is well documented that the majority of icebergs in the Central Barents Sea originates from Franz Josef Land, alternatively Svalbard, the Northern Part of Novaya Zemlya, Kara Sea (not Kara gate) or the Arctic Ocean. Due to this, 75% of all simulated icebergs were distributed uniformly along the northern boundary of the Shtokman region. Further, 12% of all icebergs were distributed along the western and eastern borders of the region. The last 1% of the icebergs was started at the southern border of the region, uniformly distributed along the border. The reason for starting the iceberg simulations along the border of the specified region is because systematic iceberg observations have been carried out by Russian sources within the periods 1949–1992 and 2002–2005. Based on these observations, it has been estimated by Statoil that totally about 880 icebergs have been within the Shtokman region within the last 100 years (Nygaard, 2009). It should be noted that there is a significant uncertainty in this estimate due to limitations in the surveillance capabilities. Further, effects of future climate changes are not taken into account.

An alternative to distributing icebergs along the border of the Shtokman region would be to start simulations from the iceberg sources into the Barents Sea and thereafter select only those trajectories going into the Shtokman region. However, this would require more and longer simulations than those presented in this work.

In total, 270 000 iceberg simulations were started along the border of the Shtokman region but only 106 635 of these entered the Shtokman region. From these simulations, it was found that the average residence time for icebergs in this region is approximately 5 days with a standard deviation of 6 days. Based on information on residence time, iceberg frequency and iceberg size distributions, the annual contact probability may be calculated based on areal density considerations (e.g. Jordaan et al., 1999). However, in order to also investigate the effect of iceberg management another approach was required. As a first step in this alternative approach, all of the trajectories which touched into the iceberg monitoring zone were selected. Thereafter these trajectories were used in simulation of iceberg detection and iceberg management. These simulations are described in the following section.

4. Iceberg management

4.1. Probability of detection

With respect to iceberg detection it is obvious that a 100% probability of detection (POD) cannot be guaranteed. Due to this, a statistical description of the quality of the detection systems is required. In this study, only the skills of traditional marine radars have been included. If a system consist of more comprehensive detection systems including satellite images, upward looking sonar's, enhanced marine radars, surveillance flights etc., the POD will increase making the results in this study somewhat conservative.

With respect to radar detection, there are a number of parameters that influence the detection capabilities, such as; sea states, distance to target, size and shape of the target, precipitation and operator skills. As it is not feasible to include all the dependencies in a statistical model, it is necessary to identify the most important factors and describe them as accurately as possible. Fuglem et al. (1999) expressed the POD for an iceberg with waterline length, L , as the cumulative probability of a normal distribution with mean $6 \cdot H_s$ and standard deviation $1.8 \cdot H_s$, where H_s is the significant wave height in a stationary sea state:

$$\text{POD}(L|H_s) = F_N(L, \mu = 6H_s, \sigma = 1.8H_s) \quad (2)$$

The POD given wave heights for different iceberg sizes are shown in Fig. 4.

4.2. Probability of successful iceberg management

For icebergs that are detected and predicted to drift into an offshore structure, the ability to physically deflect icebergs will serve as a safety function in the event tree model. However, in similarity to the detection function, the probability of successful physical iceberg management will depend on a number of parameters such as iceberg size and shape, the physical environmental conditions and available time from detection to collision. Again in similarity with the iceberg detection probability, it has been selected to focus only on a few of these parameters which are expected to be the most important ones namely H_s , L and available time for iceberg deflection (T). In the following, the definition of successful physical iceberg management is presented and thereafter the correlations between success numbers and H_s , L and T are investigated.

4.2.1. Definition of success

There are different alternatives when evaluating the outcome of a physical iceberg management operation. C-Core (2002) distinguished between two different definitions of tow success:

- Operational success
 - "A tow can be considered successful if downtime was avoided"
- Technical success
 - "A tow can be considered technically successful if: (a) a demonstrated change in course was achieved and (b) the towed iceberg achieved a course made good with one or multiple attempts."

Despite that these definitions provide a simple approach to define success, they do not provide a means of evaluating all the components of a management operation that contributed to the success. Further, when applying data on success from one region to another it is crucial to know under which conditions a success was achieved or not achieved.

Based on 1505 records of 46 individual fields on iceberg management operations conducted over a 30 year long period at the East Coast of Canada (PERD Comprehensive Iceberg Management Database), Rudkin et al. (2005) introduced an alternative way of defining iceberg management success which is considered more applicable for use in e.g. probabilistic iceberg load analyses. The approach is well described by Rudkin et al. (2005) and is therefore not repeated herein. Basically, the degree of success is described by an index, S , which is a function of parameters such as; number of tow attempts, achieved

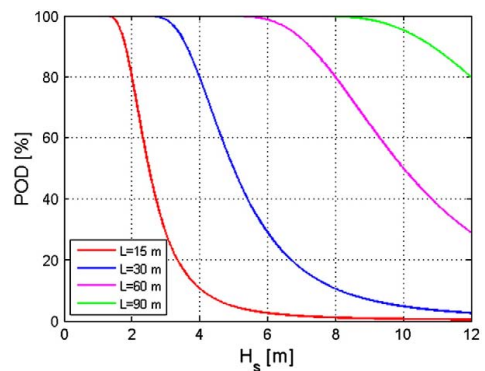


Fig. 4. Probability of detection (POD) from a marine radar given significant wave height, H_s and iceberg length, L . Based on a distribution suggested by Fuglem et al. (1999).

tow deflection, effect on operation etc. If a perfect tow is conducted, S will be 100. In order to avoid confusion, it should be noted that S does not represent the success in percentage but simply is an index where even negative values may be the outcome of a failed operation (minimum S index is -10). Further, Rudkin et al. (2005) assigned four categories to various ranges of calculated success numbers (Table 1).

For a few of the operations included in the PERD Comprehensive Iceberg Management database, the success index, S , is negative. In order to be able to describe the probability of success by a simple statistical distribution such as the two-parameter Weibull distribution, the success index was inverted. By doing this, a perfect operation would correspond to an inverted success index $S' = 0$ while a poor operation would be characterised by $S' \geq 45$. By using the method of moments, it can be seen that a two-parameter Weibull distribution, Eq. (3), describes the inverted success index well (Fig. 5).

$$P(s' < S') = 1 - \exp \left[- \left(\frac{s'}{\beta} \right)^\alpha \right] \quad (3)$$

The Weibull shape parameter is denoted α and the scale parameter, β .

4.2.2. Probability of success conditional wave height, iceberg waterline length and time available for deflection

Based on the 1505 records in the PERD CIM database, we have plotted the inverted success index, S' and corresponding recorded values for H_s , L and T in scatter plots (Fig. 6). As can be seen from the plots, there are not really any strong correlations between the success number and any of these parameters. However, by including average values and standard deviations in the plots some conclusions can be drawn:

1. The probability of success will increase slowly with increasing time available
2. The probability of success is lower for H_s in the range 4 to 6 m than in the range 0 to 4 m.
3. The probability of success will decrease slowly with increasing L .

Further, it should be noted there is no documentation on deflections of icebergs:

1. Embedded in sea ice
2. In sea states characterised by $H_s > 6$ m
3. With waterline length larger than 480 m

Consequently, the probability of successful iceberg deflections in such conditions should be assumed zero until otherwise proven. This assumption is also incorporated into the present model; i.e. if the iceberg drift model shows that sea ice occurs in the same region as an approaching iceberg, the probability of successful iceberg deflection is set to zero.

With respect to establishing a statistical distribution that represents the inverted success index and in addition includes the dependencies on H_s , L and T the following approach was used:

1. All records from the PERD CIM database were sorted into a 3-dimensional matrix depending on H_s , L and T . Each parameter was initially divided into 3 classes.

Table 1
Iceberg management success index (S) and associated grading of success in categories.

Numerator, S	Category
100–91	Complete success
90–76	Successful
75–56	Acceptable
<55	Poor

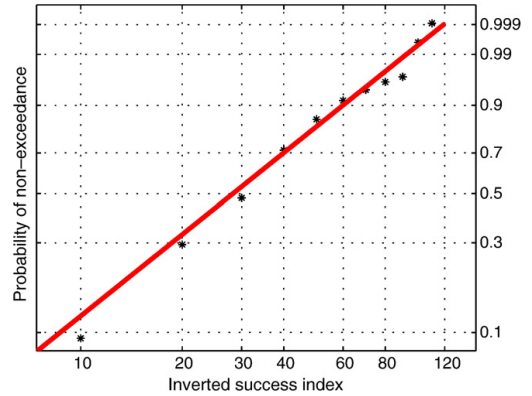


Fig. 5. Inverted success index distribution. Data from the PERD CIM database is indicated with crosses while a fitted two-parameter Weibull distribution is given by the continuous line. The Weibull shape and scale parameters are 1.598 and 35.538 respectively.

2. For each of the 3^3 combinations of H_s , L and T , density distributions for the inverted success indexes were plotted. Due to limited data in the class for the largest icebergs, the probability of successful towing of icebergs longer than 300 m was set to zero and the number of H_s , L and T combinations were reduced to 18
3. For each of the 18 combinations of H_s , L and T a two-parameter Weibull distribution was fitted to the density distributions for S' .

Fig. 7 shows one of the fitted Weibull distributions while all Weibull parameters are presented in Table 2.

4.3. Probability of successful offshore installation disconnection

As a final safety function in the iceberg management system, the offshore installation may have the capability to avoid a collision by shutting down all operations, disconnect the riser and anchor lines and escape the site. In this study, two scenarios will be considered:

1. The probability of successful disconnection is 0.98 (ref. Fuglem et al., 1999)
2. The offshore installation cannot be disconnected, i.e. the probability of successful disconnection is 0.

With respect to the first of these scenarios, it is likely that the probability of a successful disconnection of a Floating Production Unit (FPU) will depend on the actual load situation. One example would be a situation where the horizontal offset of the FPU is large and it may not be possible to disconnect without damaging the risers. The correlations between the probability of a successful disconnection and parameters such as significant wave height or sea ice conditions have not been assessed in this work.

5. Probabilistic analyses

By using the probability of successful offshore disconnection, the distributions for successful iceberg detection and successful iceberg deflection together with trajectories from the physical iceberg drift model, it is now possible to fill in the probabilities for the various sequences in the event tree (Fig. 2). For demonstration of the methodology, it was decided to consider a location somewhat to the north of the Shtokman field at position 74°N, 43°E. It should be noted that the simulation clearly showed that the iceberg density is not uniform in the selected region (Fig. 3) and the areal density of

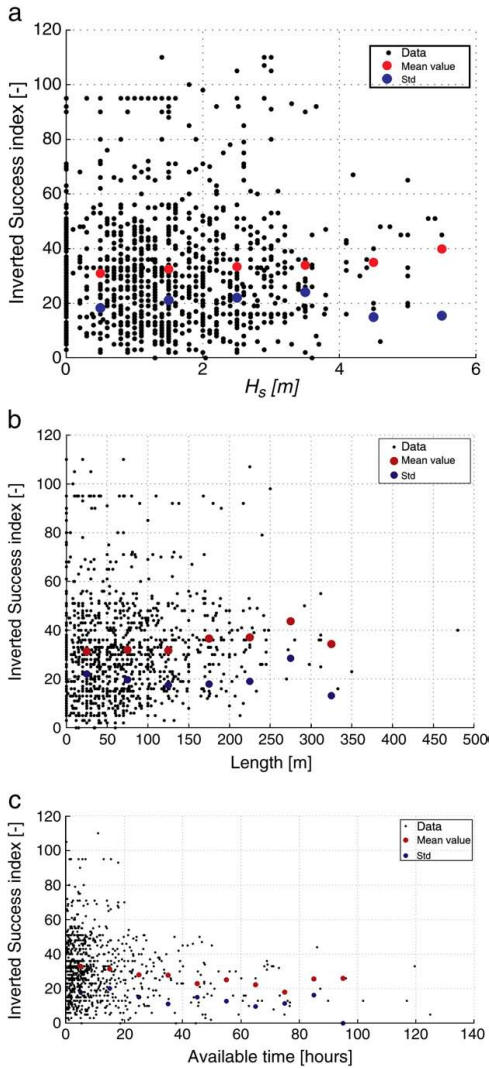


Fig. 6. Scatter plots of inverted success index versus (a) significant wave height, (b) iceberg waterline length and (c) available time.

icebergs around Shtokman is significantly less than at the selected location. The following procedure was applied:

1. All the trajectories that touched into the iceberg monitoring zone were selected (i.e. 35 km or closer to the installation).
2. A semi-probabilistic analysis was thereafter conducted by the following steps for each trajectory:
 - a. At the first time step within the iceberg monitoring zone, the iceberg waterline length (L) and corresponding significant wave height (H_s) was read.
 - b. A random number uniformly distributed within 0 and 1 was drawn from a random number generator. From the distribution

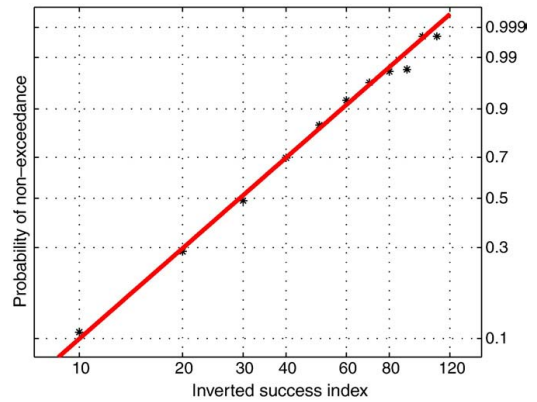


Fig. 7. Inverted success index distribution conditional $H_s < 2$ m, $L < 150$ m and $T < 20$ h. Data from 451 records in the PERD CIM database is indicated with stars while a fitted two-parameter Weibull distribution is given by the continuous line.

of iceberg detection, which is a function of H_s and L , the iceberg at that time was found to be either detected or not detected.

- c. The same procedure as described in a and b was repeated at the next time step in the same trajectory (i.e. 2 h later). In order to finally declare an iceberg for detected, two consecutive detections would be required.
3. By going through step 2 for all iceberg drift trajectories, the icebergs were divided into two classes; “detected” and “not detected.” The probability on the first branch in the event tree would simply be the ratio between the numbers of trajectories in each class divided by the total number of trajectories.
4. For all the “non-detected” icebergs, it was investigated how many of these actually touched into a collision zone. The collision zone was in this study defined as a circle with radius 500 m around the centre of the offshore installation. A collision would be defined as the event where the centre of the iceberg is within a circle with radius 500 m + 0.5 · L . The collision zone is illustrated in Fig. 8.
5. For the “detected” icebergs, all trajectories colliding with the structure were identified.
6. In all the “detected” and “colliding” trajectories, the time between point of detection and time of collision was identified (T). In addition, H_s and L at the point of detection was identified.

Table 2

Weibull parameters in distributions for inverted success indexes conditional H_s , L and T . α is the Weibull shape parameter while β is the Weibull scale parameter. If there is not sufficient data to establish a statistical distribution, the probability of successful iceberg management operations is considered to be zero (i.e. $P = 0$). Some of the parameters are also copied from classes which are considered to be identical or less favourable with respect to iceberg deflection. These numbers are enclosed by parentheses.

	$0 \leq L < 150$	$150 \leq L < 300$
Time 0–20		
$0 \leq H_s < 2$	$\alpha = 1.756 \beta = 36.119$	$\alpha = 2.858 \beta = 41.427$
$2 \leq H_s < 4$	$\alpha = 1.838 \beta = 39.683$	$\alpha = 2.231 \beta = 35.566$
$4 \leq H_s < 6$	$\alpha = 3.341 \beta = 43.769$	$P = 0$
Time 20–40		
$0 \leq H_s < 2$	$\alpha = 2.232 \beta = 32.487$	$(\alpha = 2.858) (\beta = 41.427)$
$2 \leq H_s < 4$	$\alpha = 1.898 \beta = 32.764$	$(\alpha = 2.231) (\beta = 35.566)$
$4 \leq H_s < 6$	$(\alpha = 3.341) (\beta = 43.769)$	$P = 0$
Time 40–60		
$0 \leq H_s < 2$	$\alpha = 1.654 \beta = 26.286$	$(\alpha = 2.858) (\beta = 41.427)$
$2 \leq H_s < 4$	$\alpha = 2.684 \beta = 32.208$	$(\alpha = 2.231) (\beta = 35.566)$
$4 \leq H_s < 6$	$(\alpha = 3.341) (\beta = 43.769)$	$P = 0$

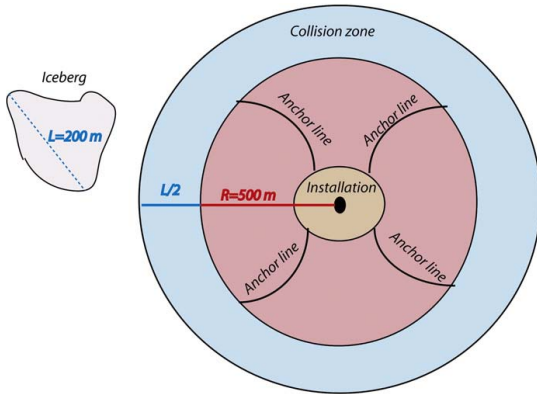


Fig. 8. Illustration of the collision zone. The radius will be a function of the waterline length of the approaching iceberg.

7. Based on the values for H_s , L and T at the moment of detection, the correct distribution for success numerator were identified. A random number between 0 and 1 was generated and from the inverted success index distribution, it could be concluded whether the ice management operation was successful or not. In this study, all inverted success indexes lower than 45 were concluded as being successful.
8. The numbers of successful versus un-successful iceberg management operations were counted and the probabilities implemented in the event tree.
9. Out of the “detected,” “colliding” and “not successfully managed” icebergs, only 2% of the icebergs would cause collisions in the scenario with a disconnectable installation.
10. In the scenario where disconnection was not allowed, information regarding iceberg drift speeds and mass were stored at the moment of collision and the kinetic energy was calculated.
11. Finally, the frequency of collisions was counted and distributions of kinetic energy were established. Together, the frequencies and the kinetic energy distributions were used to estimate extreme

iceberg collision loads for systems with and without an iceberg management system.

5.1. Concept without any iceberg management

A fixed installation without any iceberg management systems shall, as any system, maintain its structural integrity even after an accidental load. When considering an iceberg collision as an accidental event, it is required to identify the 10000 year load, i.e. the collision load with annual probability of exceedance of 10^{-4} .

The annual frequency of icebergs entering the observation zone can be found considering the ratio between iceberg observation within a certain period and the length of the period. As described in Section 3, the frequency of icebergs within the Shtokman region (Fig. 3) is assumed to be 880 within a period of 100 years. From the simulations, it is found that only 16.9% of these icebergs enter the iceberg observation zone. The rate of events per year is then found by:

$$\lambda = \frac{880 \cdot 0.169}{100} = 1.490 \text{ [events per year]} \tag{4}$$

The rate, λ , will also be the annual frequency of the initiating event in the event tree. Without any iceberg management system, it means that all icebergs are considered as undetected and consequently the event tree will be as illustrated in Fig. 9. With respect to loads, the distribution of kinetic energy will be as presented in Fig. 10.

With a frequency of 1.4898 icebergs in the observation zone per year, the number of icebergs in this region within a 10000 year period will be 14898. From the simulations, it is found that only 1.67% of these icebergs will enter the collision zone if no iceberg management system is in place. This means that the numbers of collisions are 249 within a 10000 year period. For this scenario, the installation will have to withstand the impact from the iceberg with highest kinetic energy out of these 249. This corresponds to a probability of non-exceedance, P , which is $P = 1 - \frac{1}{249} = 0.996$.

The maximum kinetic energy for the scenario without iceberg management corresponding to the 10^{-4} annual probability level of exceedance is based on the data and a fitted Weibull distribution (Eq. (5)) estimated to close to 85 MJ (Fig. 10). This could i.e. correspond

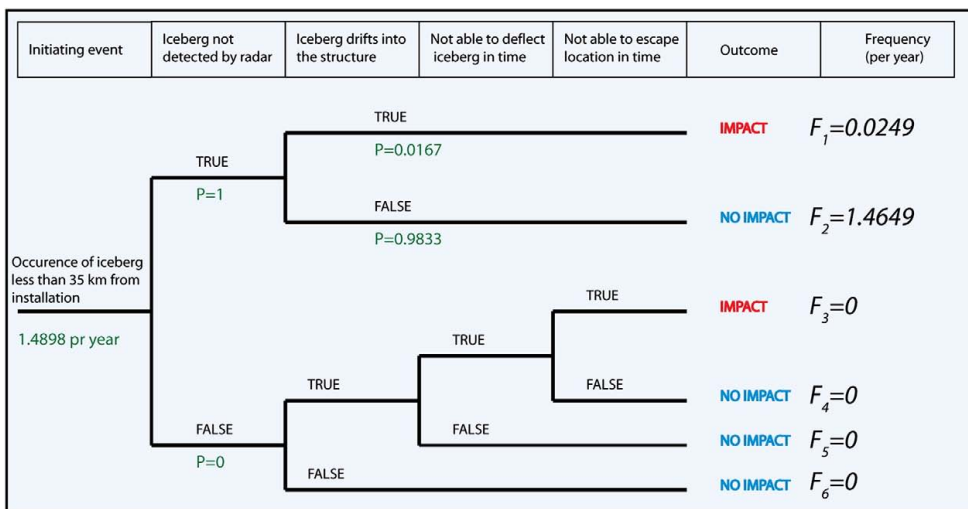


Fig. 9. Event tree including probabilities for an installation without any iceberg management functions.

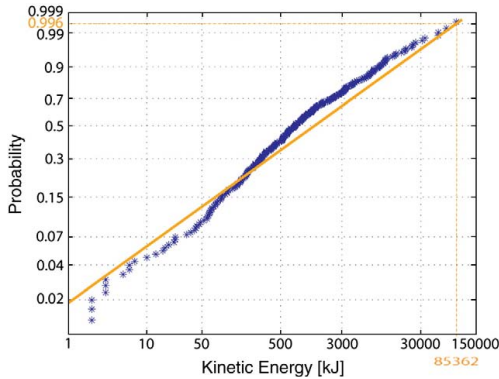


Fig. 10. Cumulative distribution function for the kinetic energy in an iceberg impact. Blue dots show data from the simulations when no iceberg management were included and the solid orange line shows a Weibull distribution fitted to the data ($\gamma=0.5$ and $\theta=2800$). The kinetic energy corresponding to a 10^{-4} annual probability level of exceedance is indicated with orange. (For interpretation of the references to colour in this figure legend, the reader is referred to the web version of this article.)

to an iceberg with mass 4.25 million tons drifting with a speed of 0.2 m/s or alternatively an iceberg with mass 170 000 tons drifting with a speed of 1 m/s.

The cumulative Weibull distribution function reads:

$$F(x) = 1 - \exp\left[-\left(\frac{x}{\theta}\right)^\gamma\right] \tag{5}$$

where γ is shape parameter, θ is the scale parameter and x is the stochastic parameter under consideration. The inverse Weibull distribution which is used to identify the extreme loads reads:

$$x = \theta \cdot [-\ln(1-F)]^{\frac{1}{\gamma}} \tag{6}$$

5.2. Concept with iceberg detection and physical iceberg management

For the concept with an offshore installation including an iceberg management system at 74°N and 43°E, the frequency of the initiating event will be the same as for the concept without iceberg management. However, since some of the icebergs will be detected and deflected around the installation, the numbers of collisions are reduced. Probabilities for the scenario with iceberg detection and deflection but without installation disconnection capabilities are presented in the event tree in Fig. 11. By summing up the frequencies for the “impact” outcomes ($F_1 + F_3$), the annual probability of an impact was found to be $6.5 \cdot 10^{-3}$. Within a period of 10000 years, 65 impacts may therefore be expected. The maximum kinetic energy will consequently correspond to the probability level $P = 1 - \frac{1}{65} = 0.9846$.

The distribution of the kinetic energy of the icebergs that actually hit the installation when iceberg management (but without disconnection) is included is presented in Fig. 12. It can be seen that the Weibull distribution fitted to the data for kinetic energy when no iceberg management was included, is not appropriate for description of kinetic energy iceberg management is included. The reason for this is that the largest icebergs cannot be deflected (length > 300 m) while the majority of the smaller one are successfully deflected. Due to this, the maximum kinetic energy corresponding to the 10^{-4} annual probability exceedance level will, for this scenario be the same as for the scenario without ice management; approximately 85 MJ (Fig. 12).

Mathematically, the probability for an iceberg-structure impact when the iceberg trajectory goes through the collision zone will be:

$$P_{\text{impact}}(H_s, L, T) = [1 - P_{\text{detection}}(H_s, L)] + P_{\text{detection}}(H_s, L)[1 - P_{\text{tow}}(H_s, L, T)] \tag{7}$$

where $P_{\text{detection}}$ and P_{tow} are the probabilities for successful detection and deflection respectively. This expression is in agreement with the approach used by Fuglem et al. (1999). Rather than using independent distributions for H_s and L as suggested by McKenna et al. (2003) and integrating over the range for these values, the probabilities are found from the simulations. Simultaneous values for wave heights and iceberg lengths plus other parameters such as the available time for towing, wind velocity, current velocity and iceberg drift velocity

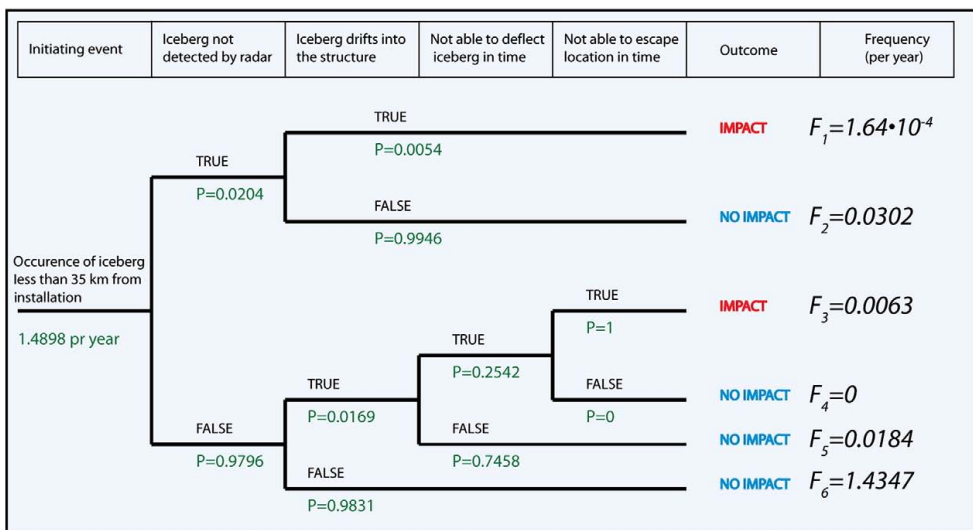


Fig. 11. Event tree including probabilities for an installation with a “standard Grand Banks” iceberg management system but no disconnection capabilities.

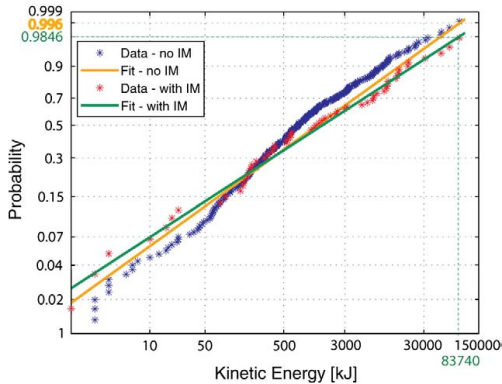


Fig. 12. Cumulative distribution function for the kinetic energy in an iceberg impact for scenarios both with and without iceberg management. The Weibull distribution fitted to the data when physical iceberg management was included ($\gamma = 0.45$ and $\theta = 3500$), is plotted as a green solid line. The maximum kinetic energy corresponding to the 10^{-4} annual probability of exceedance level when physical iceberg management is included is indicated with green numbers. (For interpretation of the references to colour in this figure legend, the reader is referred to the web version of this article.)

are available from the trajectories. This has the advantage that the correlations between the parameters, which are incorporated through the numerical drift model, are included in calculations of $P_{\text{detection}}$ and P_{tow} .

5.3. Concept with iceberg detection, physical iceberg management and disconnection capabilities excluding emergency disconnect

The frequency of impacts will be further reduced if the offshore installation has the possibility to make a planned disconnect and leave the site when threatened by one or several icebergs. The time required to perform a planned disconnection will depend on the ongoing operations and the time required to cease all activities in an orderly and safe manner. For most operations, one would expect this to take more than a few hours but less than a full day. Fig. 13 illustrates the

event tree when both physical iceberg management and planned disconnection capabilities are included in the offshore concept.

The disconnection capabilities will, in this model, not influence on the distribution of kinetic energy in the impacts compared to the scenario with only physical iceberg management but no disconnection (green line in Fig. 12). By summing up the frequencies for the “impact” outcomes ($F_1 + F_3$ in Fig. 13), the annual probability of an impact is found to be $2.9 \cdot 10^{-4}$. Within a period of 10000 years, only 3 impacts may therefore be expected. The maximum kinetic energy will consequently correspond to the probability level $P = 1 - \frac{1}{3} = 0.667$.

From Eq. (6) and the parameters in Fig. 12, the maximum kinetic energy corresponding to the 10^{-4} annual probability exceedance level will, for the scenario including physical iceberg management and disconnection, be 4.3 MJ.

Mathematically, the probability for an iceberg-structure impact when the iceberg trajectory goes through the collision zone will now be:

$$P_{\text{impact}}(H_s, L, T) = [1 - P_{\text{detection}}(H_s, L)] + P_{\text{detection}}(H_s, L)[1 - P_{\text{tow}}(H_s, L, T)] \times [1 - P_{\text{disconnect}}] \tag{8}$$

where $P_{\text{disconnect}}$ is the probability of a successful disconnection. As indicated in Section 5.3, this probability should ideally be expressed as a function of environmental parameters such as wave height or sea ice conditions. However, since only constant probability values were used in this study, these dependencies are not presented in the mathematical expression, Eq. (8).

5.4. Concept with iceberg detection, physical iceberg management and disconnection capabilities including emergency disconnect

As an additional safety barrier, some installations may have capabilities of performing an emergency disconnect (e.g. Gudmestad et al., 2009). This is of importance in scenarios were icebergs are not detected by the surveillance system but still are visible from the installation during the very last minutes before an impact. Technically, this implies that the installation release all moorings and risers immediately and starts to drift with winds and waves. It is assumed that this can be done within less than 15 min. Such disconnections may lead to significant damage to equipment and it may take long

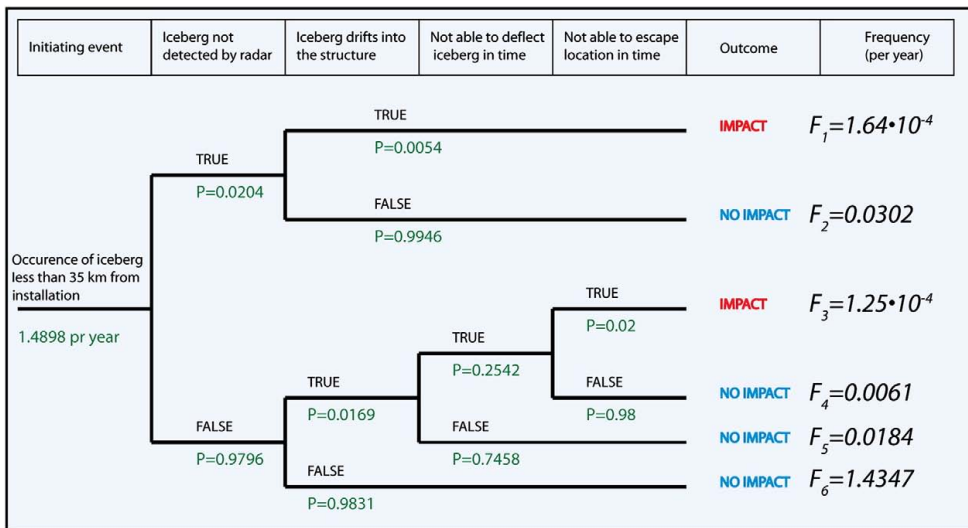


Fig. 13. Event tree including probabilities for an installation with a “standard Grand Banks” iceberg management system and capabilities for planned disconnections.

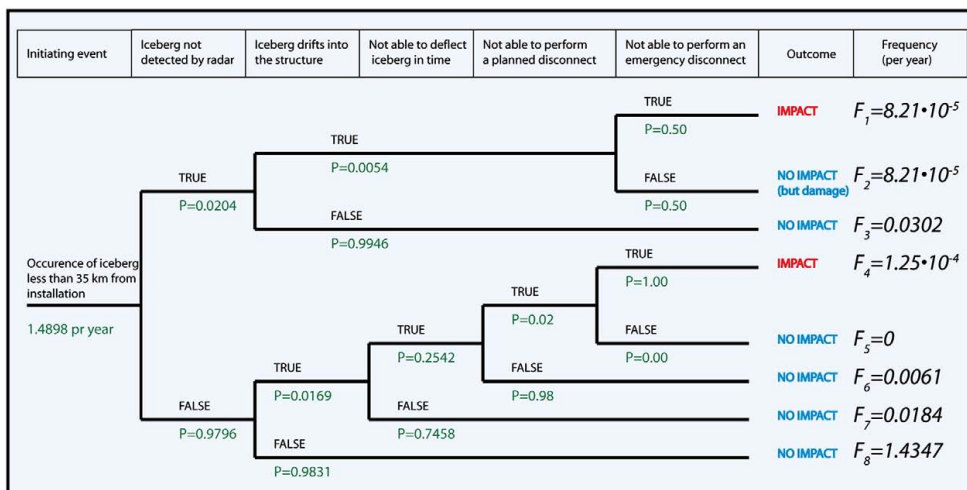


Fig. 14. Event tree including probabilities for an installation with a “standard Grand Banks” iceberg management system and capabilities both for planned disconnections and emergency disconnection.

time before a reconnection can be done. In this study, it has been assumed that there is 50% probability for a successful emergency disconnect in events where undetected icebergs are approaching. The emergency disconnect is classified as successful as long as an impact is avoided. In the events where the icebergs are detected but both deflection operations and planned disconnect have failed, the probability of a successful emergency disconnect have been assumed to be zero. The argument for this is that if the planned disconnect have failed, this is due to technical difficulties which still are present and unresolved in the moment an emergency disconnect is considered.

The total number of impacts in a 10000 year period is then further reduced and the impact frequencies will be as presented in Fig. 14. The kinetic energy corresponding to the 10^{-4} level is found by use of the same Weibull distribution as applied before (Fig. 12) and the sum of impact frequencies ($F_1 + F_4 = 2.1 \cdot 10^{-4}$ and $P = 1 \div \frac{1}{2.1} = 0.5238$). The maximum kinetic energy in an impact is now reduced to 1.8 MJ.

Mathematically, the probability for an iceberg-structure impact when the iceberg trajectory goes through the collision zone will for this scenario be expressed as:

$$P_{\text{impact}}(H_s, L, T) = [1 - P_{\text{detection}}(H_s, L)][1 - P_{\text{EDC}}] + P_{\text{det.}}(H_s, L)[1 - P_{\text{tow}}(H_s, L, T)] \times [1 - P_{\text{disc}}] \quad (9)$$

where P_{EDC} is the probability of a successful emergency disconnection.

5.5. Comparison of concepts

The impact frequencies and the abnormal values for iceberg kinetic energy have been summarised in Table 3.

Table 3
Summary of impact frequencies and abnormal values for kinetic energy for four different offshore installation concepts.

Concept	Impact frequency (per year)	Highest kinetic energy in an impact with 10^{-4} annual probability of exceedance [MJ]
No iceberg management	$2.5 \cdot 10^{-2}$	85.4
Iceberg management included but no disconnection capabilities	$6.5 \cdot 10^{-3}$	83.7
Iceberg management and planned disconnection capabilities included	$2.9 \cdot 10^{-4}$	4.3
Iceberg management and both planned and emergency disconnection capabilities included	$2.1 \cdot 10^{-4}$	1.8

6. Discussions

The presented methodology shows that the abnormal impact loads from icebergs on an offshore installation will vary significantly depending on the iceberg management capabilities for the concept. While the iceberg deflection operations have little effect on the abnormal load level as long as the largest icebergs not are towable, disconnection capabilities will provide a significant reduction in the design load. Further, it seems as the suggested methodology provides a fairly simple tool for evaluations of the effects of various iceberg management measures. However, a discussion on the advantages and disadvantages as well as comments to the results is required in order to fully understand capabilities and limitations in the model.

6.1. Iceberg drift modelling

The preferred methodology so far for evaluating the iceberg collision risk has been to use historical iceberg observations and estimates on iceberg residence time within a certain area in order to provide estimates on the density of iceberg propagation. This methodology relies however on access to systematically and reliable observations of icebergs over a large region and spanning a long time period. The use of an iceberg drift model makes it possible to provide alternative estimates on iceberg impact frequencies based on observations of glacier dynamics and precipitation. The presented work does, however, also rely on iceberg observations within a certain region over a certain time period. This initial estimate on iceberg frequency in the Shtokman region contributes to one of the major uncertainties in the presented work and should in the future be

verified by a more extensive use of the iceberg drift model in the entire Barents region.

The main argument for not using an iceberg drift model is that it is relatively laborious to set up initially and requires access to good quality hindcast databases for the metocean parameters. On the other hand, when considering an offshore development in iceberg infested regions, it seems evident that a numerical iceberg drift model will be required at some stage in the project. In particular, during production, an operational iceberg drift forecast model will be required. It should also be taken into account that once a model has been set up, it can be applied for several fields in the entire ocean basin and not only the initial project which is was developed for. Further, it should also be taken into account that metocean models also will be required independently of the iceberg threats simply because individual parameters such as winds, waves and currents are of concern both for design and operations.

With respect to the iceberg drift model used in this work, there are a number of weaknesses which are discussed in detail in Eik (2009a). The main concern is however, the quality of the ice-ocean model which the iceberg drift is based on. So far, ocean current models in the Barents region are not capable of providing “correct” currents at correct time. Further work should therefore focus on improvements in the current forecasting.

With respect to the simulations done in this work, it should first of all be recognized that considering a 6 year period only, is not sufficient to capture neither the variability from year to year nor any long term trends. The intention with this paper has been to demonstrate a methodology rather than serve as design document. In this context, the amount of data (which was limited by the extent of available ocean hindcast data) has been considered as sufficient.

6.2. Probabilistic framework

The probabilistic framework used in this study is basically very similar to the methodology presented by Fuglem et al. (1999). A Monte Carlo simulation is performed using distributions for parameters such as iceberg lengths, wave heights, detection and deflection capabilities. By dividing the Monte Carlo simulations in two stages in combination with the iceberg drift model, offers however several advantages:

- The time dependency is included in a realistic manner. This is of importance both when considering the possibility for successful iceberg deflection but also when designing the iceberg management system. A system which provides ample disconnection time may provide an increased total safety but reduced operability since disconnections are initiated more frequently than for a system with sparse disconnection time.
- The correlations between iceberg, metocean and management parameters are included. One example is the correlation between iceberg length and wave height. Initially, these parameters are independent. However, as the iceberg drifts in open water, the wave erosion will have a significant impact on the iceberg length. This is now taken into account by the implementation of an iceberg deterioration model in the iceberg drift model. In this respect, it should be noted that if the simulations are based on iceberg size data within the specified region rather than iceberg size distribution along the border, the need for a deterioration model is excluded.
- Realistic realisations of iceberg specifications and associated metocean parameters are available at the moment of impact. One example is the iceberg length, the wave height, the wave period and the wave direction. For small icebergs, it may be relevant to calculate the oscillating velocities which may be of importance when considering local loads (e.g. Fuglem, 1997).

With respect to the use of event trees, this is simply a way of visualising the probabilistic framework and ensures a systematic tool

for evaluating both the need for and the effect of various iceberg management means.

6.3. Probability of detection (POD)

The drift trajectories provide the possibility to include one of the most important ice management parameters in a simulation: the time parameter. By performing a traditional probabilistic analysis the available time for iceberg detection will be the same for all icebergs (as long as the physical management zone is defined as a function of the iceberg drift speed).

However, it is obvious that the longer an iceberg drifts within a surveillance zone, the larger is the probability of the iceberg to be detected. Reasons for this are varying weather conditions, varying concentration from the person making radar observations and that rotations of the iceberg change the radar deflections. In the proposed model, the POD will be higher for icebergs drifting slower or follow a more chaotic rather than a linear track. There is a problem that the POD found from the simulations will vary as a function of the time steps in the trajectories. By requiring detections in two consecutive steps, it is likely (but not certain) that the overall POD is conservative.

In order to utilize the presented model in a real offshore projects, a POD function taking into account not only the wave height, H_s , and iceberg length, L , but also the time spend by the iceberg within the radar range prior to detection, need to be in place. Such a function may be developed if iceberg management training courses are performed.

6.4. Results of simulations

The relatively “fat tail” in the distributions of kinetic energy require further attention. First, it should be commented that impacts with icebergs that are either large or drift very fast, are more likely to occur than smaller/slower icebergs. The reason for this is simply that these icebergs contribute to a higher iceberg density as these will swipe over larger areas than smaller/slower icebergs. By considering the iceberg drift velocity statistics, this effect seems to be captured well in the model (Fig. 15a). With respect to the iceberg lengths this effect is less obvious as the icebergs deteriorate as they drift within the region. The impacting icebergs have generally drifted within the region for a longer period than average for all icebergs and thus also been exposed to more deterioration. It was shown by Eik (2009b) that the applied iceberg deterioration model will give much higher deterioration rates for smaller icebergs. Due to this, the smaller impacting icebergs are smaller than what should be expected from the general iceberg length distribution while the largest impacting icebergs are slightly larger than indicated by the general distribution (Fig. 15b). In this respect it should be noted that the general iceberg length distribution represents all icebergs drifting within the region and is not the same as the initial distribution used to describe iceberg lengths along the border. Since both the distribution for iceberg waterline length and the iceberg drift speeds are positively skewed, the distribution of kinetic energy which is a function of mass and velocity will consequently show a significant skewness.

6.5. Comparison between swept area approach and iceberg drift simulations

In order to evaluate the uncertainty in the calculated encounter frequencies based on the iceberg drift simulations, it would be appropriate to perform a comparison with alternative established and recognized approaches. In this respect, the “swept area approach” presented by Fuglem et al. (1996) is considered relevant for such a comparison. In brief, this approach is based on an iceberg areal density estimate. The encounter probability for all iceberg lengths in all environmental conditions is then summed up. The encounter probability for one single iceberg is calculated from the ratio between

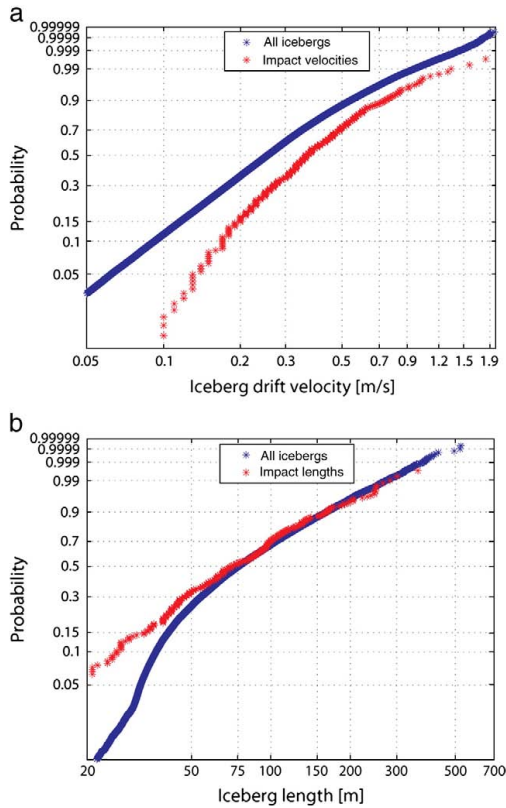


Fig. 15. Cumulative distribution function for (a) iceberg drift velocity and (b) iceberg waterline lengths. Distributions based on all trajectories in the region (blue stars) and based on impact data (red stars) are shown. (For interpretation of the references to colour in this figure legend, the reader is referred to the web version of this article.)

the area swept by the iceberg and the total area considered when calculating the areal density estimate of icebergs:

$$p_e = \frac{(w_i + w_s) \cdot v_i \cdot \Delta t}{A} \quad (10)$$

where p_e is the probability of collision during time Δt . w_i is the iceberg width, w_s is the structure width, v_i is the mean iceberg drift speed and A is the regional area through which the iceberg is transiting. The total annual expected number of iceberg encounters (η_e) is expressed by (Fuglem et al., 1996):

$$\eta_e = \rho \cdot (w_s + \bar{w}_i) \cdot \bar{v}_i \cdot T \quad (11)$$

where ρ is the average areal density of icebergs, \bar{w}_i is the mean iceberg length, \bar{v}_i is the mean iceberg drift speed and T is the number of seconds per year. It should be noted that the iceberg length is conservatively chosen to represent the swiped iceberg width.

The main complication by using the “swept area” approach in the Barents Sea is that the average areal density, ρ , depends on the residence time for the icebergs within the region. At the East Coast of Canada, where this model has been applied so far, the access to systematically collected flight track data has made it possible to establish reliable estimates for the areal density of a region. Areal reconnaissance has also been conducted in the Barents Sea (Zubakin et al., 2005), but as the recorded charts are not available in the public

domain, this type of information cannot be assessed. An additional concern by use of the “swept area” approach is that it assumes that the icebergs are uniformly distributed within the region of which the iceberg is transiting. Based on knowledge of the glaciers in the Barents Sea and the general environmental conditions it seems evident that the iceberg population within the Shtokman region (Fig. 3) is not uniform.

In order to perform a sensible comparison between the “swept area” approach and the “iceberg drift” approach, we have used the average residence time from the drift simulations (5 days). Further, it was chosen to consider a location centrally located in the Shtokman region rather than the location which has been used throughout this paper. Due to this, location “B” at 73.375°N, 43.5°E was selected for the purpose of comparing the “event tree” approach and the “swept area” approach (Fig. 16). Location B in Fig. 16 is considered to be more representative for the entire region than location A.

Based on the initial distribution of iceberg length, which is representative for icebergs observed to the north and east of the Shtokman region the mean iceberg length, \bar{w}_i , was estimated to 90 m. Based on iceberg drift observations during the IDAP campaign further east in the Barents Sea (Spring, 1994), the average drift speed was estimated to 0.19 cm/s. This value is used for \bar{v}_i . The diameter of the “collision circle” which represents the structure width, w_s , is chosen as 1000 m. With respect to the average areal density of icebergs, ρ , this is calculated as follows:

$$\rho = \frac{880 \text{ icebergs}}{100 \text{ years}} \cdot \frac{5 \text{ day residence time}}{365 \text{ days per year}} = 1.649 \cdot 10^{-12} \quad (12)$$

Consequently, the annual number of icebergs encountered is:

$$\eta_e = 1.649 \cdot 10^{-12} \cdot (1000 + 90) \cdot 0.19 \cdot (365 \cdot 24 \cdot 3600) = 0.0108 \quad (13)$$

From the iceberg drift simulations, it was found that the annual number of encounters at location B would be 0.0087 without iceberg management. The difference in the estimates from the two approaches is low and from this, one may conclude that results from the iceberg drift model are consistent with results from the “swept area” approach. However, the annual number of encounters will strongly depend on the location within the Shtokman region while the corresponding number from the “swept area” approach will

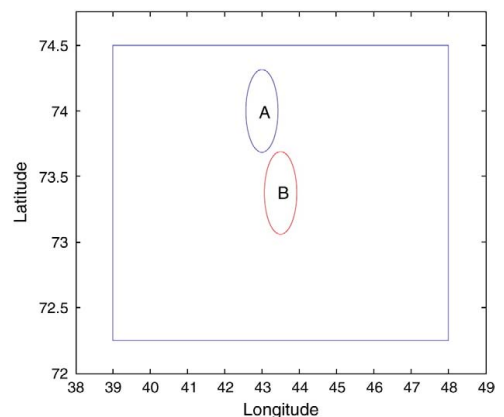


Fig. 16. Close up of the Shtokman region including the selected location used for demonstration of the “event tree” approach (A) and a location (B) used for comparison between the “event tree” approach and the “swept area” approach.

remain constant. Due to this, an unambiguous conclusion may not be made.

6.6. Further work

Even though, the presented methodology is considered to offer an adequate tool for evaluating the efficiency and need for iceberg management means, there are still a number of activities to be carried out in order to make required improvements to the approach.

The need for improvement in oceanographic modelling in Arctic regions is already mentioned and once a sufficiently good model is established a fairly long (10–15 years) current hindcast archive should be established.

The inadequacy of the distribution for detection which has been used to demonstrate the approach has been discussed. In addition to the need for including time elapsed by the iceberg within the radar range, there are also a number of other concerns:

- The applied distribution for iceberg detection does only take into account the iceberg size and sea state. It is known that iceberg shapes which are more rounded, such as the domed shaped icebergs, are more difficult to detect thus the probability of detection should also be conditional on the iceberg shape.
- Other parameters such as distance to target and precipitation are also considered as important for the detection capabilities and should consequently be incorporated into the detection model.
- Further, it will also be beneficial to have detection models quantifying the detection capabilities by other means such as satellite images and aerial reconnaissance.

As for the detection capabilities, it is also documented that domed and wedge shape icebergs are more complicated to tow. In accordance with Rudkin et al. (2005) the probability of successful tows for these shapes are about 10% lower than for tabular icebergs. This needs to be addressed if the presented model is to be used in future projects.

In the model presented, it has been assumed that it is not feasible to tow icebergs when surrounded by sea ice. Further north in the Barents Sea, the majority of icebergs will be embedded in sea ice and thus both detection and deflection capabilities on icebergs in sea ice should be investigated.

The opportunity to use the PERD iceberg management database is highly appreciated. In order to ensure a higher level of safety and efficiency in future Arctic projects all iceberg management experiences should be reported in a way which is consistent with the PERD database and eventually be merged with the PERD database. The possibility to store even more information from accomplished iceberg management operations should also be considered (i.e. full tracks).

7. Conclusions

A methodology for systematic evaluation of the need for an iceberg management system and the efficiency of various components has been presented. The approach is based on the combination of a numerical iceberg drift model and a probabilistic analysis. Experiences from the Canadian iceberg detection studies and iceberg deflection operations have been incorporated into the model.

For a selected site in the Barents Sea, it was found that the maximum impact load corresponding to a 10000 year event was 85 MJ for a concept without any iceberg management capabilities. An alternative system with iceberg detection, iceberg deflection and disconnection capabilities including emergency disconnect, indicated a corresponding abnormal load of about 1.8 MJ.

Future work should focus on improvements in oceanographic modelling and improvements in models for iceberg detection capabilities. With respect to physical iceberg management in Arctic waters, the feasibility of iceberg deflections in sea ice should be further investigated.

References

- AIChE, 1992. Guidelines for Hazard Evaluation Procedures; with Worked Examples. American Institute of Chemical Engineers, Centre for Chemical Process Safety, New York, 2nd Edition. 461 p.
- C-Core, 2002. Integrated Ice Management R&D Initiative. Physical Management, report R-01-24-605 v2 delivered to Chevron, ExxonMobil, Husky, Norsk Hydro, PERD and Petro-Canada, Vol. 2, p. p53.
- CSA S471-04, 2004. General Requirements, Design Criteria, the Environment and Loads. Canadian Standards Association, Ontario, Canada, p. 124.
- Eik, K.J., 2009a. Iceberg drift modelling and validation of applied meteocean hindcast data. *Cold Reg. Sci. Technol.* 57, 67–90.
- Eik, K.J., 2009b. Iceberg Deterioration in the Barents Sea. Proceedings of the 20th International Conference on Port and Ocean Engineering under Arctic Conditions, POAC09-113. Luleå, Sweden.
- Fuglem, M., 1997. Decision-Making for Offshore Resource Development, PhD Thesis, Memorial University of Newfoundland, Canada, 278 p.
- Fuglem, M., Jordaan, I., Crocker, G., Camaert, G. And, Berry, B., 1996. Environmental factors in iceberg collision risks for floating systems. *Cold Reg. Sci. Technol.* 24, 251–261.
- Fuglem, M., Muggeridge, K., Jordaan, I., 1999. Design load calculations for iceberg impacts. *Int. J. of Offshore and Polar Eng.* 9 (4), 298–306.
- Gudmestad, O.T., Dalane, O., Aksnes, V., 2009. On the Disconnection of a Moored Floater in Hard Ice Conditions. Proceedings of the 20th International Conference on Port and Ocean Engineering under Arctic Conditions, POAC09-137. Luleå, Sweden.
- Hibernia, 2009. About Hibernia — Hibernia Ice Management. http://www.hibernia.ca/html/about_hibernia/index.html, cited September 2009.
- ISO/CD 19906, 2007. Petroleum and Natural Gas Industries — Arctic Offshore Structures, ISO TC 67/SC 7/WG 8. Draft International Standard. International Standardisation Organization, Geneva, Switzerland. 406 p.
- Jordaan, I., Press, D., Milord, P., 1999. Iceberg Databases and Verification. Prepared for National Research Council Canada, Canada Hydraulics Centre. 45 p.
- McClintock, J., McKenna, R., Woodworth-Lynas, C., 2007. Grand Banks Iceberg Management. PERD/CHC Report 20-84. Report prepared by AMEC Earth & Environmental, St. John's, NL, R.F. McKenna & Associates. Wakefield, QC, and PETRA International Ltd, Cupids, NL. 84 p.
- McKenna, R., Ralph, F., Power, D., Churchill, S., 2003. Modelling Iceberg Management Strategy. Proceedings of the 17th International Conference on Port and Ocean Engineering under Arctic Conditions. Trondheim, Norway, pp. 645–654.
- Miller, J., Satterfield, K., 1984. Iceberg detection by radar. *Oceans 1984* 17, 405–410.
- NORSOK standard N003, 2007. Actions and Action Effects. Norwegian Technology Standards Institution, Oslo, Norway. 81 p.
- Nygaard, E., 2009. Personal Communication with Einar Nygaard, Statoil.
- Rausand, R., Høyland, A., 2004. System Reliability Theory — Models. Statistical Methods and Applications, Wiley, New Jersey, USA. 636 p.
- Rudkin, P., Boldrick, C., Barron Jr., P., 2005. PERD Iceberg Management Database. PERD/CHC Report 20-72. Report prepared by Provincial Aerospace Environmental Services (PAL), St. John's, NL. 71 p.
- Spring, W., 1994. Ice Data Acquisition Summary Report. Mobil Research and Development Corporation, Texas, US.
- Vefsnmo, S., Løvås, S.M., Mathiesen, M., 1992. Iceberg Collision — Risk Analyses, SINTEF NHL, Report STF60 F92047. 22 p.
- Wright, B., 2000. Full Scale Experience with Kulluk Stationkeeping in Pack Ice. In: Wright, B. (Ed.), PERD/CHC Report 25-44 prepared by B. Wright & Associates Ltd. 52 p.
- Zubakin, G.K., Naumov, A.K., Skutina, Ye.A., 2005. Icebergs of the Western Sector of the Russian Arctic. Proceedings of the 18th International Conference on Port and Ocean Engineering under Arctic Conditions, Vol. 2. Potsdam, NY, USA, pp. 565–574.

5 EFFICIENCY OF SEA ICE MANAGEMENT

5.1 Ice load formulations

While the efficiency of iceberg management depends strongly on the capability to predict iceberg drift and to deflect icebergs, the efficiency of sea ice management will rely on the ability to reduce the floe size of the approaching ice. In order to consider the ice management efficiency, tools must be available that describes the load reductions due to the icebreakers. An approach for how to include sea ice management in the design process of an offshore installation is presented in Section 5.3. However, the approach relies on the ability to calculate loads both from managed and un-managed ice. At present, no recognised models for calculations of loads from managed ice exist and therefore it was decided to use empirical formulations for icebreaker resistance in Section 5.3. Since the icebreaker resistance only, in the best case, can be used to represent average loads on a moored structure, an additional study of the variability of ice loads was performed. This study is presented in Section 5.2, and provides a tool to estimate the ratio between peak loads and average loads.

5.2 Ice load variability



20th IAHR International Symposium on Ice
Lahti, Finland, June 14 to 18, 2010

Characterisation of peak loads on a moored production vessel in ice

Kenneth Eik^{1,2}, Vegard Aksnes¹

1. *Norwegian University of Science and Technology (NTNU)*

2. *Statoil*

kenjo@statoil.com

vegard.aksnes@ntnu.no

For moored structures operating in ice covered waters, it is likely that the highest mooring loads are caused by sea ice rather than waves, winds or currents. This paper investigates the variability in ice loads based on recordings from physical ice tank model tests in a continuous level ice sheet. The normalised peak mooring loads (ratio between peaks in the load signal and the mean load) are found to be well represented by 3-parameter Weibull distributions. The distributions will however vary significantly as a function of ice drift speed and mooring specifications (stiffness). The load variability is reduced when the ice drift speed is increased. Further, it is discussed how information regarding the load variability may be incorporated in both operational considerations as well as in the design process of a structure.

1. Introduction

A growing number of arctic offshore developments are expected to take place within the next decade. Due to relatively large water depths in many of the Arctic Ocean basins, it is likely that solutions with moored structures, ship shaped or buoys, will be preferred in a number of the developments. Moored structures are also likely to be used if exploration drilling takes place in ice covered waters. For structures operating in sea ice, it is further likely that the highest mooring loads will be caused by actions from sea ice rather than waves, winds or currents.

With respect to loads from sea ice, the uncertainties in calculations of these are considered to be an order of magnitude higher than the uncertainties in calculations of i.e. wave loads. The variations in results from ice load calculations by different recognised ice experts are well documented in different consensus studies and most recently by Timco and Croasdale (2006). This paper does not aim at discussing techniques for ice load calculations but rather to demonstrate how the variability in ice loads may be incorporated in both operational considerations as well as in the design process of a structure.

Mooring loads recorded during tests of a vessel shaped structure in an ice tank have been studied and subjected to statistical analyses similar to those frequently used for wave loads. Statistical distributions describing the load peaks have been established and the ratio between extreme peak load and the mean peak loads from the tests have been estimated for different scenarios. Demonstrations on how this type of information can be applied both operationally and in the design process are briefly described.

This paper includes a description of the model tests (Section 2), analyses of the load data (Section 3) and demonstration of possible applications (Section 4). Discussions, Conclusions, Acknowledgements and References are found in Sections 5 to 8 respectively.

2. Model tests

Model tests of a moored ship in level ice were performed in the Large Ice Model Basin at HSVA, Germany. A detailed description of the tests can be found in Aksnes (2010). Froude scaling was used because of the importance of gravitational and inertial forces, with scaling ratio $\lambda = 25$. Lengths are scaled by λ , forces are scaled by λ^3 and speeds are scaled by $\sqrt{\lambda}$. This means that for instance model scale (ms) and full scale (fs) speeds, scale as $v_{fs} = \sqrt{\lambda} v_{ms}$. All values in this paper were scaled to represent full scale data unless other is stated.

2.1 Vessel and mooring setup

A simple hull was towed through stationary ice with constant heading along its longitudinal axis. The model was arranged such that only surge motions were possible. Further, the hull was equipped with a linear spring system (Figure 1), which acted as a simplified mooring system. The springs were interchangeable, such that two different surge natural periods could be modelled. A fixed configuration was also tested. An assembly of load cells were mounted between the fixation to the driving carriage and the spring system, and enabled measurements of mooring (or global) forces. Properties of the model and its mooring system are given in Table 1.

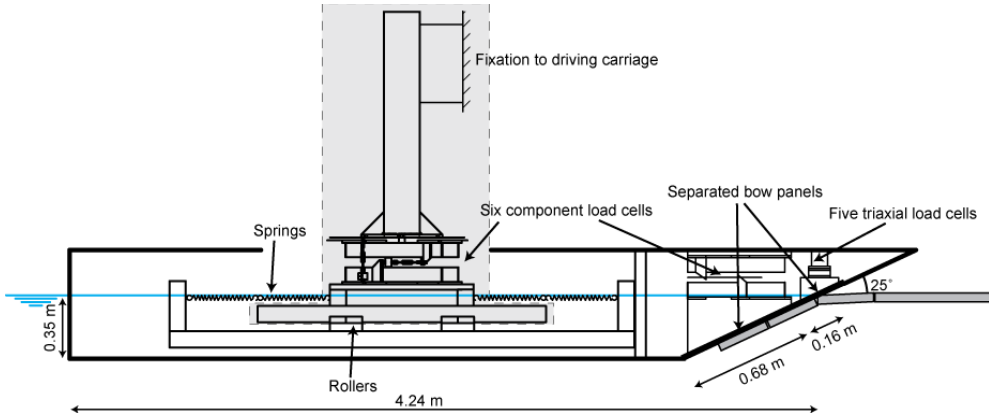


Figure 1. Cross-sectional view of the model with the mounting frame and the instrumentation. The dimensions are in model scale. The grey shaded area was fixed to the driving carriage.

Table 1. Properties of the vessel and the mooring system.

Model characteristics	Value
Length of waterline	106 m
Beam	33 m
Draught	8.8 m
Volume displacement	28000 m ³
Stem angle	25°
Surge natural period with soft mooring	67 s
Surge natural period with stiff mooring	32 s
Surge natural period with fixed springs	1.8 s

2.2 Ice properties and test matrix

Three sheets of model ice were produced according to the standard HSVA procedure (Evers and Jochmann, 1993). Ice properties were sampled as explained in Aksnes (2010) and they are summarized in Table 2.

The test runs are described in Table 3. Two test runs were performed with each of the mooring configurations, one with towing speed 0.05 m/s and one with 0.25 m/s. This gave in total six test runs. The first 100 m of each test run gave transient mooring forces, because the model was not completely embedded in the ice. This part of the tests was not included in the analysis below.

Table 2. Averaged ice properties for all the ice sheets.

Ice sheet	Ice thickness	Flexural strength	Elastic modulus	Ice density
2000	0.80 m	875 kPa	NA	NA
3000	0.73 m	675 kPa	≈1.8 GPa	NA
4000	0.70 m	625 kPa	≈1.3 GPa	929 kg/m ³

Table 3. Overview of the test runs.

Run #	Ice drift speed	Surge natural period	Length of the test run
2100	0.05 m/s	67 s (soft springs)	575 m
2200	0.25 m/s	67 s (soft springs)	775 m
3100	0.05 m/s	1.8 s (fixed)	500 m
3200	0.25 m/s	1.8 s (fixed)	825 m
4100	0.05 m/s	32 s (stiff springs)	525 m
4200	0.25 m/s	32 s (stiff springs)	750 m

3. Analyses of measured mooring loads

3.1 Data preparation

The data was sampled at 100 Hz (in model scale). Because Froude scaling was used with the scaling factor $\lambda = 25$, frequencies had to be scale as $f_{fs} = f_{ms} / \sqrt{\lambda}$, resulting in a full scale sampling frequency of 20 Hz. As can be seen from Figure 2, the amount of energy at the high frequencies was limited, thus a low-pass filtering was performed on all the data series. A 5th order Butterworth filter was applied with a cut off frequency of 0.5 Hz. It should be noted that fixed vessel showed significant energy at even higher frequencies. The reason for this is due to resonance effects which are only relevant for the fixed structure.

It should be emphasized that the absolute value of the loads are unimportant in the context of this paper as this will vary significantly depending on the size and shape of the hull under consideration. The variability in the load signals is considered as more important and it is assumed that this variability is more dependent on the ice conditions and less dependent on the hull specifications. Due to this, all recordings have been normalised by dividing the recorded value by the mean value from each dataset. It is in the following referred to a normalised load:

$$F = \frac{F_R}{\mu_F} \quad [1]$$

where F_R is the recorded load while μ_F is the mean value of F_R .

In a similar way as for wave heights, the peak mooring loads are of importance for further analyses. In wave analyses, the waves are usually assumed to be narrow banded and the wave peaks are identified as maximum values between each up-crossing of the mean water surface. With respect to the load peaks caused by ice, there is not sufficient data to decide whether the process can be considered as narrow banded or not. Due to this, a load peak, L , was simply defined as a point in the dataset where both the preceding and the following data points were lower. An example of the procedure for selecting peaks is demonstrated in Figure 3. The number of peaks and the peak frequency from each test run are given in Table 4.

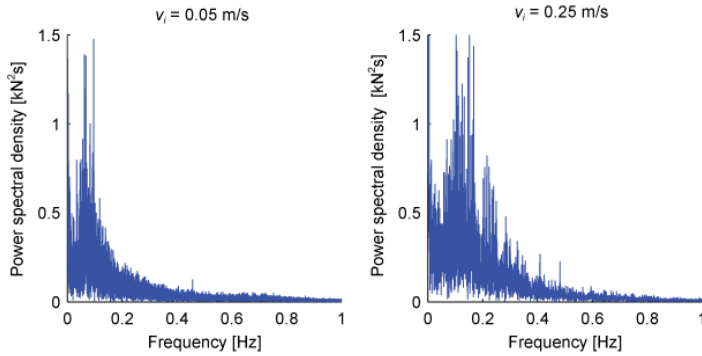


Figure 2. Load spectra from test series 4100 (left) and 4200 (right).

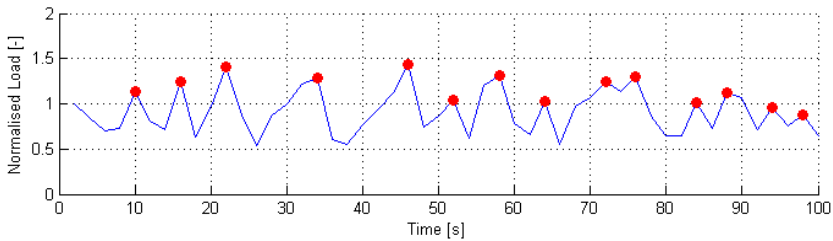


Figure 3. Example showing the identification of load peaks. The blue line shows the time history of the normalised mooring loads while the red dots show the load peaks.

Table 4. Calculated peak frequencies from each of the test runs.

Test #	Duration [min]	Total number of peaks	Peak frequency [peaks/min]
2100	157	2834	18.1
2200	49	767	15.7
3100	124	3463	27.9
3200	52	1348	25.9
4100	128	1485	11.6
4200	49	648	13.2

3.2 Distribution of load peaks

In order to estimate extreme load peaks, it is required to describe the statistical behaviour of the recorded data. By plotting the normalised load peaks in a Weibull diagram it was found that a 3-parameter Weibull distribution could represent the data well:

$$p(L) = \frac{\gamma}{\theta} \cdot \left[\frac{L - \varepsilon}{\theta} \right]^{\gamma-1} \cdot \exp \left[- \left(\frac{L - \varepsilon}{\theta} \right)^{\gamma} \right] \quad (\text{pdf})$$

$$P(L) = 1 - \exp \left[- \left(\frac{L - \varepsilon}{\theta} \right)^{\gamma} \right] \quad (\text{cdf})$$

[2]

where γ , θ and ε are the Weibull shape, scale and location parameters respectively. The cumulative distribution functions (cdfs) fitted to recordings from each test, are presented in Figure 4 while the Weibull parameters are given in Table 5. Corresponding probability density functions (pdfs) are compared in Figure 5.

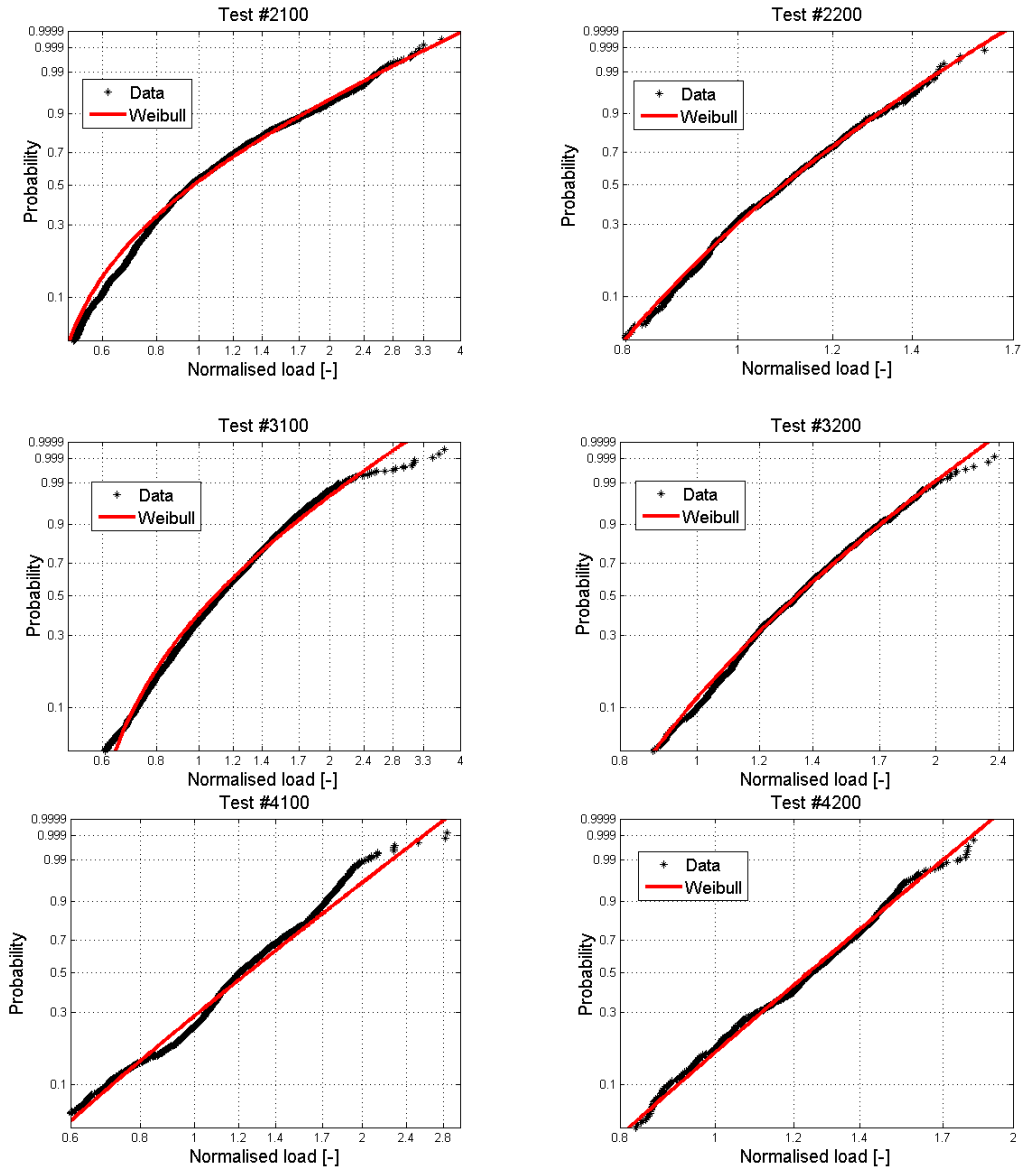


Figure 4. 3-parameter Weibull distributions fitted to recorded data by the method of moments. The distribution from test #4100 was manually adjusted in order to better capture the trend in the tail.

Table 5. Summary of the Weibull parameters which are considered to represent the recorded data distributions well.

Test #	Weibull parameters		
	Shape	Scale	Location
2100	1.3713	0.7252	0.4211
2200	3.6529	0.6250	0.5274
3100	1.7896	0.7226	0.5063
3200	3.2665	0.9218	0.5142
4100	3.0000	1.3000	0.1000
4200	5.6681	1.2288	0.0904

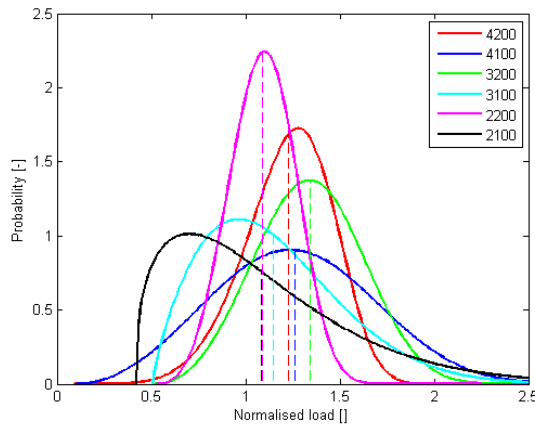


Figure 5. Comparison of distributions of local peak loads from each of the test runs. Dashed lines indicate mean values from the distributions with corresponding colours.

3.3 Extreme value analysis

The same procedure as commonly used in order to estimate the most probable maximum (mpm) individual wave height within a sea state, is adopted for estimation of the mpm load peak within a certain time interval, T . The time interval, T , should be selected so that the ice conditions within T are stationary (i.e. no significant variations in ice concentration, ice thickness, ridging intensity, ice strength etc.). It may be convenient to use the notation “ice state” for such a stationary condition. An ice state will contain totally N load peaks depending on the peak frequency, f_p , and the length of the time interval, T . Based on the Weibull distribution that represents the normalised load peaks and by counting the peaks in the recorded datasets, we can estimate the expected highest load within T . We are denoting the individual load maxima as $L_1, L_2, L_3 \dots L_N$. Amongst these; we are denoting the highest as L_{max} . The following assumptions are made:

1. All peak loads within an ice state are identically Weibull distributed.
2. All peak loads are statistically independent.

The first of these assumptions seems reasonable based on the fits presented in Figure 4. The latter is more debatable, but will probably lead to some conservatism with respect to estimation of extreme values. The cumulative distribution for the largest load peak, $P_e(L)$ can then be deduced as

$$\begin{aligned}
 \text{Prob}[L_{\max} \leq L] &= \text{Prob}[(L_1 \leq L) \cap (L_2 \leq L) \dots \dots \dots (L_N \leq L)] \\
 &= \text{Prob}(L_1 \leq L) \cdot \text{Prob}(L_2 \leq L) \dots \dots \dots \text{Prob}(L_N \leq L) \\
 &= [\text{Prob}[L_i \leq L]]^N = [P(L)]^N \tag{3} \\
 &= \left[1 - \exp \left[- \left(\frac{L - \varepsilon}{\theta} \right)^\gamma \right] \right]^N = P_e(L)
 \end{aligned}$$

The expected largest load peak can then be found by

$$E[L_{\max}] = \int_0^{\infty} L \cdot p_e(L) dL, \tag{4}$$

where $p_e(L)$ is the probability density function for the largest load peak

$$p_e(L) = \frac{dP_e(L)}{dL} = N \cdot \left[1 - \exp \left[- \left(\frac{L - \varepsilon}{\theta} \right)^\gamma \right] \right]^{N-1} \cdot \frac{\gamma}{\theta} \cdot \left[\frac{L - \varepsilon}{\theta} \right]^{\gamma-1} \cdot \exp \left[- \left(\frac{L - \varepsilon}{\theta} \right)^\gamma \right] \tag{5}$$

It is important to note that the expected largest load peak may deviate from the most probable largest load peak which is found by:

$$\frac{d}{dL} p_e(L_m) = 0 \tag{6}$$

where L_m is the most probable largest load peak. The probability distribution for load peaks in test 4200 (stiff mooring, velocity 0.25 m/s) is plotted in Figure 6 together with the corresponding extreme value distribution. Both the expected largest peak (L_{\max}) and the most probable largest peak (L_m) are indicated. A duration of 1 hour has been used in this figure. In Table 6, the number of peaks pr hour and calculated values for L_m and L_{\max} are presented. It can be seen that the extreme value distributions are slightly skewed, but that the differences in L_m and L_{\max} are insignificant. Further, it can be seen that the ratio between the maximum load and the average load is within the range 1.6 to 2.3 for the higher velocities (0.25 m/s) while it is significantly higher for the lower velocities (within the range 2.3 – 2.8 for speed 0.05 m/s when excluding test 2100).

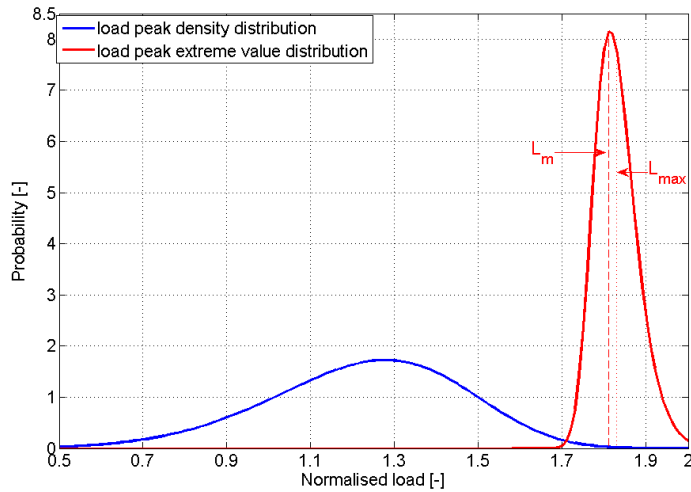


Figure 6. Probability density function for normalised load peaks from test #4200 and corresponding extreme value distribution. Duration of the ice state is 1 hour, peak frequency is 793 peaks/hour and the ice drift velocity is 0.25 m/s.

Table 6. Calculation of most probable load peak (L_m) and expected maximum load peak (L_{max}) based on normalised test recordings and load event duration of 1 hour.

Test #	# peaks	L_m	L_{max}
2100	1083	3.43	3.58
2200	939	1.59	1.61
3100	1676	2.74	2.81
3200	1554	2.21	2.25
4100	696	2.29	2.33
4200	793	1.81	1.83

4 Applications

4.1 Operational applications

During operation of a Floating Production Unit (FPU), it is likely that mooring loads are monitored continuously. For concepts that include an ice management system, the recorded load data will be crucial in order to evaluate the ice threat. Gudmestad et al. (2009) introduced an operational philosophy that applies the standard deviation of the monitored load in order to consider the need for a disconnection in the near future. While Gudmestad et al. (2009) suggested using a forecasted mean load plus two times the standard deviation of the recently recorded loads (Figure 7), it is considered rational to apply a similar approach but with a normalised extreme peak load combined with an appropriate safety factor. The following approach may be considered:

- Assume that the ice conditions are stationary over a certain period, i.e. 3 hours.
- Assume that the FPU is always capable of vaning and facing the incoming ice with the bow.
- Based on the recorded mooring loads from the recent i.e. 30 minutes, the average ice resistance is calculated and the most probable normalised load peak during the coming 2.5 hours is estimated according to the descriptions in this paper.
- The estimates are update automatically every 30 minutes.
- A time series of the estimated extreme peak load is presented in order to see if the loads are increasing or decreasing (illustrated in Figure 7).
- If the estimated extreme peak loads, which are updated every 30 minutes, follow an increasing trend and are about to exceed a pre-defined operational limit, immediate icebreaker assistance or alternatively a disconnection must be performed.
- The operational limit must include some sort of safety factor since loads up to the most probable peak load level may occur randomly within the stationary ice state.

The proposed approach should evidently be a supplement and not a substitute to traditional ice and weather forecasting. The main advantage is that the variability in the ice cover (level ice, ridges and rubbles) will be included in the estimated maximum loads. The distributions for normalised peak loads may be updated by use of the monitored load data, increasing the efficiency and safety throughout the project lifetime.

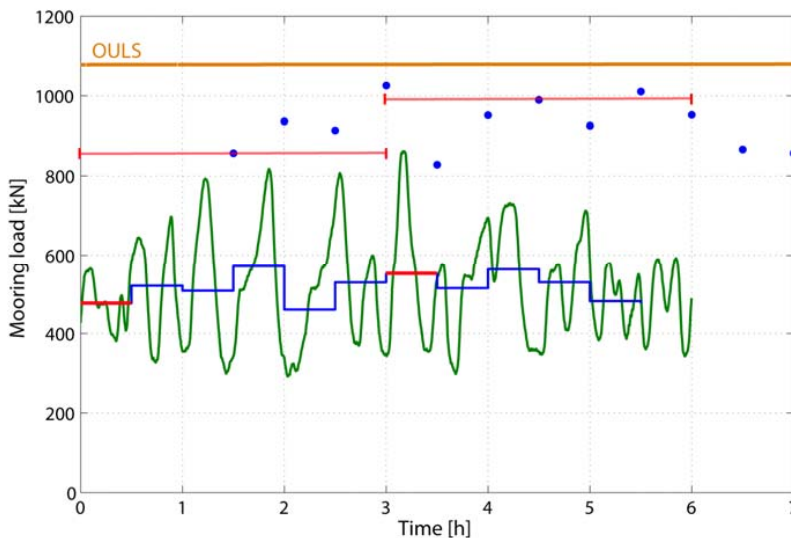


Figure 7. Illustration of operational use. The fixed green line shows how a recorded ice resistance signal may look like. The blue stair plot shows the mean resistance at 30 minute intervals. Two of the stair steps are marked with red and their associated peaks for a 3-h interval are indicated above (red lines). The blue dots show the maximum peak load within a 3-hour ice state. For the illustrated scenario, the ratio between max load and mean load is 1.8. If the maximum peak load exceeds the Operational Ultimate Limit State condition (OULS), a disconnection must be prepared.

4.2 Design applications

When designing mooring lines for an FPU, it will be required to document that the lines can resist extreme mooring loads in accordance with the relevant codes and regulations. For an FPU operating in ice covered waters, ice is likely to impose the highest mooring loads during the operational life. To estimate exact ice loads and associate these with adequate probability levels is challenging, because there are numerous parameters that are of importance for the total load (ice thickness, concentration, strength, ridging etc.). When it comes to actual load calculations, the codes (such as ISO 19906) provide limited guidance on how to make extreme predictions for moored vessels operating in varying ice regimes.

Keninonen et al. (1996) and Keinonen and Robbins (1998) studied the resistance from sea ice on different icebreakers in real operations. Further, they developed semi empirical formulations for calculations of level ice resistance on various vessel shapes. Based on observations of how much the vessels were slowed down by various ice parameters such as floe size, concentration, ice strength, snow cover, salinity and temperature, Keinonen et al. (1996) presented formulations for how to estimate an equivalent level ice thickness. Such a transformation of ice conditions is considered to be useful also when considering the ice resistance on for example an FPU in various ice conditions.

Generally, one would expect that the formulations from Keinonen et al. (1996) are reasonable for calculation of icebreaker efficiency, but more questionable for design consideration of an FPU mooring system. However, as a wide range of hull shapes has been incorporated in the “Keinonen formulation”, the ice breaking capability of an FPU should be well described also by this approach. There may be difference between a moored FPU and an operating icebreaker due to i.e. size effects which may make the sea ice clear better around the icebreaker than around an FPU. Such considerations need to be addressed in a design process of the FPU.

If it is accepted that the “Keinonen formulations” are relevant also for a moored FPU, it is possible to perform a probabilistic analysis, including statistical descriptions of all the important ice parameters and their correlations. From such an analysis, extreme ice resistance on the FPU may be estimated. Further, by using the normalised load peak distribution in the ice state providing the extreme resistance, it will be possible to estimate the most probable extreme mooring load. It should however, be emphasized that due to the number of uncertainties and assumptions made, the presented approach should be a supplement to existing tools such as analytical load calculations, numerical load calculations and physical tank model tests.

5. Discussion

5.1 Methodology

The basic idea in this work has been to adopt an approach used in wave analysis to estimate the highest ice load peaks in given ice conditions. While the expected highest individual wave height in a 3-hour sea state typically is around 1.9 times the significant wave height, we can see that the maximum ice loads compared to the mean average ice loads depend both on the ice drift speed as well as the mooring configuration.

An unambiguous conclusion regarding the effect of mooring stiffness and drift speed cannot be made since one of the tests separates significantly from the others (test #2100). The reason for why this test disunites from the others is probably that friction effects at low speeds with soft mooring systems are more dominant than ice breaking and ice clearing (Aksnes, 2010). However, it is clear that for lower speeds, the spread in normalised load is higher than for the higher speeds. Additional analyses done with data from model tests of other structures (not presented in this paper) support the finding that the load distribution is narrower for higher drift velocities.

With respect to the mooring stiffness, it seems obvious that the frequency of load peaks is higher for the fixed vessel compared to the moored vessels. Due to this, the maximum normalised load peak will be higher for the fixed vessel than for the moored vessels. There may of course be exceptions from this e.g. if the mooring configuration is designed so that resonance effects occur under influence of ice. It should also be noted that the datasets applied in this work was filtered somewhat to rough. The peak to normal ratios may vary as a function of the cut-off frequency if the cut-off is done at too low frequencies. Due to this, some efforts should be done in order to ensure that all important information is kept within the filtered datasets.

The tank model tests were only done in continuous level ice and it is not considered rational to use the same approach for a vessel exposed to ice ridges. The reason for this is that it will be complicated in a tank to create sufficiently many ice ridges in order to get a statistical description of the peak loads. However, based on real full scale operations it will, at the early stage, be possible, to establish peak load distributions even for ice conditions with ice ridges.

5.2 Applications

There are a number of critical concerns with respect to use of the normalised peak load distributions both operationally and in design. Operationally, there is a concern regarding definition and duration of an ice state. The proposed approach will only be useful as long as it is possible to describe the ice conditions into ice states. Further, different peak load distributions will be required for different ice scenarios; variable ice drift speed, variable ice concentration, variable ice thickness etc. Both monitoring of mooring loads as well as monitoring of ice parameters will be required in order to establish reliable load peak distributions for all scenarios. It should also be noted that when experience from operations in ice is gained, the safety and efficiency of future operations should be expected to increase as the variability in different ice conditions are immediately and systematically analysed.

With respect to design, there are a number of concerns. The complications regarding establishing peak load distributions when ridges are present only from tank model tests have been highlighted. Further, the use of icebreaker resistance data in order to estimate mooring loads on an FPU is debateable. If ice wedging occurs in front of the vessel, as was reported by Wright (1999) on Kulluk, the ratio between max peak load and mean peak load will be much higher than in situations with good clearing around the hull. Other concerns, such as rapid ice drift direction change has not been addressed.

The effect of managed versus unmanaged ice loads has not been addressed in this work. However, by doing tank model tests both in managed and unmanaged level ice the effect on ice management on extreme peak loads may be quantified.

6. Conclusions

- An approach for estimating the ratio between maximum horizontal mooring load and average horizontal mooring load caused by ice has been presented.
- The normalised peak mooring loads (ratio between load and mean load) are well represented by Weibull distributions. The distributions will however vary significantly as a function of ice drift speed and mooring specifications (stiffness).
- The extreme normalised peak loads are higher for a fixed vessel than a moored vessel.
- The extreme normalised peak loads are higher for low drift velocities. The spread in loads is higher for the lower drift velocities.
- Suggestions for how to use normalised peak loads both operationally and in design have been presented.
- The numbers presented in this paper are only valid for the hull shape and mooring configurations from the described model tests. For other hull shapes and mooring configurations, specific model ice tank model tests should be carried out.

Acknowledgements

The work described in this report/publication was supported by the European Community's Sixth Framework Programme through the grant to the budget of the Integrated Infrastructure Initiative HYDRALAB III, Contract no. 022441(RII3). The authors would like to thank the Hamburg Ship Model Basin (HSVA), especially the ice tank crew, for the hospitality, technical and scientific support and the professional execution of the test programme in the Research Infrastructure ARCTECLAB.

Funding of equipment by Statoil ASA was highly appreciated. The work was supported by the PetroArctic project, part of the Petromaks project of the Research Council of Norway.

References

- Aksnes, V., 2010. Model test investigation of the interaction between a moored vessel and level ice. Proceedings of the 20th IAHR International Symposium on Ice. Lahti, Finland.
- Evers, K. U. and Jochmann, P., 1993. An advanced technique to improve the mechanical properties of model ice developed at the HSVA ice tank. Proceedings of the 12th International

Conference on Port and Ocean Engineering under Arctic Conditions. Hamburg, Germany, pp. 877–888.

Gudmestad, O. T., Dalane, O. and Aksnes, V., 2009. On the disconnection of a moored floater in hard ice conditions. Proceedings of the 20th International Conference on Port and Ocean Engineering under Arctic Conditions (POAC), Luleå, Sweden.

ISO/CD 19906, 2007. Petroleum and natural gas industries – Arctic offshore structures, ISO TC 67/SC 7/WG 8. Draft International Standard, International Standardisation Organization, Geneva, Switzerland, 406 p.

Keinonen, A. and Robbins, I., 1998. Icebreaker Characteristics Synthesis – Icebreaker performance models, Seakeeping, Icebreaker escort. Report TP12812E to Transport Canada, April 1998. Vol 3 – Icebreaker Escort Model users' Guide. 49 p.

Keinonen, A., Browne, R., Revill, C. and Reynolds, A., 1996. Icebreaker Characteristics Synthesis. Report TP12812E to Transport Canada, July 1996. Vol 1 – main report. 321 p.

Timco, G. W. and Croasdale, K. R., 2006. How well can we predict ice loads? Proceedings of the 18th International Symposium on Ice (IAHR), Vol. 1, Sapporo, Japan, pp 167-174.

Wright, B., 1999. Evaluation of Full Scale Data for Moored Vessel Stationkeeping in Pack Ice. PERD/CHC report 26-200.

5.3 Sea ice management and impact on design of offshore structures

Paper accepted by the Journal of Cold Regions Science and Technology, October 2010.

**SEA-ICE MANAGEMENT AND ITS IMPACT ON THE DESIGN OF
OFFSHORE STRUCTURES**

Kenneth Eik¹

Norwegian university of Science and technology / Statoil

Trondheim, Norway

¹ Fax.: +47 73 59 70 21

Email: kenjo@statoil.com

Is not included due to copyright

6 SUMMARY

6.1 Summary and conclusions

The subject ice management has been studied with the main objective to deduce a methodology that incorporates the effect ice management systems have on the structural reliability of offshore installations. This was done by first studying Arctic projects in the past and summarizes the learning's. All available reports were unanimous and highlighted ice management as a key for the successes in the projects. Based on the reported experiences, an unambiguous definition of ice management was made and used as a bound throughout the study:

“Ice management is the sum of all activities where the objective is to reduce or avoid actions from any kind of ice features”

Despite the number of similarities between sea ice management and iceberg management, it was decided to study each of the fields individually. The motivation for doing so was that iceberg management in general focus on reducing the frequency of impacts between icebergs and installations while sea ice management generally focus on reducing the sizes in the ice floe distributions and thereby reduces the severity of the ice actions. One methodology for including iceberg management and one for including sea ice management in the offshore installation design process has been proposed.

6.1.1 Iceberg management

With respect to iceberg management, the proposed methodology considers the operations of the offshore installation as a system with certain reliability. In order to increase the reliability, various safety functions may be incorporated in the system. The occurrence of icebergs is considered as an accidental event and actions such as iceberg

detection, iceberg deflection and disconnection of the installation are considered as safety functions. This is modelled as an event tree. In order to demonstrate the methodology, an iceberg drift model has been combined with statistical distributions describing the efficiency of iceberg detection and iceberg deflection.

As the ability to calculate iceberg drift is one of the main elements in the model for calculation of iceberg management efficiency, separate studies were performed within this subject. First, a model for systematic evaluation of the skills of an iceberg drift model was presented. The ability to create reliable oceanographic models was identified as a key element required to provide reliable iceberg drift models. Further, in open waters, the iceberg drift caused by waves was considered to be of significant importance for the iceberg drift. Both physical tank model tests and numerical calculations were conducted and improved formulations for iceberg wave drift were performed. The ability to forecast iceberg deterioration was considered to be of important for the iceberg risk assessment. Due to this, a study of iceberg deterioration in the Barents Sea was performed. Existing models for deterioration calculations were used together with an iceberg drift model and the significance of iceberg deterioration in the Eastern Barents Sea was quantified. A factorial design study was conducted in order to identify the importance of environmental variables contributing to iceberg deterioration.

With respect to iceberg deflection operations, the efficiency of open water operations was well documented through records from Canadian operations. With respect to iceberg towing in ice covered waters however, there were no documentation on how it should be done or how efficient it can be. Due to this, physical tank model tests were performed by making iceberg models of fresh water ice and tow them through different sea ice conditions. It was found that the ice resistance increases significantly as the ice concentrations increases. Only iceberg towing in concentrations up to around 30% can be considered as feasible while towing in 50% ice or higher is not considered feasible due to the high ice resistance. Extensive use of icebreakers could

evidently increase the feasibility. Independent on concentrations, significant wear on the towing equipment must be expected.

6.1.2 *Sea ice management*

With respect to sea ice management, the proposed methodology focuses on the icebreaker's ability to change the load effect distributions. In order to do so, environmental data from a probabilistic type of analysis is required. In the presented study, a 1000-year long synthetic dataset was applied. Prior to the ice load calculations, the various ice conditions are transformed into an equivalent ice thickness parameter. The reason for doing so is to be able to use formulations for icebreaker resistance and icebreaker efficiency. When using the principles of ice equivalency one may consider i.e. ice of 1.1 m thickness in 90% ice concentration to cause equal icebreaker/vessel resistance as 1 m thick ice in 100% ice conditions. Also other parameters such as ice floe size, ridge intensity, ice strength, temperature etc. are included in the calculations of equivalent ice.

By first calculating equivalent ice thickness at all time steps in the 1000-year long synthetic dataset and thereafter the ice resistance on a structure, the ice load distribution without any ice management system could be derived. By reducing the equivalent ice thicknesses depending on what type of icebreaker fleets would be used, corresponding distributions for different ice management systems could be developed. It was found that icebreakers in general may contribute to significant reductions in horizontal ice loads on a moored structure. However, if the icebreakers do not have the sufficient power, they may still not be able to affect the tail in the load distributions. If it cannot be documented that the icebreakers reduce the severity of extreme and abnormal ice conditions, the robustness of the structure needs to be as without the icebreakers.

One of the key elements in the approach for calculation of horizontal loads on a moored vessel is the use of empirical formulations for icebreaker resistance in ice. When considering the required strength of mooring lines for a floating installation, it is the peak loads that are of importance and not the average loads. Due to this, the variability in ice loads in physical tank model tests was studied. By considering the ratio between peak loads and average loads for a floating system with different mooring configurations and in different ice drift speeds, distributions describing the variability in the ice loads were presented. These distributions were used in the model for efficiency of sea ice management as the calculated ice resistance was transformed to a peak load by using the variability distributions.

The reduction in ice loads due to icebreakers was demonstrated through a Structural Reliability Analysis (SRA), i.e. the probability of the loads being larger than the structural resistance was calculated. However, when considering ice management, there are a number of factors of importance not included in the SRA. Examples are the probability of failure in ice forecasting, the probability of human errors, the probability of failure in icebreaker equipment etc. In order to also take such factors into account, an approach for including the results from an SRA into a Qualitative Reliability Analysis (QRA) was proposed. Basically, this approach use a fault tree and both the events “Dangerous ice” and “Ice management failure” need to occur at the same time in order to get an accident. By doing so, the probability of an accidental event may be quantified.

6.1.3 *Disconnection*

The possibility to disconnect an installation and escape the site has been considered both in the methodologies for iceberg management and sea ice management. Details on how to physically disconnect offshore installations have not been studied in this work. However, when considering the number and magnitude of uncertainties both with respect to load calculations from icebergs and sea ice, disconnection capabilities should

be considered in all Arctic projects. In this respect, it should be noted that both distributions for kinetic energy from iceberg impacts and from sea ice loads on a moored structure shows extremely “fat tails”. This means that once in a while, there will be events that are significantly more severe than the main bulk of ice events. The possibility to disconnect an installation will contribute to an increased level of safety and to some extent compensate the uncertainties in ice load calculations.

6.2 Recommendations for further work

Both the approaches for iceberg management and sea ice management efficiency calculations require that a number of tools are used. With respect to icebergs, the lack of reliable oceanographic models has been highlighted and thus focus on further development and validations of such models such be given priority. When considering operational use of iceberg drift models, the ability to quantify the uncertainty in the drift forecasts will be crucial. Due to this, existing drift models should be used operationally for testing simultaneously with data-logging of all relevant metocean parameters such as winds, waves and currents.

Regarding sea ice management, the lack of reliable load models for unmanaged ice in general and managed ice in particular has been highlighted. It is important that the transformations the icebreakers do with the ice also are captured in the models used for calculations of ice loads. Continuous focus on numerical approaches, physical tank model tests and full scale tests will be required in order to achieve better load models.

The presented model for sea ice management do not take into account scenarios were ship-shaped installations are subjected to ice approaching perpendicular to the hull. There are reasons to expect that icebreakers will be extremely important in order to assist such installations to vane and reduce the severity of such events. Priority should be given to studies on this subject as ship-shaped installations may be preferred in a number of Arctic projects.

7 REFERENCES

Crocker, G., Wright, B., Thistle, S. and Bruneau, S., 1998. An assessment of Current Iceberg Management Capabilities. Contract report for National Research Council Canada, Prepared by C-CORE and B. Wright and Associates Ltd., C-CORE Publication 98-C26, 108 p.

Faltinsen, O. M., 1990. Sea Loads on Ships and Offshore Structures. Cambridge University Press, 328 p.

Isaacson, M., 1988. Influence of wave drift force on ice mass motions. In: Proceedings 17th International Conference on Offshore Mechanics and Arctic Engineering, Houston, US, pp. 125-130.

Kudou, K., 1977. The drifting force acting on a three-dimensional body in water. Journal of Soc. Naval Arch. 141, pp. 71-77.

Mauro, H., 1960. The drift on a body floating on water. Journal of Ship Research 4, pp. 1-10.

McClintock, J., McKenna, R. and Woodworth-Lynas, C., 2007. Grand Banks Iceberg Management. PERD/CHC Report 20-84, Report prepared by AMEC Earth & Environmental, St. John's, NL, R.F. McKenna & Associates, Wakefield, QC, and PETRA International Ltd., Cupids, NL., 84 p.

PERD Iceberg Management Database, 2005. <http://www.nrc-cnrc.gc.ca/eng/ibp/chc/reports/ice-engineering.html>, cited November 2009.

Timco, G. W. and Gorman, R., 2007. Survey of Canadian Arctic Captains: Current Status and Research needs. Proceedings of the 19th International Conference on port and Ocean Engineering under Arctic Conditions, Dalian, China, pp. 695-704.

Wamit, Inc. 2006. Wamit[®] User Manual version 6.3PC, USA.